University of Hamburg
Faculty of Mathematics, Informatics, and Natural Sciences,
Department of Biology

Binding properties determine the cytoadhesion of *Plasmodium falciparum* infected erythrocytes with the host

by

Johannes Allweier

A thesis submitted in fulfillment of the requirements

for the degree of

Doctor rerum naturalium

2026

Day of oral defense: 24.04.2026, Klein Flottbeck

Chair: Prof. Dr. Esther Schnettler
Member: Prof. Dr. Thomas Gutsmann

1. Dissertation reviewer: Prof. Dr. Iris Bruchhaus

Bernhard Nocht Institute for Tropical Medicine
Department of Host-Parasite Interaction
Bernhard-Nocht-Straße 74, 20359 Hamburg

2. Dissertation reviewer: Prof. Dr. Tim-Wolf Gilberger

Bernhard Nocht Institute for Tropical Medicine
Department of Cellular Parasitology
Bernhard-Nocht-Straße 74, 20359 Hamburg

Eidesstattliche Versicherung:

Hiermit versichere ich an Eides statt, die vorliegende Dissertationsschrift selbst verfasst und keine anderen als die angegebenen Hilfsmittel und Quellen benutzt zu haben. Sofern im Zuge der Erstellung der vorliegenden Dissertationsschrift generative Künstliche Intelligenz (gKI) basierte elektronische Hilfsmittel verwendet wurden, versichere ich, dass meine eigene Leistung im Vordergrund stand und dass eine vollständige Dokumentation aller verwendeten Hilfsmittel gemäß der Guten wissenschaftlichen Praxis vorliegt. Ich trage die Verantwortung für eventuell durch die gKI generierte fehlerhafte oder verzerrte Inhalte, fehlerhafte Referenzen, Verstöße gegen das Datenschutz- und Urheberrecht oder Plagiate.

Affidavit:

I hereby declare and affirm that this doctoral dissertation is my own work and that I have not used any aids and sources other than those indicated. If electronic resources based on generative artificial intelligence (gAI) were used in the course of writing this dissertation, I confirm that my own work was the main and value-adding contribution and that complete documentation of all resources used is available in accordance with good scientific practice. I am responsible for any erroneous or distorted content, incorrect references, violations of data protection and copyright law or plagiarism that may have been generated by the gAI.

Hamburg, the 02/18/2026

_____

Johannes Allweier

Abstract

The pathogenicity of *Plasmodium falciparum* malaria is primarily driven by the sequestration of infected erythrocytes in the microvasculature, mediated by the interaction between *P. falciparum* erythrocyte membrane protein 1 (*Pf*EMP1) and various host human endothelial cell receptors (ECRs). Investigating the distinct adhesion properties of the approximately 60 different *Pf*EMP1 variants encoded by the *var* gene family has historically been hindered by the parasite's ability to switch the actively presented *Pf*EMP1 and the heterogeneity of *in vitro* cultures. This study characterized transgenic IT4 parasite lines, generated via the selection linked integration (SLI) system, to link specific genotypes to adhesive phenotypes under static and flow conditions.

Adhesion assays of the SLI-activated parasite lines to ECRs presented on transgenic Chinese hamster ovary cells confirmed known receptor interactions for several *Pf*EMP1s. Known binding partners for IT4var01-HA^{endo} and IT4var16-HA^{endo} such as CD36 and intercellular adhesion molecule 1 (ICAM-1) were confirmed, along with the identification of novel binding partners. Flow chamber assays using the IT4var01-HA^{endo} line revealed distinct binding dynamics, characterized by rolling adhesion on CD36 and static adhesion on ICAM-1. The placental malaria-associated variant, IT4var04-HA^{endo} (VAR2CSA), demonstrated known cytoadhesion to chondroitin sulfate A (CSA), however, additionally a novel, broadly unspecific binding to all tested Chinese hamster ovary (CHO) cells was observed as well. Conversely, the investigation of more complex variants presented significant challenges. The severe malaria-associated candidate IT4var19-HA^{endo} initially lacked expected endothelial protein C receptor (EPCR) binding, which could only be induced by multiple rounds of binding enrichment. Subsequently, static adhesion was observed to EPCR and ICAM-1, with the latter contradicting earlier descriptions of *var19* as an EPCR-only binder. Furthermore, attempts to characterize the A-type IT4var08-HA^{endo} and the expected EPCR-binder IT4var20-HA^{endo} revealed genomic plasticity and transcriptional instability of theses two transgenic parasite lines. RNA-seq analysis indicated that IT4var08-HA^{endo} cultures did not maintain the SLI mediated mutually exclusive expression of the IT4var08 target gene, while IT4var20-HA^{endo} formed three potential fusion genes with *var27*. The discovery and initial characterization of the mutually exclusive expression defective phenotype of IT4var08-HA^{endo} provided a promising tool to further

study the complex mechanisms of *var* gene switching. The transcriptomic analysis of a large set of IT4 lines of different *var* expression patterns revealed novel insights into coexpression of *var*-adjacent genes, based on relative gene orientation.

Finally, the study utilized the earlier characterized multi-binding IT4var01-HA^{endo} line to screen synthetic peptide libraries derived from CD36 and ICAM-1 binding domains for their ability to inhibit cytoadhesion to these to ECRs. While identifying potential inhibitory candidates, such as the CD36-derived peptides P03^{CD36} and P05^{CD36}, the screening revealed significant cytotoxicity and hemolysis-related artefacts, highlighting the complexity of peptide-based interference strategies. Only one peptide, P07^{CD36}, out of the ten peptides each tested to inhibit CD36 and ICAM-1 cytoadhesion, showed a moderate binding inhibition of 15 % relative to the non-inhibited positive control. These findings demonstrate the utility of SLI-based systems for characterizing specific *var* expression while underscoring the substantial impact of genomic recombination, transcriptional switching, and compound toxicity on experimental validation.

Zusammenfassung

Die Pathogenität der *Plasmodium falciparum*-Malaria wird maßgeblich durch die Sequestrierung von *P. falciparum*-infizierten Erythrozyten (iEs) in den Kapillaren bestimmt, welche durch die Interaktion zwischen *P. falciparum* erythrocyte membrane protein 1 (*Pf*EMP1) und verschiedenen menschlichen Wirtsendothelzellrezeptoren (ECRs) vermittelt wird. Die Untersuchung der unterschiedlichen Adhäsionseigenschaften der ca. 60 verschiedenen *Pf*EMP1-Varianten, kodiert durch die *var*-Genfamilie, wurde bislang durch die Fähigkeit des Parasiten zum Wechsel der präsentierten *Pf*EMP1, sowie durch die Heterogenität deren Expression in *in vitro*-Kulturen erschwert. In dieser Studie wurden transgene IT4-Parasitenlinien charakterisiert, die mittels des *selection linked integration* (SLI)-Systems generiert wurden, um spezifische Genotypen unter statischen und Flussbedingungen mit adhäsiven Phänotypen zu verknüpfen.

Adhäsionsassays der SLI-aktivierten Parasitenlinien an ECRs, präsentiert auf transgenen CHO-Zellen, bestätigten bekannte Rezeptorinteraktionen für mehrere *Pf*EMP1s. So konnten für IT4var01-HA^{endo} und IT4var16-HA^{endo} Bindungspartner wie CD36 und *intercellular adhesion molecule 1* (ICAM-1) verifiziert sowie neue Bindungspartner identifiziert werden. Flusskammer-Assays der IT4var01-HA^{endo}-Linie zeigten distinkte Bindungsdynamiken, charakterisiert durch rollende Adhäsion auf CD36 und statische Adhäsion auf ICAM-1. Die mit plazentarer Malaria assoziierte Variante IT4var04-HA^{endo} (VAR2CSA) wies die bekannte Cytoadhäsion an *chondroitin sulfate A* (CSA) auf, zeigte darüber hinaus jedoch auch eine neue, breit unspezifische Bindung an alle getesteten CHO-Zellen.

Die Untersuchung komplexerer Varianten stellte hingegen eine größere Herausforderung dar. Der mit schwerer Malaria assoziierte Kandidat IT4var19-HA^{endo} zeigte anfänglich nicht die erwartete *endothelial protein C receptor* (EPCR)-Bindung, diese konnte erst durch mehrfache Bindungsanreicherung induziert werden. Anschließend ließ sich eine statische Adhäsion an EPCR und ICAM-1 beobachten. Letztere widerspricht früheren Beschreibungen von *var19* als reinem EPCR-Binder. Des Weiteren offenbarten Versuche zur Charakterisierung der Linien IT4var08-HA^{endo} und IT4var20-HA^{endo} eine genomische Plastizität und transkriptionelle Instabilität im Parasitengenom. RNA-Seq-Analysen deuteten darauf hin, dass IT4var08-HA^{endo}-Kulturen die durch SLI vermittelte, gegenseitig ausschließende Expression des IT4var08-Zielgens nicht aufrechterhielten, während

IT4var20-HA^{endo} drei potenzielle Fusionsgene mit *var27* bildete. Die Entdeckung und erste Charakterisierung des *mutually exclusive expression defective* (MEED)-Phänotyps von IT4var08-HA^{endo} lieferte ein vielversprechendes Werkzeug, um die komplexen Mechanismen der *Pf*EMP1-Expression weiter zu untersuchen. Eine transkriptomische Analyse einer großen Anzahl an IT4-Linien mit unterschiedlichen *var*-Expressionsmustern gab zudem neue Einblicke in die Koexpression von *var*-benachbarten Genen in Abhängigkeit ihrer relativen Genorientierung.

Abschließend wurde die zuvor charakterisierte, multibindende IT4var01-HA^{endo}-Linie genutzt, um synthetische Peptidbibliotheken, abgeleitet von CD36- und ICAM-1-Bindungsdomänen, auf ihre Fähigkeit zur Hemmung der Cytoadhäsion an diese ECRs zu prüfen. Zwar wurden potenzielle inhibitorische Kandidaten wie die CD36-abgeleiteten Peptide P03^{CD36} und P05^{CD36} identifiziert, jedoch enthüllte das Screening auch signifikante Zytotoxizität und Artefakte durch Hämolyse, was die Komplexität peptidbasierter Bindungsinhibition verdeutlicht. Von den jeweils zehn getesteten Peptiden zur Hemmung der CD36- und ICAM-1-Cytoadhäsion zeigte lediglich P07^{CD36} eine moderate Bindungshemmung von 15 % relativ zur nicht-inhibierten Positivkontrolle.

Diese Ergebnisse demonstrieren den Nutzen SLI-basierter Systeme zur Charakterisierung spezifischer *var*-Expression, unterstreichen jedoch gleichzeitig den erheblichen Einfluss von genomischer Rekombination, transkriptionellem Umschalten und Substanztoxizität auf die experimentelle Validierung.

Abbreviations

ACT	artemisinin-based combination therapies
AFM	atomic force microscopy
AMP	antimicrobial peptides
APC	allophycocyanin
ATS	acidic terminal sequence
BM	binding media
CAM	cell adhesion molecule
CPP	cell-penetrating antimicrobial peptide
CD	cluster of differentiation
CHO	Chinese hamster ovary
CIDR	cysteine-rich interdomain region
CM	cerebral malaria
CS	chondroitin sulfate
CSA	chondroitin sulfate A
CSP	circumsporozoite protein
CSPG	chondroitin sulfate proteoglycan
DBL	duffy-binding like
DC	domain cassette
DDT	dichlorodiphenyltrichloroethane
DE	differentially expressed
DGE	differential gene expression
DMSO	dimethyl sulfoxide
DPBS	Dulbecco's Phosphate-Buffered Saline

DSB	double-strand break
DSS	DNA secondary structure
EC	endothelial cell
ECR	endothelial cell receptor
EMP	erythrocyte membrane protein
EPCR	endothelial protein C receptor
fc	fold change
GA	genetic algorithm
G4	G-quadruplex
gff	general feature format
GHB	glycophorin-binding protein
GFP	green fluorescent protein
GTS	global technical strategy for malaria
h2h	head-to-head
h2t	head-to-tail
HBEC-5i	human brain endothelial cells
HBMEC	primary human brain endothelial cell
hDHFR	human dihydrofolate reductase
HRP2	histidine-rich protein 2
HR	homologous recombination
ICAM-1	intercellular adhesion molecule 1
iE	infected erythrocyte
IFA	immunofluorescence assay
IFN-γ	interferon gamma
ITN	insecticide-treated mosquito net
Il-1	interleukin-1
KAHRP	knob-associated histidine-rich protein
LFA-1	lymphocyte function-associated antigen-1
lncRNA	long noncoding RNA
l2fc	$\log_2$ fold change

MDR1	multidrug resistance protein 1
MEED	mutually exclusive expression defective
MFE	minimum folding energy
MTS	malaria thawing solution
MTT	(3-(4,5-Dimethylthiazol-2-yl)-2,5-Diphenyltetrazolium Bromide)
NC	negative control
NF-$\varkappa$B	nuclear factor-$\varkappa$B
nt	nucleotides
NTS	n-terminal segment
PAM	pregnancy-associated malaria
PBS	phosphate-buffered saline
PC	positive control
PE	Phycoerythrin
PCA	principle component analysis
PCR	polymerase chain reaction
PEV	pre-erythrocytic vaccines
P. falciparum	*Plasmodium falciparum*
***Pf*CRT**	*P. falciparum* chloroquine resistance transporter
***Pf*EMP1**	*P. falciparum* erythrocyte membrane protein 1
PHIST	*Plasmodium* helical interspersed subtelomeric family
PQS	putative quadruplex-forming sequences
PS	phosphatidylserine
PTP3	erythrocyte membrane protein trafficking protein 3
PV	parasitophorous vacuole
RDT	rapid diagnostic test
RIFIN	repetitive interspersed families of polypeptides
RT	room temperature
t2t	tail-to-tail
t2h	tail-to-head
SAM	sequence alignment/map

SBP1	skeleton binding protein 1
SCFS	single cell force spectroscopy
SLI	selection linked integration
SM	severe malaria
SNP	single nucleotide polymorphism
SIP2	SPE2-interacting protein
STEVOR	subtelomeric open reading frame
TM	transmembrane domain
TNFα	tumor necrosis factor alpha
TNFR	tumor necrosis factor receptor
TPM	transcripts per million
uE	uninfected erythrocyte
UPS	upstream sequence
VSA	variant surface antigen
VCAM-1	vascular adhesion molecule 1
WHO	World Health Organisation

Contents

Abbreviations **vii**

List of Figures **xiv**

List of Tables **xvi**

1 Introduction **1**

1.1 Malaria . . . 1
1.1.1 Overview . . . 1
1.1.2 Disease . . . 2
1.1.3 Diagnosis . . . 3
1.1.4 Treatment . . . 4
1.1.5 Transmission . . . 4
1.1.6 Vaccines . . . 6

1.2 *Plasmodium falciparum* . . . 8
1.2.1 Life cycle . . . 8
1.2.2 Cytoadhesion and sequestration . . . 10
1.2.3 *Pf*EMP1 . . . 10
1.2.4 Genetics . . . 10
1.2.5 Sequestration . . . 16
1.2.6 Endothelial cell receptors . . . 17

2 Materials and Methods **23**

2.1 Material . . . 23
2.1.1 Consumables . . . 25
2.1.2 Biologicals . . . 28
2.1.3 Media and Solutions . . . 30

2.2 Methods . . . 34
2.2.1 Mammalian cell culture . . . 34
2.2.2 *Plasmodium* culture . . . 36
2.2.3 Preparation of peptide stocks and working solution . . . 37
2.2.4 Limited dilution and plaque assay . . . 38

2.2.5 Static binding assay . . . 38
2.2.6 Flow binding assay . . . 42
2.2.7 Panning . . . 44
2.2.8 Immunofluorescence microscopy . . . 45
2.2.9 RNA isolation . . . 45
2.2.10 Genomic DNA isolation . . . 46
2.2.11 RNA-seq data processing and relative *var* gene expression analysis 46
2.2.12 Scatterplot of *var* gene and neighbouring genes co-expression . . 47
2.2.13 *De novo* gene assembly . . . 48
2.2.14 Recombination identification . . . 48
2.2.15 Agarose gel electrophoresis . . . 50

3 Parasite adhesion 51

3.1 Results . . . 51
3.1.1 IT4 wild type . . . 53
3.1.2 IT4var01- and IT4var16-HA^{endo} . . . 58
3.1.3 IT4var04-HA^{endo} . . . 63
3.1.4 IT4var19-HA^{endo} . . . 65
3.1.5 IT4var08-HA^{endo} . . . 67
3.1.6 IT4var20-HA^{endo} . . . 70
3.1.7 IT4var66-HA^{endo} . . . 72
3.2 Discussion . . . 76

4 Genomics of SLI-transfectants 83

4.1 Results . . . 83
4.1.1 Co-regulation of *var* proximal genes . . . 83
4.1.2 Defective mutually exclusive expression in IT4var08-HA^{endo} . . 86
4.1.3 Transcriptomal differences between binding enriched and non-binding IT4var19-K2-HA^{endo} parasite lines . . . 92
4.1.4 *Var* chimera – IT4var20/27 . . . 93
4.2 Discussion . . . 99

5 Peptides for inhibition of cytoadhesion 107

5.1 Results . . . 107
5.1.1 Antimalarial peptides . . . 107
5.1.2 CD36 cytoadhesion inhibition . . . 109
5.1.3 CD36 peptide cytotoxicity . . . 110
5.1.4 ICAM-1 cytoadhesion inhibition . . . 112

5.1.5 ICAM-1 peptide cytotoxicity 113
5.2 Discussion 115
6 Conclusion **119**
A Appendix **121**
A.1 Introduction 121
A.2 Material and Methods 127
A.3 Results 138
A.3.1 Genomics of SLI-transfectants 138
A.3.2 Antimalaria peptides 214
Publications **215**
Bibliography **217**
B Acknowledgments **245**

List of Figures

1.1 Prevalence of malaria around the world in 2024 2
1.2 Life cycle 9
1.3 *var* gene structure 13
1.4 Location of *var* genes and PQS on chromosomes of *Pf*IT 14
1.5 Model of catch- and slip bonds 17

2.1 Binding assay plate washing setup 39
2.2 Bound erythrocyte quantification pipline 41
2.3 Setup of flow binding experiment with Ibidi pumps system 44
2.4 RNA-seq data processing 47
2.5 *De novo* gene assembly 48

3.1 SLI schematic for *var* genes 52
3.2 Cytoadhesion of IT4 wt without shear stress 55
3.3 Cytoadhesion of IT4 wt under shear stress 56
3.4 Number of bound IT4 wt iEs under shear stress 57
3.5 Rolling velocity and distance of IT4 wt under shear stress 57
3.6 Cytoadhesion of IT4wt without shear stress 58
3.7 Cytoadhesion of IT4var16-HA^{endo} without shear stress 59
3.8 Number of bound IT4var01-HA^{endo} wt iEs under shear stress 60
3.9 Cytoadhesion of IT4var01-HA^{endo} under shear stress 61
3.10 Rolling velocity and distance of IT4var01-HA^{endo} under shear stress 62
3.11 Static cytoadhesion of IT4var04-HA^{endo} 63
3.12 Binding enrichment of IT4var19-K2-HA^{endo} 65
3.13 Binding comparison of IT4var19-K2-HA^{endo} against IT4var19-K2-HA^{endo}-P5-EPCR 67
3.14 Binding enrichment of IT4var08-HA^{endo} 68
3.15 Binding comparison of IT4var08-HA^{endo} against IT4var08-HA^{endo}-P4-ICAM1 70

3.16 Binding comparison of IT4var20-HA^{endo} against IT4var20-HA^{endo}-P4-ICAM1 71
3.17 Cytoadhesion of IT4var66-HA^{endo} 72
3.18 Cytoadhesion of IT4var66-HA^{endo} under shear stress 74
3.19 Rolling velocity and distance of IT4var66-HA^{endo} under shear stress 75
3.20 Number of bound IT4var66-HA^{endo} iEs under shear stress 75

4.1 Coexpression of neighboring genes. 85
4.2 Clustering of IT4var08-HA^{endo} before and after enrichment 87
4.3 Volcano plot of differential gene expression of IT4var08-HA^{endo}-LC against IT4var08-HA^{endo}-P4-ICAM1 89
4.4 Location of differentially expressed (DE) genes on chromosomes of *Pf*IT . 90
4.5 RNA-seq analysis of binding enriched and unenriched IT4var19-K2-HA^{endo} 93
4.6 RNA-seq analysis of *var* expression profile and coverage of IT4var20-HA^{endo} and IT4var20-HA^{endo}-c32 94
4.7 Coverage of IT4var20-HA^{endo}-c32 to proposed var27–20 fusion reference sequence 95
4.8 Agarose gel of PCR products for recombination check of *var20* and *var27* . 98

5.1 Relative binding inhibition of CD36 peptides 109
5.2 Cytotoxicity analysis of CD36-derived antimalarial peptides 111
5.3 Relative binding inhibition of ICAM-1-derived peptides 112
5.4 Cytotoxicity analysis of ICAM-1-derived antimalarial peptides 113

A.1 *Var* gene repertoire and respective domains of IT4/FCR3 isolate 123
A.2 Genomic *var* gene orientation of the IT4/FCR3 isolate 126
A.3 *Var* expression in relationship to neighbouring genes 138
A.4 IFA of IT4var08-HA^{endo} 139
A.5 Coverage of R1F2 paired reads of IT4var20-HA^{endo} and IT4var20-HA^{endo}-c32 212
A.6 Folding free energy of *var27* (top) and *var20* (bottom) with R1F2 paired reads of IT4var20-HA^{endo} as indicators for possible recombination sites . . 213
A.7 Static binding inhibition of CD36 and ICAM1 derived peptides 214

List of Tables

1.1 Overview over common *Pf*EMP1 domain sequences classified by binding phenotype 13

2.1 Consumables 25
2.2 Sequence of *Pf*EMP1 antagonistic peptides derived from CD36 and ICAM-1 28
2.3 Primary antibodies 28
2.4 Secondary antibodies 28
2.5 List of primers SLI 29
2.6 List of primers for genotyping 29
2.7 Sequence of decreasing shear stress in flow binding assay. 43
2.8 Orientations for aligned, paired-end reads 49
2.9 PCR reaction mix (left) and thermal cycler settings (right) for a 20 µL plasmid amplification reaction. 49

4.1 Genes co-regulated to *var* genes in DESeq2 IT4var08-HA^{endo} 91
4.2 Homology sequences of recombination sites 96
4.3 Tabular results of agarose gel with PCR amplificates of genomic of IT4var20-HA^{endo} recombination sites 97

A.1 Non-telomeric putative G-quadruplex forming sequences in FCR3/IT4 . . 124
A.2 Genes co-regulated to *var* genes in DESeq2 IT4var08-HA^{endo} 140
A.3 Expression of *Pf*EMP1 in the IT4var08-HA^{endo} lines 141
A.4 Expression of *Pf*EMP1 in the IT4var19-K2-HA^{endo} lines 142
A.5 Expression of *Pf*EMP1 in the IT4var20-HA^{endo} and IT4var20-HA^{endo}-c32 lines 143
A.6 Differential gene expression between IT4var19-K2-HA^{endo} and IT4var19-K2-HA^{endo}-P5-EPCR 144

A.7 Differential gene expression between IT4var08-HA^{endo}-LC and IT4var08-HA^{endo}-P5-EPCR 147

1 Introduction

1.1 Malaria

1.1.1 Overview

The malaria disease, caused by the protozoan parasites of the genus *Plasmodium*, plagues humans in tropical climates for at least 5000 years, as the disease was already described in the oldest known medical book, the Chinese *Nei Ching*. It nevertheless took until the 19th century until the malaria transmission was linked to mosquito bites by Sir Patrick Manson and later proven experimentally by Ronald Ross which earned the latter the Nobel Prize in 1902 [1]. Today the disease still claims 610 000 lives every year with 282 million reported cases in the year 2024. The African continent is the most affected region shouldering 94 % of cases and 95 % of fatalities respectively (Fig. 1.1). Furthermore, children under the age of five years make up the majority of fatalities with 73.7 % in 2023. This concentration of the disease burden on the African continent is on the one hand owed to the optimal environmental conditions such as rainfall, humidity and temperature for the vector, the *Anopheles* mosquito in the sub-Saharan region, and on the other hand also owed to the poverty and therefore lack of adequate healthcare opportunities [2]. Fighting malaria does not only reduce the vast human suffering caused by the disease in endemic regions, it would also boost the development of the mostly poor affected countries. A study commissioned by Oxford Economics Africa estimates that Africa's economy would be 16 billion, dollars a year larger if the World Health Organisation (WHO)'s global technical strategy for malaria (GTS) goals of curbing malaria by 90 % by 2030 were achieved [3]. For the

year 2022, it is estimated that an increase in worldwide total funding in malaria control and elimination from 4.1 billion to 7.8 billion would be sufficient to reach this target [4]. Other studies determined an expected increase in GDP growth of 0.11 % per year for each 10 % points of decrease in malaria incident rate [5].

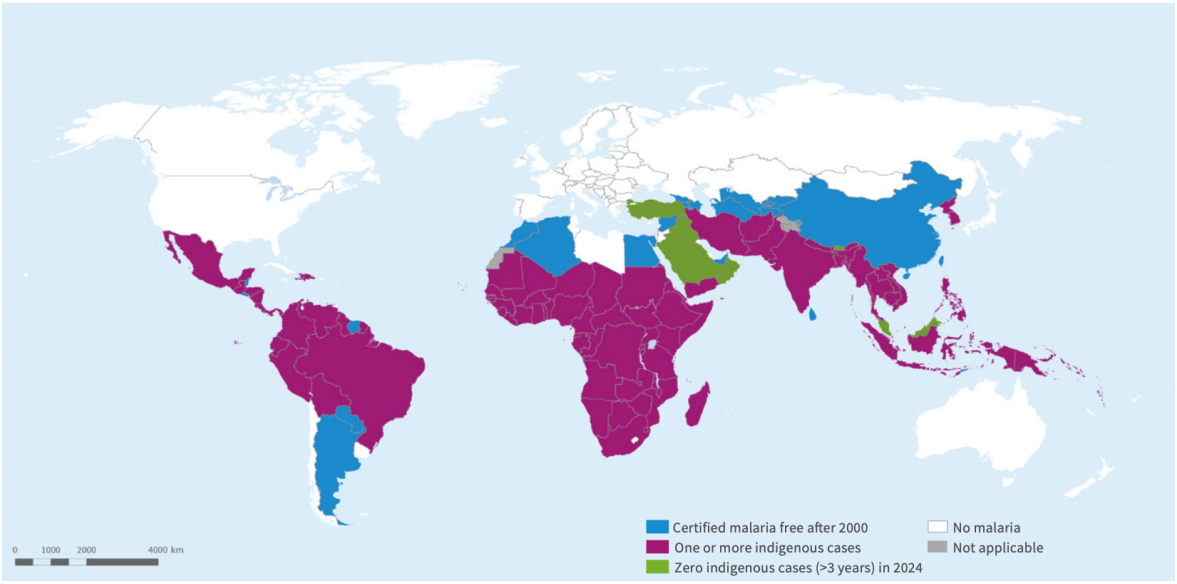


Figure 1.1: **Prevalence of malaria cases around the world in 2024**. Countries with indigenous cases are compared to countries without cases for >3 years, no new cases since the year 2000 and countries without cases since before the year 2000 [2].

1.1.2 Disease

An infection of the human host with the *Plasmodium falciparum* (*P. falciparum*) parasite causes a form of malaria disease, which is also known as malignant tertian, or subtertian malaria and manifests generally in continuous episodes with only short, intermittent breaks of fever. These episodes tend to synchronize with the parasite's 48 h replication rhythm during prolonged infections [6, 7]. The second most relevant, human pathogenic member of the same genus, *P. vivax*, causes benign tertian malaria, with fever occurring on the first and third day of the infection. The rarer, *P. malariae*-induced quartan malaria is marked by the occurrence of fever in 72-hour cycles, corresponding to the parasite's 72-hour life-cycle [7, 8]. Recently, increased numbers of

human infections with *P. knowlesi*, a malaria parasite of macaque monkeys, have been discovered in Malaysia and neighbouring south east Asian countries. Increased case numbers are likely due to improved molecular diagnostics, as the *P. knowlesi* infections were often misdiagnosed as *P. malariae* [9]. As implied by the origin of the nomenclature of the different malaria manifestations, periodic episodes of fever are the most prominent symptom of malaria. The periodicity of the fever originates from the interplay between the host's circadian rhythm and the parasite's replication rate during the asexual blood stage [6]. The periodic rupture of infected erythrocytes releases antigens and waste products that trigger pro-inflammatory cytokine release (e.g., TNFα, IL-1), endothelial activation, and activation of the human immune response [7, 10].

1.1.3 Diagnosis

Diagnosis is mainly performed through light microscopic analysis of stained blood smears, immunochromatographic-based rapid diagnostic tests (RDTs) specific for the detection of *P. falciparum* histidine-rich protein 2s (HRP2s), and diagnostic polymerase chain reaction (PCR) tests [11]. Clinically, manifestations of *P. falciparum* malaria are further subdivided into uncomplicated, severe malaria (SM), and pregnancy-associated malaria (PAM).

Severe malaria Adverse outcomes of the disease occur most frequently in children under five living in high-transmission areas, where 4.5 % of malaria-infected children present with symptoms of SM [12]. In adults, the risk of developing severe malaria mostly stems from comorbidities, immune deficiencies, high age (>65 years) or delayed or no treatment [13]. Based on the definition of the WHO, cases of SM must include one (or more) of the following signs if no other cause can be determined: Impaired consciousness, coma, generalized weakness, convulsions, acidosis, hypoglycemia, hyperparasitemia, shock, renal impairment, pulmonary edema, and bleeding from the nose or gums [11].

Uncomplicated malaria Uncomplicated malaria is diagnosed in patients that test positive with at most mild symptoms and without the features of SM [11].

Pregnancy-associated malaria Infection with *P. falciparum* during pregnancy causes may cause low birthweight in infants, pregnancy loss, and anemia [11]. PAM shows a distinct cytoadhesion pattern of infected erythrocytes (iEs) that accumulate in the tissue of the placenta. The adhesion is in this cased redominantly mediated by only one member of the roughly 60 *var* gene members, the among isolates highly conserved *var2csa*. *Var2csa* binds chondroitin sulfate A (CSA) of chondroitin sulfate proteoglycans (CSPGs) in the placenta [14, 15].

1.1.4 Treatment

The outcome of the malaria disease depends severely on a rapid diagnosis and treatment of the patients. The first major antimalarial drug, Quinine, an alkaloid extracted from the bark of the cinchona tree, has been used to treat malaria for over 300 years, until parasite drug resistance and the discovery of more potent drugs superseded it [16]. Today, first-line therapy for uncomplicated *P. falciparum* malaria are artemisinin-based combination therapies (ACT), most commonly artemether-lumefantrine or dihydroartemisininpiperaquine, administered over three days [17]. Globally, 4 billion ACT doses were produced between 2010–2022 with a generally high efficacy; however, concerns arise in the African and Asian regions where (partially) artemisinin-resistant parasites are suspected to be responsible for treatment failure rates greater than 10 %. In such cases, artesunate plus mefloquine, halofantrine, or artesunate in combination with the long-acting sulfadoxine-pyrimethamine may be administered [17, 18]. Generally, drug treatment usually proves effective and capable of clearing *Plasmodium* parasites from the bloodstream.

1.1.5 Transmission

All human malaria parasite vectors are mosquitoes of the genus *Anopheles* which consists of 465 named members of which ~70 are capable of infecting humans. The three species *Anopheles gambiae*, *An. arabiensis* and *An. funestus* are prevalent in the sub-Saharan region and epidemiologically the most relevant [19]. The regional prevalence

of the malaria disease is dependent on the habitat of the mosquitoes. Therefore, vector control became early on a key tool in combating malaria transmission. The WHO states that insecticide-treated mosquito nets (ITNs) are the main method of vector control for the most burdened countries of sub-Saharan region where an estimated 243 million out of the 255 million produced ITNs where distributed. Indoor spraying of pesticides may complement ITNs which protects ~55 million people [4].

Initial efforts in eradicating malaria involved draining mosquito breeding grounds and administering larvicides, which later, in the 1950s, was performed by by mass application of the highly effective insecticide dichlorodiphenyltrichloroethane (DDT). Both approaches had severe adverse effects on the ecology and more targeted approaches were developed. These range from novel insecticides that only affect specific species to the genetic control of pests. The first field tested approach made use of radiation-sterilised male mosquitoes, which, when released into the wild and mate with indigenous females, do not produce fertile offspring. Other approaches aim at taking advantage of recent advancements in genetic modification to create genetically modified mosquitoes that are immune to the *Plasmodium* infections. However this poses still many challenges as for one the fitness gained from being able to clear the infection must be larger than the additional cost of expressing the desirable gene constructs. Secondly, in order to robustly and quickly spread the desired modification, a genetic driver system is required. [20] made use of a CRISPR gene-drive system to insert a range of antimalarial proteins into the *An. stephensi* genome, with more than 99.97 % of first generation offspring carrying the mutation, as compared to ~50 % expected in regular Mendelian segregation patterns. Long term stability studies on effector gene stability are not yet available and a lot of work is still required to even reach the subsequent hurdles of convincing the regulatory agency, environmental groups and the general public on the safety and efficacy of the genetic modification approach.

1.1.6 Vaccines

Given the massive economic and humanitarian burden of malaria and other widespread parasitic infections, it is notable that, until October 6, 2021, no vaccine against any parasitic disease was available. The first efforts to develop such vaccines began in the 1960s, with the first successful candidate, RTS,S/AS01 (Mosquirix™), under development since the 1980s. The difficulties in creating vaccines for parasitic diseases are primarily due to their complex life cycles, consisting of multiple morphological stages, and their ability to modulate and evade the host's immune response [21]. Compared to viruses, parasite antigens comprise only a small percentage of the whole organism ($< 1\,\%$) and are highly stage-specific. Consequently, individuals exposed to malaria can achieve only partial immunity [22]. This partial immunity takes years and multiple infections to develop, which is reflected in the fact that most fatalities occur in malaria naïve children. Current vaccines are therefore administered mainly as childhood immunizations. In a 2019 pilot program for RTS,S, the vaccine was administered in three doses followed by a fourth booster dose 18 months later to infants and children. The study demonstrated the vaccine's safety profile and achieved a 30 % reduction in severe malaria and fatal outcomes among participants [21]. As of December 2024, RTS,S/AS01, together with a second vaccine (R21/Matrix-M), has been rolled out in 17 African countries, with more than 8 million doses administered [4, 23]. Both vaccines are recombinant protein vaccines targeting a fragment of the circumsporozoite protein (CSP), the major antigen of the parasite's sporozoite stage. To overcome CSPs low immunogenicity, the vaccines are formulated with adjuvants, such as the virus-like particles in RTS,S or nanoparticles from saponins in Matrix-M. These adjuvants are not required in other pre-erythrocytic vacciness (PEVs), such as whole-sporozoite vaccines. One such PEV candidate, marketed by Sanaria Inc. as PfSPZ-CVac (*Plasmodium falciparum* sporozoite Challenge under chemoprophylaxis), involves inoculating participants intravenously with 3,200 or 12,800 live sporozoites in combination with the antimalarial drug chloroquine. In a controlled infection study, this approach provided 33 % protection at the lower dose and 100 % protection at the higher dose in

malaria-naïve participants [24]. Other PEVs target *P. falciparum*–infected hepatocytes or aim to inhibit merozoite invasion. Erythrocytic vaccines mainly target the PAM antigen VAR2CSA. VAR2CSA is a highly conserved member of *P. falciparum* erythrocyte membrane protein 1 (*Pf*EMP1) that is strongly expressed during PAM, where it mediates placental-specific CSA binding of iEs. During non-pregnancy-associated malaria, parasites rarely express VAR2CSA. As a result, women in affected areas typically acquire immunity against PAM only after multiple pregnancies [25]. The WHO estimates that 12.4 million women, which are about one-third of all pregnancies in high-transmission African countries, were infected with malaria in 2023, leading to low birth weight and markedly higher infant mortality rates [4]. Two vaccine candidates in Phase 1a/b trials, PAMVAC (University of Copenhagen) and PRIMVAC (Inserm, France), aim to combat this issue. Both include N-terminal fragments of VAR2CSA to induce antigen-specific IgG production [26]. Transmission-blocking vaccines (TBVs) target the parasite's sexual stages to block its replication in the mosquito and thereby interrupt disease transmission. Target antigens include the gamete surface proteins Pfs48/45 and Pf230, as well as Pf25 on zygotes and ookinetes. All of these candidates remain in early Phase 1 trials [27].

1.2 *Plasmodium falciparum*

1.2.1 Life cycle

The *P. falciparum* life cycle begins when an infected female *Anopheles* mosquito injects sporozoites into a human host during a blood meal, which then migrate to the liver to mature and multiply. After maturing, parasites are released into the bloodstream as merozoites, where they invade erythrocytes and undergo a 48-hour asexual replication cycle. The periodic rupture of these infected cells releases new merozoites to continue the cycle, while a fraction of parasites develop into sexual-stage gametocytes. These gametocytes are ingested by another mosquito during a blood meal, allowing the parasite to sexually reproduce and migrate in the process from the gut to the salivary glands, ready to infect a new host. For a more detailed illustration of this process, please see Figure 1.2.

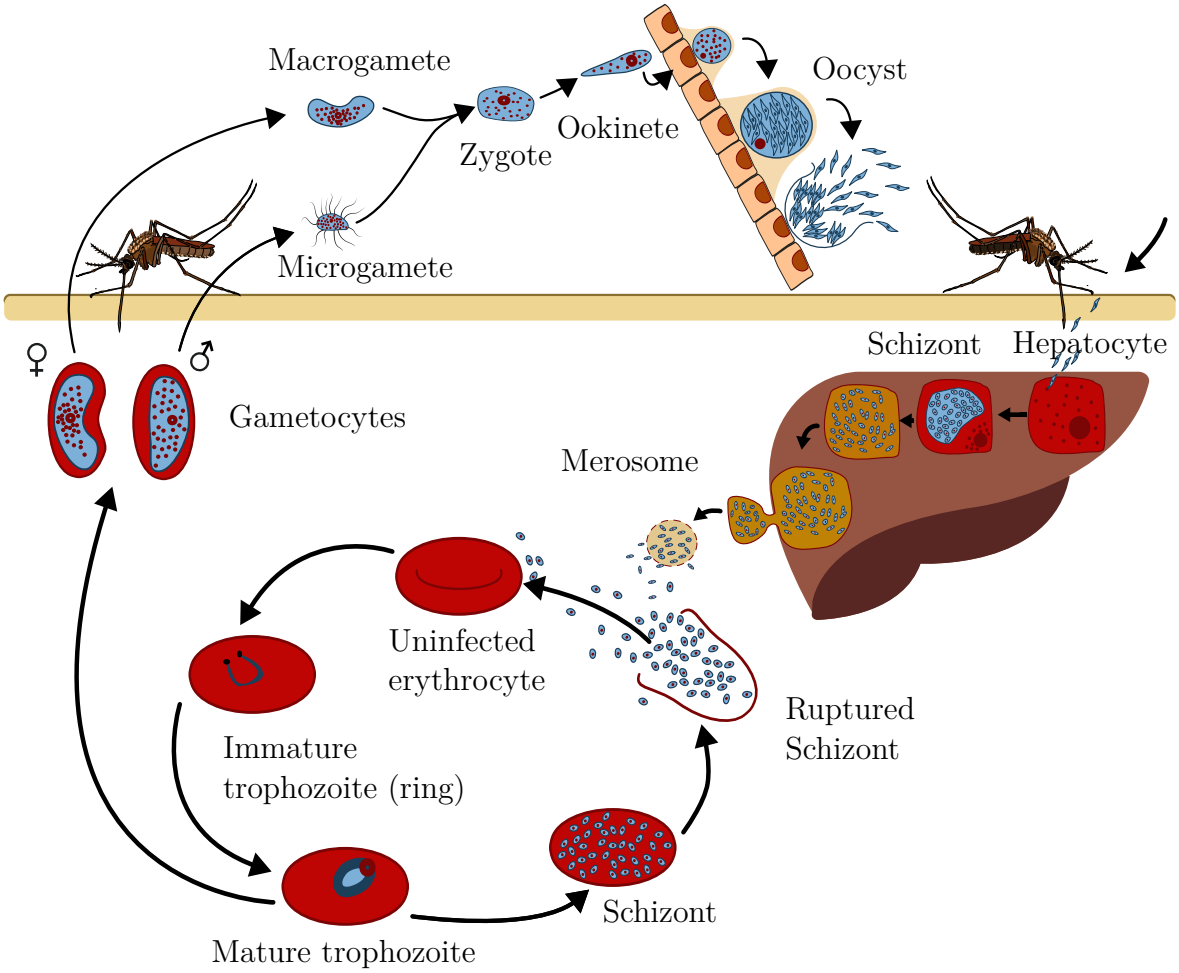


Figure 1.2: ***P. falciparum* life cycle**. The female *Anopheles* mosquito injects the sporozoite form of the parasite into the human dermis while taking a blood meal. The motile sporozoites migrate to the liver and proliferate to mature liver schizonts within the hepatocytes. Up to 40,000 daughter merozoites develop, separated by a parasite-derived parasitophorous vacuole (PV), in each infected hepatocyte. After several days to a week, the PV ruptures within the hepatocytes, releasing the merozoites into its cytoplasm. There they agglomerate into bundles of 10 to 1000 merozoites. These so called merosomes, then traverse the endothelial barrier to reach the vasculature [28]. In the bloodstream, the host cell-derived merosome membrane dissolves, and the merozoites are released into circulation, where they invade mature erythrocytes [10]. This marks the beginning of the asexual blood stage replication cycle (schizogony). Within 48 hours, the infected erythrocyte matures from immature trophozoite (ring) to mature trophozoite to schizont stage. In the final step, the schizont ruptures and releases 16–32 merozoites back into the blood stream [10]. A fraction of trophozoites develop into the gametocytes, the sexual stages of the parasite. Gametocytes are ingested by a subsequent blood meal of a mosquito where they shed their erythrocytic membrane. The male microgamete and the female macrogamete fuse to form a zygote, which transforms into an ookinete. The ookinete is mobile and able to traverse the epithelial wall from the mosquito midgut to the haemolymph. The ookinete develops into an oocyst which matures into sporozoites within 7–10 days. The sporozoites migrate to the mosquito's salivary glands where they are available as co-cargo to be injected into another human host with the mosquitos saliva. Modified from *Wikimedia Commons*.

1.2.2 Cytoadhesion and sequestration

The cytoadhesion of mature *P. falciparum*-infected erythrocytes to microvascular endothelial cells represents a critical pathophysiological mechanism underlying the pathogenesis of malaria [29]. The sequestration of mature parasitized erythrocytes in microvascular beds prevents their clearance by the spleen, but simultaneously causes microvascular obstruction, impaired tissue perfusion, and organ dysfunction that characterizes SM [30, 31]. Upon erythrocyte invasion, the parasite extensively remodels the host cell to facilitate binding. The cytoskeleton is stiffened and serves as an anchor for newly formed, knob-like protrusions which enhance cytoadherence under physiological flow and febrile conditions [32, 33]. The knobs' main function is to anchor the major adhesion molecule of the *Pf*EMP1 multigene family on the iEs surface. Other parasite-derived variant surface antigens (VSAs) include the repetitive interspersed families of polypeptides (RIFIN) and subtelomeric open reading frame (STEVOR) protein families [34]. The *P. falciparum* reference genome 3D7 contains 157 *rifin* and 32 *stevors* (PlasmoDB, `Pf3D7_68`, protein coding genes only).

1.2.3 *Pf*EMP1

*Pf*EMP1 is the major facilitator of cytoadhesion and erythrocyte rosetting. Additionally, *Pf*EMP1 is the major inducer of host-protective antibodies. The ability to switch *var* gene expression enables the parasite to evade the adaptive immune response. *Pf*EMP1 is encoded by the *var* multigene family, consisting of 45–60 members per isolate [35, 36]. The genome of the FCR3/IT isolate used for this study contains 56 *var* genes (Fig. A.1) (PlasmoDB, `PfIT_58`, including the non-coding *var1csa*).

1.2.4 Genetics

1.2.4.1 *var* gene expression

A prominent and frequently highlighted feature of the *var* gene family is the mutually exclusive expression of a single *var* gene at a time [37]. Work in recent years has shown

that this process is less strict than previously thought. For instance, populations of parasites have been shown to completely switch off *var* gene expression, as observed in a splenectomized patient by Bachmann and colleagues [38]. Similarly, chronic asymptomatic malaria infections, where the antigenic repertoire is exhausted, are linked to lower *Pf*EMP1 surface expression to evade the anti-*Pf*EMP1 immune response [39].

A single-cell RNA-seq study of the lab strains IT4/FCR3 and 3D7 showed that, at least *in vitro*, a parasite population can consist of three different *var* gene-expressing phenotypes: parasites expressing a single *var* gene, multiple *var* genes, or expressing none to very few *var* genes [40].

Selective *var* transcription is epigenetically controlled and inherited across multiple asexual cell divisions, allowing the parasite to keep the switching rate low and conserve its antigenic repertoire [37, 41]. This epigenetic memory of the *var* expression profile is largely reset after passage through the mosquito to the next human host [42].The genomic loci of silenced *var* genes are held in a condensed state by the heterochromatin mark H3K9me3, which silences upstream promoters. Active *var* genes lie in the euchromatin, which is associated with the permissive histone modifications H3K9ac, H3K4me2, and H3K4me3. In the active state, transcription factors and RNA polymerase II can access the gene and transcribe both mRNA and the antisense long noncoding RNAs (lncRNAs) of the *var* gene. Antisense lncRNAs are thought to play a role in the activation of *var* genes at the transcriptional level by competing with silencing factors [43, 44].

A range of methyltransferases, including PfSET1, PfSET2, PfSET3 and PfSET10, as well as acetyltransferases (PCAF/GCN5-like) have so far been identified as responsible for histone modifications that induce changes in chromatin condensation [39, 45].

1.2.4.2 Structure

All *var* genes consist of two exons and a conserved intron of ~1 kb (Fig. 1.3) [46]. Lavstsen *et al.* further classifies the *var* genes into the major upstream sequence (UPS) groups UPS A, UPS B, UPS C and UPS E and the intermediates UPS A/B UPS B/Cs based on their genomic location and upstream sequence. UPS E consists of only one

member, the across isolates conserved var2CSA (see Appendix A.1) [47]. A-type *var* genes are largely located at telomeric or near-telomeric chromosome regions (Fig: 1.4), with the head being oriented towards the centromere and often have a *rif* or *var* gene oriented in the opposite direction (see Appendix A.2). B-types are similarly located at the chromosome ends but are generally smaller and less complex in their extracellular domain structure. Most of them end on the DBLα-CIDRα-DBLδ-CIDR2 domain structure. Group C consists of centromeric *var* genes that point towards the telomeres (Fig. 1.4) [47].

- **DC4** (DBLα1.4-CIDRα1.6-DBLβ3)
- **DC5** (DBLγ12-DBLδ5-CIDRβ3/4-DBLβ7/9)
- **DC8** (DBLα2-CIDRα1.1-DBLβ12-DBLγ4/6)
- **DC13** (DBLα1.7-CIDRα1.4)

Even though the extracellular domain of *var* genes is highly polymorphic, it is classified in three recurring building blocks: duffy-binding like (DBL), cysteine-rich interdomain region (CIDR) and C2 and the cell membrane distal n-terminal segment (NTS). DBL further clusters to subgroups (α – ε) and CIDR (α, β, γ) [48]. Conserved, recurring clusters of DBL and CIDR domains are called domain cassettes (DCs). The DCs 1, 2 and 3 belong to the only three *var* genes that are highly conserved across all *P. falciparum* isolates, even though the reference strain 3D7 and the strain non-reference IT4 used in this study lack the exon 2 part of the gene.

1.2.4.3 Recombination of *var* genes

High rates of recombination within the *var* gene family are responsible for antigenic diversification during the asexual blood stage. It is estimated that this frequent ectopic recombination can provide millions of opportunities daily within a single infected

	Binding phenotype	*Var* group	Domain position			
			1	**2**	**3**	**4–9**
Regular	Unknown	A	NTSA	DBLα1	CIDR$\delta/\beta/\gamma$	DBLβ, DBLγ, DBLδ, DBLζ, DBLε, CIDR$\delta/\beta/\gamma$
	EPCR	A	NTSA	DBLα1	CIDRα1.4–7	
	EPCR	B	NTSB	DBLα2	CIDRα1.1/8	
	CD36	B & C	NTSB	DBLα0	CIDRα2–6	
Conserved	CSA	E, *var2CSA*	NTSpam	DBLpam1	DBLpam2	CIDRpam, DBLpam3–6
	Unknown	A, *var1-3D7*	NTSA	DBLα1.4	CIDRα1.3	DBLβ1, DBLγ15, DBLε1, DBLγ8, DBLζ1, DBLε5
	Unknown	A, *var1-IT*	NTSA	DBLα1.1	CIDRα1.2	DBLβ11, DBLγ1, DBLε1, DBLγ8, DBLζ2, DBLε5
	Unknown	A, *var3*	NTSA	DBLα1.3	–	DBLε8

Table 1.1: **Overview over common *Pf*EMP1 domain sequences classified by binding phenotype and *var* group as well as 'regular' and conserved *var* genes.** Modified from [49].

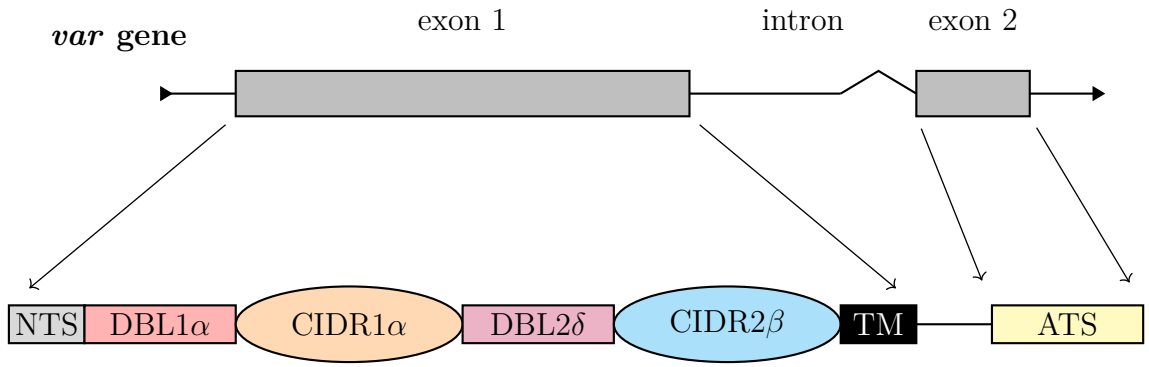


Figure 1.3: **Structure of *var* genes**. Exon 1 codes for the extracellular *Pf*EMP1 domains and the transmembrane domain (TM). The highly conserved exon 2 codes for the cytoplasmic acidic terminal sequence (ATS).

individual to significantly expand the parasite's antigenic repertoire [50]. The parasite's extremely AT-rich genome (80.7 % A/T) increases the frequency of secondary DNA structures such as hairpins and stem-loops, which in turn may induce replication fork stalling, triggering double-strand breaks that are repaired via error-prone pathways such as microhomology-mediated repair [51]. Another motif for secondary DNA structures, the G-quadruplex (G4) DNA motifs, which are made up of multiple guanine tetrads linked by short loops, are for the same reason rare in the *P. falciparum*

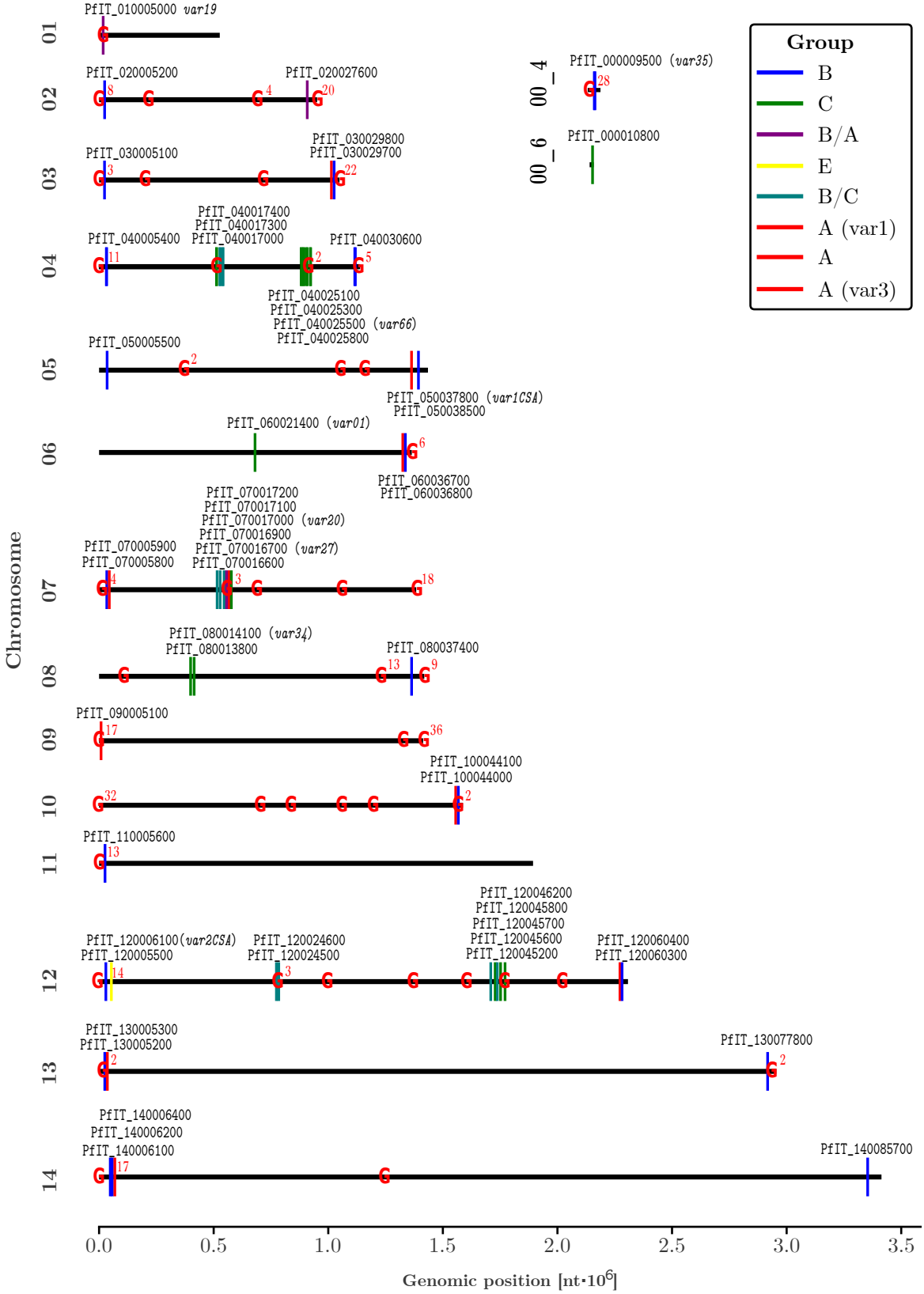


Figure 1.4: **Location of *var* genes and putative quadruplex-forming sequencess on *Pf*IT genome.** `00_4` and `00_6` are genomic fragments of unknown chromosomal association. G: putative quadruplex-forming sequences (PQS). If PQS are closer than 50 kb to each other, number of occurrences is indicated.

genome [52]. Even though G4 motifs are rare in *P. falciparum*, their chromosomal location highly correlates with *var* genes, leading to speculation about their role in transcription and recombination [52, 53]. In the 3D7 clone, 16 out of the 63 putative quadruplex-forming sequences (PQS) are located in 1.6–17 kb upstream of B-type *var* genes and another 15 were found within *var* genes making almost half of non-telomeric PQSs *var* gene related [52]. The same can be observed for FCR3/IT4 which contains 67 non-telomeric PQSs of which 11 are precisely 1.6–1.7 kB upstream of B-type *var* genes (Fig. 1.4 and Tab. A.1). Another 19 PQSs of all *var* types are located in exon 1 of *var* genes. The frequent recombination of *var* genes can benefit the parasite by creating antigenic diversity that evades the immune system, as long as the other roles of *Pf*EMP1, such as cytoadhesion, are conserved. Studies of field isolates confirm that *var* genes are highly divergent between isolates. Only *var1csa*, *var2csa* and *var3* are conserved across isolates [54, 55]. *Var* diversity has long been attributed to meiotic recombination of the gametocytes in the mosquito host [50]. In 2000, Freitas-Junior and colleagues conducted a study that revealed a physical clustering of subtelomeric as well as internal *var* loci of chromosomes at the nuclear periphery during mitosis [50, 56]. This finding explained how homologous recombination (HR) mediated double-strand break (DSB) repair, which requires co-located long homologous sequences that are rare in the mostly heterologous parasite, could come together to recombine to novel *var* genes. The identified mechanism explained the drive in genetic diversity in the *var* gene family, which occurs faster than would be possible through homologous crossover during meiosis alone [56]. A systematic approach on ectopic recombination during asexual replication was performed by Claessens and colleagues, who investigated recombination events in progeny of >200 clones. It was found that *var* genes recombine asexually at a frequency that is comparable to that of single nucleotide polymorphisms (SNPs) [50]. The *var* genes recombined at general regions of high sequence identity between two genes (~80 bp) and especially at perfect homology regions of on average 15 bps. The authors also established that recombination of *var* genes is possible either intragenomically or across chromosomes. However, this process occurs almost exclusively within equal domain classes (e.g. CIDRa with CIDRa, etc.) [50].

1.2.5 Sequestration

Sequestration of *P. falciparum* within the microvasculature of vital organs is a central driver of malaria's adverse pathological effects. This process leads to mechanical obstruction of blood flow, promotes local tissue hypoxia and swelling, and in the case of cerebral malaria (CM) contributes directly to the neurological manifestations and mortality associated with CM. In addition to vascular blockage, accumulation of parasitized cells triggers local inflammation and may disrupt physiological homeostasis, resulting in brain edema, petechial haemorrhages, and increased intracranial pressure. These factors are strongly linked to fatal outcomes. The process of parasite sequestration and cytoadhesion is often compared to leukocyte extravasation [57]. In both cases, circulating blood cells must attach themselves to the endothelial lining of blood vessels while being subjected to shear stress. Importantly, neither process occurs spontaneously under physiological conditions; instead, they rely on a multi-step cascade that dynamically alters the adhesive properties of the endothelium [58, 59]. The most prominent endothelial cell receptors (ECRs) receptors involved in parasite sequestration are CD36, intercellular adhesion molecule 1 (ICAM-1), CSA, and endothelial protein C receptor (EPCR). Their role in cytoadhesion is complex and dependent on the involved endothelial tissue, as well as a range of other host and disease factors [60]. As reviewed by Bachmann and colleagues (2022), observations vary regarding the extent of rolling or static adhesion mediated by ICAM-1 and CD36. However, there is increasing consensus that CD36 predominantly facilitates rolling, whereas ICAM-1 primarily mediates firm, static adhesion [61].

For the *Pf*EMP1–CD36 interaction, the mechanistic basis has been described by the catch-bond model. In this model, whether static or rolling adhesion occurs depends strongly on the local shear rate, since the lifetime of the bond decreases proportionally with the applied pulling force [62, 63]. At very low shear forces, the bond stability is limited. As tensile force increases, bond lifetime paradoxically increases until a maximum stability is reached. Beyond this point, further increases in tensile force reduce bond stability, corresponding to the canonical slip-bond regime (Fig. 1.5).

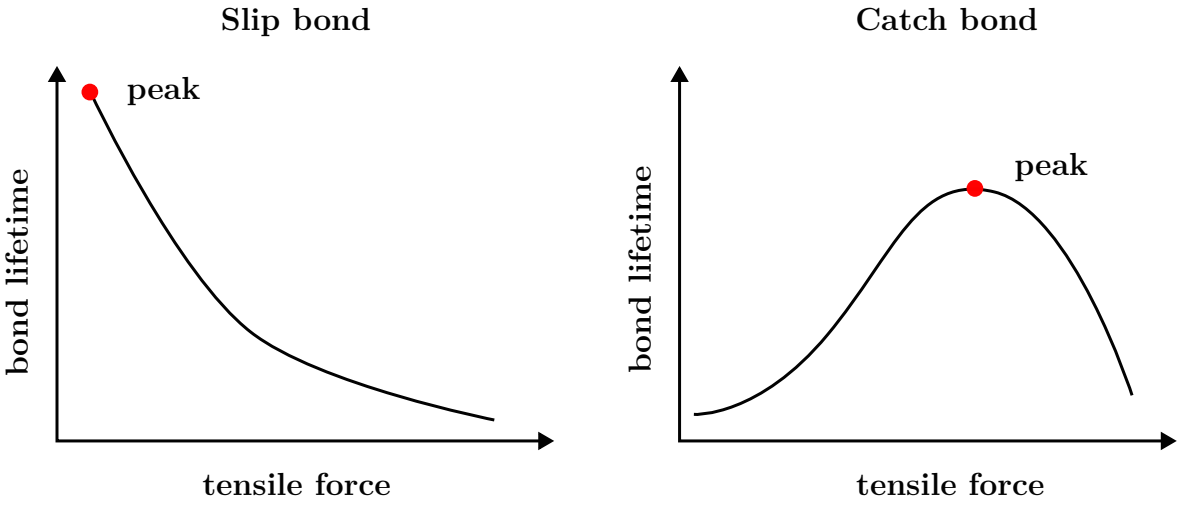


Figure 1.5: **Model of catch- and slip bonds**. Model for the lifetime of the bond in relationship to an applied tensile force. **Left**: Slip bonds experience their maximal lifetime at a minimal force. **Right**: Catch bonds exhibit an optimal stability at a tensile force > 0. After the optimal force, their behaviour resembles slip bonds.

1.2.6 Endothelial cell receptors

1.2.6.1 CD36

The scavenger receptor CD36 is the most common host ligand for *Pf*EMP1. More than 75 % of *var* genes have the CD36 binding domains CIDRα2—6. which is typically found in C- and B-type *var* genes (Tab. 1.1) [61, 64]. In the disease setting, C- and B-type expression, and therefore mostly CD36-binding parasites, are associated with uncomplicated malaria [61, 65]. The multifunctional scavenger protein is expressed in different mammalian cell types, namely platelets, macrophages, monocytes, hepatocytes, epithelial cell, and the microvascular endothelium relevant to malaria disease, where it is preferentially expressed in the heart, muscles, dermis, and lung and absent in the brain and umbilical vein [66–69]. In endothelial cells, CD36 recognizes specific pathogens and mediates the inhibition of growth factor induced angiogenesis and fatty acid uptake [67]. *P. falciparum* iEs make use of this widely available receptor to cytoadhere to the endothelium through the same binding site involved in essential fatty acid uptake. The phenylalanine residue on membrane-distal region of CD36 (F153), which binds a hydrophobic pocket in the CIDRα domains, is also vital for fatty acid recognition [64]. Its interaction with the parasite *Pf*EMP1 proteins tethers iEs to

the microvasculature. However, studies disagree on whether CD36 yields purely firm adhesion or rolling adhesion.

1.2.6.2 ICAM-1

ICAM-1 is a member of the immunoglobulin superfamily and is expressed on various cell types including lymphocytes, adherent macrophages, and at low levels on endothelial cells. Endothelial ICAM-1 expression is, however, significantly upregulated in response to inflammatory cytokines such as tumor necrosis factor alpha (TNFα), interleukin-1 (Il-1) and interferon gamma (IFN-γ), which are abundant during malaria infections [70–72]. The 80–115 kDa surface receptor is heavily glycosylated and consists of five tandem immunoglobulin-like domains, of which the the outermost domain, D1, contains different binding sites for the β2-integrins and lymphocyte function-associated antigen-1 (LFA-1) during leukocyte rolling and transmigration as well as a binding site for rhinoviruses [73]. The binding site for *P. falciparum*-iEs is located in the first two domains, overlapping with, but distinct from, the binding site for LFA-1 [74, 75]. Cytoadhesion to ICAM-1 is mediated by specific DBLβ domains of *Pf*EMP1, which are found in both group A and group B/C *var* gene types [76]. Group A DBLβ subgroups 1 and 3 and DBLβ5 in group B have been shown to mediate ICAM-1 binding [77, 78]. The recently, as part of this work, discovered binding phenotype of the B/A type *var* gene *IT4var19* is suspected to be mediated by DBLβ12, which is structurally highly similar to DBLβ5 [79].

1.2.6.3 TNFR1 (CD120a) and TNFR2 (CD120b)

Tumor necrosis factor receptor (TNFR)1 and TNFR2 are type I transmembrane glycoproteins and the main receptors for the cytokine TNFα, which play distinct roles in activating endothelial cells. TNFR1 is broadly expressed, and its activation is a primary driver of inflammation in endothelial cells, leading to the expression of the adhesion molecules ICAM-1, vascular adhesion molecule 1 (VCAM-1), and E-selectin [80]. In contrast, TNFR2 expression is more restricted, and its signaling is associated with promoting endothelial cell survival, proliferation, and angiogenesis, often coun-

teracting the inflammatory effects of TNFR1 [81]. In *P. falciparum* malaria, secretion of the major TNFR1 and TNFR2 ligands IL-1 and TNFα is upregulated, and plasma concentrations correlate with the severity of the disease [82]. Binding assays of pooled field isolates showed binding of the iEs to human TNFR1 and TNFR2 recombinantely expressed on CHO-745 cells [83].

1.2.6.4 Endothelial protein C receptor

Endothelial protein C receptor (EPCR) is a vital receptor in the anticoagulant protein C pathway. Activated protein C, with protein S acting as a cofactor, inhibits hemostasis by inactivating coagulation factors V and VIII. EPCR is expressed constitutively, albeit at low levels, on the endothelium of all organs, though its expression is decreased in the brain [84]. Moxon and colleagues propose that the low levels of cytoprotective EPCR make the blood vessels of the brain especially vulnerable to disruption by sequestered iEs, impacting the anti-inflammatory and endothelial barrier protective function of the protein C pathway [84]. In the same year, Turner and colleagues discovered that iEs are capable of directly cytoadhering to EPCR through *Pf*EMP1's CIDRα1 domains (See Tab. 1.1) [85]. Additionally, *P. falciparum* parasite populations from patients with SM are enriched in EPCR-binding *Pf*EMP1 variants, further corroborating the role of EPCR in the pathogenesis of SM [86, 87]. A recent cryo-electron microscopy study showed that the hydrophobic EPCR binding site around the two α-helices is covered by the neighboring DBLα domain under physiological conditions and becomes available for binding only after EPCR-induced conformational changes of the two domains [88].

1.2.6.5 Multidrug resistance protein 1

Multidrug resistance protein 1 (MDR1), also known as P-glycoprotein, encodes an ATP-dependent efflux transporter and is highly expressed in the microvasculature of the human brain and the testes [89]. A pool of field isolates showed binding of iEs to MDR1 expressed on CHO-745 cells [83].

1.2.6.6 VCAM-1

The 110 kDa immunoglobulin superfamily protein is inducibly expressed on NF-ϰB/IRF-activated endothelium to facilitate leukocyte adhesion and transendothelial migration by binding to the integrin VLA-4 [90]. VCAM-1 has been shown to bind iEs of laboratory strains under static conditions, as well as some field isolates, via rolling adhesion [91, 92]. However, no correlation with the severity of malaria disease has been identified [29].

1.2.6.7 Chondroitin sulfate

Chondroitin sulfate (CS) chains are unbranched polysaccharides of variable length. They always consist of two alternating monosaccharides, d-glucuronic acid (GlcA) and N-acetyl-d-galactosamine (GalNAc), which may vary by different sulfation patterns of C-4 and C-6 of GalNAc and the C-2 position of GlcA. CSA is defined as chains consisting of mostly C-4 sulfation on GalNAc [93, 94]. CSPGs of the placenta have long been identified as the preferred receptor for cytoadhesion of infected erythrocytes in PAM [14, 95]. The binding affinity of the iEs is thereby dependent on the amount, and probably the pattern, of sulfation of the CSA variant (C-4) of the polysaccharide [93, 94]. The organ-specific variants of CS chains on CSPGs define the distinct cytoadhesion of iEs to the placenta, even though CS is expressed on almost all mammalian cells [94]. The CHO-745 mutant lacks the xylosyltransferase necessary for CS biosynthesis and therefore is often used in iE adhesion assays recombinantly expressing other human ECRs without CS interference [96]. The parasite-derived ligand that facilitates this binding is VAR2CSA, a unique and conserved member of the *Pf*EMP1 family [97]. Multiple VAR2CSA domains show binding affinity with the strongest being the tandem DBL1X—DBL2X, but DBL3X and DBL6ε also show weak binding affinity. The strongest CSA adhesion is displayed by full-length var2csa [98].

1.2.6.8 CD55

CD55 (decay-accelerating factor) regulates the complement system and is present on the surface of a wide range of cells in the blood vessels, including erythrocytes, vascular endothelial cells as well as cells of the adaptive and innate immune system [99]. On uninfected erythrocytes (uEs), CD55 functions as a host factor required for the merozoite attachment to uEs prior to subsequent cell invasion [100].

1.2.6.9 Tetraspanins CD9, CD37, CD81 and CD151

CD9, CD37, CD81 and CD151 are members of the tetraspanin protein family, which play a key roles in influencing cell fusion, adhesion, and motility. They interact with a wide variety of other proteins forming tetraspanin-enriched microdomains [101]. On activated endothelial cells, CD9, CD81 and CD151 contribute to the recruitment of the adhesion molecules ICAM-1 and VCAM-1 for leukocyte extravasation by supporting the formation of adhesive clusters [102–104]. CD37 is only found on immune cells, where it regulates T cell and B cell interactions. CD37 is not present on endothelial cells [105]. CD9 was identified as binding partners for pooled parasite isolates from Gambian patients [83].

2 Materials and Methods

2.1 Material

2.1.0.1 Organisms

Organism	Strain \Clone	Origin
Plasmodium falciparum	IT4\FCR3S1.2	[106]; [107]
Cricetulus griseus	CHO-K1	[108]
Cricetulus griseus	CHO-pgsA-745	[96]

2.1.0.2 Transgenic organisms

Name	Clone\Isolate	Vector
IT4-SLI-var01 IT4-SLI-var02 IT4-SLI-var03 IT4-SLI-var04 IT4-SLI-var16 IT4-SLI-var19 IT4-SLI-var20 IT4-SLI-var66	FCR3S1.2\IT4 Integrated with pSLI-varX-3xHA plasmid	[79, 109]
CHO-GFP CHO-ICAM1 CHO-CD36 CHO-ICAM1 CHO-TNFR1 CHO-TNFR2 CHO-VCAM CHO-MDR1 CHO-CD37 CHO-CD55 CHO-CD81	CHO-pgsA-745 with pAc-GFP1-N1 vector with respective human ECRs	Lisa Roth; [110]
CHO-CD9 CHO-CD151	CHO-pgsA-745 with pEGFP-N1 vector with with respective human ECRs	Lisa Roth; [110]

2.1.0.3 Software

Name	Version	Source
Anaconda	23.10.0	https://www.anaconda.com
bioinfokit	v2.0.9	[111]
CellProfiler	4.2.6	[112]
DESeq2	1.42.0	[113]
FastQC	0.12.1	[114]
featureCounts	2.0.4	[115]
Fiji	1.54p	https://imagej.net/software/fiji
gffutils	0.13	https://daler.github.io/gffutils
HISAT2	2.2.1	[116]
INKSCAPE	1.4.2	https://inkscape.org/
Ibidi Pump Control	–	Ibidi, Martinsried, Germany
iDEP	2.01	[117]
Ilastik	1.4.0.b21	[118]
matplotlib	3.9.3	https://matplotlib.org
Prism 10	10.4.1	GraphPad Software, LLC
Python	3.11	http://www.python.org
QGRS mapper	–	[119]
R	4.5.0	[120]
samtools	1.22.1	[121]
seaborn	0.13.2	[122]
SPAdes	4.0.0	[123]
Spyder IDE	6.0.1	www.spyder-ide.org
trackdem	0.7.2	[124]

2.1.1 Consumables

Table 2.1: Consumables

Name	Distributor
1.5/2 mL Safe-Lock reaction tubes	Eppendorf, Hamburg
24-well-tissue culture plate	Sarstedt, Nümbrecht
96-well-tissue culture plate	Thermo Scientific, Waltham, USA
Cell culture flask T25	Thermo Scientific, Waltham, USA
Cell culture flask T75	Thermo Scientific, Waltham, USA
Cell strainer, 70 µm	Sarstedt, Nümbrecht
CellTrics 30 µm	Sysmex Partec, Görlitz
Conical centrifuge tubes (15 mL)	Falcon, Schwerte
Conical centrifuge tubes (50 mL)	Falcon, Schwerte
Coverslips (Plastic, 13 mm)	Sarstedt, Nümbrecht
Cryovials	Sarstedt, Nümbrecht
EVE cell counting slide	NanoEntek, Seoul, Korea
Filter paper	Machery-Nagel, Hoerdt Cedex, France
Glass Slide	Engelbrecht, Edermünde
Low Protein Binding Microcentrifuge Tubes (1.5 mL)	Thermo Scientific, Waltham, USA
Microplate, 96 well, PS, F-bottom	Greiner Bio-One, Kremsmünster, Austria
Millipore Stericup Sterile Vacuum Filter (0.22 mm)	Merck, Darmstadt
Parafilm	GE Healthcare, Chicago, USA
Petri dish (5/10 mL)	Sarstedt, Nümbrecht
Pipette tips, filter (10/20/200/1000 µL)	Sarstedt, Nümbrecht
Serological pipettes (5/10/25 mL)	Sarstedt, Nümbrecht
Stericup Milipore vacuum filter (0.45 µM)	Merck, Darmstadt
Syringe 20 mL	B.Braun, Dresden
Syringe filter, Filtropur S 0.2 mm	Sarstedt, Nümbrecht

2.1.1.1 Instruments

Name	Type	Manufacturer
RNA gel electrophoresis	4150 TapeStation	Agilent Technologies, Santa Clara, USA
Automatic cell counter	Countess II FL	Thermo Scientific, Waltham, USA
Bioanalyser	Agilent 2100	Agilent Technologies
Cell counting chamber	Neubauer	Marienfeld Superior, Marienfeld
Cell freezing container	Mr. Frosty	Thermo Scientific, Waltham, USA
Centrifuge	5415 D	Eppendorf, Hamburg
Centrifuge	5427 R	Eppendorf, Hamburg
Centrifuge	Megafuge 1.0	Thermo Scientific, Waltham, USA
CO_2 Incubator	Function Line	Heraeus Instruments, Hanau
Electronic microscope	EVOS XL	Thermo Scientific, Waltham, USA
Electronic pipette	Pipetboy acu 2	INTEGRA Biosciences, Biebertal
Fluorescence microscope	Axioscope M1, M2	Zeiss, Jena
Freezer (-80°C)	FORMA 700	Thermo Scientific, Waltham, USA
Agarose gel chamber	Horizon 11.14	Gibco, Life Technologies, USA
Ibidi Pump System	System-10902	Ibidi, Martinsried
Inverted microscope	Axioscope M1	Zeiss, Oberkochen
Microscope	CX31	Olympus, Hamburg
PCR cycler	Peqstar	Peqlab, Erlangen
Perfusion tubing sets	Yellow and green	Ibidi, Martinsried
pH-Meter	CG840	Sartorius AG, Göttingen
Photometer	NanaDrop 2000	Thermo Scientific, Waltham, USA
Power supply	EPS 301	Amersham pharmacia biotech, Sweden
Pipettes	2/20/200/1000 µL	Gilson
Scale	SPO 51	Scaltec, Hollywood, USA
Scale	BP210S	Sartorius, Göttigen
Sequencer	NextSeq 550	Illumina, USA
Sterile workbench	Class II BSC	ESCO Labculture, Friedberg
Thermomixer compact	5355R	Eppendorf, Deutschland
Vortex	Genie 2	Scientific Industries, USA
Water bath	SW20	Julabo, Seelbach

2.1.1.2 Chemicals

Name	Distributor
Accutase	PAN Biotech, Aidenbach
Acetic acid	Roth, Karlsruhe
Aceton	Roth, Karlsruhe
Albumax II	Life Technologies, Carlsbad, USA
Ampicillin	Roche, Mannheim
Biocoll	Biochrom, Berlin
D-Glucose	Sigma, Missouri, USA
D-Sorbitol	Sigma, Missouri, USA
Dako Fluorescence Mounting	Dako, Waldbronn
di-Sodium hydrogen phosphate	Roth, Karlsruhe
DMSO-Dimethylsulfoxid 250 mL	Roth, Karlsruhe
Ethanol	Merck, Darmstadt
Ethylenediaminetetraacetic acid (EDTA)	Biomol, Hamburg
G418 disulfate salt	Sigma, Missouri, USA
Gas (1 % O_2, 5 % CO_2, 94 % N_2)	Air liquide, Düsseldorf
Gelatin (175 g Bloom, Type A)	Sigma, Missouri, USA
Gentamicin	Ratiopharm, Ulm
Giemsa solution	Merck, Darmstadt
Glutaraldehyde (25%)	Merck, Darmstadt
Glycerol	Merck, Darmstadt
Hoechst33342	Chemodex, St. Gallen, Switzerland
Human blood (0+)	UKE, Hamburg
Hypoxanthine	Sigma, Missouri, USA
Hydrochloric acid Immersion oil 518N	Zeiss, Oberkochen
Leica CV Mount	Leica Biosystems, Wetzlar
Methanol	Roth, Karlsruhe
Penicillin/Streptomycin	Life Technologies, Carlsbad, USA
Potassium chloride	Merck, Darmstadt
Potassium dihydrogen phosphate	Merck, Darmstadt
RNase away	Roth, Karlsruhe
Sodium bicarbonate	Sigma, Missouri, USA
Sodium chloride	Roth, Karlsruhe
Sodium dihydrogen phosphate	Roth, Karlsruhe
Sodium hydroxide	Roth, Karlsruhe
Tris base	Roth, Karlsruhe
Trizol	Life Technologies, Carlsbad, USA
Zeocin	InvivoGen, San Diego, USA

2.1.2 Biologicals

Table 2.2: Amino acid sequence of *Pf*EMP1 antagonistic peptides derived from CD36 (left) and ICAM-1 (right). Peptides kindly synthesized by Dr. Niels Röckendorf.

CD36	
Name	**Amino acid sequence**
Peptide 1	FTVLNLAVAAASHIYQNQFV
Peptide 2	VLNLAVAAASHIYQNQFVQM
Peptide 3	NLAVAAASHIYQNQFVQMIL
Peptide 4	AVAAASHIYQNQFVQMILNS
Peptide 5	AAASHIYQNQFVQMILNSLI
Peptide 6	ASHIYQNQFVQMILNSLINK
Peptide 7	HIYQNQFVQMILNSLINKSK
Peptide 8	YQNQFVQMILNSLINKSKSS
Peptide 9	NQFVQMILNSLINKSKSSMF
Peptide 10	FVQMILNSLINKSKSSMFQV

ICAM-1	
Name	**Amino acid sequence**
Peptide 1	GNAQTSVSPSKVILPRGGSV
Peptide 2	TSVSPSKVILPRGGSVLVTC
Peptide 3	PSKVILPRGGSVLVTCSTSC
Peptide 4	ILPRGGSVLVTCSTSCDQPK
Peptide 5	GGSVLVTCSTSCDQPKLLGI
Peptide 6	LVTCSTSCDQPKLLGIETPL
Peptide 7	STSCDQPKLLGIETPLPKKE
Peptide 8	DQPKLLGIETPLPKKELLLP
Peptide 9	LLGIETPLPKKELLLPGNNR
Peptide 10	ETPLPKKELLLPGNNRKVYE

Table 2.3: Primary antibodies

Antigen	**Organism**	**Fluorophore**	**Manufacturer**
CD120a/TNFR1	mouse	PE	BioLegend
CD120b/TNFR2	mouse	APC	BioLegend
CD151	mouse	APC	BioLegend
CD36	mouse	APC	BioLegend
CD37	mouse	APC	ThermoFisher
CD55	mouse	APC	BioLegend
CD81	mouse	APC	BioLegend
CD9	mouse	PE	BioLegend
EPCR	mouse	APC	BioLegend
HA	rat	–	Roche Diagnostics
ICAM-1	mouse	APC	BioLegend
KAHRP	rabbit	–	RG Spielmann, BNITM
MDR1	mouse	APC	ThermoFisher
VCAM-1	mouse	APC	BioLegend

Table 2.4: Secondary antibodies

Antigen	**Organism**	**Fluorophore**	**Source**
anti-Rabbit	goat	Alexa Fluor™ 488	ThermoFisher, A11008
anti-Rat	donkey	Alexa Fluor™ 594	ThermoFisher, A21209

2.1.2.1 Plasmids

pSLI-plasmid [125] was kindly provided by Tobias Spielmann.

Table 2.5: **List of primers for selection linked integration.** Primers ordered from Eurofins GmBH, recognition sequence for restriction enzyme, homology region

Name	Direction	Sequence ($5' \mapsto 3'$)
var11_HR_FWD	forward	GCTATTTAGGTGACACTATAGAATACTCAAGCTGCGGCCGCTAA GTTCCTGGTAGTCCTAAATATAAAAC
var11_HR_REV	rev	GCGTAATCTGGAACATCGTATGGGTACATGGTGGTACCTATATC CCACACATCTGCTATAGGATATTTC
var14_HR_FWD	forward	GCTATTTAGGTGACACTATAGAATACTCAAGCTGCGGCCGCTAA ATGATATATATGCACCACGTGCTC
var14_HR_REV	rev	GCGTAATCTGGAACATCGTATGGGTACATGGTGGTACCTATATC CCACACATCCGCTATAGG
var31_HR_FWD	forward	GCTATTTAGGTGACACTATAGAATACTCAAGCTGCGGCCGCTAA GATAGAAGTAGTACTTGAACCTAG
var31_HR_REV	rev	GCGTAATCTGGAACATCGTATGGGTACATGGTGGTACCTATATC CCATACATCTGCTATAG
var59_HR_FWD	forward	GCTATTTAGGTGACACTATAGAATACTCAAGCTGCGGCCGCTAA CAAATGATTATACAAGTGGAAATAGTTC
var59_HR_REV	rev	GCGTAATCTGGAACATCGTATGGGTACATGGTGGTACCGATATT CCATATATCTGATATAGGATATTCC

Table 2.6: **List of primers for genotyping.** All primers ordered from Eurofins GmBH except 5_FWD from SigmaAldrich. GAGA added for better synthesis.

Name	Cluster	Location	Direction	Sequence ($5' \mapsto 3'$)
3_FWD	1	*var20*	forward	GAGATGCTGCAGCGTCATTGTAG
4_REV	1	*var27*	reverse	GAGAGGTGATGGGTCACAACAAGC
5_REV	2	*var20*	forward	GAGAGGGTGCCAGGAACAAACAC
4_FWD	2	*var27*	reverse	GAGATTTTGGGGATGTTCTGGGTTG
5_FWD	3	*var20*	forward	GTTACATCCCACGGTCCTCC
1_REV	3	*var27*	reverse	GAGAGGTAGAAGTGCGTTGAGAGGTG
3_REV	3	*var20*	reverse	GAGAAACTCAAGCGACGGTCTATACG
2_FWD	3	*var27*	forward	GAGAGGCGTGATAAGCCACTAGGAG

2.1.3 Media and Solutions

2.1.3.1 10 % Giemsa stain

Name	**Quantity**
Giemsa's azure, eosin methylene blue solutionl	10 mL
dH_2O	90 mL

→ Prepare fresh after 2 days.

2.1.3.2 10x CHO-PBS

Name	Concentration
NaCl	1.37 M
KCl	27 mM
Na_2HPO_4	101 mM
KH_2PO_4	18 mM
dH_2O	–

→ Adjust ph = 7.4, autoclave, store at room temperature (RT). Dilute 1:10 with dH_2O and autoclave again for 1x CHO-PBS.

2.1.3.3 10x PBS

Name	Concentration
NaCl	1.37 M
KCl	29 mM
Na_2PO_4	81 mM
KH_2PO_4	15 mM
dH_2O	–

→ Adjust pH = 7.4, autoclave, store at RT. Dilute 1:10 with dH_2O and autoclave again for 1x PBS.

2.1.3.4 Parasite growth medium

Name	**Quantity**
RPMI 1640	1.587 % (w/v)
$NaHCO_3$	12 mM
Glucose	6 mM
Albumax II	0.5 % (v/v)
Hypoxanthine	0.2 mM
Gentamycin	0.4 mM
dH_2O	–

→ Adjust pH = 7.2, sterile filter, store at 4°C. Complete medium was kindly provided by RG Spielmann.

2.1.3.5 Binding medium (BM)

Name	Quantity
RPMI 1640	16.4 g/L
Glucose (water free)	20 g/L
dH_2O	–

→ Adjust pH = 7.2, sterile filter, store at 4°C.

2.1.3.6 Hoechst 33342 stock solution (10x)

Name	Quantity
Hoechst333442	4.5 mg
DMSO	1 mL

→ Dilute 1:10 in DMSO for 1x working solution, store at -20°C.

2.1.3.7 RPMI without serum

Name	Quantity
RPMI 1640	16.4 g/L
Hypoxanthine	5 mg/L
Gentamycin	250 µL/L
$NaHCO_3$ (7,5 %)	30 mL/L
dH_2O	–

→ Adjust pH = 7.2, sterile filter, store at 4°C.

2.1.3.8 Gelatine for knob enrichment

Name	Quantity
Gelatine (175 bloom)	1 g
RPMI without serum	100 mL

→ Solubilize at 37°C, sterile filter, store at 4°C.

2.1.3.9 Malaria Thawing Solution (MTS)

Name	Quantity
NaCl	3.5 g
dH_2O	100 mL

→ Sterile filter, store at 4°C

2.1.3.10 Malaria Freezing Solution (MFS)

Name	Quantity
D-Sorbitol	3 g
NaCl	0.65 g
Glycerol	28 mL
dH_2O	72 mL

→ Sterile filter, store at 4°C

2.1.3.11 HBEC-5i growth medium

Name	Quantity
DMEM/F-12	500 mL
Fetale bovine serum	50 mL
Endothelium Cell Growth Supplement	15 mg
Penicillin/Streptomycin (100x)	5 mL

→ Store at -4°C.

2.1.3.12 CHO growth medium

Name	Quantity
Ham's F12 with L-Glutamin and 25 mM HEPES	500 mL
Fetale bovine serum	50 mL
Penicillin/Streptomycin (100x)	5 mL

→ Store at -4°C.

2.1.3.13 CHO freezing solution

Name	Quantity
Complete CHO growth medium	90 mL
DMSO	10 mL

→ Store at -4°C.

2.1.3.14 TAE Buffer (50x)

Name	Concentration
Tris base	2 M
Acetic acid	1 M
EDTA	50 mM
dH_2O	–

→ Adjust pH = 8.5, store at room temperature. Dilute 1:100 in dH_2O before use.

2.1.3.15 G418 stock solution

Name	Concentration
G418 disulfate salt e	50 mg/mL
dH_2O	–

→ Sterile filter, store at -20°C.

2.1.3.16 Glutaraldehyde fixing solution (1%)

Name	Quantity
25 % Glutaraldehyde solution	20 µL/well
1x PBS	480 µL/well

→ Prepare fresh before use.

2.1.3.17 Synchronization solution

Name	Quantity
Sorbitol	5 g
dH_2O	100 mL

→ Sterile filter, store at 4°C

2.1.3.18 WR99210 stock solution

Name	Quantity
WR99210	20 mM
DMSO	1 mL

→ Sterile filter, dilute 1:1000 for working solution. Store at -20°C. WR99210 stocks were kindly provided by RG Spielmann.

2.2 Methods

2.2.1 Mammalian cell culture

2.2.1.1 CHO-cell culture

Chinese hamster ovary (CHO) cells were cultured either in T25 or T75 culture flasks in 5 or 15 mL of CHO growth medium respectively. For cells transfected with pAc-GFP1-N1 or pEGFP-N1 vector (see Tab. 2.1.0.2), 1 mg/mL of G418 was added. CHO-K1-EPCR cells were cultured with 0.5 mg/mL of Zeocin. Cells were kept at a confluence of 20–90 % at 37°C in an atmosphere of 5 % CO_2. For subcultureing or experiments, cells where washed 1–2x in the flask with 5 mL of phosphate-buffered saline (PBS) and treated with 0.5 mL of Accutase® for a T25 or 1.5 mL for a T75 flask at 37°C until the majority of cells were detached (2–5 min). Loose cells were detached by gently knocking the flask on a hard surface. Subsequently, 5 mL was added to the flasks to block the digest. At the end, the whole suspension was transferred to a 5-mL falcon for further use.

2.2.1.2 Thawing of CHO-cells

The frozen cryovials were thawed in a water bath at 37°C for approx. 1 minute and afterwards transferred into 5 mL of pre-warmed CHO growth medium. The cells were subsequently pelleted at 300 g for 2 minutes, resuspended in 5 mL of growth medium with the respective selection marker and transferred to a T25 flask.

2.2.1.3 Freezing of CHO-cells

Cells from a T25 or T75 flask were detached as described in 2.2.1.1 and pelleted at 300 g for 2 minutes. The cell pellet was resuspended in 4 mL (8 mL) of CHO freezing solution and aliquoted 1 mL each into cryotubes, and transferred to a freezer at -80°C in a Mr. Frosty cell freezing container. The next day, the cells were transferred to liquid nitrogen for long term storage.

2.2.1.4 Fluorescence-Activated Cell Sorting (FACS) of transgenic CHO cells

To enrich for a pure population of CHO cells expressing a high density of a specific human receptor on the cell surface, cells were sorted using a BD FACS Aria III cell sorter. CHO cells were detached as described in 2.2.1.1 and washed first with 3 mL of complete CHO growth medium to inactivate residual Accustase and subsequently with cold, serum-free Ham's F12 medium. All centrifugation steps were carried out at 4°C at 300 g for 5 minutes. After discarding the supernatant, the pellet was resuspended in 1 mL of cold, serum-free Ham's F12 medium. CHO cells were stained by addition of 2 µL of either an allophycocyanin (APC) or Phycoerythrin (PE)-conjugated primary antibody specific to the human receptor of interest and were kept for 60 minutes on ice and protected from light. Afterwards, cells were washed twice with 3 mL of cold, serum-free Ham's F12 medium. After the final wash, the cell pellet was resuspended in 500 µL of serum-free Ham's F12. To ensure a single-cell suspension and prevent clogging of the cell sorter, the suspension was passed through a 30 µm cell strainer into a fresh FACS tube. Samples were kept on ice until sorting. Cell sorting was performed based on a double-positive fluorescence signal. The green fluorescent protein (GFP) signal, indicating successful transfection, as well as the stained surface receptor-specific signal from either PE or APC fluorophores (Tab. 2.3), was detected using the appropriate laser excitation and emission filters. The exception was CHO-K1-EPCR, which was sorted only for APC-antiEPCR signal, since the respective vector of this cell line does not express GFP. The sorted cells were collected into 15 mL conical tubes pre-filled with 3 mL of complete CHO growth medium containing the respective selection marker. The collected cells were pelleted, washed twice, and resuspended in complete growth medium and transferred to a new culture flask. Freshly sorted cells were expanded in the following week and cryopreserved as described before.

2.2.2 *Plasmodium* culture

Plasmodium culture was carried out as first established by Trager & Jensen in petri dishes with nocs, ø60 mm and ø90 mm with growth media volume of 5 and 10 mL respectively [126]. Hematocrit of human erythrocytes (O+) was kept between 2.5–5 %. Dishes were incubated in airtight boxes with atmosphere of 5 % CO_2, 1 % O_2, and 94 % N_2 at 37 °C. Parasitaemia was kept below 10 % and the medium was changed accordingly every 0.5–3 days. For selection linked integration (SLI)-integrant cell lines, 400 µg/mL G418 or 4 nM WR99210 for the SLI-transfectants.

2.2.2.1 Thin film blood smear

For thin film blood smears, ~1 µL of blood was aspirated from across the bottom of the petri dish and put on the end of a microscope slide. A second slide was angled at 30 ° to it and slid to the drop. Once the drop was dispersed along the seam, the top slide is pushed along the bottom slide until the whole drop is dispersed. The smear was then fully air-dried, fixed in 100 % methanol for 30 s and subsequently stained in 10 % Giemsa's solution for 5–10 minutes. Then the smear was rinsed under tap water, air-dried and inspected at 100x magnification via light microscopy.

2.2.2.2 Freezing of *P. falciparum* infected erythrocytes

The parasites culture was pelleted at 700 g. One milliliter of malaria freezing solution was added dropwise per freezing and transferred into a 1.5 mL cryovial. The vials were transferred promptly to the -80°C freezer for short-term storage. For long-term storage, the vials were transferred from the -80°C freezer to liquid nitrogen.

2.2.2.3 Thawing of *P. falciparum* infected erythrocytes

The 1.5 mL cryovials containing the parasite freezings were thawed for 2 minutes at 37°C in a water bath. The cell suspension was then transferred to a 15 mL centrifuge tube, to which an equal volume of pre-warmed malaria thawing solution (MTS) was added. Following subsequent centrifugation at 300 g, the supernatant was discarded

and the sediment washed twice with 3 mL of MTS. Finally, the pellet was resuspended in 5 mL of RPMI growth medium and cultured under standard conditions.

2.2.2.4 Gelatin floatation

Gelatine floatation was performed as described by [127]. In short, knob-forming parasites (K^+) in the trophozoites and schizont stages float in 0.7 % gelatine whilst knobless trophozoite iEs (K^-), ring-stage iE (K^+ and K^-) and uE, sediment on the bottom. This was done by diluting the *Plasmodium* culture pellet in an equal amount of RPMI medium and carefully mixing it 4x the pellet amount of 1 % gelatine in RPMI in a 15-mL falcon. The suspensions was then allowed to sediment for 20–30 minutes at 37 °C. Then the top layer with suspended iEs was transferred into a new falcon, centrifuged at 700 g and washed with 5 mL of growth medium. Parasitaemia and blood stage were determined by Giemsa smear (2.2.2.1).

2.2.2.5 Sorbitol synchronisation

Sorbitol synchronization was carried out to select for ring-stage parasites as described in [128]. Parasite culture was pelleted at 700 g and 5x of pellet volume aqueous D-sorbitol was added (5 %, 0.274 M). The suspension was then incubated at 37°C for 15–20 minutes whilst being shaken every 5 min. Afterwards the suspension was pelleted at 700 g, the supernatant discarded and the pellet washed twice in 5 mL of RPMI growth medium. Successful synchronization was determined by blood smear (2.2.2.1).

2.2.3 Preparation of peptide stocks and working solution

Lyophilized CD36 and ICAM-1 derived peptides were dissolved in 100 % dimethyl sulfoxide (DMSO) to prepare stock solutions at a concentration of 10 mM. Stocks were stored at −80 °C. On the day of the assay, 500 µL subdilutions with a peptide concentration of 200 µM in 2 % DMSO were prepared, by adding 10 µL of the 10 mM peptide stocks to 490 µL of binding media (BM). The peptide working solutions were thawed and mixed with 500 µL 4×10^6 knob-enriched iEs. The resulting 1 mL was used

for two wells à 500 µL as technical replicates in the static binding experiments. The final concentration amounted to $1 \times 10^6 \frac{iEs}{well}$ with peptide concentration of 100 µM. The sequences of the newly synthesized antagonistic peptides are listed in Table 2.2.

2.2.4 Limited dilution and plaque assay

A limited dilution was carried out to isolate single clones of parasite cultures, as described in [129]. This meant that parasites were set to 1 % (1 % parasitaemia at 0.75 % hematocrit). From there on a 1 : 10 dilution series was carried out until a final concentration of $1 \times 10^{-8} \frac{iE}{uE}$. Hematocrit was kept at 0.75 % by addition of blood in each step. 200 µL of each dilution, starting at $1 \times 10^{-3} \frac{iE}{uE}$ until $1 \times 10^{-8} \frac{iE}{uE}$ was added in 10 replicates each to a flat-bottomed 96-well microplates and incubated undisturbed for 12 days at 37 ℃and 4 % CO_2, 1 % H_2O and 94 % N_2.

2.2.5 Static binding assay

CHO cells were seeded at a concentration of $1 \times 10^5 \frac{cells}{mL}$ ($0.5 \times 10^5 \frac{cells}{ml}$) two (three) days before the assay in 24-well plates with plastic coverslips under standard CHO culture conditions. On the day of the assay, the confluence of seeded CHO cells was verified under an inverted microscope to ensure a minimum confluence of 90 %. Parasite cultures at the trophozoite stage with an initial parasitemia of at least 5 % were selected and subjected to knob enrichment as described in 2.2.2.4. Following knob enrichment, the parasite pellet was resuspended in 2 mL of BM. Prior to resuspension, a smear from the parasite culture was prepared to determine the parasitemia, ideally exceeding 60 %. The total erythrocyte concentration was determined using a Neubauer counting chamber after preparing a 1:100 dilution. The iE concentration was calculated by multiplying the total erythrocyte count from the Neubauer chamber with the parasitemia and the suspension was diluted with BM to a concentration of $2 \times 10^6 \frac{iEs}{ml}$. The medium from each well of a 24-well plate containing CHO cells was aspirated and replaced with 0.5 mL binding medium. The plate was incubated at 37°C for 30 minutes to equilibrate. Subsequently, the binding medium was aspirated, and

500 µL of iE suspension (1×10^6 $\frac{iEs}{ml}$) were added. For antagonistic peptide inhibition assays, iE-peptide solutions were prepared as described in section: 2.2.3. The plate was incubated at 37°C with 5 % CO_2 for 75 minutes, with gentle agitation performed every 15 minutes to ensure even distribution and optimal binding.

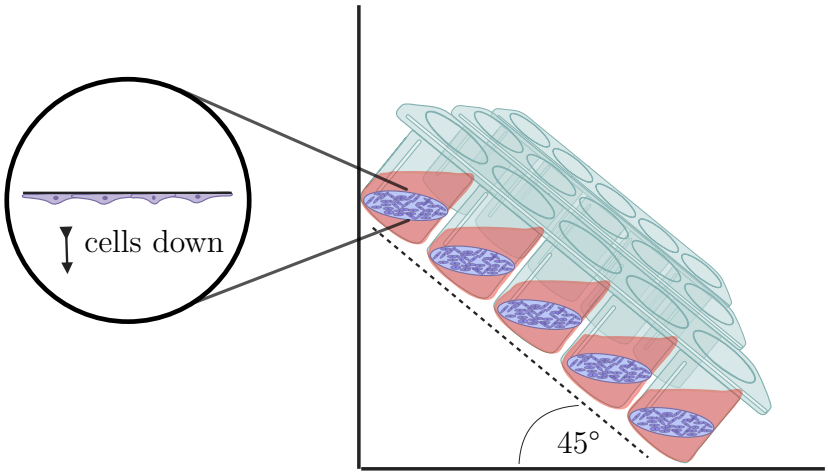


Figure 2.1: **Setup to remove unbound erythrocytes by gravity of after binding assay** 24-well plate is angled at 45°. Coverslips with bound and unbound erythrocytes are placed cells face-down, parallel to the table.

Afterwards, unbound erythrocytes were washed away by dipping the coverslip twice into a beaker of BM, blotting off excess medium on tissue each time. The coverslips were then placed face down on an angled 24-well plate filled with 500 µL of BM (Fig. 2.1) to allow unbound erythrocytes to fall off for 30 minutes. The coverslips were then transferred to a new 24-well plate to be fixed in 500 µL of 1 % glutaraldehyde in Dulbecco's Phosphate-Buffered Saline (DPBS) for 30 minutes at RT. This was followed by staining them for 3 minutes in 10 % Giemsa solution. Subsequently, the coverslips were washed by submerging them in water, air-dried and finally glued face down with a drop of Leica CV Mount on microscope slides. 10–15 pictures were taken per coverslip using the EVOS XL microscope. Images were analysed with a custom build pipeline based on Cronshagen with image segmentation by Ilastik, followed by object identification with CellProfiler. Differences include the preprocessing of the images, the classification in multiple classes by Ilastik as well as the visualization of identified iEs in the

original image. The full, modified, pipeline is described in Figure 2.2 Cronshagen. The number of iEs/picture was converted the iEs/mm^2 with the correction factor 6.173. To quantify the effect of the antimalarial peptides on cytoadhesion, all measurements where normalized relative the positive control (PC), which was determined to be 100 % cytoadhesion and the negative control (NC) with 0 % cytoadhesion. For the test of the CD36-peptide library, Peptide 10 of ICAM-1 was used for the PC as unspecific peptide and vice versa. CHO-GFP cells without human endothelial receptor were used as NC. Normalization was performed separately for each assay according to equation 2.1.

$$z_i = \frac{n_i - \bar{n}_{NC}}{(\bar{n}_{PC} - \bar{n}_{NC})} \cdot 100\,\% \qquad (2.1)$$

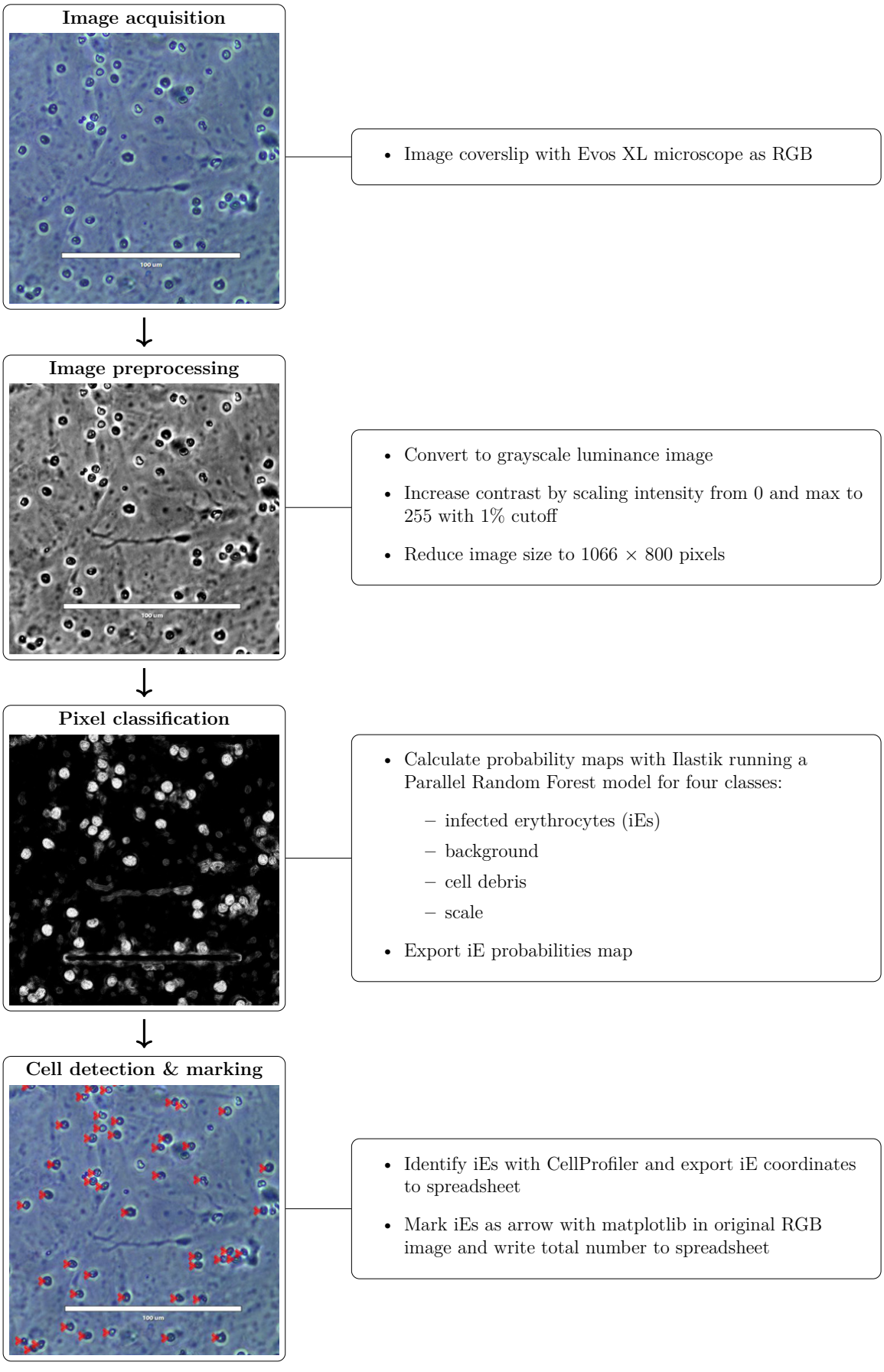
$z_i = \text{i}^{\text{th}}$ normalized measurement [%]

$n_i = \text{i}^{\text{th}}$ measurement $\left[\frac{\text{iEs}}{\text{mm}^2}\right]$

$\bar{n}_{NC} =$ average iEs negative control $\left[\frac{\text{iEs}}{\text{mm}^2}\right]$

$\bar{n}_{PC} =$ average iEs positive control $\left[\frac{\text{iEs}}{\text{mm}^2}\right]$

Figure 2.2: **Bound erythrocyte quantification pipeline**. Automated sequences to batch analyse images of static binding assay slides.



2.2.5.1 MTT viability assay

Two days before the assay, CHO-ICAM1 and CHO-CD36 cells were seeded in flat-bottom 96-well plates at $1 \times 10^3 \frac{\text{cells}}{\text{well}}$ in 100 µL CHO growth medium containing G418 (8 µL/mL) and incubated overnight at 37°C, 5 % CO_2. In the morning of the following day, fresh CHO growth medium was added and peptides aliquots were prepared by a two-step dilution (1:25, then 1:20) to yield 20 µM peptide in BM with 0.2 % DMSO. In the afternoon, the media were exchanged for peptide-containing medium or controls. The positive control contained of BM with 0.2 % DMSO and the cytotoxic NC with 50 % DMSO, keeping a final volume of 100 µL per well. After 24 hours of exposure, 15 µl of (3-(4,5-Dimethylthiazol-2-yl)-2,5-Diphenyltetrazolium Bromide) (MTT) dye solution reagent was added and incubated at RT for 4 hours. Finally, the formazan was solubilized in 100 µl of Stop mix and absorbance of each well was recorded at 570 nm on a microplate spectrophotometer. Background (blank) values were subtracted and viability for each condition was normalized to the PC (0.2 % DMSO) as described for static binding inhibition in formula 2.1. Data were reported as mean ± standard deviation.

2.2.6 Flow binding assay

Two days before the assay, CHO cells were detached, pelleted for 2 minutes at 300 g and resuspended in 1–2 mL CHO growth medium. The concentrations of the cell suspension was determined either by Countess II FL or Neubauer chamber and further diluted to a concentration of $7.5 \times 10^5 \frac{cells}{ml}$ and 200 µL was seeded per 0.8-LUER Ibidi flow slide. The slides were checked two hours later for cell adhesion and the medium was exchanged for fresh CHO growth medium containing the respective selection markers. Similarly, the medium was changed the next day. On the day of the assay, the Ibidi fluidic system was equilibrated with 14 mL of BM in the CO_2 incubator at least 30 minutes before the start of the experiment according to the the manufacturer's instructions. Trophozoite stage parasites were enriched by gelatine floatation and diluted to $1 \times 10^7 \frac{iEs}{mL}$ as described for the static binding assay (see 2.2.5). Once the pump system was set-up and under a 37°C climate controlled hood and running with the slide under a

digital microscope (EVOS FL Auto), 1 mL of the knob-enriched parasites, with a total number of $1 \times 10^7 \frac{iEs}{ml}$ was added to system (Fig. 2.3). The experiments started at the highest investigated shear stress of $6 \frac{\text{dyn}}{\text{cm}^2}$ and was decreased in steps of 10 minutes to $0.9 \frac{\text{dyn}}{\text{cm}^2}$ (see Tab. 2.7). The Ibidi Pump Control software calculates the required flow rates Φ according to Equation 2.2 to generate the set shear stress in the flow slide. The parameters used were a slide-factor F = 34.7 for the 0.8 LUER Ibidi slide and a viscosity $\tau = 0.0072\,\text{dyn}\,\text{s/cm}^2$. Meanwhile the microscope took pictures at the highest possible framerate of one picture per 3 seconds. A time series of 120 pictures was used to track the bound erythrocytes with the R-Software and the trackdem package as described by Wu *et al.*. The script plots the tracked particles over a still image of the video and connects the tracked iEs with a line of the same color to visualize the trajectories. Additionally, each x-coordinate for each particle at each frame was written into a `.txt` file. A python script was used to calculate the distance travelled for each particle from the x-coordinates and plot each measurement in a dot plot. Additionally, for each identified particle, the distance was divided by the duration of the tracked particle by counting the respective frames and dividing by frame rate (3 seconds).

$$\tau = \eta \cdot \text{F} \cdot \Phi \qquad (2.2)$$

$$0.1\,\text{Pa} = 1\,\text{dyn/cm}^2 \qquad (2.3)$$

τ = shear stress $\left[\text{dyn/cm}^2\right]$

η = dynamical viscosity $\left[\text{dyn}\,\text{s/cm}^2\right]$

Φ = flow rate [mL/min]

F = slide-factor [mL/min]

Table 2.7: Sequence of decreasing shear stress in flow binding assay.

Shear stress	6.0 $^{\text{dyn}}/_{\text{cm}^2}$	4.0 $^{\text{dyn}}/_{\text{cm}^2}$	3.0 $^{\text{dyn}}/_{\text{cm}^2}$	2.0 $^{\text{dyn}}/_{\text{cm}^2}$	1.5 $^{\text{dyn}}/_{\text{cm}^2}$	0.9 $^{\text{dyn}}/_{\text{cm}^2}$
Time	10 min	10 min	10 min	10 min	10 min	10 min

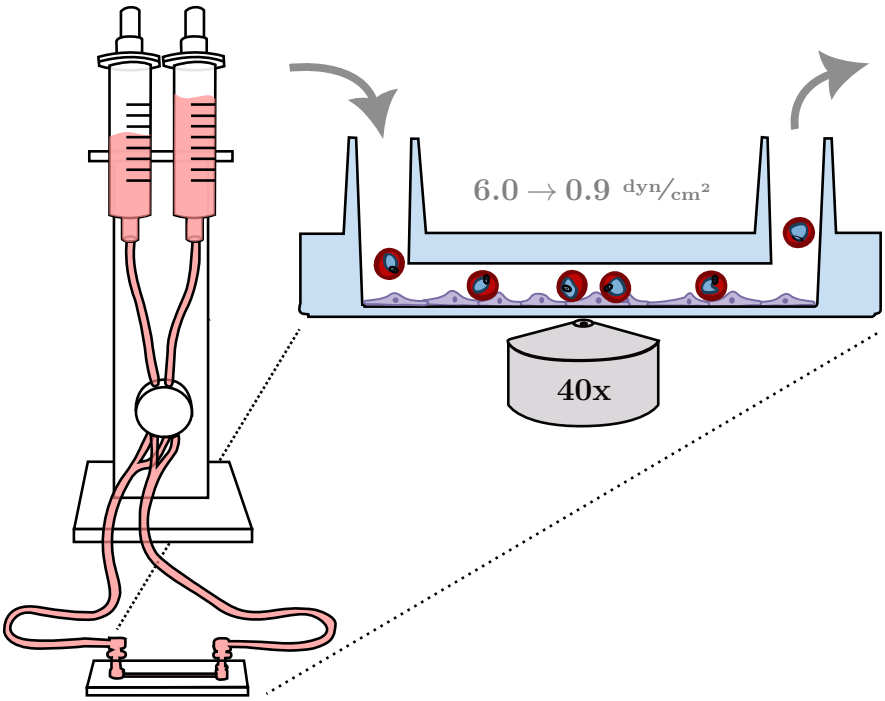


Figure 2.3: **Setup of flow binding experiment with Ibidi pumps system**. iEs are pumped unidirectionally across cells attached to a flow cells with a shear rate ranging from $6 - 0.9 \frac{\text{dyn}}{\text{cm}^2}$.

2.2.7 Panning

Trophozoite stage parasites were enriched by gelatine floatation (see 2.2.2.4). The medium of a confluent T25 flask with the cells of interest was changed against BM and incubated for 30 minutes at 37 °C. Then the BM was replaced by the enriched iEs, resuspended in 3 mL of BM. The iEs and CHO/endothelial cells (ECs) were then coincubated at 37 °C and 5 % CO_2 in the incubator for 75 minutes. In-between the iEs were agitated every 15 minutes by gently rocking the flasks in all directions. After 75 minutes the iE suspension was aspirated and the cells were washed five times by gently pipetting 5 mL of BM into the wall of the flask, gently shaking it and aspirating it again. Pictures of the flask were then taken with the EVOS® XL inverted microscope for documentation and to check for binding and cell health. In the last step, 3 mL of complete malaria growth medium was added with 100 µL of blood. Subsequently the flask with the bound iEs was put in an airtight box, gassed with 5 % CO_2, 1 % O_2, and 94 % N_2 and incubated at 37 °C. The next day the supernatant from the flask was harvested, pelleted at 700 g and resuspended in 7 mL of RPMI medium. The

suspension was carefully layered on top of 7 mL of Biocoll separating solution and centrifuged for 20 minutes at 950 g without brakes. The supernatant was then removed up to the blood pellet and the cells were washed with 10 mL of complete malaria growth medium. Afterwards, blood was added to achieve 5 % hematocrit and cells were regularly cultured as described in 2.2.2.

2.2.8 Immunofluorescence microscopy

To increase parasitaemia, the parasite culture was knob-enriched as described in 2.2.2.4. The pellet was washed once in 1x PBS and subsequently resuspended in 1x PBS to achieve a hematocrit of 1–2.5%. The suspension was applied as a thin film onto a 10-well glass slide and air dried. Cells were then fixed in acetone at RT for 30 minutes. Subsequently, they were rehydrated with 1x PBS and washed five times by applying and removing fresh 1x PBS. Primary antibodies (anti-KAHRP, 1:1000; anti-HA, 1:500) were diluted in 1x PBS containing 3% BSA and ampicillin (1:1000). Primary antibodies were added to the slide and incubated in a humid chamber overnight at 4°C. After five washing steps with 1x PBS, secondary antibodies were diluted (anti-rabbit Alexa Fluor™ 488, 1:500; anti-rat Alexa Fluor™ 594, 1:2000) in 1x PBS containing 50 ng/mL Hoechst 33342 and 3% BSA. Secondary antibodies were incubated in a humid chamber at RT for 1 hour, then removed, and the fixed cells were washed an additional five times with 1x PBS. Subsequently, three drops of Dako mounting medium were added along with a glass cover slide. Slides were imaged at 63x or 100x magnification using Zeiss AxioImager M1 or M2 microscopes equipped with a Hamamatsu Orca C4742-95 camera. Additional image processing was performed using Fiji.

2.2.9 RNA isolation

Plasmodium culture pellet was incubated with 5–10x of Trizol at 37 °C for 5 minutes after shaking it for 30 seconds. Trizolized samples where either stored at -80 °C or directly processed for RNA isolation. RNA isolation was carried out by adding 200 µL of chloroform (4°C) per 1 mL of Trizol in 1.5 mL RNase free reaction tubes, 15 s of

shaking and 2 minutes of incubation at RT. Afterwards the suspension was centrifuged for 30 minutes at 4°C at 18000 g. Subsequently, the clear supernatant was transferred to new reaction tubes and an equal amount of 70 % ethanol (4°C) was added. The solution was then added on RNA spin columns from the PureLink RNA Mini Kit and following steps were performed as per kit protocol. RNA was eluded in RNase free water in two steps à 20 µL and RNA concentration was measured with NanoDrop 2000 spectrophotometer (ThermoFisher). Depending on RNA concentration, samples were tested for RNA degradation either with the High Sensitivity RNA ScreenTape (1–25 ng) or with RNA ScreenTape (25–500 ng) with the 4200 TapeStation (Agilent). Isolated RNA was stored at -80 °C.

2.2.10 Genomic DNA isolation

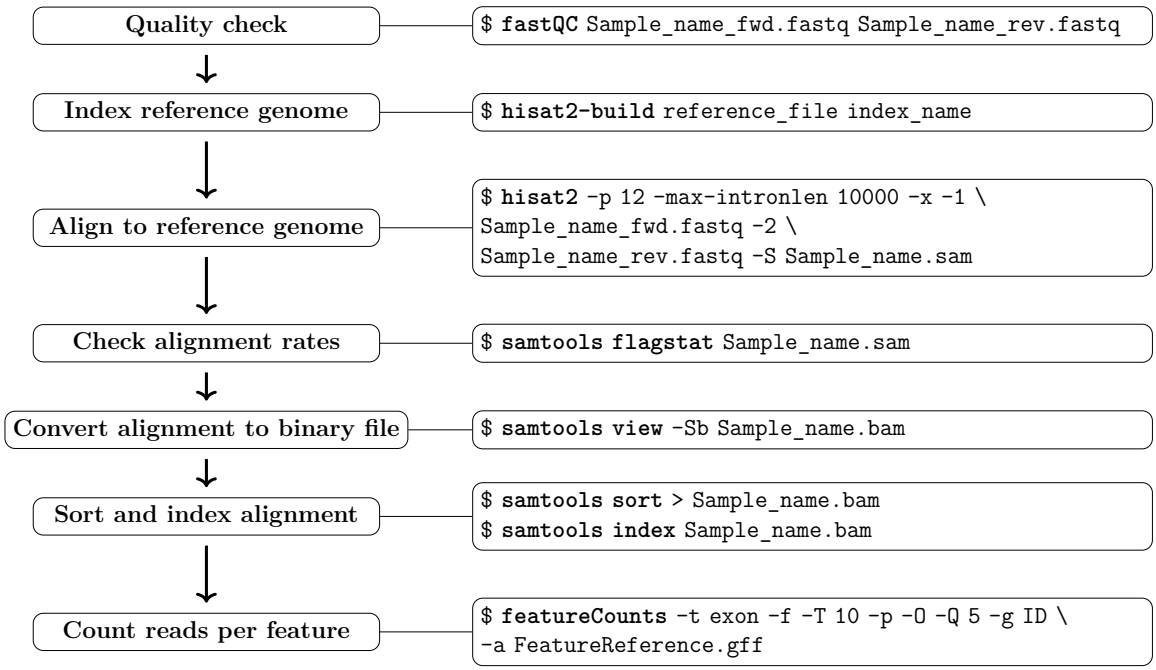
A blood pellet of 250–500 µL of iE was collected in a 15-ml falcon. The pellet was split into fractions of 200 µL of blood per 1.5 mL reaction tube, to which 20 µL of Proteinase K was added. The samples were then processed using the QIAMP® DNA Mini Kit according to the manufacturer's instructions. The concentration of genomic DNA in the sample was determined photometrically using a NanoDrop™ 2000 at 260 nm, and the DNA was stored at -20°C.

2.2.11 RNA-seq data processing and relative *var* gene expression analysis

RNA-sequencing was kindly performed by Dr. Dániel Cadar of the in-house sequencing facility. In short, rRNA was removed using QIAseq FastSelect RNA Removal Kit. The QIASeq Stranded mRNA Library Kit was used for library preparation and sequenced on an Illumina NextSeq550 system with the NextSeq 500/550 Mid Output Kit v2.5 (150 cycles). Raw sequencing data quality was checked with FastQC and mapped to the respective reference genome (PlasmoDB, IT4 version 58) with HISAT2. The resulting alignment quality was checked with samtools flagstat. Read counts per feature were determined with featureCounts. See Figure 2.4 for more details. For the relative *var*

expression profiles, the raw read counts per exon determined with featureCounts were normalized to transcripts per million (TPM) with the bioinfokit python package. Due to the highly conserved nature of ATS domain, only reads mapping to exon 1 (see Fig: 1.3) were used for the analysis. Pie charts were created with python and matplotlib.

Figure 2.4: **RNA-seq data processing**. Schema and parameters for the processing of *Plasmodium* RNA-seq data.



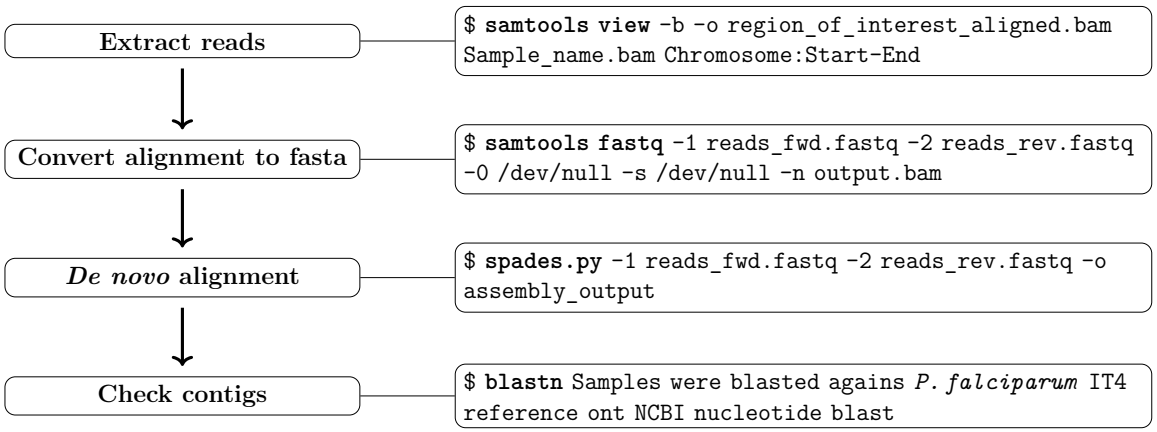
2.2.12 Scatterplot of *var* gene and neighbouring genes co-expression

The python package gffutils was used to parse the gff-file of the `PfIT` reference genome to determine gene ID, strand and gene type (rifin, *Pf*EMP1 etc.) of the neighbouring genes. The gene IDs were then used to look up the gene expression in the TPM normalized expression data. The resulting data was plotted with matplotlib and seaborn as a scatter plot. A full list of RNA-seq samples is attached at A.1.

2.2.13 *De novo* gene assembly

A new alignment file including only reads mapping to the region of suspected recombination was created with samtools view. All reads covering the region of suspected recombination where extracted from the original alignment file. The new alignment was converted back to paired-end reads and used as an input for the *de novo* assembler SPAdes. See Fig. 2.5 for more details.

Figure 2.5: ***De novo* gene assembly**. Schema and parameters to create a *de novo* gene assembly from an **RNA-seq** alignment file.



2.2.14 Recombination identification

Correctly aligned reads with the aforementioned Illumina based sequencing pipeline show the characteristic "inward-facing" orientation ($\rightarrow \leftarrow$) that flanks the insert. For these reads the first alignment is always to the forward strand, and the second alignment to the reverse strand `FXRX`. If the first and second alignment both map to the same strand (`FXFX` or `RXRX`), the reads are oriented in the same direction ($\rightarrow \rightarrow$ or $\leftarrow \leftarrow$), indicating either a mapping error by the aligner, or a deviation of the sample from the reference genome. The same is indicated if the first reads maps to the reverse strand, and the second read to the forward strand (`RXFX`) which leads to reads facing outwards from the insert ($\leftarrow \rightarrow$). In the case of IT4var20-HA^{endo} an irregular accumulation of (`RXFX`) read pairs could be observed. Custom sequence alignment/map (SAM) files

were filtered for only such reads based on the alignment flags `81`, `161`, `145` and `97`. The read number (1 or 2) and orientation are noted for each aligned read in the SAM file.

Table 2.8: **Orientations for aligned, paired-end reads.** Orientation flags in numeric code as set by aligner in SAM file

Code	Strand: read 1	Strand: read 2	Orientation to insert		Flag: read 1	Flag: read 2
F1R2	Forward	Reverse	→ ←	Inward-facing	99	147
F2R1	Forward	Reverse	→ ←	Inward-facing	163	83
R1F2	Reverse	Forward	← →	Outward-facing	81	161
R2F1	Reverse	Forward	← →	Outward-facing	145	97
F1F2	Forward	Forward	→ →	Same-direction	65	129
F2F1	Forward	Forward	→ →	Same-direction	129	65
R1R2	Reverse	Reverse	← ←	Same-direction	113	177
R2R1	Reverse	Reverse	← ←	Same-direction	177	113

2.2.14.1 Standard PCR

Diagnostic PCRs were carried out with GoTaq® direct to gel reagents from Promega. Genomic *P. falciparum* DNA was used as template. The reaction mix and amplification were carried out according to the parameters specified in Table 2.9 using a Peqlab peqSTAR 96X thermocycler.

Reagent	Volume
Template DNA	1 µL
Forward Primer (10 µM)	2 µL
Reverse Primer (10 µM)	2 µL
dNTPs (2.5 mM each)	2 µL
5x Buffer (Promega)	4 µL
$MgCl_2$ (25 mM)	1.5 µL
GoTaq® G2 (Promega)	0.2 µL
Nuclease-free water	to 20 µL

Temp	Time	Cycles
95°C	10:00 min	1×
95°C	1:00 min	35×
55°C	1:30 min	
72°C	2:00 min	
72°C	10:00 min	1×

Table 2.9: PCR reaction mix (left) and thermal cycler settings (right) for a 20 µL plasmid amplification reaction.

2.2.15 Agarose gel electrophoresis

Gels of 1 % agarose in TAE buffer were cast with two drops of 0.025 % ethidium bromide solution per 50 mL in the gel chamber (Horizon 11.4, Gibco Life Technologies). 6 µL of 1 kb Ladder (Thermo Scientific) or 2.5 µL of sample were added per pocket. The fragments were separated at 100–100 V in TAE buffer. The gels were imaged using a UV transluminator (PHEROlum 289, Biotec Fischer) at 254 nm.

2.2.15.1 Identification of putative quadruplex forming sequences

Fasta sequences of chromosomes were extracted from the `PfIT` reference genome (PlasmoDB, version 58) and analyzed using QGRS Mapper with the following parameters adopted from [52] : Max length: 33; Min G-group: 3; loop size: 0 to 11. The results were plotted using Python and matplotlib.

2.2.15.2 Differential gene expression

A differential gene expression (DGE) was carried out with the R package DESeq2 and standard parameters with raw read counts as input.

3 Parasite adhesion

3.1 Results

The main cause of pathogenicity in *P. falciparum* malaria is *Pf*EMP1-mediated cytoadhesion, which allows iEs to adhere to the endothelial lining of blood vessels. This sequestration occurs in the microvasculature of vital organs, causing many of malaria's morbidities. By obstructing blood flow, it leads to anaerobic glycolysis, inflammation, and vascular dysfunction [131]. Additionally, sequestered iEs are protected from the natural clearance of abnormal erythrocytes by the spleen. The second major trait of *Pf*EMP1 is the parasite's ability to switch between the approximately 60 *var* genes encoding different *Pf*EMP1 variants. This not only alters the adhesion profile, but also changes the antigenic profile, which allows the parasite to evade the adaptive immune response [42, 47, 132].

Until recently, the most prominent method to enrich iE cultures for different surface expression profiles of *Pf*EMP1 was through selecting the parasites in a process called 'panning' on selective binding partners. These could be naturally-occurring ligands on ECs, on transgenic CHO cells expressing human ECRs, or as immobilized purified ECRs. The panning process then involved multiple cycles of incubating iEs with the *Pf*EMP1-ligand surfaces or cells, washing away non-adherent parasites, and culturing the bound parasites [110, 133]. This rarely led to monovariant-expressing parasite cultures, as multiple *Pf*EMP1s contain adhesion domains for the same ECRs [110, 134, 135]. This resulted in a majority enrichment of parasites expressing the *Pf*EMP1 variant with the highest binding affinity. Even though this method remains the *de facto* standard for researching different *var* genes, it does not facilitate the enrichment of *var*

genes transcribing for *Pf*EMP1s with unknown or low binding affinities. Furthermore, for each generation of the culture, a fraction of the parasites switches to express different *var* genes if the selection pressure is not kept up [136]. Clonally isolating parasites can produce monovariant *var* gene cultures, however the likelihood of selecting a specific *var* gene of interest is extremely low if that gene is rarely or not transcribed in the parent population [78].

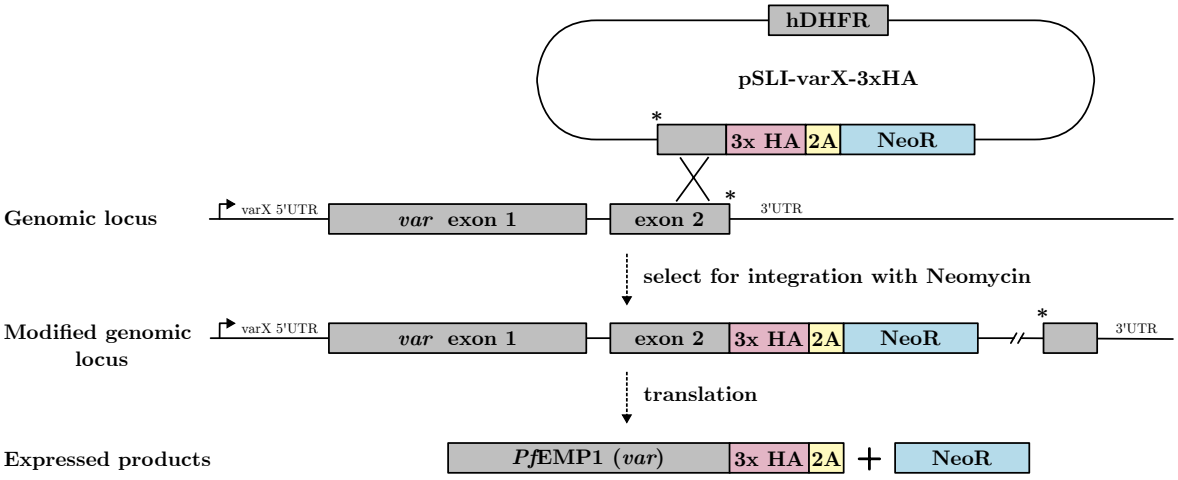


Figure 3.1: **SLI schematic for *var* genes**. The exosomal pSLI-varX-3xHA plasmid is integrated into its targeted genomic locus through homologous recombination of a ~500 bp sequence at the 3' end of exon 2 in the *var* gene of interest. The modified genomic locus extends the *var* gene by an HA-tag (`3x HA`), a T2A skip peptide (`2A`) and a Neomycin resistance (`NeoR`). By means of the skip peptide, the expressed products consist of two separate proteins, the tagged *P. falciparum* erythrocyte membrane protein 1 (*Pf*EMP1) and the neomycin resistance. human dihydrofolate reductase (hDHFR); $*$, stop-codon; ⅃, promotor. Modified from [79, 125]

A variety of targeted gene editing methods exist, with the majority relying on single- or double-crossover recombination using plasmids carrying sequences homologous to the target region [125]. The novel SLI system improves upon this mechanism by enabling rapid integration of a plasmid into the *P. falciparum* genome by linking a resistance marker via a ribosomal 'skip' peptide directly to the endogenous promoter of the target gene, allowing parasites with successful integration to be positively selected within weeks. In the case of a SLI-*var* integrants, homologous recombination occurs through a 500 bp sequence of the 3' end of the exon 2 of the target *var* gene, followed by an

HA-tag, the 2A-skip peptide and a Neomycin resistances gene (Fig. 3.1). Furthermore, SLI permits targeting of essential genes and can be combined with functional tags for protein localization and knockdown studies, in contrast to conventional knockout or conditional expression systems that often struggle with low integration efficiency or require expensive reagents [125]. In cooperation with RG Spielmann, Jan Stäcker, and Jakob Cronshagen, a range of SLI-activated *var* cell lines were generated from the IT4 and 3D7 parent isolates. Initial experiments with SLI lines expressing the known CD36 binders `PF3D7_0809100` and IT4var66 (`PfIT_040025500`), as well as the conserved *var2CSA*, in both parasite lines (3D7: `PF3D7_1200600` and IT4: `PfIT_120006100`) confirmed the anecdotal observation that the IT4 line exhibits increased stability of cytoadherence phenotype *in vitro* compared to the 3D7 *P. falciparum* line [109]. Early binding assays by Jana Brehmer (RG Host-Parasite Interaction, BNITM) using iEs with *var01* and *var16* on transgenic CHO cells showed the expected CD36 and ICAM-1 dual binder phenotype and additionally identified potential new endothelial receptor binding partners such as TNFR-2, VCAM-1, and CD9 [137]. Other newly generated SLI lines, for which at least one ECR binding partner has been described in literature, exhibited absent or variable adherence phenotypes (unpublished data, Jana Brehmer). This included the expected EPCR binders var19-HA^{endo} and IT4var20-HA^{endo}, the placental malaria-associated variant IT4var04-HA^{endo} binding CSA [75, 85, 97]. Furthermore, SLI-*var* lines with unknown binding properties such as IT4var02-HA^{endo}, IT4var03-HA^{endo}, and IT4var08-HA^{endo} did not show binding to a panel of nine tested ECRs [137].

3.1.1 IT4 wild type

The unmodified IT4 wild type parasite line, which was used to create the SLI-var-HA^{endo} parasite lines, was the first to be investigated for its adhesion phenotype. The binding capacity of iEs to various human ECRs was assessed using an adhesion assay to transgenic CHO cells that express different human ECRs or only an intracellular GFP with no surface modification as control. Plotted in Fig. 3.2, A are the bound iEs per

mm^2 after washing away loose or unbound iEs and uEs. Among the receptors tested, the highest binding was observed for CHOs expressing CD36, with a mean adhesion of 398 ± 50 iEs/mm^2 ($p_{adj} = 0.005$). This was followed by low to moderate binding to VCAM-1 ($\sim$75 iEs/mm^2, $p = 0.104$), MDR-1 ($\sim$70 iEs/mm^2, $p = 0.130$) and CD55 (70 iEs/mm^2, $p = 0.130$). With the exception of CD37 (12 iEs/mm^2), the other receptors examined, such as ICAM-1, K1-EPCR, CD9, CD37, CD81, TNFR1 and TNFR2, all showed slightly higher binding compared to the GFP control ($\sim$15 iE/mm^2), with average binding ranging from 32 – 52 iEs/mm^2, but without statistical significance.

To investigate the molecular basis of the binding phenotype, the expression profile of the *var* gene family in the IT4 wild type parasite line was analysed by RNAseq (Fig. 3.2, B). The relative expression levels of individual *var* transcripts were visualized as a pie chart. The data shows that *var66* (`PfIT_040025500`), making up 63.0 % of the total *var* transcript pool, is the dominant *var* gene in long-term *in vitro* culture of the IT4 line. The second most expressed *var* gene is *var34* (`PfIT_080014100`). The highly conserved pseudogene *var1CSA* (`PfIT_050037800`) is expressed at 5.3 %. The exon 2 and intron of *var1CSA* are truncated in the IT4 line and most isolates, but the gene is nevertheless included in the analysis due to its unique features and unique expression pattern [54]. Additionally, only *var21* (`PfIT_040017000`) and *var59* (`PfIT_040017400`) are expressed above 1 %.

Flow binding assay

To get a clearer insight into the binding dynamics, cytoadhesion of IT4wt was investigated under shear stress. Starting at 6 $^{dyn}/_{cm^2}$, the shear stress was gradually reduced to 0.9 $^{dyn}/_{cm^2}$ in steps of 10 minutes (Tab. 2.7) while images were taken every 3 seconds. The image series was used to track bound or retarded iEs with an R-based tracking pipeline. Additionally, the total amount of bound iEs after each 10-min segment was determined by a manual count of the last image.

While no iEs were found binding to the CHO-GFP control, a negligible amount of iEs bound to CHO-ICAM1 after 10 minutes of shear rates of 1.5 $^{dyn}/_{cm^2}$ ($\sim$ 6 iEs/mm^2) and 0.9 $^{dyn}/_{cm^2}$ ($\sim$ 15 iEs/mm^2). For CHO-CD36, first bound parasites appeared at

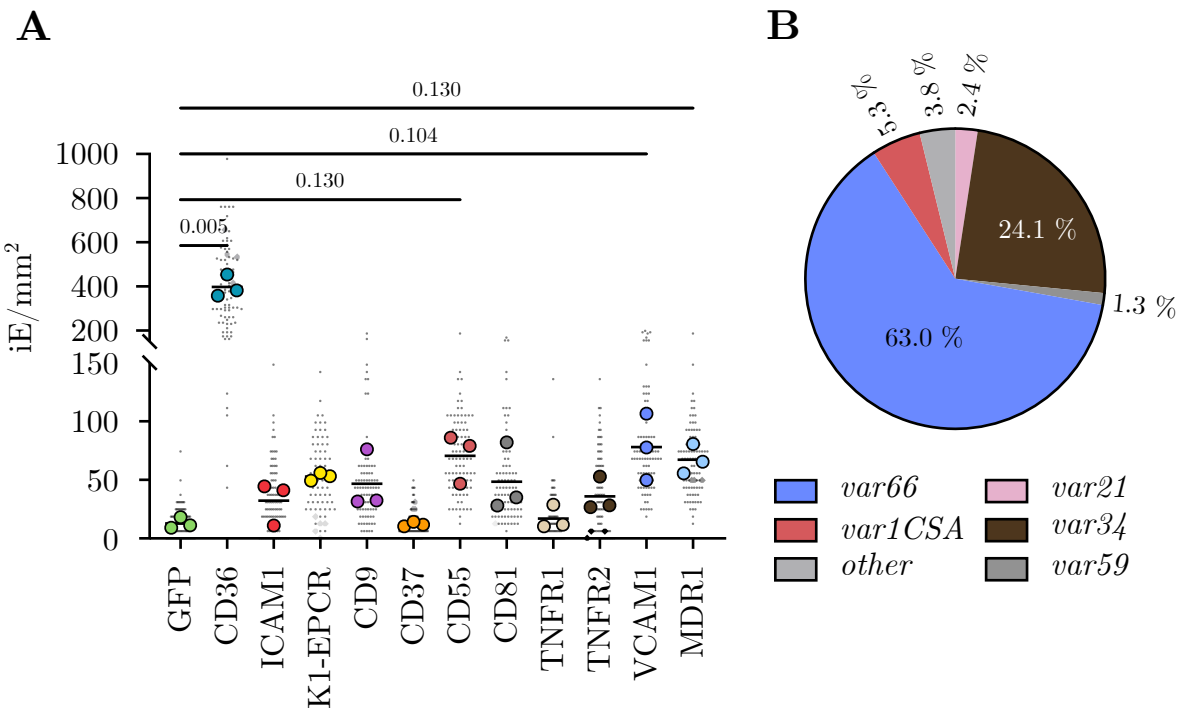


Figure 3.2: **Cytoadhesion of IT4 wt without shear stress A:**.Static binding assay of IT4 wt against ECRs on CHO cells. Statistic with nonparametric Kruskal-Wallis test for comparisons enriched/unenriched and for each receptor against the respective CHO-GFP controls. **B:** *Var* expression profile of IT4 wt.

4.0 $^{dyn}/_{cm^2}$, increasing gradually to 818 iEs/mm^2 at 0.9 $^{dyn}/_{cm^2}$ (Fig. 3.8; A and B). Due to the low amount of bound iEs on CHO-ICAM1, tracking could only be applied to CHO-CD36. There, iEs could be tracked starting at a shear rate of 3 $^{dyn}/_{cm^2}$ with a sharp increase at 2.0, 1.5, and 0.9 $^{dyn}/_{cm^2}$ (Fig. 3.3). At the shear rates of 2.0 – 0.9 $^{dyn}/_{cm^2}$, the average tracked velocities decreased from 29.9 μm/min to 42.2 μm/min (Fig. 3.5, A). Similarly, the tracked distance of the particles increased from 27.9 to 40.0 μm (Fig. 3.5, A). The iEs displayed a rolling motion at shear rates from 3.0 – 1.5 $^{dyn}/_{cm^2}$ indicated by the path of the trajectories running aligned to the flow (Fig. 3.3, A – D). At 0.9 $^{dyn}/_{cm^2}$, iEs were mostly bound stationary, which is displayed as localized wiggle of lines in all directions (Fig. 3.3, D).

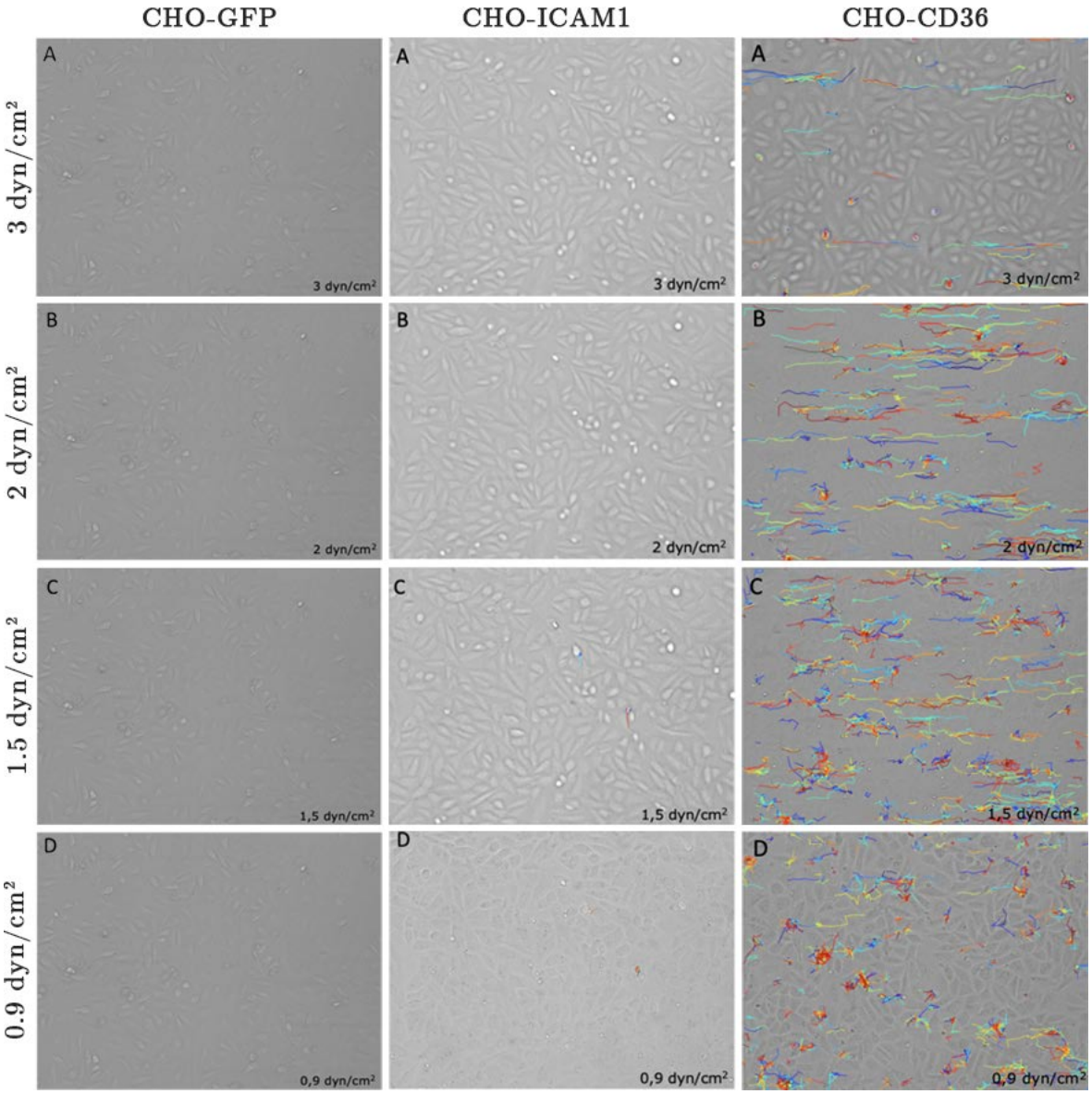


Figure 3.3: **Cytoadhesion of IT4 wt under shear stress**. iEs flow unidirectionally from left to right at a shear rate of $3 - 0.9\,\mathrm{dyn/mm^2}$. Left: CHO-GFP as control of CHO without ECR on surface, Center: CHO-ICAM1, Right: CHO-CD36. Paths of iEs tracked over >10 frames are marked in color. Experiments performed by D. Rauchberger (RG Host-Parasite Interaction, BNITM).

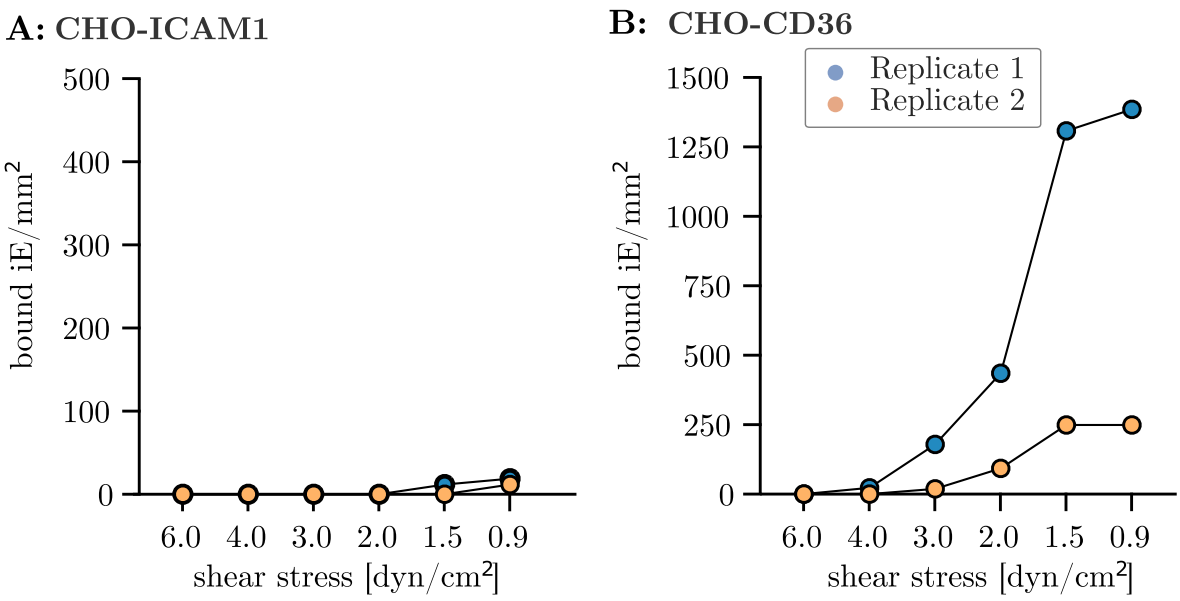


Figure 3.4: **Bound IT4 wt iEs under shear stress**. Number of bound iEs in iE/mm^2 after 10 min of respective shear stress decreasing from 6.0 – 0.9 dyn/mm^2 over **A:** CHO-ICAM1 and **B:** CHO-CD36 cells; Experiments performed by D. Rauchberger.

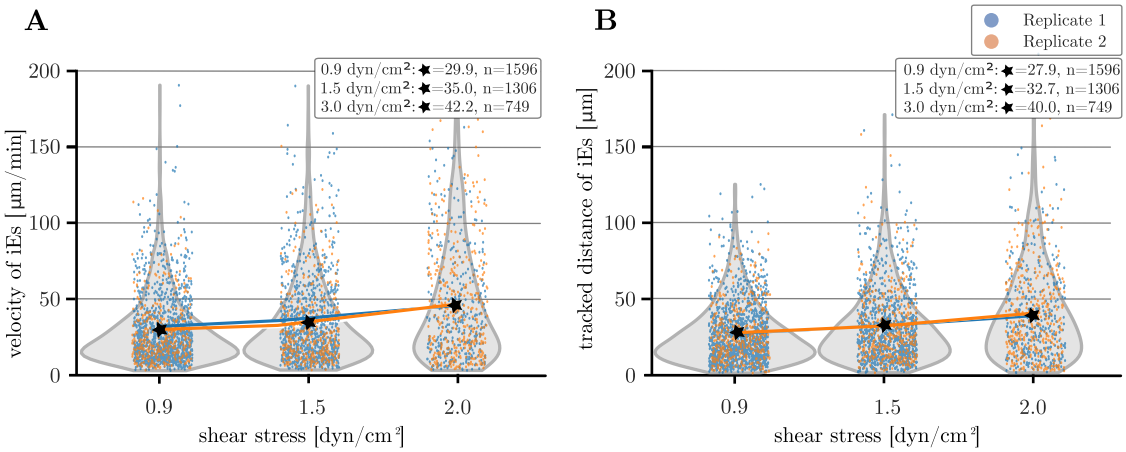


Figure 3.5: **Rolling velocity and distance of IT4 wt under shear stress**. **A:** Rolling velocity of iEs in µm/min and **B:** tracked rolling distances of iEs for shear rates of 0.9, 1.5 and 2 dyn/mm^2. ★ = mean; n = tracked iEs; Experiments performed by D. Rauchberger.

3.1.2 IT4var01- and IT4var16-HA^{endo}

The IT4var01-HA^{endo} line showed significant binding to CD36 (1460 ± 783 iEs/mm^2, p = 0.004), ICAM-1 (p = 0.010, 910 iEs/mm^2), CD55 (p = 0.145, 340 iEs/mm^2) and VCAM-1 (p = 0.024, 630 iEs/mm^2) as compared to the CHO-GFP control (15 iEs/mm^2) (Fig. 3.6, A) under static conditions. CD81, TNFR1, TNFR2 and MDR1 show a mean binding higher than the control with 150 iEs/mm^2, 140 iEs/mm^2, 440 iEs/mm^2 and 270 iEs/mm^2 respectively. The *var01* gene accounts for 95.9 % of the total *var* gene expression. The remaining transcripts are distributed among *var1CSA* (2.2 %), *var66* (1.0 %), and other *var* genes (1.8 %) (Fig. 3.6, B).

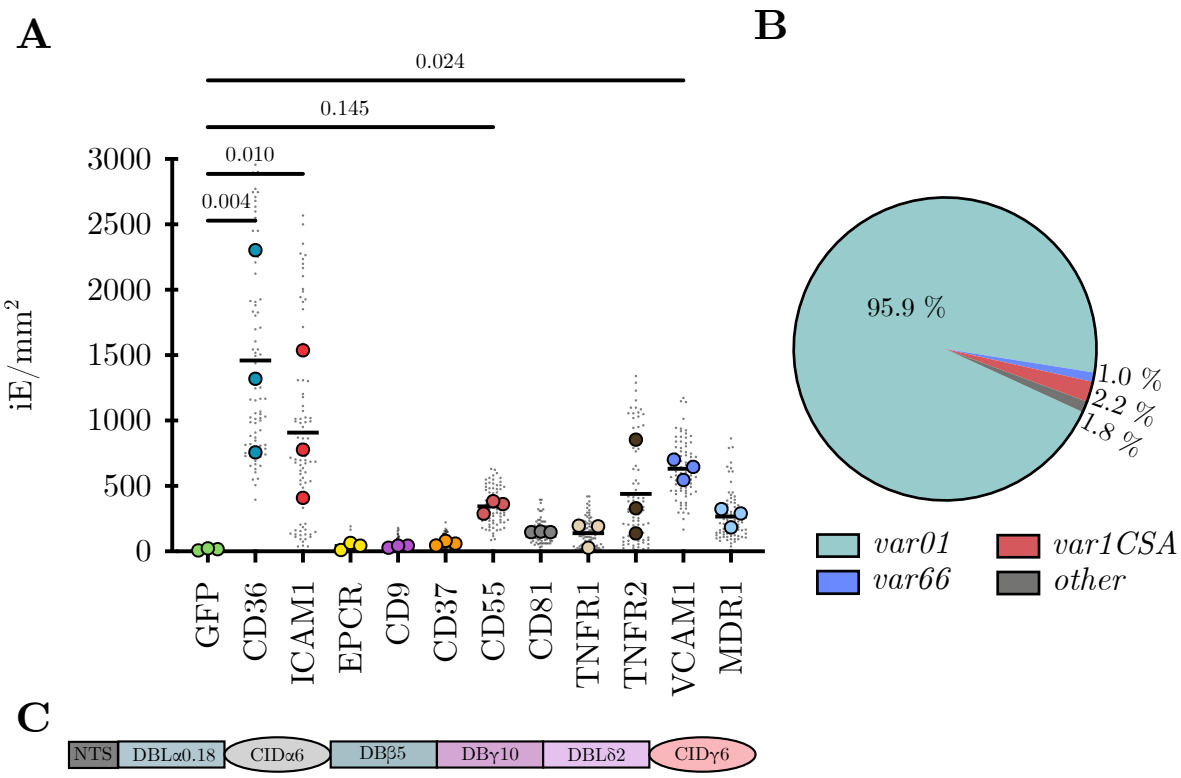


Figure 3.6: **Cytoadhesion of IT4var01-HA^{endo} without shear stress A:**. Statistic with nonparametric Kruskal-Wallis test for comparisons for each receptor against the respective CHO-GFP control. **B:** *Var* expression profile of IT4var01-HA^{endo}. **C:** Domain structure of *var01*.

The static binding assay for IT4var16-HA^{endo} (Fig. 3.7, A) showed a similar binding pattern as IT4var01-HA^{endo}. The parasite line facilitated a significant binding to the same CHO-ECRs, namely CD36 (540 ± 211 iEs/mm², p = 0.116), ICAM-1

(p = 0.004, 2540 iEs/mm^2), CD55 (p = 0.058, 750 iEs/mm^2) and VCAM-1 (p = 0.024, 910 iEs/mm^2). The CHO-GFP control bound on average with 42 iEs/mm^2.

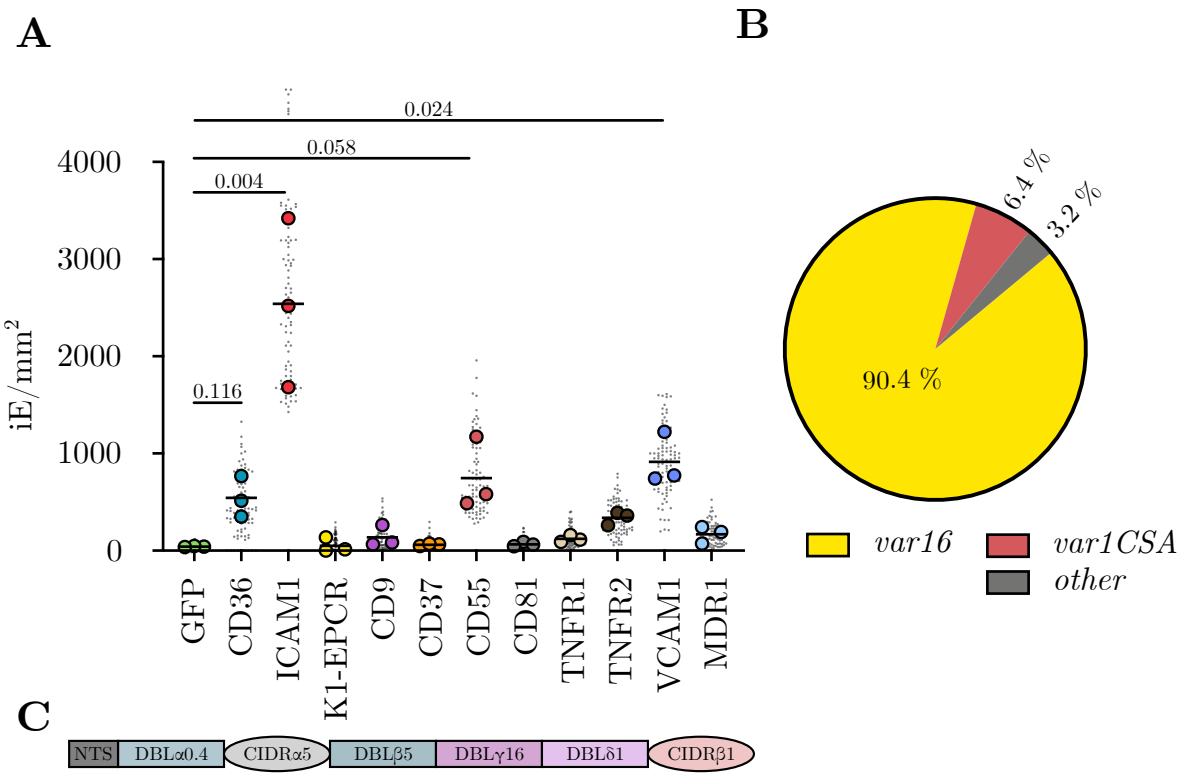


Figure 3.7: **Cytoadhesion of IT4var16-HA^{endo} without shear stress A:**.Static binding assay of IT4var16-HA^{endo} against ECRs on CHO cells. Statistic with nonparametric Kruskal-Wallis test for comparisons for each receptor against the respective CHO-GFP control. **B:** *Var* expression profile of IT4var16-HA^{endo}. **C:** Domain structure of *var16*.

Flow binding assay

IT4var01-HA^{endo} is a well-known ICAM-1 and CD36 dual binder and therefore of interest to compare the dynamics of two different *Pf*EMP1-ECRs interactions with one parasite line. The flow experiments revealed binding against both receptors starting at shear stress of 4 dyn/cm^2 with a steady increase to 0.9 dyn/cm^2. The amount of bound iEs was roughly twice as much to CHO-CD36 than to CHO-ICAM1 at the respective time points (Fig. 3.8, A and B). After 10 minutes of 0.9 dyn/cm^2, 300 iEs/mm^2 bound to CHO-ICAM1 and 547 iEs/mm^2 bound to CHO-CD36. The path of the trajectories

revealed further differences. At shear rates from 3.0 – 1.5 $^{dyn}/_{cm^2}$, IT4var01-HA^{endo} parasitized iEs displayed a rolling behaviour on CHO-CD36, while they were immobilized on CHO-ICAM1 (Fig. 3.9, A – C). At 0.9 $^{dyn}/_{cm^2}$, the difference was less discernible with parasites mostly static over both ECRs (Fig. 3.9, D). The same could be observed, when the tracked iEs were evaluated for velocity and distance travelled. While both velocity and tracked distance decreased at lower shear stress for iEs over CHO-CD36 from 70.4 μm/min at 3.0 dyn/cm^2 to 28.2 μm/min at 0.9 dyn/cm^2 and 55.4 μm to 25.5 μm (Fig. 3.10, A and B), this was not observed for CHO-ICAM1. Here the iEs velocity stayed constant at $\sim$ 23 μm/min and the tracked distance at $\sim$ 26 μm (Fig. 3.10, C and D).

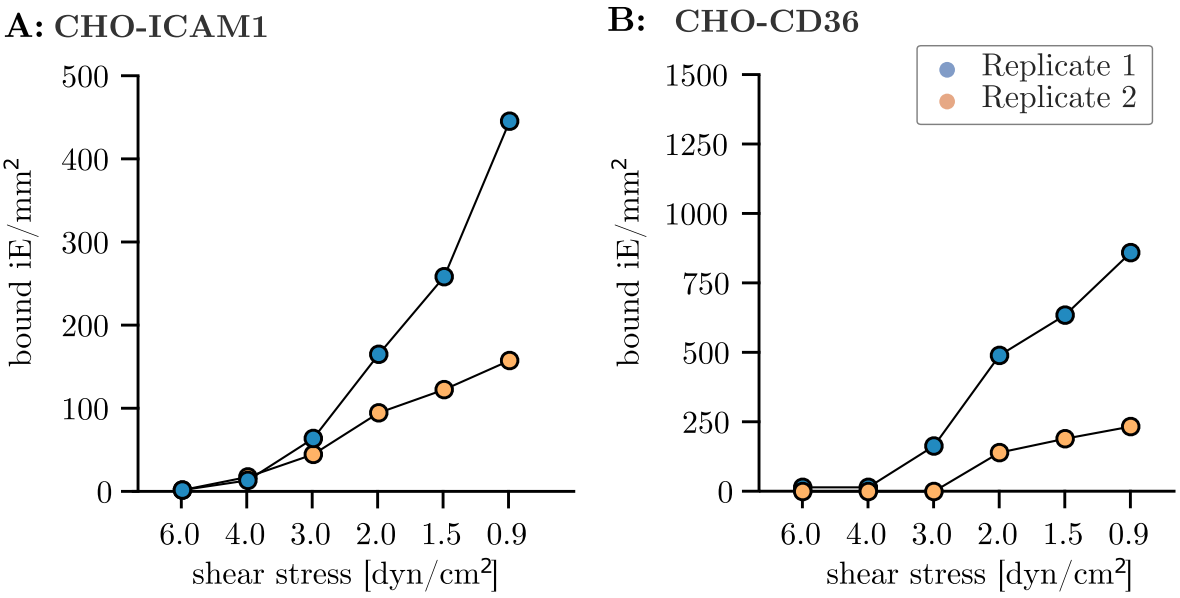


Figure 3.8: **Bound IT4var01-HA^{endo} wt iEs under shear stress**. Number of bound iEs in iE/mm^2 after 10 min of respective shear stress decreasing from 6.0 – 0.9 dyn/mm^2 over **A:** CHO-ICAM1 and **B:** CHO-CD36 cells; Experiments performed by D. Rauchberger.

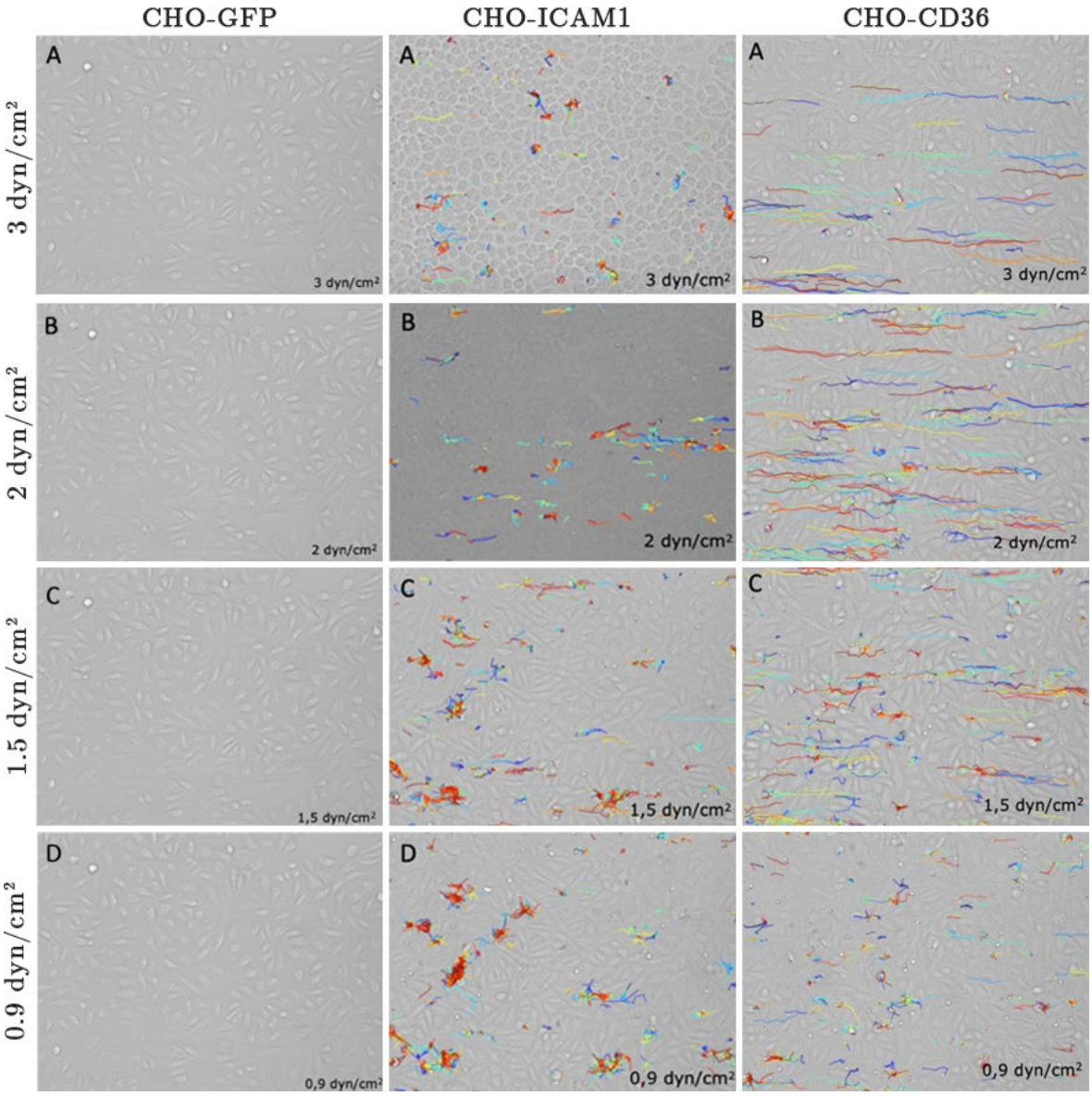


Figure 3.9: **Cytoadhesion of IT4var01-HA^{endo} under shear stress**. iEs flow unidirectionally from left to right at a shear rate of $3 - 0.9\,\mathrm{dyn/mm^2}$. Left: CHO-GFP as control of CHO without ECR on surface, Center: CHO-ICAM1, Right: CHO-CD36. Paths of iEs tracked over >10 frames are marked in color. Experiments performed by D. Rauchberger.

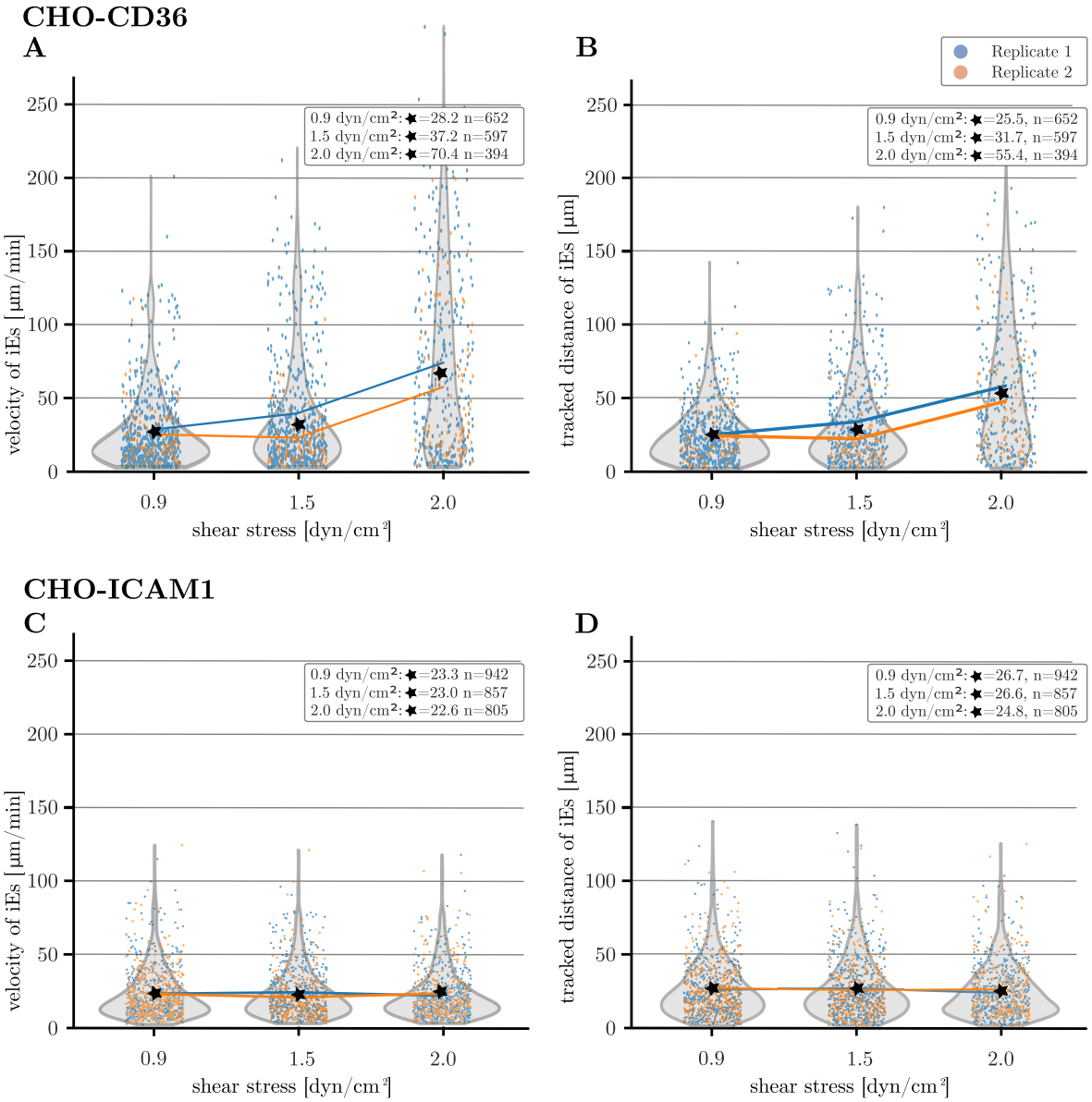


Figure 3.10: **Rolling velocity and distance of IT4var01-HA^{endo} under shear stress**. **A:** Rolling velocity of iEs in µm/min and **B:** tracked rolling distances of iEs for shear rates of 0.9, 1.5 and 2 dyn/mm^2. ★ = mean; n = tracked iEs; Experiments performed by D. Rauchberger.

3.1.3 IT4var04-HA^{endo}

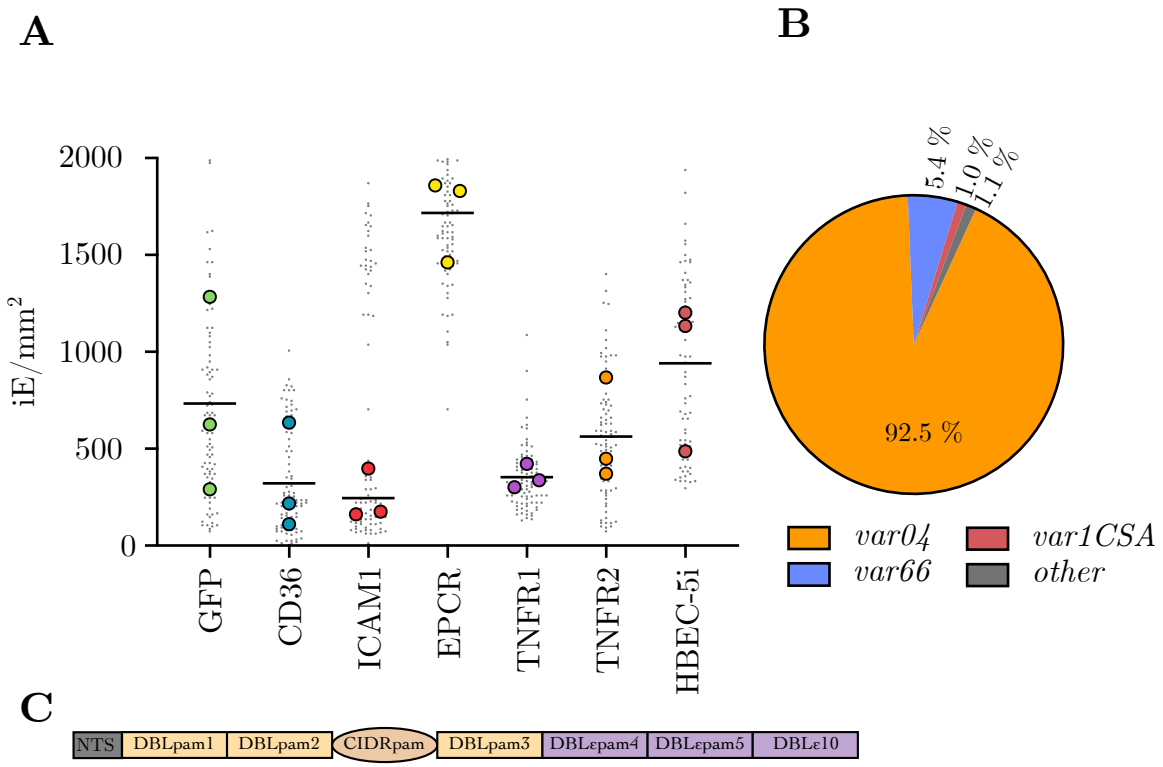


Figure 3.11: **Static cytoadhesion of IT4var04-HA^{endo} A:** Static binding assay of IT4var04-HA^{endo} against ECRs on CHO cells. Statistic with nonparametric Kruskal-Wallis test for comparison of each sample against the CHO-GFP control. **B:** *Var* expression profile of IT4var04-HA^{endo}. **C:** Domain structure of *var04*.

The IT4var04-HA^{endo} SLI line selects for the expression of var2CSA, the across isolates highly conserved placental malaria associated *Pf*EMP1 variant. CSA is absent on the CHO-745 cell line used for the transfection of CHO-GFP, CHO-ICAM1, CHO-TNFR1 and TNFR2, but present on the CHO-K1 cell line used for CHO-EPCR (Methods: 2.1.0.2) as well as on the immortalized human brain endothelial cellss (HBEC-5is). The expected cytoadhesion to CHO-K1-ECPR, as well as HBEC-5is was observed at high rates of 1717 iEs/mm^2 and 940 iEs/mm^2 respectively (Fig. 3.11, A). However, various degrees of cytoadhesion could be observed for all CHO-745 derived ECRs cell lines as well. Out of the five additionally tested cell lines, CHO-GFP, which does not present any recombinant protein on the outer cell membrane showed the highest binding

with 733 iEs/mm^2. This was followed by CHO-TNFR2 (562 iEs/mm^2), CHO-TNFR1 (353 iEs/mm^2), CHO-CD36 (320 iEs/mm^2) and CHO-ICAM1 (245 iEs/mm^2). No significant p-values could be determined, as the replicate values for the control exhibit a hight deviation (σ = 505 iE/mm^2), as well as a binding affinity in the same magnitude as the other samples. The transcriptome analysis of IT4var04-HA$^{\text{endo}}$ showed a transcription of the target *var04* gene of 92.5 %, followed by *var66* with 5.4 % and *var1CSA* with 1.0 % (Fig. 3.11, B).

3.1.4 IT4var19-HA^{endo}

IT4var19-HA^{endo} was of special interest, as its DC8 together with DC13 domain cassette are enriched in patients of severe and cerebral malaria [86, 87, 138]. In our own group Yifan Wu showed that a dominantly *var19* expressing IT4 parasite line would also strongly bind to CHO-ICAM1 cells (unpublished). The line was selected for *var19* expression by panning five rounds over TNFα activated primary human brain endothelial cell (HBMEC) and once over CHO-K1-EPCR [139]. TNFα activated HBMEC were shown to display EPCR and ICAM-1 on the surface [140]. Binding assays of the SLI activated IT4var19-K2-HA^{endo} however did not display the widely published EPCR adhesion [85, 141, 142], nor did it adhere to CHO-ICAM1 (Fig: 3.13, A). An immunofluorescence assay (IFA) of acetone fixed trophozoites, showed through anti-HA staining, that the IT4var19-HA fusion protein was expressed in IT4var19-K2-HA^{endo} line (Fig. 3.13, B ○). A simultaneous stain against knob-associated histidine-rich protein (KAHRP), equally indicated the presence of knobs.

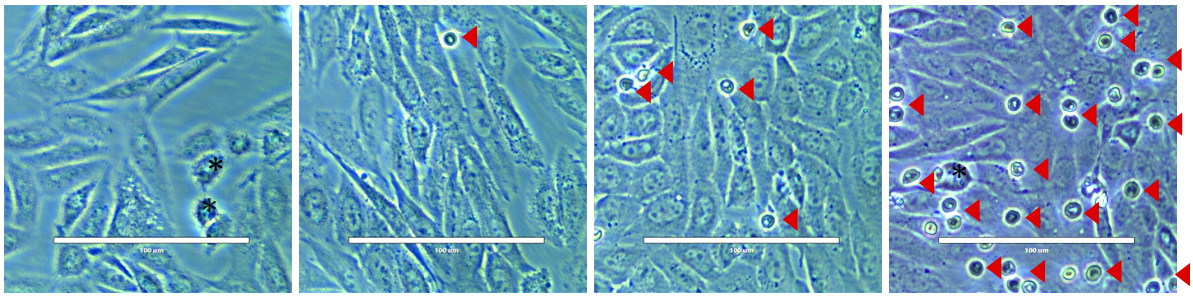


Figure 3.12: **Binding enrichment of IT4var19-K2-HA^{endo}**. Four rounds of subsequent binding enrichement (panning) of IT4var19-K2-HA^{endo} over CHO-K1-EPCR cells. ∗: apoptotic CHO cells. ◀: bound iEs (exemplary). Scale bar = 100 µm. Round 1–3 were kindly performed by Yifan Wu.

Since the RNA-seq *var* gene profile showed that *var19* was with 79.5 % the dominantly expressed *var* gene (Fig. 4.5, A ○), a trypsin digest of surface exposed iE proteins was conductedm which indicated, by the absence of a protected fragment, that *Pf*EMP1 was not present in the outer erythrocyte membrane (Fig. 3.13, B ○,

kindly performed by Jakob Cronshagen). As a trypsin digest is not sensitive enough to completely exclude *Pf*EMP1 on the iEs surface, it was tried to enrich the IT4var19-K2-HA^{endo} line over CHO-K1-EPRC cells, to select for potential cytoadherent members of a majority non-binding population. After three rounds of enrichment, a first distinct increase of bound parasites was observed, with extensive binding after the fourth round (Fig. 3.12). A fifth round did not lead to a discriminable binding increase. Subsequently, the parasites binding phenotype was maintained by panning them monthly, while in culture.

The binding enriched IT4var19-K2-HA^{endo}-P5-EPCR expressed with 93.2 % *var19* a higher percentage of *var19*, however, over four replicates between the unenriched and enriched IT4var19-K2-HA^{endo}, no significant difference in total *var* gene expression ($p = 0.34$) nor in *var19* expression ($p = 0.34$) could be observed (Fig. 4.5, C; App. A.4). A subsequent trypsin digest showed that *Pf*EMP1 was now detectable on the iE surface of the enriched IT4var19-K2-HA^{endo}-P5-EPCR (Fig. 3.13, A ◇). Similarly the parasites now displayed the expected binding phenotype (Fig. 3.13, A ◇). IT4var19-K2-HA^{endo}-P5-EPCR bound CHO-ICAM1 cells at 666 iEs/mm^2 and CHO-K1-EPCR at 1172 iEs/mm^2.

This binding phenotype could not be observed when shear stress was applied. For a the whole investigated shear stress range from 0.9 to 6 dyn/cm^2 no binding was observed for iEs over CHO-ICAM1. For CHO-K1-EPCR cells, a total 36 iEs/mm^2 where bound after 10 minutes at the lowest shear stress of 0.9 dyn/cm^2.

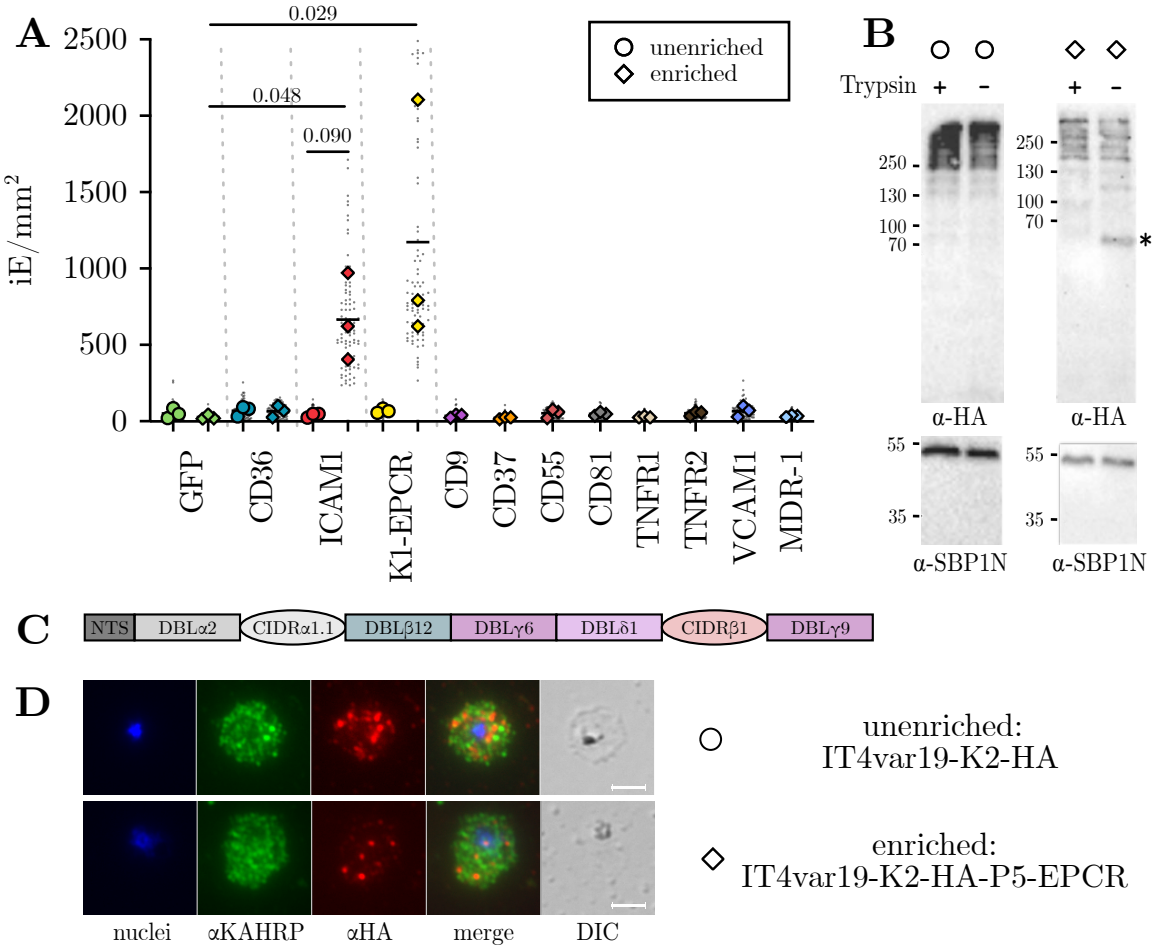


Figure 3.13: **Binding comparison of IT4var19-K2-HA^{endo} against IT4var19-K2-HA^{endo}-P5-EPCR**. **A:** Static binding assay of iE on human receptor expressing CHO cells. Statistis with nonparametric Kruskal-Wallis test for comparisons unenriched (○) / enriched (◇) and for each receptor against the respective CHO-GFP controls. **B:** Trypsin digest of erythrocytes surface proteins. Western blot with α-HA antibodies for HA-tagged *Pf*EMP1 identification. The asterix ∗ indicates the intraerythrocytic protected *Pf*EMP1 fragment. The full length of the in the Maurers' cleft located SBP1 protein serves as control for erythrocyte cell wall integrity and the absence of intracellular trypsin. The trypsin digest was kindly performed by Jakob Cronshagen [109]. **C:** Domain structure of *var19*. **D:** Fluorescence microscopy images of acetone fixed parasites with α-HA to detect the HA-tagged *var19* and α-KAHRP to check for knobs and deletion of chromosome 2. Nuclei stained with Hoechst; DIC: differential interference contrast. Size bars 5 µm. Assays of the non-binding IT4var19-K2-HA^{endo} were kindly performed by Agnes Murk.

3.1.5 IT4var08-HA^{endo}

The binding partner for the IT4var08-HA^{endo} line could not be identified by Jana Brehmer in her PhD project [137], even though, her RNAseq results, taken immediately after successful genomic intergration of the SLI-plasmid, showed a *var08* expression of

94.4 % in the IT4var08-HA^{endo} (Fig. 4.2, A ▲) parasite line. As enrichment of the SLI line was necessary to achieve surface presentation of the respective *Pf*EMP1 in the IT4var19-K2-HA^{endo} line, a similar approach was applied to the IT4var08-HA^{endo} line. However, in contrast to var19, no binding partner for var08 is known [54]. As the CD36 binding CIDRα2–6 domains are well defined and absent in IT4var08-HA^{endo}, the initial enrichment experiments were performed on the ECRs of ICAM-1 and EPCR, which are commonly found in other A-type variants [64, 76]. Notably, the ICAM-1 binders are described to belong to a diverse set of DBLβ domains [76]. Additionally, further experiments performed in this work with *var* genes of the B/A-type *var19* and *var20* (Fig. 3.13 and 3.16) showed that binding motif-based predictions are not without fault [109]. An attempt was therefore made to enrich the IT4var08-HA^{endo} line for binding to CHO-K1-EPCR and CHO-ICAM1 cells. While four rounds of enrichment did not display any binding to the CHO-K1-EPCR cells, the IT4var08-HA^{endo} bound strongly to CHO-ICAM1 cells after the second round of enrichment, plateauing after the third round (Fig. 3.14).

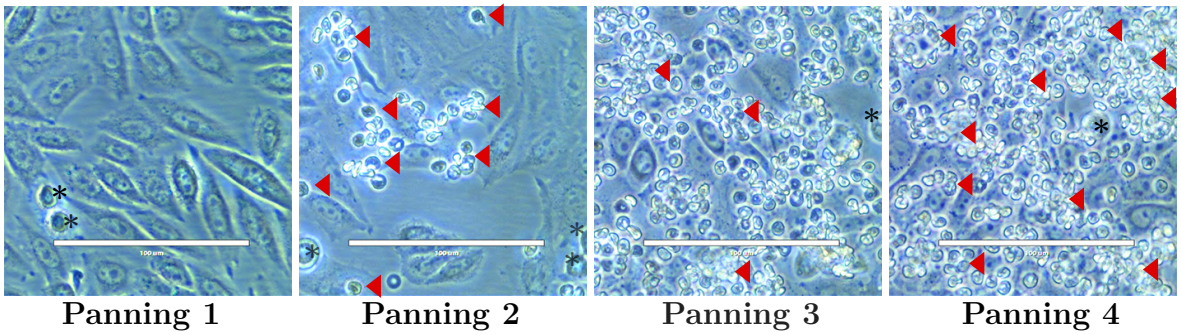


Figure 3.14: **Binding enrichment of IT4var08-HA^{endo}**. Four rounds of subsequent binding enrichement (panning) of IT4var08-HA^{endo} over CHO-ICAM1 cells. ∗: apoptotic CHO cells. ◀: bound iEs (exemplary). Scale bar = 100 µm.

Consistent with previous results by Jana Brehmer, a repetition of the not binding enriched IT4var08-HA^{endo} showed very low to no binding to the investigated receptors (Fig. 3.15, A ○), [137]. All tested CHO-ECRs as well as the control showed means ranging from 25 ± 10 iEs/mm^2 (mean ± SD) for CHO-GFP to 107 ± 35 iEs/mm^2 for

CHO-CD36 to the highest binding of 117 ± 96 iEs/mm^2 for CHO-TNFR2. Upon binding enrichment on CHO-ICAM1, increased binding to all ECRs was observed. The lowest binding of IT4var08-HA^{endo}-P4-ICAM1 (◇) was exhibited by CHO-K1-EPCR with 158 ± 78 iEs/mm^2, whereas this time the CHO-GFP control was only the second lowest with 194 ± 90 iEs/mm^2. Compared to the unenriched sample, this marks a substantial, almost 8-fold increase ($p = 0.07$) in binding to the non-ECRs control. Additionally, the IT4var08-HA^{endo}-P4-ICAM1 bound CHO-CD36 (1094 ± 427 iEs/mm^2), CHO-ICAM1 (2155 ± 646 iEs/mm^2) and to a lesser degree CHO-CD9, CHO-CD55, CHO-TNFR1, and CHO-TNFR2. As the binding enriched line showed increased binding to multiple ECRs, as well as the strong and unexpected binding to the CHO-CD36, which is not described for A-type *var* genes, lead to doubt into the integrity of the SLI-line, the unenriched parasites immediately before and after enrichment were sequenced to validate the *var* expression profile. The data revealed that the IT4var08-HA^{endo}, in prolonged *in vitro* culture had not retained the 94 % *var08* (Fig. 4.2, A ▲) expression and showed a reduced *var08* expression of only 64.7 % (Fig. 4.2, A ●). The culture was therefore termed IT4var08-HA^{endo}-LC (LC = long culture). Other *var* genes expressed in significant amounts were *var1csa* (8.6 %), *var04/var2csa* (8.2 %) and *var66* (6.3 %). After binding enrichment over CHO-ICAM1, *var08* made up only 31 % of total expressed *var* genes (Fig. 4.2, A ◆). The second most expressed *var* gene was *var04/var2csa* (12.6 %) followed by *var66* (12.0 %) and *var16* (7.4 %).

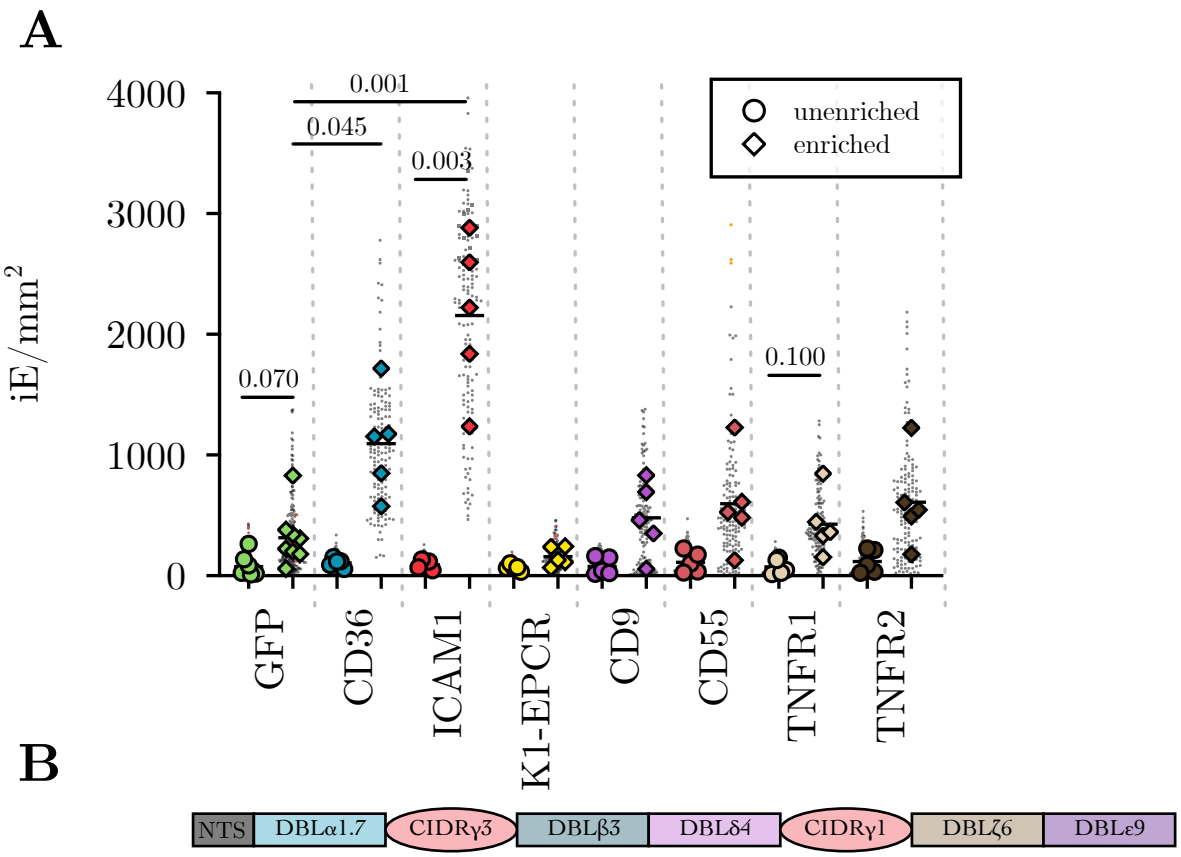


Figure 3.15: **Binding comparison of IT4var08-HA^{endo} (unenriched) against IT4var08-HA^{endo}-P4-ICAM1 (enriched)**. Statistic with nonparametric Kruskal-Wallis test for comparisons enriched/unenriched and for each receptor against the respective CHO-GFP controls. **Control LC ○**: IT4var08-HA^{endo}. **P4-ICAM1 ◇**: IT4var08-HA^{endo} enriched four times over CHO-ICAM1. **B:** Domain structure of *var08*.

3.1.6 IT4var20-HA^{endo}

The IT4var20-HA^{endo} line was designed to mutually exclusively express IT4var20 through genetically adding the SLI-cassette at the 3' genomic region of the target gene. As described further in section 4.1.4 , it was later discovered that our IT4var20-HA^{endo} line deviates from the IT4 reference genome, as it is in fact a chimera with the 3'-terminal IT4var27 and an N-terminal IT4var20. It is made up of the intracellular ATS, as well as the membrane proximal CIDRβ6 and DBLδ1 of IT4var20, followed by the membrane distal DBLγ5, DBLβ5, CIDRα3.1, DBLα0.6 and NTS. The first binding assays of IT4var20-HA^{endo} were performed, before the RNA-seq analysis was available. As the expected distinct EPCR binding phenotype induced by the IT4var20-CIDRα1.1 domain could not be observed (Fig. 3.16), an enrichment of the IT4var20-HA^{endo} over CHO-K1-EPCR was performed to potentially enrich for surface presentation of the ex-

pressed *Pf*EMP1 as it was required for IT4var19-HA^{endo} (See. 3.1.4). Four successive rounds of panning led only to a weak increase in CHO-K1-EPCR binding, starting from initially, only sporadically binding starting culture. The resulting IT4var20-HA^{endo}-P4-K1-EPCR showed increased cytoadhesion with CHO-ICAM1 (1678 ± 92 iEs/mm^2) (mean $\pm$ SD) compared to the already high basal binding of binding to CHO-ICAM1 with 1071 ± 349 iEs/mm^2. Binding to CHO-CD36 behaved similarly with a respective increase from 330 ± 251 iEs/mm^2 to 591 ± 90 iEs/mm^2. A less pronounced trend could be observed for CHO-CD9, CHO-CD55, CHO-TNFR1 and CHO-TNFR2, for all of which the mean of the enriched culture lay above the unenriched. The two- to three biological replicates, as well as the small differences in the means are not sufficient to draw conclusions. The CHO-GFP control and CHO-K1-EPCR showed low baseline levels of 71 ± 55 iEs/mm^2 and 48 ± 22 iEs/mm^2, respectively. Upon binding enrichment over CHO-EPCR, no specific increase of binding to CHO-K1-EPCR was detected. The binding to CHO-K1-EPCR remained negligible at 59 ± 20 iEs/mm^2, which was lower

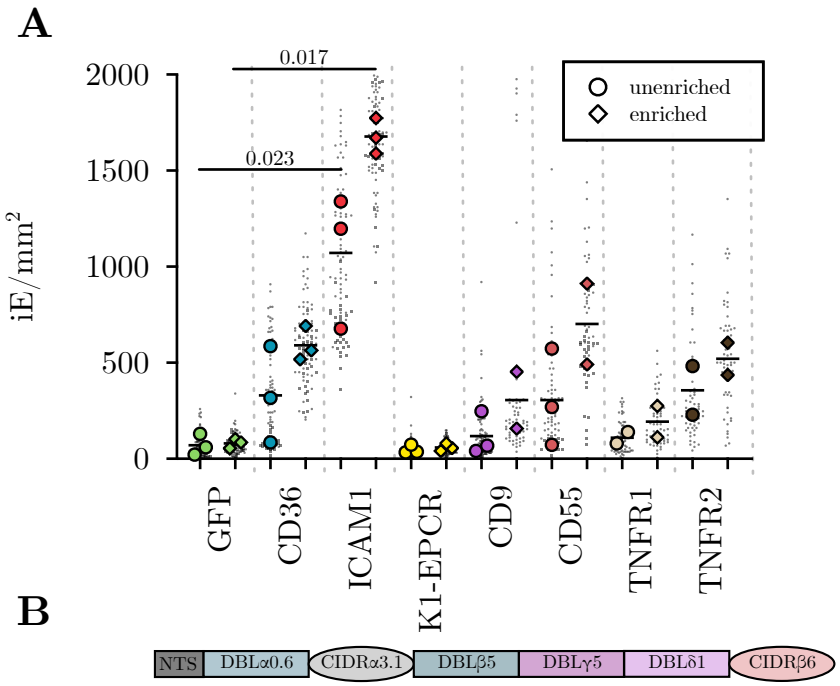


Figure 3.16: **Binding comparison of IT4var20-HA^{endo} (unenriched) against IT4var20-HA^{endo}-P4-EPCR (enriched).** **Unenriched ○**: IT4var20-HA^{endo}. **enriched over K1-EPCR ◇**: IT4var20-HA^{endo}-P4-EPCR enriched four times over CHO-K1-EPCR. Statistic with nonparametric Kruskal-Wallis test for comparisons enriched/unenriched and for each receptor against the respective CHO-GFP controls. **B:** Domain structure of the fusion gene *var20–27*.

than the CHO-GFP control (81 ± 24 iEs/mm^2). However, the selection process resulted in an increase in binding to other receptors. The IT4var20-HA^{endo}-P4-EPCR population retained and increased its high affinity for CHO-ICAM1 (1678 ± 92 iEs/mm^2). Additionally, elevated binding was observed for CHO-CD55 (701 ± 297 iEs/mm^2) and CHO-CD36 (591 ± 90 iEs/mm^2) compared to the unenriched condition.

3.1.7 IT4var66-HA^{endo}

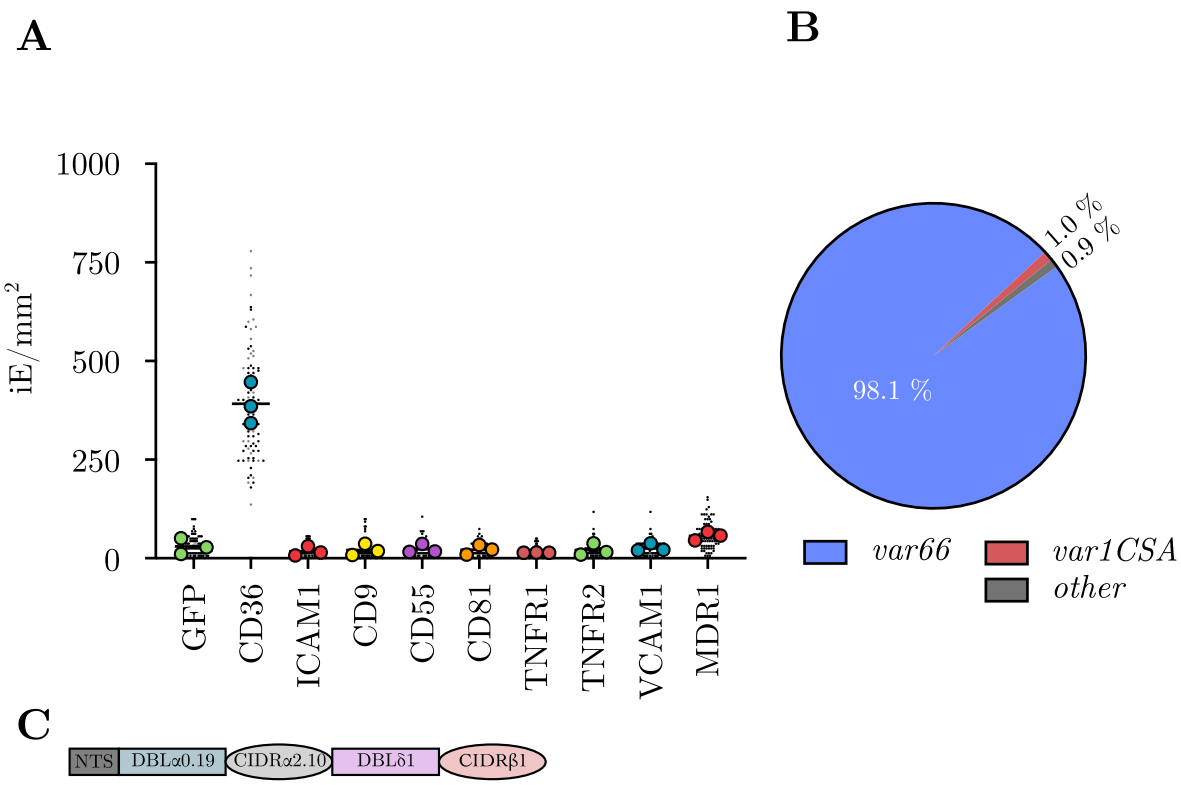


Figure 3.17: **Cytoadhesion of IT4var66-HA^{endo} A:**.Static binding assay of IT4var66-HA^{endo} against ECRs on CHO cells. Statistic with nonparametric Kruskal-Wallis test for each receptor against the respective CHO-GFP control. **B:** *Var* expression profile of IT4var66-HA^{endo}. **C:** Domain structure of *var66*.

The RNA-seq data revealed that the IT4var66-HA^{endo} line showed the highest percentage of the activated target *var* gene compared to other SLI-var lines investigated in this work. *var66* made up 98.1 % followed by *var1CSA* with 1 % and the sum of the remaining *var* genes with 0.9 % (Fig. 3.17, B). *var66* is a classical C-type *var* gene with a CD36-binding CIDRα2.10 domain in position 3 of the *Pf*EMP1 [64]. This binding phe-

notype could be replicated with IT4var66-HA^{endo} iEs binding to CHO-CD36 cells under static conditions at 391 ± 52 iEs/mm^2. Out of the additionally tested CHO-ECRs, only CHO-MDR1 (56 ± 11 iEs/mm^2) showed slightly increased adhesion compared to the CHO-GFP control (30 ± 20 iEs/mm^2). As the mixed IT4 wt cultures expressed mostly *var66* (Fig. 3.6, A), the flow binding assay for the IT4var66-HA^{endo} lead to similar results. However, in this cases not a single iE bound to CHO-ICAM1 and the total amount of iEs bound to CHO-CD36 was slightly higher than that by IT4 wt. The highest amount bound again at 0.9 dyn/mm^2 with 1030 iEs/mm^2. Rolling was observed a shear rates from 3 – 1.5 dyn/mm^2 with mostly stationary iEs at 0.9 dyn/mm^2 (Fig. 3.18). The tracked data revealed a large deviation between the replicates 1 and 2, especially at 2.0 dyn/mm^2 (Fig. 3.19). Whilst iEs in replicate 1 showed an average velocity of 51.5 µm/min, replicate 2 was only 19.3 µm/min. A look at the video of the tracked particles revealed, that the software had problems tracking the iEs in this replicate. This was previously seen at higher shear rate >2 dyn/mm^2 which is why those are generally excluded from the analysis. At shear rates of 1.5 dyn/mm^2, the velocity far exceeded that of IT4 wt with 56 µm/min whilst it was roughly the same at 0.9 dyn/mm^2 with 30.5 µm/min. As tracked distance was calculated from the same data as the the average velocity, the outliers appeared also for replicate 2 at 2 dyn/mm^2. Here, replicate 2 lies with 19.9 µm (Fig. 3.19, B) tracked distance even below statically bound IT4var01-HA^{endo} over CHO-ICAM1 which where tracked at 24.8 µm at 2 dyn/mm^2 (Fig. 3.10, B).

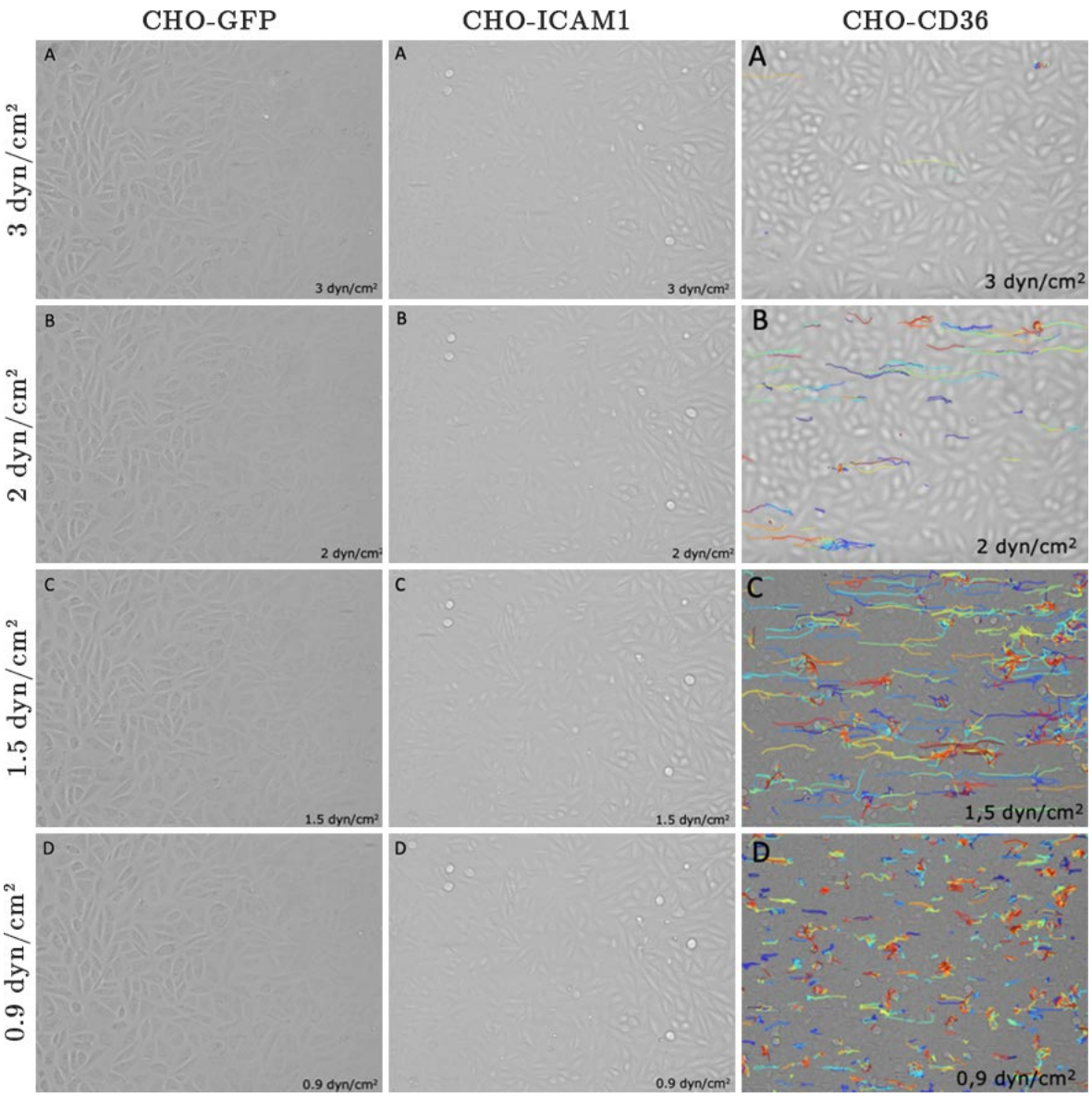


Figure 3.18: **Cytoadhesion of IT4var66-HA^{endo} under shear stress**. iEs flow unidirectionally from left to right at a shear rate of $3 - 0.9\,\mathrm{dyn/mm^2}$. Left: CHO-GFP as control of CHO without ECR on surface, Center: CHO-ICAM1, Right: CHO-CD36. Paths of iEs tracked over >10 frames are marked in color. Experiments performed by D. Rauchberger.

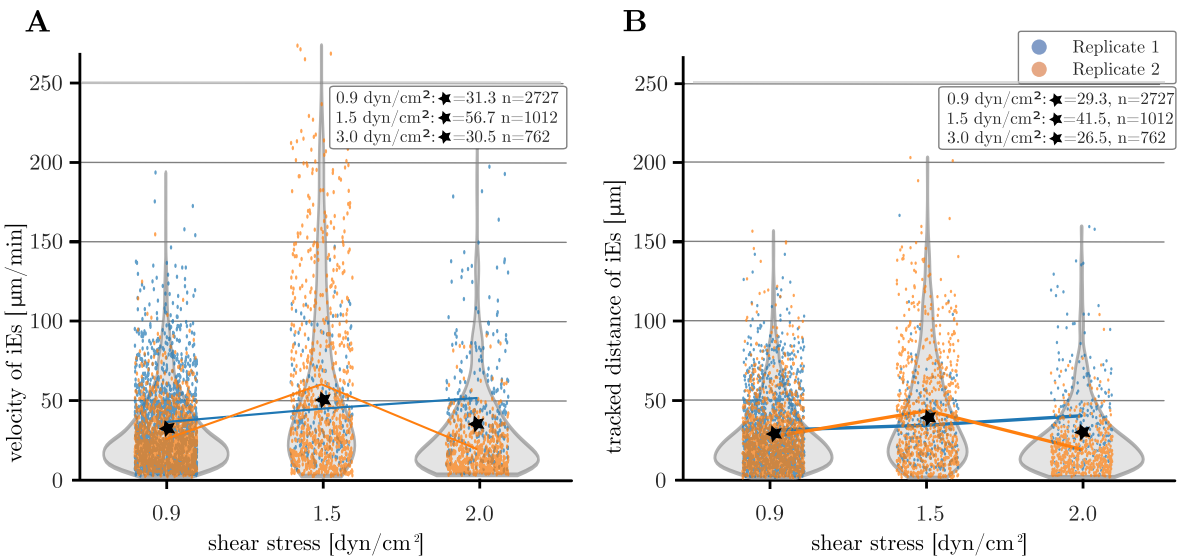


Figure 3.19: **Rolling velocity and distance of IT4var66-HA^{endo} under shear stress**. **A:** Rolling velocity of iEs in µm/min and **B:** tracked rolling distances of iEs for shear rates of 0.9, 1.5 and 2 dyn/mm^2. ★ = mean; n = tracked iEs; Experiments performed by D. Rauchberger.

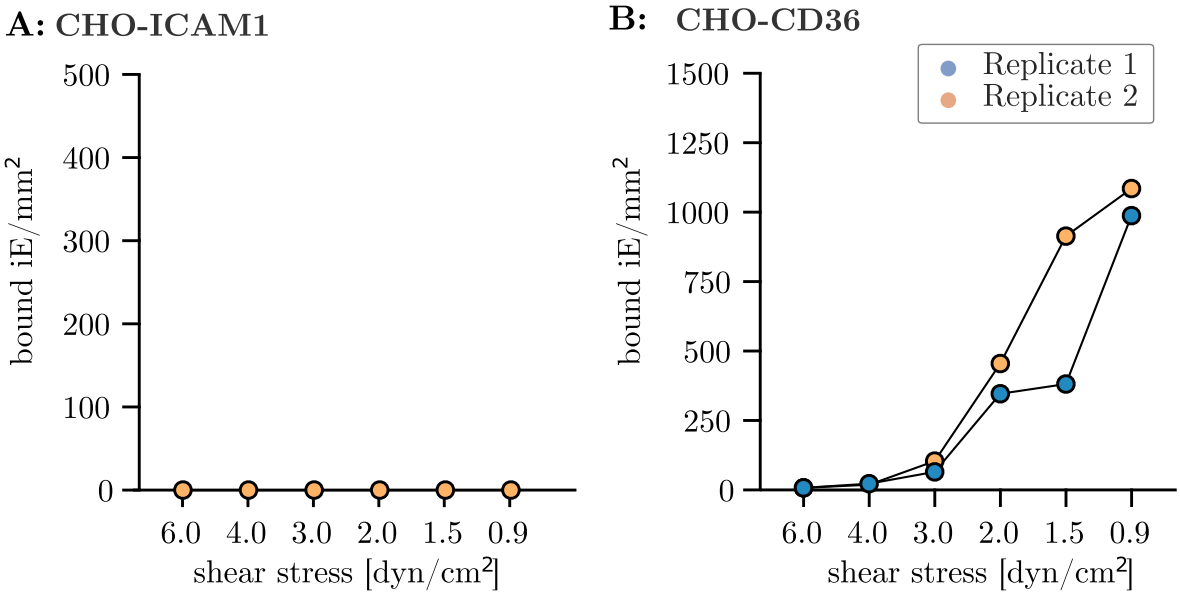


Figure 3.20: **Bound IT4var66-HA^{endo} iEs under shear stress**. Number of bound iEs in iE/mm^2 after 10 min of respective shear stress decreasing from 6.0 – 0.9 dyn/mm^2 over **A:** CHO-ICAM1 and **B:** CHO-CD36 cells; Experiments performed by D. Rauchberger.

3.2 Discussion

Var01 (PfIT_060021400) and *var16* (`PfIT_120024500`) are fairly similar based on their domain structure (Fig. 3.6, C and Fig. 3.7, C) and are both centrally located on their respective chromosomes. Their major differences are their upstream regions with *var01* defined as C-type and *var16* as B/C type *var* gene. Their CIDRα2–6 domains predicted both *var* genes to bind CD36 as common binding phenotype for C and B/C type *var* genes (Tab. 1.1) [143, 144]. Additionally both lines share a DBLβ5 domain which has been identified as an ICAM-1 binder in multiple studies [77, 144]. Even though the two *var* genes share a similar domain structure and sequence, IT4var01-HA^{endo} shows higher CD36 binding than ICAM-1 with the opposite being the case for IT4var16-HA^{endo}, where ICAM-1 is by far the most prominent binding partner. Janes *et al.* saw the same with an *var01*-enriched line (3G8) and an *var16*-enriched IT4 line (ItG-ICAM1) where the *var16*-enriched line bound immobilized ICAM-1-Fc about twice as well as the *var01* line. In their additional binding assay against CHO-745 cells expressing ICAM-1, the *var16* enriched line showed ~10 % lower binding than the *var01* enriched line. Considering that *var16* made up only 66 % of the total *var* genes in their *var16*-enriched line, compared to the *var01* line with 99 % *var01* this would still indicate a higher binding affinity of the *var16* line to ICAM-1 than that of the *var01* candidate. Experiments from Bengtsson *et al.* attest DBLβ5 from *var16* the highest ICAM-1 binding affinity out of a total of nine different tested recombinantly expressed DBLβ5 domains. Unfortunately, the study did not include IT4var01-DBLβ5 as a comparison [76]. The same two *var01* and *var16* enriched lines from Janes *et al.*, were also tested for CD36 binding, where both lines showed a high binding affinity without a major difference between the two lines as well as against VCAM-1, where their lines did not cytoadhere in contrast to our results [78]. We could identify significant CHO-VCAM1 cytoadhesion in IT4var01-HA^{endo} and IT4var16-HA^{endo} with 910 and 630 iEs/mm^2 respectively (Fig. 3.6 and 3.7) but not in var19-K2 and IT4var66-HA^{endo} (Fig. 3.13 and 3.17). The *Pf*EMP1 domains responsible for VCAM-1 cytoadhesion has not yet been identified, but a possible candidate could be the DBLβ5 as it is present

in the two tested binding lines and absent in the latter non-binding one [92].

Both IT4var01-HA^{endo} and IT4var16-HA^{endo} show that a single type of expressed *var* gene facilitates binding to at least four endothelial receptors with a potential of five if TNFR2 would become statistically significant with more biological replicates. This corresponds well with data from Ockenhouse *et al.* who found that parasite lines enriched over multiple cell adhesion molecules (CAMs) and subsequently clonally isolated, were also able to bind ICAM-1, VCAM-1 and CD36 without testing for CD55 [92].

The IT4var04-HA^{endo} line, which expresses VAR2CSA (*var2csa*), exhibited the expected preferential binding to cells presenting surface CSA. This specific adhesion was observed in both CHO and endothelial cells (Fig. 3.11, A) and aligns with the well-established CSA-binding phenotype of VAR2CSA, the primary placental adherence receptor [14, 97, 98]. The CSA specificity of IT4var04-HA^{endo} was further confirmed by Jakob Cronshagen via cytoadhesion experiments on spotted decorin (bovine-derived CSPG with CSA side chains); moreover, adhesion was successfully inhibited by the addition of soluble CSA [109, 145]. However, substantial background binding was also observed across CHO-745-derived cell lines, including negative controls. Adhesion of iEs to CHO-745 wild-type cells has been reported previously by Andrews et al. (2005), who challenged the validity of CHO-745 as a genuinely inert control [146]. Similarly, Metwally et al. (2017) described a CHO-745-binding phenotype, demonstrating the enrichment of non–CHO-745-binding IT4 and 3D7 wild-type strains on CHO-745 controls. Although this enrichment altered the *var* expression profile in both cultures, *var2csa* was not enriched in either case [110]. Specifically, *var34* remained the dominant transcript in the IT4 line both before (~60 %) and after (~70 %) enrichment. The CHO-745-enriched line also exhibited significant increases in *var28* (~8 % of total *var* genes), *var32a/b* (~15 %), *var28* (~1 %), and *var14* (~1 %). Neither variant contained discernible levels of *var04/var2csa* (< 0.2 %), and no single *var* gene was common to both CHO-745-binding lines (IT4var04-HA^{endo}, Fig. 3.11, B, and the panning-enriched IT4–CHO-745) [110]. Although CHO-745 cells are typically characterized as CS-deficient due to the absence of xylosyltransferase required for CSPG biosynthesis,

it was shown that CS remains present on the cell surface, albeit at only 3 % of baseline levels [147]. It is therefore plausible that this residual CS expression supports low levels of *var04/var2csa*-mediated adhesion. Given the complexity of var04/var2csa-mediated binding, which involves a minor CSA-binding channel and two non-continuous binding sites [98], interactions with other components of the CHO glycocalyx cannot be excluded.

The *var* gene profile of IT4var19-K2-HA^{endo} was skewed by a high percentage of *var66* (44.9 %) expression in the first replicate of IT4var19-K2-HA^{endo}, where the cell line was under Neomycin pressure for less than a month. The three subsequent replicates of the prolonged cultured IT4var19-K2-HA^{endo} parasites showed that *var66* made up less than 5 % of their total *var* genes (App. A.4). Additionally, a *var66* phenotypical CD36 binding could not be observed (Fig. 3.17 and 3.13, A). The delayed disappearance of the wild type associated *var66* expression could be and indication of a low 'off' rate of *var66*. While exact switching rates for this *var* gene are not known, central *var* genes have been described to have lower 'off' rates than their telomeric counterparts [136, 148].

Similarly to *in vitro*, where *Pf*EMP1-mediated adhesion does not benefit the parasite's survival, this can also be the case in rare *in vivo* settings. One such case was described by Bachmann and colleagues who found a high parasitaemia of non-*Pf*EMP1 presenting iEs in a semi-immune patient that recently underwent a splenectomy [38]. In this case, the parasites were not dependent on vascular adhesion to avoid clearance by the spleen and could therefore be selected by the host immune system for the less immunogenic non-*Pf*EMP1 presenting variants. Similarly, when single clones are picked *in vitro* from parental laboratory strains, these clones can vary vastly in total *var* gene expression [49, 149]. An equal transcription count of total *var* gene and *var19* transcription counts for the enriched and unenriched IT4var19-K2-HA^{endo} lines showed that the differing binding phenotype was not mediated through *var* gene transcription (Fig. 4.5, C). A non-quantitative IFA with the HA-tagged var19-*Pf*EMP1 also showed the protein translated in both lines (Fig. 4.5, D).

The IT4var08-HA^{endo} line expresses a complex A-type *var* gene characterized by

the domain head structure NTS-DBLα1.7-CIDRγ3-DBLβ3-DBLδ4. RNA-seq analysis immediately after the integration confirmed that the correct *var08* gene was expressed mutually exclusively (94.4 % of total *var* genes; Fig.,4.2, A, ▲). Consistent with the initial characterization by J. Brehmer, the unenriched SLI cell line displayed a non-binding phenotype against the tested panel of ECRs [137]. As initial trypsin surface digests were unsuccessful in generating conclusive evidence on whether the var08-*Pf*EMP1 molecule of the correct size is present on the surface, a binding enrichment was performed, as was successfully done for IT4var19-K2-HA^{endo}.

As the binding enrichment over CHO-ICAM1 cells led to an adherent IT4var08-HA^{endo}-enriched phenotype, the full set of CHO-ECRs was tested again. However, the enrichment process also resulted in a broad binding profile, including increased binding to the supposed non-binding control CHO-GFP. Other than the already observed CHO-ICAM1 adhesion, the IT4var08-HA^{endo}-P4-ICAM1 line exhibited strong binding to CHO-CD36 (1094 iEs/mm^2), a phenotype typically restricted to B- and C-type *var* genes possessing CIDRα2–6 domains [64, 144]. A subsequent repetition of the trypsin surface digest of iEs by Charlotte Wapler of Lab Group Bachmann and Susann Ofori of RG Host-Parasite Interaction (unpublished), showed a protected *Pf*EMP1 fragment indicating surface exposure of tagged HA-tagged *Pf*EMP1 in both the IT4var08-HA^{endo} as well as the IT4var08-HA^{endo}-P4-ICAM1 parasite lines. It can therefore be excluded that one of the eight investigated ECRs is the binding partner of *var08*, and the observed binding of IT4var08-HA^{endo}-P4-ICAM1 is not owed to surface enrichment of *Pf*EMP1 but to the enrichment of the mutually exclusive expression defective (MEED) phenotype. In short, the data revealed that cultivating the SLI-line under Neomycin pressure did not succeed in maintaining the mutually exclusive expression phenotype of the parasite line. A subsequent IFA of IT4var08-HA^{endo} showed, however, that all inspected iEs also express the HA tag fused to var08. Although the genomic instability of the IT4var08-HA^{endo} makes it not suitable for the investigation of *var08* cytoadhesion, it could serve as a model to investigate mutually exclusive expression of *var* genes. The RNA-seq data of the various stages of the IT4var08-HA^{endo} line were therefore further analyzed in the genomic of *var* genes chapter (Chapt. 4).

The IT4var66-HA^{endo} is a classical C-type *var* gene containing the widely published CD36-binding CIDRα2.10 domain (Fig. 3.17, C) [61, 144]. Even though the three replicates as well as the chosen non-parametric Kruskal-Wallis with Dunn's multiple testing correction were not sufficient to generate a significant p-value for CD36 cytoadhesion, the CD36 binding phenotype can be validated by the results (Fig. 3.17, C). Although the cytoadhesion for IT4var66-HA^{endo} to CD36 was with only (391 ± 52 iEs/mm^2) on average much lower than the CD36 binding of IT4var01-HA^{endo} (1460 ± 782 iEs/mm^2) and slightly lower than that of IT4var16-HA^{endo} (540 ± 211 iEs/mm^2). Despite the high diversity of CIDRα2–6 domains, which share less than 33 % pairwise sequence similarity, they retain a conserved hydrophobic pocket that binds to a phenylalanine residue (F153) at the distal tip of the CD36 receptor. This variety has been experimentally shown to affect the cytoadhesion strength of the different CIDRα2–6 domain-ECRs combinations [64]. As we lack quantitative information about the amount of surface exposed *Pf*EMP1, our experimental set-up is not capable of differentiating the binding strength of different domains across parasite lines.

The binding analysis under shear-stress identified distinct differences between CD36 and ICAM-1-mediated cytoadhesion. Flow assay of the ICAM-1-CD36 dual binder line IT4var01-HA^{endo} showed in the flow regime between $0.9 - 2.0\,\mathrm{dyn/cm^2}$ iEs bound firmly to CHO-ICAM1, while the same parasite line displayed a rolling phenotype over CHO-CD36 cells (Fig. 3.9 and Fig 3.10). The increase of rolling velocity and distance proportional to the increase could be observed for the CD36-only binder *var66* in the IT4var01-HA^{endo} and as the major *var* gene in the IT4 wt. Subsequent experiments with more ICAM-1 binding parasite lines would strengthen the case for ICAM-1 as a mediator of mostly static adhesion, but were not available at the time of the experiments.

During the flow assays, significant technical challenges with the IBIDI pump system and tracking software were encountered, particularly at higher shear stress levels where maintaining consistent focus and tracking became problematic. The low maximal frame rate of one image every three seconds caused the trackdem R-software to frequently fail to detect infected erythrocytes iEs when the microscope lost focus during extended

runs or high-velocity phases, leading to incomplete data capture for shear stresses above 3 $^{dyn}/_{cm^2}$. Furthermore, while we successfully measured binding at 0.9 $^{dyn}/_{cm^2}$, the current setups tubing configuration prevented us from testing shear rates below this threshold (0.1–0.9 $^{dyn}/_{cm^2}$). Consequently, the inability to reliably track high-velocity rolling events and the lack of low-shear data likely resulted in an underestimation of binding events for weaker receptor-ligand interactions.

Published biochemical and structural studies have previously classified the DC8 in *IT4var19*-encoded *Pf*EMP1 as an EPCR-specific binder, with the DBLβ12 domain predicted to interact with complement receptor qC1qR rather than ICAM-1 [134, 150, 151]. Avril *et al.* identified cytoadhesion of a IT4var19 parasite line, which was generated by enriching a majority *var16* expressing cell line (ItG-ICAM1) over HBMEC, to immobilized EPCR but not immobilized ICAM-1. Although upon working with cell-to-cell assays, the authors saw moderate cytoadhesion to CHO-ICAM1, and a reduction of HBMEC cytoadhesion by 30 % upon addition of anti-ICAM-1 antibodies. However, they did attribute this cytoadhesion to ICAM-1 but rather to residual *var* genes of the progenitor ICAM-1 adherent ItG-ICAM1 cell line [134]. Furthermore, the authors used a DBLβ12-coupled Dynal Bead binding assays to immortalized HBMEC also suggested that CIDRα1.1 is not the only domain involved in cytoadhesion to brain ECs [134]. A subsequent study by Gillrie *et al.*, who worked with the same binding enriched IT4var19 line, concluded that *var19* must cytoadhere through an additional receptor to EPCR alone, as they were unable to inhibit binding to various endothelial cells where EPCR was either blocked through anti-EPCR antibodies, or knocked down through siRNA [152].

IT4var19-K2-HA^{endo}-P5-EPCR did not show CHO-ICAM1 adhesion under shear stress, even though it bound the cells under static conditions at 666 iEs/mm^2 (Fig. 3.13, A). This stands in stark contrast to the other ICAM-1 binder IT4var01-HA^{endo}, which bound CHO-ICAM1 only moderately stronger (36 %, 910 iEs/mm^2, Fig, 3.6) than IT4var19-K2-HA^{endo}-P5-EPCR under static conditions but also displayed a strong cytoadhesion under shear stress with 300 iEs/mm^2 (10 minutes of 0.9 $^{dyn}/_{cm^2}$, Fig. 3.8). Generally, the flow experiments showed, that shear rates below 0.1–1.0 $^{dyn}/_{cm^2}$ should

be investigated as well, which requires a technical modification of the used IBIDI Pump system with a different tubing set. This is especially important for var19-EPCR cytoadhesion, which in our experiments only slightly bound after 10 minutes of $0.9\,^{\mathrm{dyn}}/_{\mathrm{cm}^2}$. Similar results were obtained by Bernabeu *et al.* who, in a 3D brain microvessel, observed IT4var19 mediated cytoadhesion only at shear rates shear rates of $\leq 0.9, ^{\mathrm{dyn}}/_{\mathrm{cm}^2}$ [153].

Further experimentation is necessary, to determine whether the suspected novel DBLβ12-ICAM1 cytoadhesion differs under under dynamic binding conditions compared to the more canonical DBLβ5-ICAM-1 binding phenotype. Other than replication of flow binding assays of IT4var19-K2-HA$^{\mathrm{endo}}$-P5-EPCR under a more suitable shear range of $0.1–1.0\,^{\mathrm{dyn}}/_{\mathrm{cm}^2}$, single cell force spectroscopy (SCFS) could be a promising tool to further characterize the dynamic binding behavior of *Pf*EMP1–ECRs bonds. By linking a single iEs to the cantilever of an atomic force microscopy (AFM), the force between individual receptor-antigen bonds can be measured.

In this set-up, a single SLI *var*-monovariant iE is immobilized on a concanavalin A–coated, tipless cantilever and repeatedly brought into contact with monolayers of various CHO-ECRs, allowing rupture forces and loading-rate dependencies to be extracted for individual receptor–ligand bonds in their physiological membrane environment [137]. Studies using related AFM-based single-molecule assays have already demonstrated that CD36–iE interactions behave as classical slip bonds, whereas ICAM-1–iE interactions exhibit catch-bond behavior, with lifetimes increasing over an intermediate force range before decaying at higher loads [62, 154]. The combination of SCFS with SLI-transfectants therefore overcomes the ambiguity inherent to panning-enriched cultures, as all recorded force–lifetime pairs can be attributed to a single, genetically defined *Pf*EMP1 variant, enabling quantitative comparison of bond type (catch- versus slip-bond), off-rates and energy barrier distances across distinct *Pf*EMP1–ECR pairs, including DBLβ5– and DBLβ12–ICAM-1 interactions.

4 Genomics of SLI-transfectants

4.1 Results

4.1.1 Co-regulation of *var* proximal genes

The coexpression of proximal genes is a common phenomenon across multiple species. Approximately 10 % of human genes are transcribed by bidirectional promoters, and this fraction is even higher in yeast, which serves as a model organism for studying the coexpression of genes in pairs or larger clusters [155]. More than 400 genes are potentially coregulated in *P. falciparum* by bidirectional promoters [156]. The highest correlation is observed for head-to-head (h2h) oriented genes, with an additional inverse relationship between gene distance and expression correlation. Specifically, the shorter the distance between the 5'UTR regions, the higher the likelihood of coexpression [156]. Lavstsen *et al.* observed in their analysis of the *var* gene organization in 3D7 that most A-type *var* genes are arranged h2h with a *rifin*, and hypothesized a functional link between the encoded *Pf*EMP1s and RIFINs [47]. Follow-up studies confirmed that these gene pairs are indeed coregulated; however, the evolutionary reason for the conserved h2h *rif*-*var* architecture in the SM-associated upsA type remains unclear [157, 158]. In IT4, eight out of nine A-type *var* genes are oriented h2h with a *rifin*, while B-types are predominantly arranged tail-to-tail (t2t) (see Fig. A.2). The genomic neighborhood of C-type *var* genes, which are located in central and subtelomeric regions, is considerably more diverse (Fig. 1.4 and Fig. A.2). In this study, and in related work by our group, a multitude of RNA-seq datasets from IT4 parasite lines with diverse *var* expression profiles were available. This provided an opportunity to

screen for potential coregulation of *var* genes with their neighboring genes across 61 samples (see A.1). The resulting expression matrix was visualized as a scatterplot, with normalized expression counts for *var* genes (> 5 TPM) on the x-axis and expression levels of neighboring genes on the y-axis (see Fig. 4.1). When a *var* gene had both an upstream and downstream neighbor, both relationships were included. Correlation coefficients were then calculated based on the orientation of *var* gene groups relative to their neighboring genes.

The Pearson correlation test revealed a statistically significant co-regulation for *var* genes oriented in the h2h and head-to-tail (h2t) orientation both with $p \leq 0.001$ and correlation factors $r = 0.349$ and $r = 0.318$ respectively. The other two orientations, t2t and tail-to-head (t2h) show no correlation with r-values close to zero and $p > 0.5$ (Fig. 4.1, A and C). When subdividing the members of the *var* gene family into their respective groups, significant positive correlation could only be observed for A-type *var* genes ($r = 0.284$, $p < 0.001$) as well as E-types*var* gene and *var2csa*) ($r = 0.569$, $p < 0.001$) with their neighbors. In contrast, no similar significant transcriptional correlation was detected for group B ($r = -0.058$, $p = 0.494$) or group C ($r = 0.004$, $p = 0.959$) *var* genes, nor for the transition groups B/A and B/C.

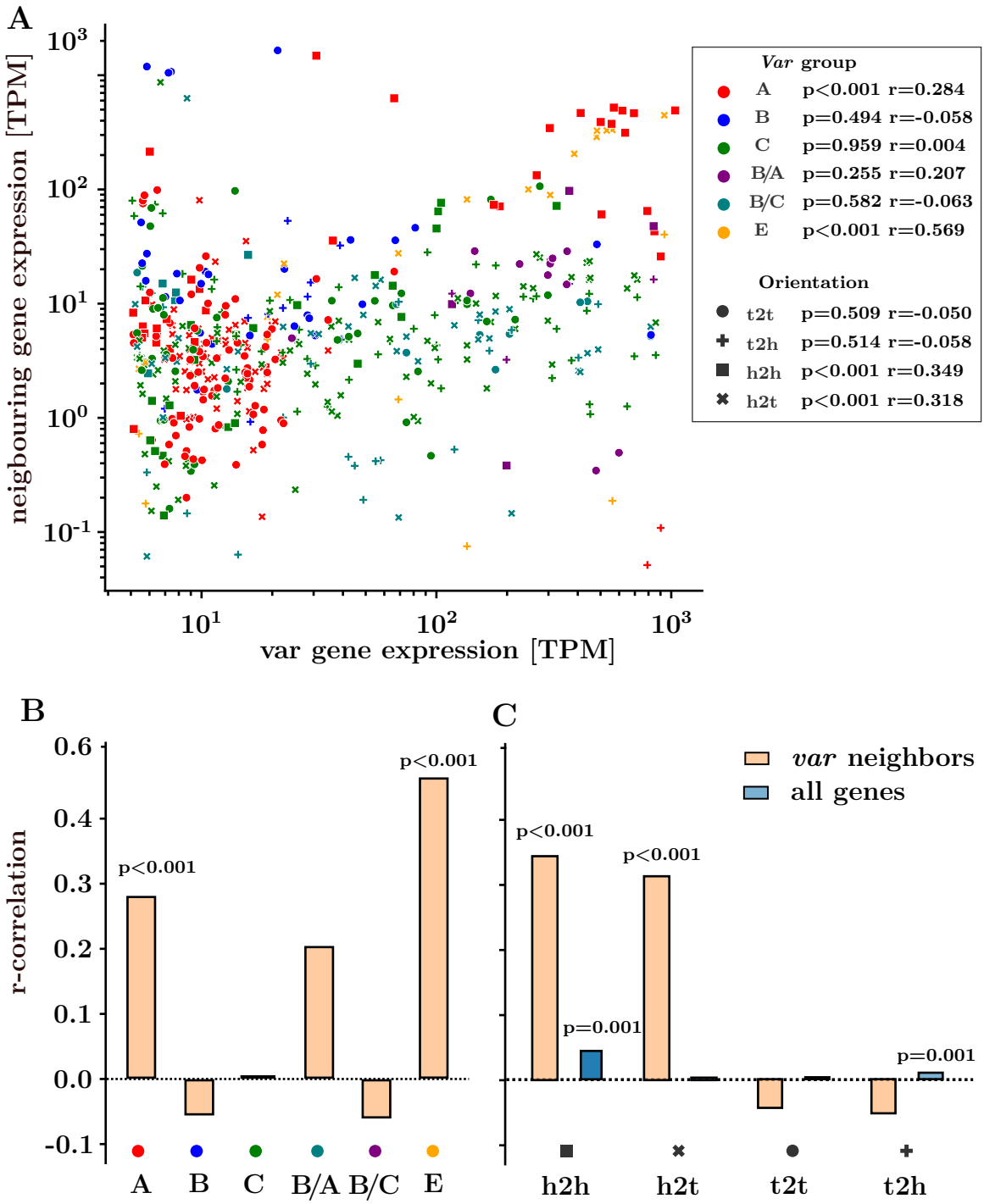


Figure 4.1: **Coexpression of neighboring genes. A:** Scatterplot of *var* expression from RNA-seq data of 61 SLI-transfectants (see A.1). *Var* expression with TPM > 5 plotted on the x-axis, whilst expression of the neighbouring gene is plotted on the y-axis. Each *var* gene is depicted as one or two markers, once each in relationship to the upstream and once to the downstream neighbour if available. Pearson correlation coefficients (r) and corresponding two-tailed p-values are provided in the legend. Possible orientations: t2t = tail-to-tail; t2h = tail-to-head; h2h = head-to-head; h2t = head-to-tail. **B:** Bar chart visualization of r-correlation scores of *var* group statistics of scatterplot from A. p-values for p $\leq$ 0.1 are depicted. **B:** Correlation of gene expression to orientation of neighboring gene as r-correlations scores for *var* genes (orange) and all genes compared (blue).

4.1.2 Defective mutually exclusive expression in IT4var08-HA^{endo}

Understanding *var* gene switching mechanisms as well as the processes governing mutually exclusive expression is crucial in the fight against the malaria disease, as it enables the parasites to systematically cycle through its antigenic repertoire, driving chronic infections and immune evasion that sustain malaria transmission. Dissecting these processes holds potential for novel interventions that disrupt antigenic variation, increasing parasite clearance by the adaptive immune system and thereby reduce disease severity [39]. Until recently, mutually exclusive expression of *var* genes of only one gene out of the multiple member *var* gene family at a time was considered the fundamental paradigm governing *Pf*EMP1 display on the surface of iEs. However, more recent single-cell transcriptomic studies have revealed that individual parasites can simultaneously express multiple *var* genes or enter states with little to no *var* transcription, challenging the strict exclusivity model [40]. Additionally, surface co-expression of two different *Pf*EMP1 variants on iEs has been directly demonstrated, facilitating binding to multiple host receptors and suggesting greater transcriptional plasticity than previously recognized [159]. The genomic analysis of IT4var08-HA^{endo} and its derivative lines with deviated *var* gene control mechanisms thus offers the opportunity to correlate changes in adhesion phenotypes and receptor specificity with shifts in *var* gene usage and modifications in the gene regulatory networks.

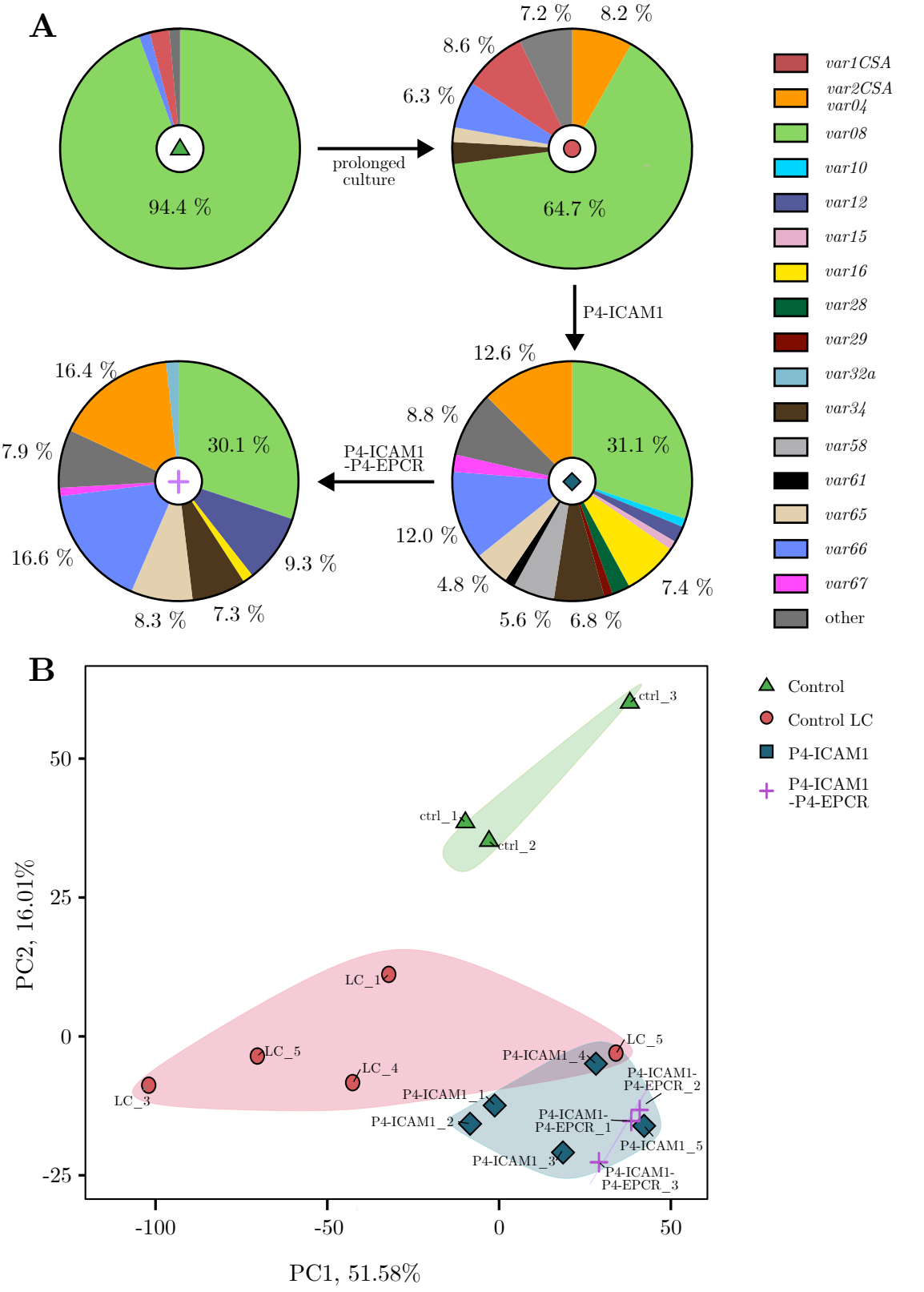


Figure 4.2: **Clustering of IT4var08-HA^{endo} before and after enrichment** Control (ctrl) ▲: IT4var08-HA^{endo}. Control LC ●: IT4var08-HA^{endo} after prolonged *in vitro* culture. P4-ICAM1 ◆: IT4var08-HA^{endo} enriched four times over CHO-ICAM1; P4-ICAM1-P4-EPCR +: IT4var08-HA^{endo} enriched four times over CHO-ICAM1 and afterwards four times over CHO-K1-EPCR. **A:** Expression profile of *var* genes. **B:** principle component analysis of RNA-seq samples with PC1 on X-axis and PC2 on Y-axis. Detailed results in Appendix A.3.

The origin of the IT4var08-HA^{endo} line is described in Chapter 3.1.5. In brief, IT4var08-HA^{endo} was generated by Jakob Cronshagen, and an RNA sample was collected shortly after plasmid integration for sequencing [79, 137]. The initial *var* expression profile of the SLI line showed the expected dominance of the targeted *var08* gene, accounting for 94.4 % of total transcripts (▲). Following prolonged *in vitro* cultivation, and as no cytoadhesion was detected in the initial binding assays, the parasites were subsequently enriched by panning over CHO-ICAM1 cells. The culture prior to enrichment is referred to as IT4var08-HA^{endo}-LC (●), while the enriched line is termed IT4var08-HA^{endo}-P4-ICAM1 (◆). Binding assays with these two lines against a panel of seven CHO-ECRs revealed varying degrees of cytoadhesion across all tested cell types (Fig. 3.15). Transcriptome analysis showed that the P4-ICAM1 line exhibited a mixed *var* gene expression profile that diverged substantially from the long-term cultured IT4 wild-type line lacking selection pressure (Fig. 3.2, B). Early indications of this transcriptional diversification were already apparent in the unenriched LC culture (●), which displayed a reduced proportion of *var08* transcripts (64.7 %) along with relative upregulation of *var1CSA*, *var04/var2CSA*, *var66*, and *var34* (Fig. 4.2, A ●). To assess whether this heterogeneous expression pattern resulted from enrichment on the ICAM-1 receptor, the parasites were subsequently panned over CHO-K1-EPCR cells. Even after four rounds of enrichment, the resulting line, designated P4-ICAM1-P4-EPCR (+), did not display cytoadhesion to CHO-K1-EPCR cells. The *var* gene expression profile remained largely unchanged after this second enrichment, consistent with the observed non-EPCR-binding phenotype. Notably, *var* genes containing CIDRα1 domains, characteristic of EPCR-binding *Pf*EMP1 variants, remained absent in both parasite lines (Fig. 4.2, A ◆ – +). The limited transcriptional effect of this final CHO-K1-EPCR panning step was not confined to *var* genes but was also evident in the principle component analysis (PCA) of all four IT4var08-HA^{endo}-derived parasite lines (Fig. 4.2, B). The PCA revealed a distinct cluster for the newly created SLI integrant (▲), whereas the two panned lines (◆ – +) overlapped almost completely, indicating minimal transcriptional variation between the two populations.

To gain a more detailed picture of the transcriptomic differences between the multi-

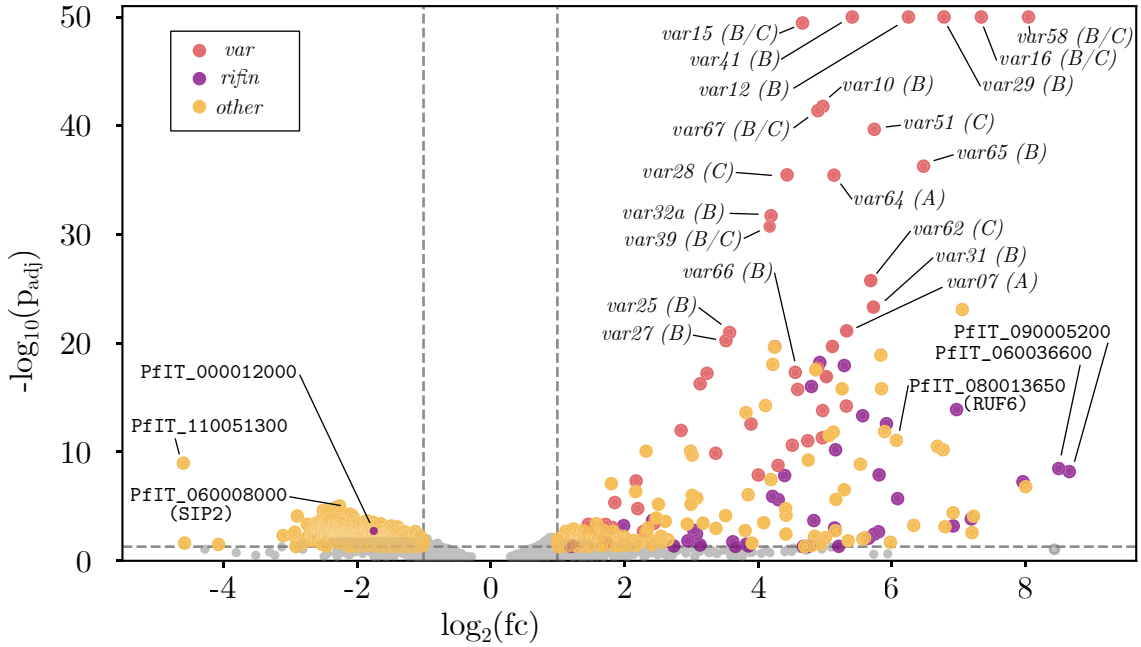


Figure 4.3: **Volcano plot of differential gene expression of IT4var08-HA^{endo}-LC against IT4var08-HA^{endo}-P4-ICAM1.** Grey ●: Genes expressed below threshold of $p_{adj} \leq 0.05$ and fold change (fc) ≥ 2. Red: ●: *var* genes, Purple: ●: *rifin*, Yellow: ●: other significantly differentially expressed genes. Analysis performed with DEseq2. Detailed results in Appendix A.3

ECR-binding IT4var08-HA^{endo}-P4-EPCR line and the non- to low-binding IT4var08-HA^{endo} control, a differential gene expression analysis was performed. The results, visualized in a volcano plot, showed that, when using a threshold of $p_{adj} \leq 0.05$ and fold change ≥ 2 is used, the majority (1047) of the 1362 differentially expressed (DE) genes is upregulated in the IT4var08-HA^{endo} line compared to only 315 genes upregulated in the IT4var08-HA^{endo}-P4-EPCR line (Fig. 4.3). In contrast, the DEs genes identified in the -P4-EPCR line exhibited substantially higher fold changes (fcs) and much stronger statistical significances. As already indicated by the *var* expression profile (Fig. 4.2, A), the DGE analysis revealed a strong upregulation of VSA families in the IT4var08-HA^{endo}-P4-EPCR population compared to the original, unenriched -LC line. In total, 49 out of the 315 upregulated genes were *var* genes, and 40 were *rifins*. Eleven out of the 40 *rifins* directly flank a significantly upregulated *var* gene (Tab. 4.1). A total of 19 genes neighboring the upregulated *var* genes, including the aforementioned eleven *rifins*, are DE. Only two genes neighboring *var* genes are DE in the opposite direction, and both are oriented t2t with the neighboring *var* gene. Overall, when the

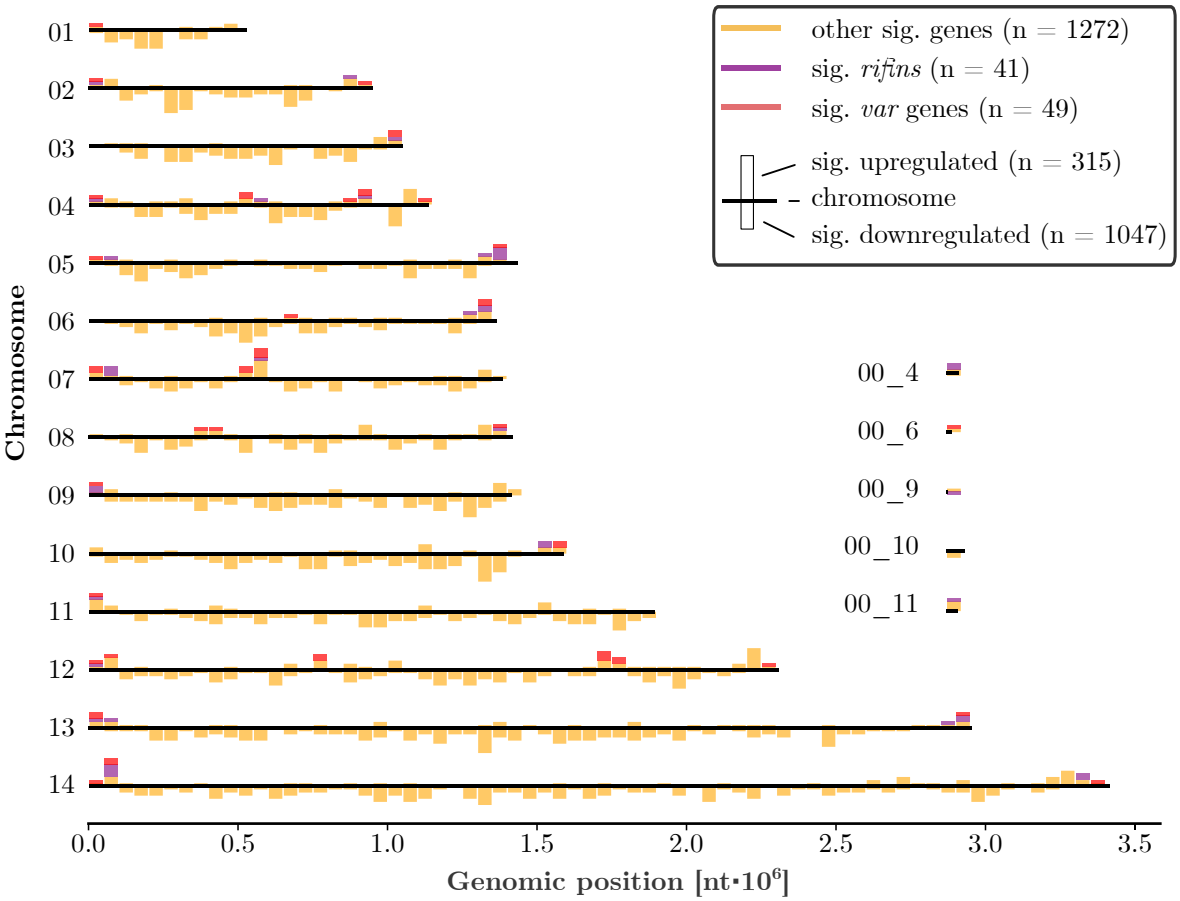


Figure 4.4: **Location of differentially expressed (DE) genes on chromosomes of *PfIT***. Significance threshold: $p_{adj} \leq 0.05$ and fold change ≥ 2. DEs plotted in bins of size 50 kB, genes overexpressed in IT4var08-HA^{endo}-P4-ICAM1-P4-EPCR are plotted above chromosome line and overexpressed in IT4var08-HA^{endo}-LC below. `00_XX` are genomic fragments of unknown chromosomal association.

var-neighboring genes are ranked by fc, the strongest and most significant changes are typically observed for h2h or t2h orientations relative to the switched-on *var* gene, whereas the five bottom-most genes are oriented t2t. A plot of the DEseq results according to their chromosomal location further reveals, that the significantly upregulated non-*var* genes are located in the vicinity of transcriptionally active *var* genes, whilst the 1047 downregulated genes are spread evenly across the 14 chromosomes (Fig. 4.4).

No *var* gene and only a single *rifin* was significantly downregulated in the P4-ECPR samples, (`PfIT_000012000`, fc $= 4, p_{\text{adj}} = 0.0017$). The downregulated *rifin* is located on the `PfIT_00_9` scaffold without any neigbouring *var* genes (Fig. 4.4). The most significantly upregulated genes in the P4-ECPR line were *var58* (fc = 263.3), *var16*

Table 4.1: Filtered list of DESeq2 results of Tab. A.3. Listed are all genes that are significantly differentially expressed ($p_{adj} \leq 0.05$ and fold change (fc) ≥ 2) between IT4var08-HA^{endo}-LC and IT4var08-HA^{endo}-P5-EPCR, located directly upstream or downstream of a significantly regulated *var* gene. Orientation of neighboring gene as t2t = tail-to-tail; t2h = tail-to-head; h2h = head-to-head; h2t = head-to-tail. More detailed results in Appendix Tab. A.2.

var Name	*var* fc	Neighbor ID	Neighbor description	Orient.	Neighbor fc
IT4var02	29.64	PfIT_090005200	rifin	h2h	401.88
IT4var07	40.04	PfIT_060036600	rifin	h2h	360.09
IT4var39	18.04	PfIT_120045100	acidic terminal segments, variant surface antigen of PfEMP1, putative	h2h	255.73
IT4var65	88.77	PfIT_080013650	RNA of unknown function RUF6	h2h	102.34
IT4var28	21.60	PfIT_070017300	rifin	h2h	60.46
IT4var22	24.10	PfIT_100043900	rifin	h2h	56.04
IT4var61	31.22	PfIT_080037300	rifin	t2h	19.71
IT4var04	31.14	PfIT_120006200	hypothetical protein	h2t	13.98
IT4var63	10.32	PfIT_120024700	PfEMP1 pseudogene	h2t	8.48
IT4var54	5.45	PfIT_110005700	rifin	t2t	8.45
IT4var08	4.88	PfIT_070006000	rifin	h2h	5.36
IT4var30	7.20	PfIT_040025700	rifin	t2h	3.97
IT4var66	23.52	PfIT_040025700	rifin	h2t	3.97
IT4var18	4.60	PfIT_030029600	rifin	h2h	3.32
IT4var12	75.96	PfIT_130077700	rifin	t2t	2.29
IT4var45	2.77	PfIT_120005600	rifin	t2t	2.28
IT4var34	32.45	PfIT_080014200	asparagine-rich antigen Pfa55-14	t2t	2.19
IT4var62	51.38	PfIT_040025000	conserved protein, unknown function	t2t	-2.53
IT4var01	26.75	PfIT_060021200	conserved protein, unknown function	t2t	-4.61

(fc = 161.5), *var29* (fc = 109.7), *var12* (fc = 76.0), and *var41* (fc = 42.4), all with $p_{\text{adj}} \leq 1 \times 10^{-50}$. Additionally to the *vars* and *rifins*, the two DE genes; ApiAP2 and RUF6 are marked in the volcano plot for their potential role in *var* gene transcription (Fig. 4.3) [109, 160, 161]. The ApiAP2 protein encoding SIP2 (`PfIT_060008000`, $p_{\text{adj}} = 5.5 \times 10^{-4}$, fc $= -5.2$), was downregulated in the MEED line, and the RUF6 gene was upregulated (`PfIT_080013650`, $p_{\text{adj}} = 2.9 \times 10^{-11}$, fc = 102.3).

4.1.3 Transcriptomal differences between binding enriched and non-binding IT4var19-K2-HA^{endo} parasite lines

RNAseq data of four biological replicates each of the non-binding IT4var19-K2-HA^{endo} as well as the CHO-ICAM1 and CHO-EPCR cytoadherent IT4var19-K2-HA^{endo}-P5-EPCR was used to screen the transcriptome for differences to reveal potential factors involved in cytoadhesion. A first look at the *var* genes revealed, that fraction of *var19* transcript from total *var* gene transcript count increased from 79.5 % in the unenriched, to 93.2 % in the binding enriched IT4var19-K2-HA^{endo}-P5-EPCR parasite line (Fig. 4.5, A). A quantitative analysis of normalized gene counts showed no statistical difference neither in total *var* transcript count, nor in *var19* transcript count between the two parasite lines where the gene is transcibed at 294.29 TPM and 283.68 TPM respectively (Fig. 4.5, C).

Whole transcriptome analysis with DESeq2 between IT4var19-K2-HA^{endo}-P5-EPCR and IT4var19-K2-HA^{endo} lines resulted in three differentially expressed genes with a fc $\geq |2|$ and $p_{adj} \leq 0.1$. These are the putative glycophorin-binding protein (GHB) ($p_{adj} = 0.024$, fc $= 7.67$), the erythrocyte membrane protein (EMP)-trafficking protein PTP3 ($p_{adj} = 0.037$, fc $= 13.29$) and the *Plasmodium* helical interspersed subtelomeric family (PHIST)a ($p_{adj} = 0.099$, fc $= 2.86$) (Fig. 4.5, B). A second PTP3 protein is up-regeulated 5.7 fold but below below the significance threshold with an adjusted p-value of 0.538.

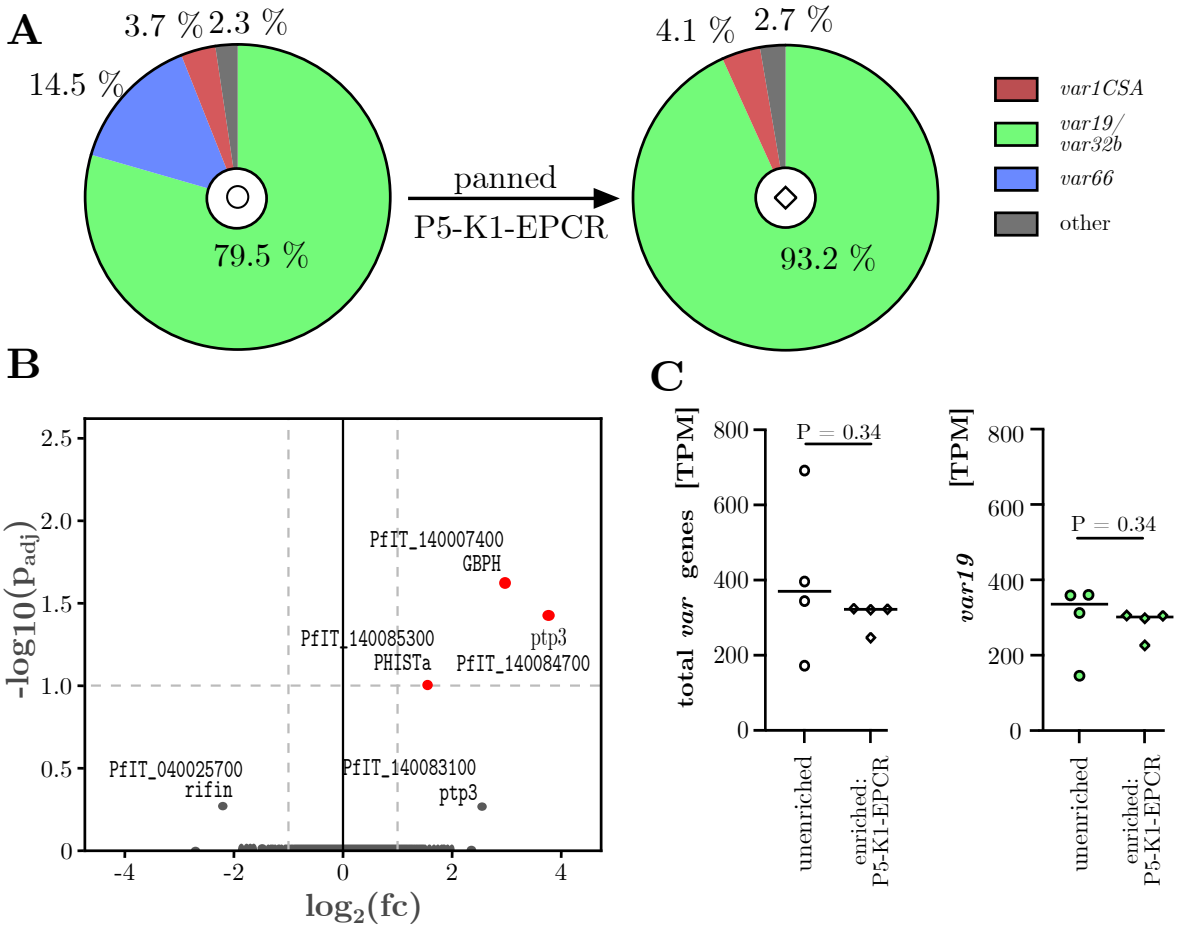


Figure 4.5: **RNA-seq analysis of binding enriched and unenriched IT4var19-K2-HA^{endo}. A:** *Var* expression profile of IT4var19-K2-HA^{endo} before (○: unenriched) and after five rounds of binding enrichment over CHO-K1-EPCR cell (◇: enriched). **B:** Volcano plot of differential gene expression (DESeq2) between unenriched and enriched IT4var19-K2-HA^{endo}. Genes marked in red are over the threshold of $p_{adj} \leq 0.1$ and fold change (fc) ≥ 2. **C:** Normalized transcript counts in TPM of all *var* genes (left) and *var19* (right). Statistical comparison with Mann-Whitney U test.

4.1.4 *Var* chimera – IT4var20/27

The expression profile of IT4var20-HA^{endo} showed that the SLI target gene, *var20* (`PfIT_070017000`), accounts for only 46.0 % of total gene expression, followed by *var27* (`PfIT_070016700`) with 26.6 % (Fig. 4.6, A, left). Both genes are located on the central region of chromosome 7 (`PfIT_07`). They are only 28 kb apart from each other and flank a pseudogenic *rifin* (`PfIT_070016800`) as well as another *var* gene; (`PfIT_070016900`) (App: A.6).

A look at the RNA-seq coverage showed that both genes are only partially transcribed (Fig: 4.6, B). *Var27* shows high transcription for the first 5.2 kb of the 5' part of

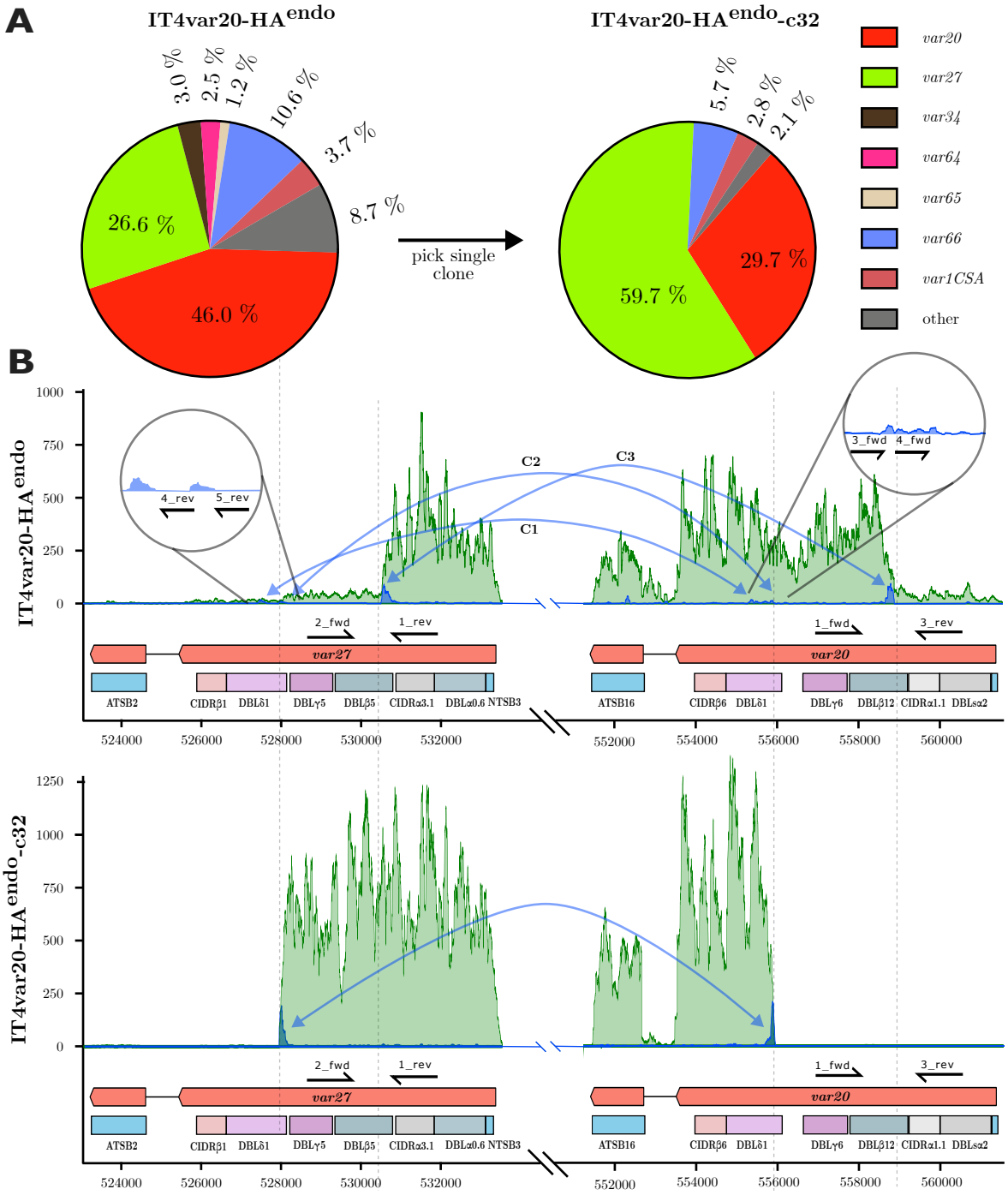


Figure 4.6: **RNA-seq analysis of *var* expression profile and coverage of IT4var20-HA^{endo} and IT4var20-HA^{endo}-c32.** **A:** *Var* expression profile of IT4var20-HA^{endo} and the single clone IT4var20-HA^{endo}-c32. **B:** Read coverage plot of *var27* (left) and *var20* (right) on `PfIT_07`. Green — : Reads correctly paired to reference genome in the F1R2 or F2R1 orientation (read pair pointing at each other). Blue — : Reads in the R1F2 orientation (read pair pointing away from each other). Dashed - - - : Proposed gene recombination sites. C1 – C3 : Clusters of R1F2 paired-reads with inserts spanning from *var27* to the *var20* locus

the gene. In *var20*, transcription covers the second half of the gene, starting at 5.3 kb, covering part of exon 1 and the full exon 2 until the stop codon. Illumina's paired-end

sequencing protocol used to sequence the transcriptome generated two reads pointing towards each other, the so-called `FR` orientation (Tab: 2.8), with an insert of ~150 bp. By sorting the reads into correctly `FR` oriented (green) and discordantly paired (blue), the coverage plot revealed three clusters of reads mapping from *var20* to *var27* in an `RF` orientation with an insert size of 2 kb. This indicated that a genomic recombination may have taken place at those positions, creating novel variations of a fusion gene consisting of the head of *var27* and the tail of *var20*. The first cluster, cluster 1, consisted of 18 `RF` paired-reads, cluster 2 of 11, and cluster 3 of 95 reads (App: A.6). The recombination sites for all three recombination clusters are homology regions in *var27* and *var20* of 26, 34 and 43 bp length (Tab. 4.2). Whilst the first two are exact matches, the cluster 3 recombination contains three mismatches with a maximal concordant sequences of 21 bp.

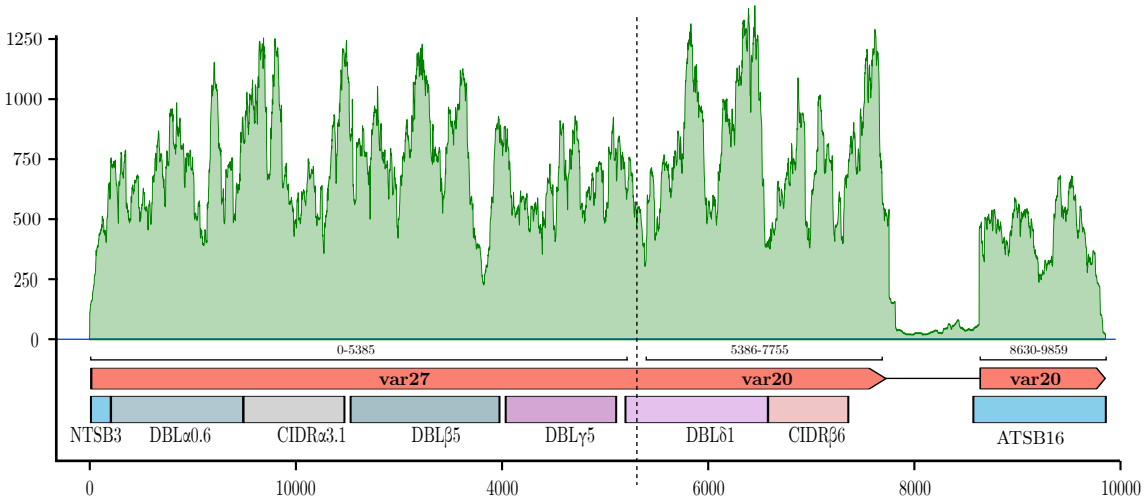


Figure 4.7: **Coverage of IT4var20-HA^{endo}-c32 to proposed var27–20 fusion reference sequence**. Green — : Reads correctly paired to reference genome in the F1R2 or F2R1 orientation (read pair pointing at each other). Blue — : Reads in the R1F2 orientation (read pair pointing away from each other). Dashed - - - : Proposed gene recombination site.

Even though correctly oriented coverage significantly dropped from ~500 to ~100 reads at the excluded segments of *var27* and *var20*, respectively, the low transcription could still be attributed to a mixed population of parasites, with some carrying the reference concordant *var20* and *var27* loci. By means of PCR, specific

Table 4.2: **Homology sequences of *var27* – *var20* recombination sites.**

Name	Homology sequence	Locus *var27*	Locus *var20*
Cluster 1	TGGTGGCAAAAAAATGGTGAAC ATAT	PfIT_07: 527394 - 527419	PfIT_07: 555401 - 555426
Cluster 2	TAGTGGTAGTATTTGTATCCCA CCCAGGAGGCGA	PfIT_07: 527954 - 527987	PfIT_07: 555928 - 555961
Cluster 3	TCATGCGCACACCTCCGT$\frac{T}{G}$A$\frac{C}{T}\frac{T}{C}$ TCCATCTTTGCCTGTACATGG	PfIT_07: 530524 - 530566	PfIT_07: 558864 - 558906

primer pairs were designed to screen the IT4var20-HA^{endo} for the original loci of *var27* (2_fwd/1_rev), *var20* (5_fwd/3_rev) and for the suspected recombination var27-20fusion (5_fwd/1_rev) (Fig. 4.6, B). Separation of the replication products on an agarose gel confirmed that amplicons of the expected sizes for all three primer pairs were present, showing that the IT4var20-HA^{endo} line consists of parasites carrying the original loci as well as the fusion gene. The fusion gene could not be detected in the IT4 wt culture (Fig. 4.8). In order to mitigate this genetic variation, a single clone of the IT4var20-HA^{endo} line was picked and is henceforth referred to as IT4var20-HA^{endo}-c32. The expression profile of IT4var20-HA^{endo}-c32 shows, like the parent line, a majority expression of *var27* and *var20*. It is of note that the ratio of the two genes is, however, inverted, with the majority of reads mapping to *var27* (59.9 %) instead of *var20* (29.7 %) (Fig: 4.6, A, right). Similarly, the coverage plots indicate that the clone also carries a genomic recombination (Fig: 4.6, B, top). Instead of the four different variants in the *var20* locus (clusters 1–3 and the original locus), the IT4var20-HA^{endo} line consists solely of the fusion gene *var27—var20* of the variant described by the reads of cluster 2 (App: A.6).

Finally, the RNA-seq data was used to create a novel reference for the novel fusion gene. In short, the reads from IT4var20-HA^{endo}-c32 from `PfIT_07:520000-580000` were used in an *de novo* alignment with SPAdes (Fig. 4.7). The resulting dominant assembled contig was over 9 kb long and aligned with 0 mismatches to a manually created sequence which consisted of the *var27* head (`PfIT_07:527987-533338`) and *var20* tail (`PfIT_07:551454-555961`). Consequently the domain structure of fusion gene var27-20-cluster-2 identical to *var27* (NTS-DBLα0.6-CDIRα3.1-DBLβ5-DBLγ5-

DBlδ1-CIDRβ6-ATS) but with the two membrane proximal domains DBlδ1-CIDRβ6 as well as the intracellular ATS originating from the IT4var20-HA^{endo}-c32 line showed light binding to CHO-ICAM1 ($p = 0.023$) and elevated but non-significant levels to CD36, CD55 and TNFR2. At the time point of the experiments, only a cluster 3 type recombination was suspected which could not be identified in preliminary qPCR experiments of IT4var20-HA^{endo}-c32. It was therefore suspected that the clonal IT4var20-HA^{endo}-c32 was expressing full-length original locus *var20*. Since the parasites did not display the expected CIDRα1.1-mediated EPCR binding, it was tested whether the line needed to be enriched for surface presentation of the *var20 Pf*EMP1 molecule. Therefore, IT4var20-HA^{endo}-c32 was enriched four times over CHO-K1-EPCR cells. The resulting IT4var20-HA^{endo}-c32-P4-EPCR line likewise did not display EPCR adhesion and showed a similar but increased binding profile to the aforementioned receptors (Fig. 3.16).

Table 4.3: **Tabular results of agarose gel with PCR amplificates of genomic IT4var20-HA^{endo} recombination sites.** CL = Cluster. See agarose gel in Fig. 4.8.

	CL-1	**CL-2**	**CL-3**	**no CL-3**	**no CL-3**
Expected amplificate	957 bp	1782 bp	1218 bp	1882 bp	1693 bp
IT4 wt	+	+	+	+	+
Sli-var20	+	+	+	+	+
Sli-var20-c32	None	+	+	+	+
Sli-var20-P4-EPCR-C6	None	+	+	+	+
Sli-var20-P4-EPCR-F5	None	+	+	+	+
Water control	None	None	None	None	None

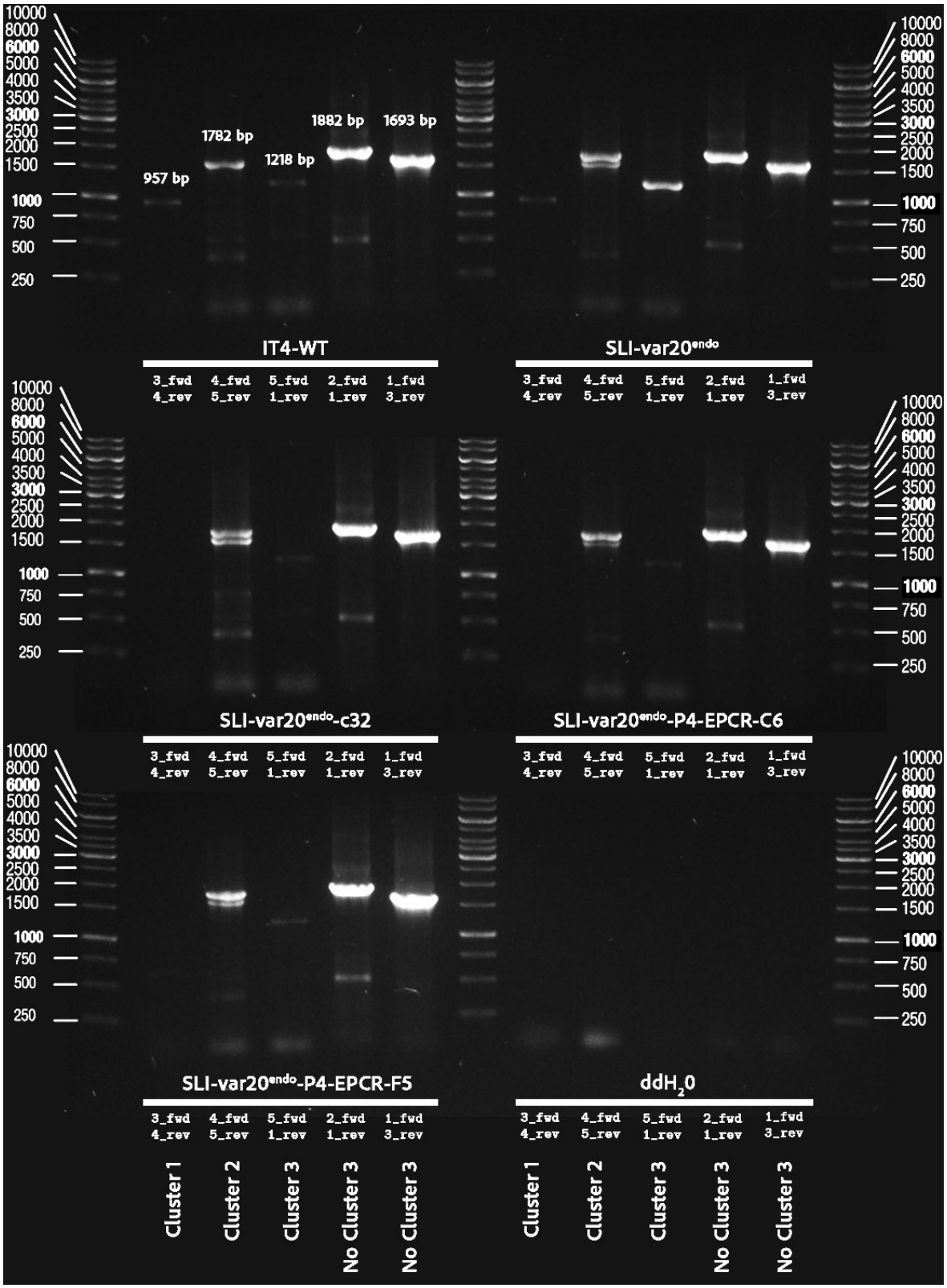


Figure 4.8: **Agarose gel of PCR products for recombination check of *var20* and *var27*.** PCR products of Primer pairs: 3_fwd – 4_rev : `Cluster 1` recombination;; 4_fwd – 5_rev : `Cluster 2` recombination; 5_fwd – 1_rev : `Cluster 3` recombination; 2_fwd – 1_rev : original locus for `Cluster 3` recombination site in *var27* locus; 1_fwd – 3_rev : original locus for `Cluster 3` recombination site in *var20*.

4.2 Discussion

The availability of a large RNAseq dataset, containing parasite populations of diverse *var* gene expression profiles originating from the same IT4 strain, offered the unique opportunity to investigate co-expression patterns of *var* adjacent genes. Regulation of *rifins* transcription is still poorly understood and even though more than 400 gene pairs are potentially regulated via bidirectional promoters in *P. falciparum*, only little research has been done on the topic [156]. Consistent with the general organization of the *P. falciparum* transcriptome, where gene pairs sharing a h2h orientation exhibit the highest expression correlation [156], the strongest co-regulation was observed for group A ($r = 0.284$) *var* genes, which are predominantly arranged head-to-head with *rif* genes (Fig. A.2). This aligns with observations by Claessens *et al.*, who noted that the specific up-regulation of group A *var* genes in HBEC-5i-selected parasites was consistently accompanied by the increased transcription of the adjacent, h2h oriented *rif* genes [151]. Similarly, Wang *et al.* described the preferential transcription of the conserved *rifA1* subfamily alongside their neighboring Group A *var* genes in parasites expressing SM-associated surface antigens [157]. This phenomenon is likely driven by bidirectional promoter activity from the shared 5' intergenic region. Chappell *et al.* demonstrated that transcription from bidirectional promoters is a pervasive feature of the *P. falciparum* genome, with the likelihood of co-expression increasing inversely with the distance between transcriptional start sites [156]. Interestingly, the correlation co-efficients observed for *var* gene neighbors in h2h and even h2t orientations significantly exceeded those calculated for the general genome (Fig. 4.1, B and C). It is not clear whether this is a background feature owed to a gene dense genomic locus around the *var* genes, or linked to the specific regulatory mechanisms of *var* neighboring gene activation. A further investigation taking the distance of gene pairs into account could clarify this, as the effect of bidirectional promotors in h2h oriented genes is dependent on the distances of the respective 5' UPSs to each other.

Especially the increase of the genes adjacent to *var* genes in the h2t orientation is not explained by bidirectional promotors. Active *var* genes are described to physically

relocate to a specific perinuclear expression site, characterized by an euchromatic environment and the recruitment of specific factors such as the non-coding RNA RUF6 [161, 162]. It is plausible that this transcription active chromatin environment facilitates the transcription of adjacent genes through increased accessibility, as suggested by the coregulation of h2t pairs ($r = 0.318$). This hypothesis is supported by Wang *et al.*, who argued that the structured diversity and organization of *rif* genes alongside *var* genes evolved to ensure functional coupling, potentially implicating RIFINs in the adhesion complex or immune evasion strategy alongside the dominant *P. falciparum* [157]. Somewhat contradicting this theory is that t2t ($r = -0.050$) and t2h ($r = -0.058$) oriented genes did not show signs of coregulation. In yeast and other eukaryotes, convergent transcription often leads to negative correlation due to transcriptional interference [156]. However, Chappell *et al.* found that while t2t gene pairs in *P. falciparum* frequently exhibit overlapping 3' UPSs, this does not generally result in strong negative correlations [156].

The maintenance of mutually exclusive gene expression of the blood stage parasite's most immunogenic surface protein is central to the immune evasion strategy of *P. falciparum* [163]. The transcriptomic analysis of the IT4var08-HA^{endo}-LC line revealed a breakdown of this regulation, termed here as the MEED phenotype. Unlike typical mixed cultures where diverse subpopulations each express a single *var* gene, the MEED line exhibited a global upregulation of surface antigen families, with 49 *var* genes and 40 *rifins* significantly upregulated compared to the binding-enriched control. This massive switch from monoallelic expression suggests a fundamental failure in the epigenetic silencing machinery. It is not clear whether only the mutually exclusive expression mechanism of the *var* genes is defective, as almost 30x more genes are DE than the *var* genes alone. Even though more genes are downregulated in the MEED line, the earlier observed coexpression of *var* adjacent VSAs, especially in the head-to-head and head-to-tail orientation, is still present (Fig. 4.3 and Tab. 4.1). The upregulation of genes not sharing a bidirectional promotor but in the vicinity of the *var* genes is indicative of changes in chromatin structure leading to an increased accessibility of the surrounding promotors [164]. In contrast, genes oriented tail-to-tail

were less frequently affected, suggesting that transcriptional termination sites might still offer some boundary protection even in the absence of robust heterochromatin.

A likely driver of this phenotype is the significant downregulation of the ApiAP2 transcription factor SPE2-interacting protein (SIP2) (`PfIT_060008000`, $p_{\text{adj}} = 0.0012$, fc $= -5.35$) observed in the MEED line. SIP2 is known to bind to SPE2 motifs located in the subtelomeric regions as well as in the upstream region of *var* genes and plays a critical role in tethering chromosome ends to the nuclear periphery, thereby facilitating the formation of heterochromatin [160, 165]. Flueck et al. (2010) demonstrated that the disruption of *var*-SPE2 interactions leads to the loss of heterochromatin markers like HP1 and H3K9me3, resulting in the derepression of *var* genes and other subtelomeric families. The SPE2 motif is especially enriched in upsB type promotors where it plays a crucial part in upsB promoter-mediated silencing. Deletion of the SPE2 motif *in vitro* switched the promotor from default inactive, into an active state [160]. The RNA-seq results of the MEED line support this, as preferential activation of the upsB type *var* genes could be observed. Eight out of the 50 DE *var* genes ranked by p-value were members of the upsB containing B and B/C *var* groups (Fig. 4.3).

Another gene described to play a role in *var* gene regulation is the non-coding RNA of RUF6 (`PfIT_080013650`, fc = 102.3). RUF6 is encoded within the *var* gene expression site and has been implicated in the activation and memory of *var* gene expression. Guizetti et al. (2016) proposed that RUF6 functions in trans or cis to modulate the "counting" mechanism that restricts expression to a single *var* gene [161]. The overexpression of RUF6 in the MEED line could be a consequence of the simultaneous activation of multiple *var* loci, each producing RUF6 transcripts. Alternatively, the high levels of RUF6 might actively contribute to the destabilization of the silencing machinery, potentially by saturating the regulatory complexes required for singular gene choice.

The disparity between *var19* transcription levels and the observed binding phenotype in IT4var19-K2-HA$^{\text{endo}}$ parasites suggests a missing cofactor required for *Pf*EMP1 surface exposure. Despite no significant difference in either total *var* gene expression ($p = 0.34$) or *var19*-specific transcription ($p = 0.34$) between the binding-enriched

and unenriched parasites, surface presentation of var19-*Pf*EMP1 was dramatically altered following selective panning over CHO-K1-EPCR cells. The unenriched IT4var19-K2-HA^{endo} line expressed *var19* at 79.5 % of total *var* transcripts (294.29 TPM), yet showed no detectable cytoadhesion to ICAM-1 or EPCR. Trypsin digestion of surface-exposed erythrocyte proteins confirmed the absence of protected *Pf*EMP1 fragments in the unenriched parasites, indicating that var19-*Pf*EMP1 was not presented on the infected erythrocyte surface despite successful translation, as shown by IFA through detection of the HA tag fused to *var19*. The observation that the binding-competent IT4var19-K2-HA^{endo}-P5-EPCR line exhibited only marginally increased *var19* transcription, indicates that the panning-mediated selection enriches for parasites with enhanced capacity to present var19-*Pf*EMP1 at the infected erythrocyte surface, independent of transcriptional upregulation of the *var19* gene itself. A DGE analysis between the binding-enriched and unenriched IT4var19-K2-HA^{endo}populations identified three significantly DE genes between the two populations (fc $\geq |2|$, $p_{adj} \leq 0.1$). The most prominent candidate is the erythrocyte membrane protein trafficking protein 3 (PTP3) (`PfIT_140084700`), which is upregulated 13.29-fold in the binding-enriched parasites ($p_{adj} = 0.037$). A second PTP3 gene (`PfIT_140083100`) is similarly upregulated 5.7-fold, though below the significance threshold. A knockout of the single PTP3 gene in the 3D7 reference strain by Meier and colleagues in 2008 equally disrupted the surface presentation of *Pf*EMP1 on the surface of iEs [166]. Two additional significantly DE genes provide further evidence for upregulation of the virulence complex trafficking machinery in the enriched population. The putative GHB (`PfIT_140007400`) is upregulated 7.67-fold ($p_{adj} = 0.024$), while the exported protein PHIST (`PfIT_140085300`) is upregulated 2.86-fold ($p_{adj} = 0.099$). `PfIT_140085300` shares 100 % sequence identity to `PF3D7_1449600` (former id: `PF14_0472`) which was also identified by Claessens *et al.* to be the only gene upregulated at least three-fold in enrichment experiments of three separate parasite isolates (HB3, 3D7, and IT4) over HBEC-5i endothelial cells. Their panning over brain endothelial cells simultaneously enriched SM related A and B/A type *var* genes with EPCR binding CIDRα1.X domains in all isolates [151]. It is therefore possible that `PfIT_140085300` plays a substantial role in mediating SM related

cytoadhesion. The 23 PHISTa paralogues of *P. falciparum* are known to share different affinities to the different *Pf*EMP1-ATS domains, which led Oberli *et al.* to hypothesize that individual PHISTa variants are optimized for different groups of *Pf*EMP1 [167, 168]. As PHISTa, other than PHISTb and PHISTc, are generally unique in *P. falciparum*, they might be an interesting target in the treatment of SM malaria [168].

In this work, three different recombination events were identified in the vicinity of the SLI modified locus. Even though the IT4var20-HA^{endo} line passed through multiple bottlenecks, that should decrease, or in the case of single clone picking, completely eliminate genomic variations in the haploid genome of the parasite line, the different recombinations could still be identified via genomic PCR in progeny lines. The IT4var20-HA^{endo} line underwent selection for plasmid transfection into the parasite with WR99210, selection for plasmid integration into the genome with G418 and one round of single clone selection by Jakob Cronshagen [79]. It is unclear whether multiple parasites of containing each of the three chimeras survived these bottlenecks or the recombination on this locus happens so frequently that they reoccurred after cloning. The subsequent cloning resulting in the c32, C6 and F5 lines reduced the number of chimeras to two but still did not fully eliminate the diversity (Fig. 4.5). Recent publications point to *var* recombinations being frequent for select genomic loci and sequences. Otto *et al.* found a high frequency of shared sequences accumulated in chromosomes 7 and 4. The authors argue that these genomic island of reduced diversity may be induced by a selective sweep of the chloroquine resistance transporter *P. falciparum* chloroquine resistance transporter (*Pf*CRT) (`PfIT_070013900`). *Pf*CRT was found to confer a strong fitness advantage under chloroquine pressure. As a result, parasites strains carrying this mutation such as the parental line of IT4/FCR3, rapidly expanded *in vivo*, and the loci of 200 kB surrounding *Pf*CRT experienced a significant reduction in genetic diversity [35, 169, 170]. As *var20* and *var27* are located only 125 and 160 kb downstream of *Pf*CRT respectively, this region experienced an increased frequency of sequence identity of homologous regions relevant for the multiple recombination events observed.

A systematic approach on ectopic recombination during asexual replication was performed by Claessen and colleagues who investigated recombination events in progeny of > 200 clones. It was found that *var* genes recombine asexually at a frequency that is comparable to that of single SNP [50]. The authors also established that *var* genes recombined at general regions of high sequence identity between two genes (80 bp) with a perfect homology regions of on average 15 bps. Additionally, they determined that recombination of *var* genes is possible either intragenomically in the immediate vicinity or across chromosomes [50].

Other instigators for recombinations can be found in DNA secondary structure forming motifs. It was observed that these motifs are highly enriched around *var* genes and are hypothesized to induce replication fork stalling and collapse, which in turn increases errors through DSB repair mechanisms [52, 171]. A search for a common DNA secondary structures (DSSs), DNA G-quadruplexes, revealed two PQS in proximity of the observed recombinations (`PfIT_07:543522-543550` and `PfIT_07:557137-557168`, see Tab. A.1). One is in exon 1 of *var20* between cluster 1 and cluster 2 , and second one in exon 1 of *var15* (`PfIT_070016900`) , which is located in between *var27* and *var20* at a distance 10 kb and 8 kb respectively (Fig. 4.6 or Fig. A.6). It is unclear how accurate *in silico* based prediction of G4 is in *P. falciparum*. Even tough Smargiasso and colleagues could verify the upsB specific G4s *in vitro*, an G4-seq based approach in a later study by [53] found that QGRS Mapper predicted only one third of G4 sites [52, 53]. Unfortunately, G4-seq data is only available for the isolates `3D7` and `HB3` so far. Another study looking at DSS (folding free energy of 50-mers calculated with RNAfold) found them at boundaries of *Pf*EMP1 structural domains which allows for functional domain conservation [171]. Especially the 'mid-var' DBL domains, which were previously identified as recombination hotspots were significantly enriched for 50-mer DSS with a low minimum folding energy (MFE) below a threshold of $-6.27\frac{\text{kcal}}{\text{mol}}$ [171]. The calculations were kindly provided by Prof. Thomas Lavstsen, and were used to check for correlations of low MFEs values to the breaking points in var20/var27. The two *var* genes, that are already low in MFE compared to other *P. falciparum* genes, show a significant increase in DSS forming motifs between the DBLδ and DBLγ

domains with a MFE of $-20\frac{\text{kcal}}{\text{mol}}$ and $-15\frac{\text{kcal}}{\text{mol}}$ at cluster 2 (Fig. A.6). The definite trigger for the recombination hotspot cannot be conclusively determined. It is likely that a multitude of factors play together. These are namely the close proximity of two closely *var* genes of the same *var* group with similar domain structures and multiple homology regions. Additionally, it could be shown that affected regions are enriched in DSS forming motifs increasing which are known inducers of replication fork stalling and DSBs.

5 Peptides for inhibition of cytoadhesion

5.1 Results

5.1.1 Antimalarial peptides

Adhesion of *P. falciparum*-infected erythrocytes iEs to vascular endothelium is a key pathological process in severe malaria, causing microvascular obstruction and tissue hypoxia. Disrupting this cytoadhesion is a promising therapeutic strategy to prevent severe complications like cerebral malaria and multi-organ failure [31, 172]. Such an approach would complement current antimalarials, which, despite killing the parasite, leave the adhesive *Pf*EMP1 protein on the iEs surface, maintaining cytoadherence and contributing to endothelial dysfunction [70, 131]. This persistent adhesion contributes to the high mortality rates seen within 24 hours of hospital admission [173] and motivates the investigation of novel anti-cytoadhesion therapies [172, 174, 175].

This study established an *in vitro* screening method that closely mimics *in vivo* conditions to identify binding inhibitory peptides. The data provide the foundation for a molecular evolutionary approach to develop antimalarial peptides using genetic algorithms (GAs), as described by Röckendorf and colleagues [176, 177]. This strategy combines computational evolution involving cycles of *in silico* recombination and mutation with experimental fitness data from *in vitro* assays to optimize peptides over multiple generations.

Two peptide libraries were generated as a starting point for the optimization by

systematically fragmenting the suspected *Pf*EMP1-binding ECR domain. The first library targeted to inhibit CD36 adhesion, and the second ICAM-1, with each consisting of ten peptides of 20 amino acid length. The libraries were designed as a series of overlapping fragments, created by shifting the reading frame by 2–4 residues along the binding domain sequence to ensure comprehensive coverage of potential binding epitopes.

To assess peptide functionality, a reproducible static binding assay was established using the transgenic parasite line IT4var01-HA$^{\text{endo}}$. This line expresses a single *Pf*EMP1 variant (IT4*var01*) and specifically adheres to CHO cells expressing either CD36 or ICAM-1, providing a well-defined screening system (Fig. 3.6). An MTT cytotoxicity assay was also implemented to evaluate peptide safety. Together, the binding inhibition and cytotoxicity data serve as the experimental fitness functions for the GA, enabling a multi-objective optimization process that simultaneously selects for high inhibitory potency and low toxicity.

5.1.2 CD36 cytoadhesion inhibition

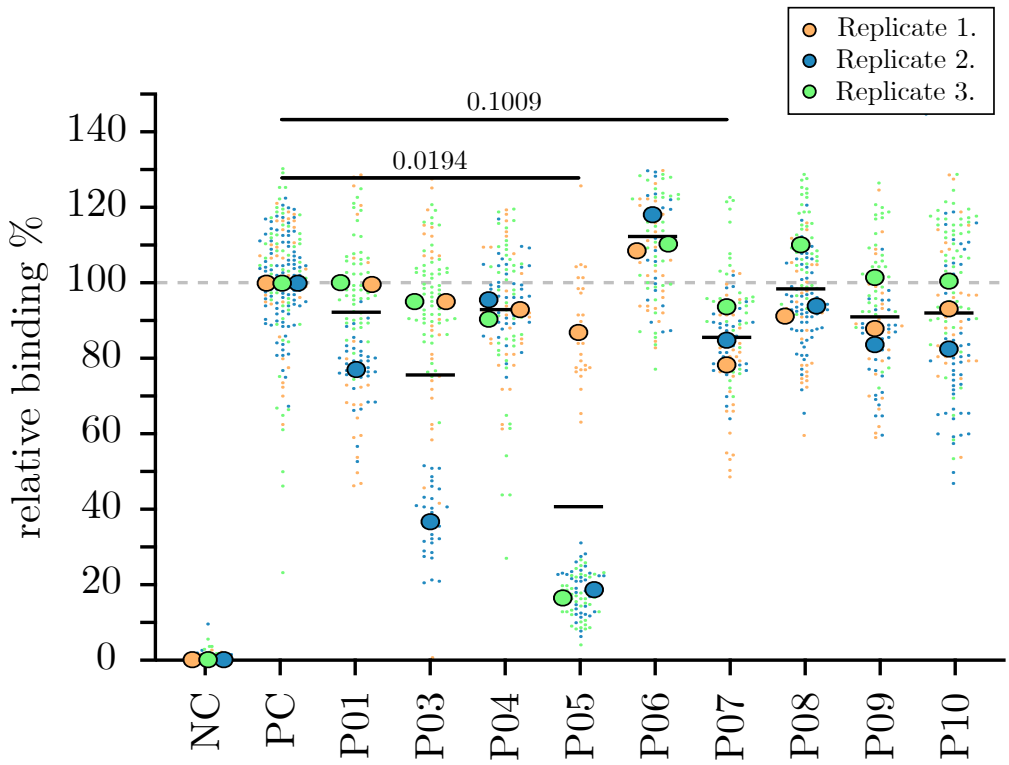


Figure 5.1: **Effect of CD36 derived peptides on binding of IT4var01-HA^{endo} iEs to CHO-CD36 cells**. NC: CHO-GFP cells without peptides; PC: CHO-CD36 cells with (P10^{ICAM1}); P01–P10: CHO-CD36 with peptides P1^{CD36}–P10^{CD36}. All measurements normalized relative to controls NC (0 %) to PC (100 %). Statistic with nonparametric Kruskal-Wallis test for comparison of each peptide sample with PC.

The library of CD36-binding domain-mimicking peptides, P01–P10^{CD36}, was screened for inhibitory effects using a static binding assay with CD36-binding IT4var01-HA^{endo} on CD36-expressing transgenic CHO cells. Binding is expressed as a percentage relative to a negative control (NC) 0 % and positive control (PC) 100 % to which all samples are normalized. The experiment was conducted in three independent replicates. For the negative control (NC), iEs were co-incubated with CHO cells lacking the CD36 receptor (CHO-GFP). This combination revealed the baseline cytoadhesion to the CHO cells of on average, 39 ± 27 iEs/mm^2 was observed (for unnormalized values, see App. A.7). The positive control consisted of iEs binding to CHO cells expressing the CD36 receptor (CHO-CD36) in the presence of a non-inhibitory peptide

($P10^{ICAM1}$). This condition established the baseline for 100 % relative binding with mean binding across the three replicates of 1502 ± 370 iEs/mm^2, reflecting the results of earlier binding assays performed without peptides (Fig. 3.6, A).

Peptides $P01^{CD36}$, $P04^{CD36}$, and $P07$–$P10^{CD36}$ exhibited varying degrees of moderate inhibition, with mean relative binding values generally between 85 % ($P07^{CD36}$) and 112 % ($P06^{CD36}$). The largest reductions were seen for $P03^{CD36}$, with 25 % less binding than the PC, and $P05^{CD36}$, with an inhibition of 59 % (to 41 % relative binding). However, both peptides showed high variability among replicates, with standard deviations of ±34 % and ±40 %, respectively.

A visual inspection of the imaged slides revealed an increase in deformed iEs (Fig. 5.2, B). In particular, replicates 2 and 3 for $P05^{CD36}$ showed a large amount of cell debris, likely consisting of ruptured erythrocytes. The only peptide that significantly reduced IT4var01-HA^{endo} binding was $P07^{CD36}$, which decreased the number of cytoadherent cells by 14 % ($p = 0.10$). In contrast, $P06^{CD36}$ was the only peptide that increased cytoadhesion, with 12 ± 5 % more adherent iEs than the control.

5.1.3 CD36 peptide cytotoxicity

To assess whether the antimalarial peptides at a final concentration of 20 µM and 0.2 % in BM induced cytotoxic effects on CHO cells, their impact on metabolic activity was measured using an MTT viability assay (Fig. 5.2). In this assay, CHO cells were grown in 96-well plates and, on the second day, coincubated for 24 hours with different peptides in 0.2 % DMSO, alongside a negative control containing 50 % DMSO to induce cell death as NC. The NC served as the baseline for 0 % viability. Cells co-incubated with only BM and no DMSO were assigned 100 % viability (PC3). Additionally, the static binding experiment's PC condition with $P10^{ICAM1}$ and 0.2 % DMSO (PC1), as well as 0.2 % DMSO alone (PC2), was investigated. PC1 and PC2 both reduced viability by approximately 10 %, to 91 ± 4 % and 90 ± 8 %, respectively. Similarly, $P05^{CD36}$, and $P06$–$P10^{CD36}$ maintained viabilities between 90–100 % relative to PC3 with standard deviations smaller ±5. Higher losses of relative viability was observed

for P01^{CD36}, P03^{CD36} and P04^{CD36}, with viabilities of 53 ± 4, $54 \pm 2\,\%$ and $60 \pm 0.3\,\%$ respectively.

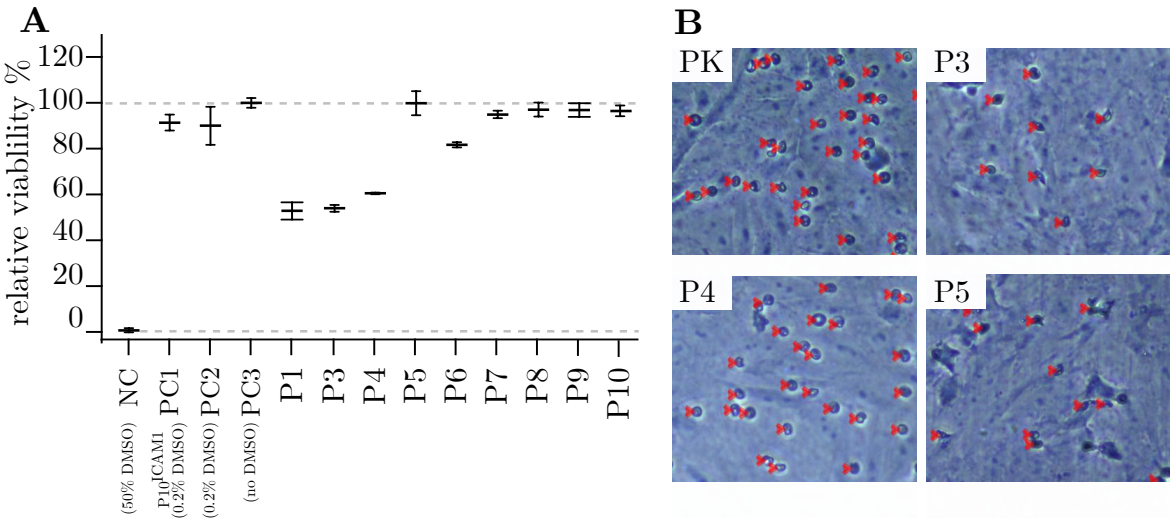


Figure 5.2: **Cytotoxicity analysis of CD36-derived antimalarial peptides**. **A:** MTT cytotoxicity analysis of peptides P1^{CD36}–P10^{CD36} on CHO-CD36 with 0.2 % DMSO. All measurements were normalized relative to controls NC (0 %) and PC3 (100 %). **B:** Example images showing the effects of peptides P3^{CD36}, P4^{CD36}, P7^{CD36}, and PC (P10^{ICAM1}) on CHO-CD36 cells during the static binding assay.

5.1.4 ICAM-1 cytoadhesion inhibition

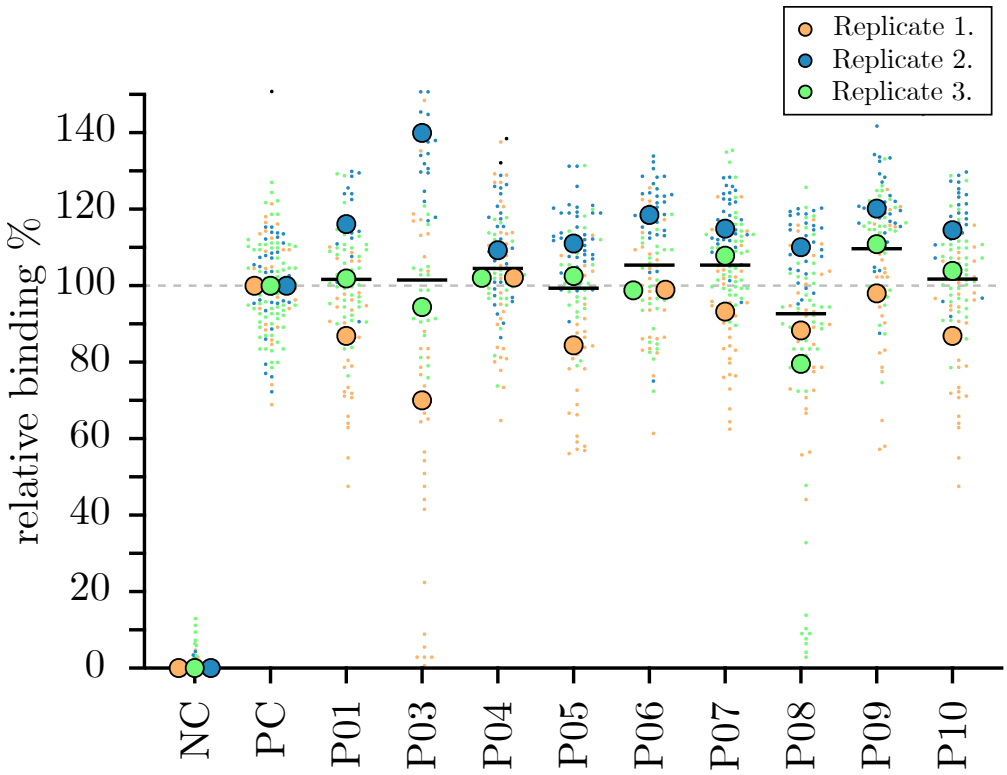


Figure 5.3: **Effect of ICAM1-derived peptides on binding of IT4var01-HA^{endo} iEs to CHO-ICAM1 cells**. NC: CHO-GFP cells without peptides; PC: CHO-ICAM1 cells with (P10^{CD36}); P01–P10: CHO-ICAM1 with ICAM-1-derived peptides P1^{ICAM1}–P10^{ICAM1}. All measurements were normalized relative to controls NC (0 %) and PC (100 %). Statistical analysis was conducted using the nonparametric Kruskal-Wallis test for comparison of each peptide sample against PC.

In the same manner as for the CD36-derived peptides, the library of ICAM-1-derived peptides was assessed in a static binding assay using the same IT4var01-HA^{endo} parasite line incubated with CHO cells expressing ICAM-1. Binding was expressed as a percentage relative to a PC defined by a peptide of equal length derived from CD36 (P10^{CD36}), with all conditions measured across three independent replicates. In absolute numbers, the mean binding of the PC, P10^{CD36}, was 2030 ± 781 iEs/mm^2 (Fig. A.7). For the NC, iEs were co-incubated with CHO-GFP and showed only minimal background binding of 57 ± 31 iEs/mm^2.

All ICAM-1-derived test peptides (e.g., P01^{ICAM1}, P03^{ICAM1}–P10^{ICAM1}) exhibited

little to no inhibition, with mean relative binding values spread around the 100 % baseline. No peptides showed a significant change in binding compared to the control at a p-value cut-off of 0.1. The largest reduction was observed for $P08^{ICAM1}$, at 7 %, while $P09^{ICAM1}$ yielded 10 % more adherent parasites than the PC. Even though $P03^{ICAM1}$ did not affect the mean number of bound iEs, it stood out for having the largest spread between replicates, with a standard deviation of 35 %. All other peptides ranged from 4 % ($P04^{ICAM1}$) to 15 % ($P08^{ICAM1}$).

5.1.5 ICAM-1 peptide cytotoxicity

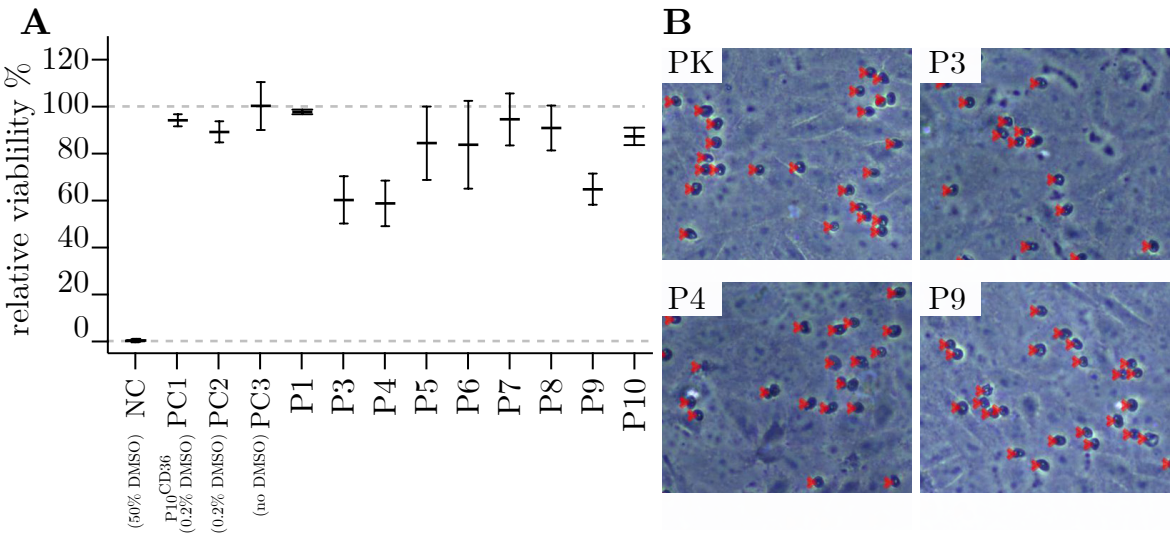


Figure 5.4: **Cytotoxicity analysis of ICAM-1-derived antimalarial peptides**. **A:** MTT cytotoxicity analysis of peptides $P1^{ICAM1}$ and $P3^{ICAM1}$–$P10^{ICAM1}$ on CHO-ICAM1 with 0.2 % DMSO. All measurements were normalized relative to controls NC (0 %) and PC3 (100 %). **B:** Example images showing the effects of peptides $P3^{ICAM1}$, $P4^{ICAM1}$, $P7^{ICAM1}$, and PC ($P10^{CD36}$) on CHO-ICAM1 cells during the static binding assay.

The effects of the ICAM-1-derived peptides on cell viability were tested on CHO-ICAM1 cells, following the same protocol as for the static adhesion experiments. The controls PC1 and PC2 produced similar reductions in viability to 94 ± 3 % (Fig. 5.4, A), consistent with the measurements for CHO-CD36 cells under identical conditions (Fig. 5.2, A). The smallest effects were observed for $P01^{ICAM1}$ (97 ± 1 %), $P05^{ICAM1}$

($84 \pm 16\,\%$), P06$^{\mathrm{ICAM1}}$ ($84 \pm 19\,\%$), P07$^{\mathrm{ICAM1}}$ ($94 \pm 11\,\%$), P08$^{\mathrm{ICAM1}}$ ($90 \pm 10\,\%$), and P10$^{\mathrm{ICAM1}}$ ($87 \pm 4\,\%$). The largest decreases were measured with P03$^{\mathrm{ICAM1}}$, P04$^{\mathrm{ICAM1}}$, and P09$^{\mathrm{ICAM1}}$, yielding viabilities of $60 \pm 10\,\%$, $58 \pm 10\,\%$, and $65 \pm 7\,\%$, respectively. No visual effects of these decreased viabilities on cell morphology in the static binding experiments were discernible (Fig. 5.4, B), consistent across all other tested ICAM-1-derived peptides.

5.2 Discussion

The screen of the CD36-derived peptide library yielded complex results. While initial data suggested that peptides $P03^{CD36}$ and $P05^{CD36}$ were potent inhibitors, these results were accompanied by high variability between replicates and were associated with signs of cytotoxicity. Visual inspection of the binding assays for $P03^{CD36}$ and $P05^{CD36}$ revealed cell debris and deformed iEs, suggesting that the observed reduction in adherent cells was likely an artefact of peptide-induced cell lysis rather than true competitive inhibition of the *Pf*EMP1-CD36 interaction (Fig. 5.2).

An investigation of the effect of peptides on CHO cells through MTT viability assays showed that $P03^{CD36}$ and $P04^{CD36}$ significantly reduced CHO cell metabolic activity, indicating a cytotoxic effect. Interestingly, $P05^{CD36}$ did not demonstrate significant toxicity on CHO-CD36 cells in the MTT assay, even though it visually affected the iEs (Fig. 5.2, B). This discrepancy suggests that the damaging effects observed in the binding assay may be specific to iEs. The peptide may, for instance, selectively destabilize the erythrocyte membrane, leading to rupture. Hemolytic properties are a known issue in the development of antimicrobial peptides and are therefore experimentally assessed if a therapeutic application is considered [176, 178, 179]. Incorporation of peptides into phospholipid membranes may form ionophore-like structures, which in turn increases Ca^{2+} influx, a known trigger for eryptosis. The *P. falciparum* iEs are even more sensitive to this process than uEs, as the parasite's remodeling of the erythrocytes additionally leads to increased membrane Ca^{2+} permeability [180]. Other known changes of iE membranes compared with uEs include the translocation of phosphatidylserine (PS) from the inner to the outer leaflet of the erythrocyte membrane, in combination with a depletion of cholesterol and other phospholipids used for parasite growth [181, 182]. $P05^{CD36}$ could be a candidate for an antimicrobial peptides (AMP) that selectively induces hemolysis in transformed iE membranes without affecting uEs and other eukaryotic cell membranes, as suggested by the lack of cytotoxicity observed on CHO-CD36 cells.

The mode of action of AMPs is still not well understood and varies between struc-

turally different AMPs; however, the formation of pores from peptide oligomers is thought to be the primary mechanism [176, 178]. A number of AMPs have been investigated previously as potential antimalarials for their ability to selectively target the membrane of iEs compared with uEs [178, 179, 183]. AMPs often carry a net positive charge to adhere to the negatively charged membranes of prokaryotes. An increased concentration of negatively charged head groups of PS on the extracellular side of iEs could be the differentiating factor explaining why so many AMPs selectively target iEs without affecting other eukaryotic host cell membranes [179, 181]. Prominent examples are LK-2, a 28-amino-acid-long fragment of the lymphocytic effector protein NK-lysin [179], a truncated form of cecropin B from *Anopheles arabiensis* (An-cecB-1), and dermaseptin S3 (DS3) [184]. These peptides were able to reduce the viability of the iEs *in vitro* at concentrations that did not negatively affect other host cells. All three AMPs are strongly positively charged with a net positive charge of +10 (LK-2), +9 (An-cecB-1), and +5 (DS3); however, this cannot be the mode of action of $P05^{CD36}$, since it is neutral at physiological pH [178, 179, 184].

The results of the ICAM-1-derived peptide library showed more homogeneous outcomes, without any indication of inhibition. Even without the three outliers $P03^{CD36}$, $P05^{CD36}$, and $P03^{ICAM1}$, there was still a significant spread between replicates, with an average standard deviation for CD36 inhibition experiments of $\overline{\sigma} = 8.1\%$ and $\overline{\sigma} = 11.9\%$ for ICAM-1 inhibition. The standard deviation was therefore only slightly smaller than the inhibition observed for the most promising peptide, $P07^{CD36}$. The sensitivity of the assay, as performed here with three replicates, was therefore not sufficient to generate a ranked list of peptides with varying degrees of inhibition, which would be optimal as input for the second generation of peptides. To increase the quality of the results, a higher number of replicates would be required. Another strategy that would increase the probability of finding active peptides would be to increase the library size of tested filial peptides. Commonly, the library sizes for evolutionary peptide development are > 50 in comparison with the ten filial peptides used in this study [177, 185, 186]. To increase the chance of success with current library sizes, one could focus on identifying potent inhibitory peptides with effects strong enough to measure. Instead of

solely generating peptides by fragmenting the ECRs binding domain, the resulting peptides could be computationally modified with *in silico* tools to increase solubility and reduce toxicity [176]. A range of tools exists that calculate physicochemical properties of peptides and could be used to rationally modify detrimental properties of peptides of the filial generation [187]. Recent advances in protein folding prediction would even allow high-throughput computational estimation of peptide–protein interfaces [188].

6 Conclusion

This thesis successfully demonstrated that the application of the selection linked integration (SLI) system to the *var* gene family provides a robust platform for the study of *P. falciparum*-mediated cytoadhesion. These SLI-modified lines facilitate the in-depth investigation of single, mutually exclusively expressed *var* genes without the confounding effects of a heterogeneous parasite population. This advancement is particularly significant for studying *Pf*EMP1–ECR interactions, as it ensures that observed adhesion phenotypes are directly attributable to a genetically defined *Pf*EMP1 variant. Additionally, the stabilization of these phenotypes enables future single cell force spectroscopy (SCFS) experiments, where defined *Pf*EMP1–receptor pairs can be characterized at the single-molecule level to extract bond lifetimes and rupture forces in a physiological membrane environment [137].

The characterization of these lines in cell binding assays under shear stress confirmed the system's applicability for studying cytoadhesion dynamics. While it was possible to successfully track iEs and quantified rolling velocities across various ECRs, such as CD36 and ICAM-1, the setup ran into the limitation of the capture framerate. A modification of the current pump setup would enable the investigation of a broader shear range (below $0.9\,{}^{\mathrm{dyn}}/_{\mathrm{cm}^2}$) which is essential to accurately characterize weaker receptor-ligand interactions that are otherwise underestimated in the current setup.

The integration of bulk RNA-seq analysis provided a detailed picture of the genomic and transcriptomic landscape of multiple IT4-SLI lines. The data allowed to investigate the coregulation of *var* proximal genes, specifically the h2h orientation of A-type *var* genes and *rifins*, underscore the complexity of the parasite's gene regulatory networks

[47, 156]. However, the modification of transiently low-expressed A-type *var* genes presented significant challenges in both the creation of new lines and the achievement of the desired cytoadherent phenotype. In the specific case of the MEED line, these difficulties led to the discovery of a promising tool for further research into *var* gene transcription and the mechanisms governing mutually exclusive expression. This line serves as a valuable model for studying the processes that allow parasites to cycle through their antigenic repertoire and evade the host immune response [39].

Finally, this work gathered first valuable data and experience regarding ECR-mimicking peptide-based cytoadhesion inhibition. Although the initial sensitivity of the inhibition assays was not sufficient to generate a comprehensive ranked list of peptide efficacy, the observed effects for promising candidates like $P07^{CD36}$ provide a foundation for second-generation peptide development. Future experiments should implement an increased library size with previous *in silico* optimization of physico-chemical properties will be instrumental in identifying potent inhibitory peptides that could eventually serve as novel antimalarial therapies [176, 188].

A Appendix

A.1 Introduction

A.1.0.1 Domain structures

Gene ID	var gene	Group	Domain structure
PfIT_030029700	IT4var18	A	DBLα1.2 CIDRα1.6 DBLβ3 DBLγ16 DBLγ2 DBLδ1 CIDRβ1
PfIT_060036700	IT4var07	A	DBLα1.7 CIDRα1.4 DBLβ1 DBLβ3 DBLγ10 DBLδ1 CIDRβ1
PfIT_070005900	IT4var08	A	DBLα1.7 CIDRγ3 DBLβ3 DBLδ4 CIDRγ1 DBLζ6 DBLε9
PfIT_070017100	IT4var64	A	DBLα1.5 CIDRδ1 DBLβ7 DBLγ11 DBLγ11
PfIT_090005100	IT4var02	A	DBLα1.5 CIDRδ1 DBLβ3 DBLγ12 DBLδ5 CIDRβ3 DBLβ9
PfIT_100044000	IT4var22	A	DBLα1.4 CIDRα1.7 DBLβ3 DBLγ10 DBLγ11 DBLδ1 CIDRβ1
PfIT_120060300	IT4var60	A	DBLα1.8 CIDRβ2 DBLγ7 DBLζ5 DBLε11 DBLε12
PfIT_130005300	IT4var09	A	DBLα1.6 CIDRγ3 DBLγ15 DBLε1 DBLδ1 CIDRβ1
PfIT_050037800	VAR1CSA	A (var1)	DBLα1.1 CIDRα1.2 DBLβ11 DBLγ1 DBLε1 DBLγ8 DBLζ1 DBLε5
PfIT_140006400	IT4var03	A (var3)	DBLα1.3 DBLε8
PfIT_080037400	IT4var61	B	DBLα0.9 CIDRα2.7 DBLδ1 CIDRβ1
PfIT_100044100	IT4var41	B	DBLα0.4 CIDRα5 DBLβ5 DBLγ5 DBLδ1 CIDRβ1
PfIT_110005600	IT4var54	B	DBLα0.1 CIDRα3.1 DBLδ1 CIDRβ1
PfIT_120005500	IT4var45	B	DBLα0.5 CIDRα2.9 DBLδ1 CIDRβ1
PfIT_140085700	IT4var10	B	DBLα CIDRα DBLβ DBLδ CIDRγ DBLγ DBLζ
PfIT_130077800	IT4var12	B	DBLα0.18 CIDRα6 DBLβ4 DBLδ1 CIDRβ1
PfIT_140006100	IT4var29	B	DBLα0.3 CIDRα3.2 DBLδ1 CIDRγ5
PfIT_140006200	IT4var31	B	DBLα0.18 CIDRα4 DBLβ3 DBLγ9
PfIT_070005800	IT4var44	B	DBLα0.16 CIDRα3.4 DBLβ13 DBLδ1 CIDRβ6
PfIT_130005200	IT4var14	B	DBLα0.23 CIDRα5 DBLβ5 DBLδ1 CIDRγ2 DBLγ3 DBLζ4
PfIT_060036800	IT4var32a	B	DBLα0.23 CIDRα3.2 DBLγ6 DBLδ1 CIDRβ1
PfIT_120060400	IT4var26	B	DBLα0.23 CIDRα3.3 DBLδ1 CIDRβ1
PfIT_050005500	IT4var11	B	DBLα0.3 CIDRα2.4 DBLβ10 DBLδ1 CIDRβ1
PfIT_040030600	or IT4var23 IT4var24	B	DBLα0.10 CIDRα2.2 DBLδ1 CIDRγ5
PfIT_040005400	IT4var33	B	DBLα0.11 CIDRα2.4 DBLδ1 CIDRβ5
PfIT_030029800	IT4var46	B	DBLα0.10 CIDRα2.2 DBLδ1 CIDRγ4 DBLε2 DBLζ3 DBLε3
PfIT_030005100	IT4var40	B	DBLα0.12 CIDRα2.11
PfIT_020005200	IT4var17	B	DBLα0.11 CIDRα2.4 DBLβ8 DBLδ1 CIDRγ4 DBLγ10
PfIT_000009500 (00_4)	IT4var35	B	DBLα0.8 CIDRα5 DBLδ1 CIDRβ1
PfIT_050038500	IT4var25	B	DBLα0.11 CIDRα2.4 DBLδ1 CIDRβ1
PfIT_070017000	IT4var20	B/A	DBLα2 CIDRα1.1 DBLβ12 DBLγ6 DBLδ1 CIDRβ1
PfIT_020027600	IT4var06	B/A	DBLα2 CIDRα1.1 DBLβ12 DBLγ6 DBLδ1 CIDRβ4
PfIT_010005000	or IT4var19 IT4var32b	B/A	DBLα2 CIDRα1.1 DBLβ12 DBLγ6 DBLδ1 CIDRβ1 DBLγ9
PfIT_120045700	IT4var67	B/C	DBLα0.10 CIDRα2.2 DBLε2 DBLζ3 DBLε12
PfIT_120045200	IT4var39	B/C	DBLα0.5 CIDRα2.5 DBLδ1 CIDRβ6
PfIT_120024600	IT4var63	B/C	DBLα0.7 CIDRα3.4 DBLδ1 CIDRβ1
PfIT_070016900	IT4var15	B/C	DBLα0.8 CIDRα3.5 DBLβ8 DBLδ1 CIDRβ1
PfIT_120024500	IT4var16	B/C	DBLα0.4 CIDRα5 DBLβ5 DBLγ16 DBLδ1 CIDRβ1

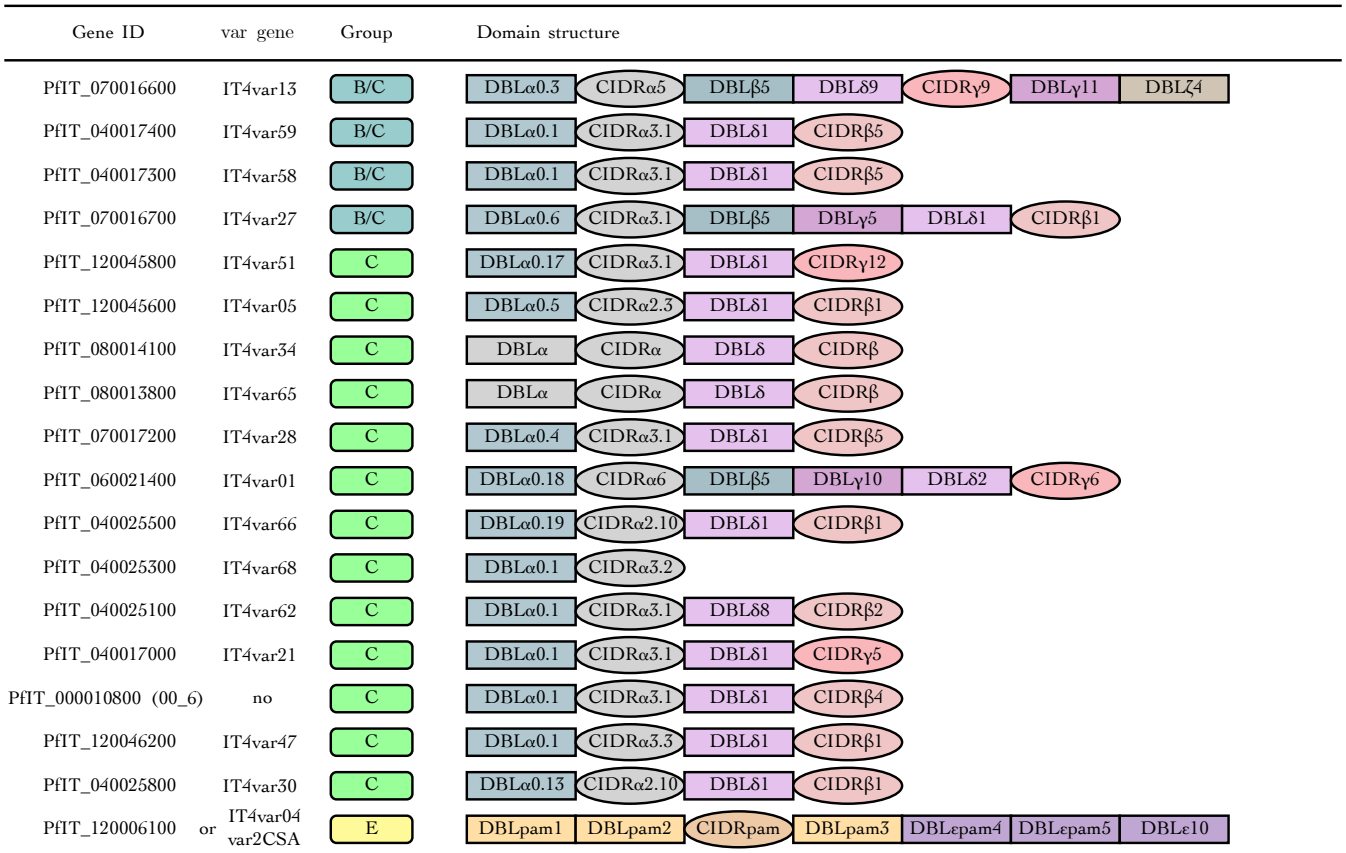


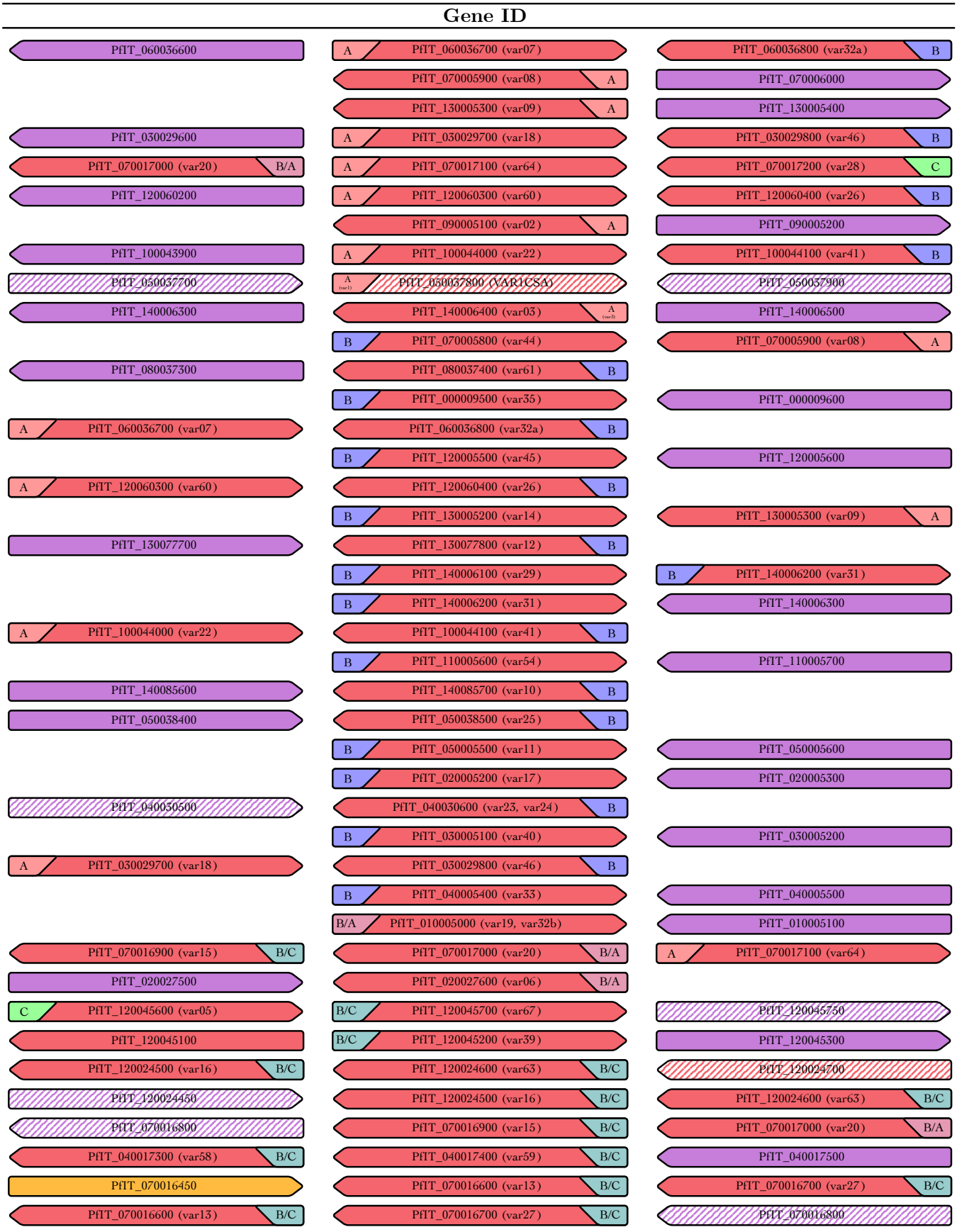
Figure A.1: *Var* gene repertoire and respective domains of IT4/FCR3 isolate. Modified from Dr. Anna Bachmann and [189]

A.1.0.2 Putative G-quadruplex forming sequences

Table A.1: **Non-telomeric putative G-quadruplex forming sequences in FCR3/IT4**. Calculated with QGRS Mapper, Max length: 33; Min G-group: 3; loop size: 0 – 11.

Chrom.	Position	Strand	Length	Putative quadruplex sequences	G-Score	Comment
1	18441	-	30	GGGGGATGTGGGGGAGGCGGGAGCGTTGGG	48	exon1 of *var19/var34b* B/A, PfIT_010005000
2	215619	-	20	GGGAAAGGGATGGGAATGGG	47	
2	690844	+	14	GGGAGGGGGGGGGG	47	
3	200795	-	19	GGGGGGGAGGGGTAAAGGG	45	
3	714344	+	15	GGGGGGGGGGGGGGG	48	
3	1026025	+	32	GGGGATCAAGGGTTTTGTCACTAGGGGAGGGG	40	exon1 of *var46* B, PfIT_030029800
3	1032420	-	30	GGGTTAAGGGTATAACTTTAGGGGTTAGGG	42	1.6 kb ups of *var46* B, PfIT_030029800
4	27647	+	30	GGGTTAAGGGTATAACTTTAGGGGTTAGGG	42	1.6 kb ups from *var33* B, PfIT_040005400
4	512553	+	24	GGGTGAGGGGTTTTGGGGTTTGGG	48	exon1 of *var21* C, PfIT_040017000
4	904658	+	31	GGGCGGTTTTAAGGGGGGGTGGTAAGTAGGG	40	exon1 of *var66* C, PfIT_040025500
4	920079	+	27	GGGGGGGTGGTAAGTAGGGTTGAGGGG	40	exon1 of *var66* C, PfIT_040025500
4	1116138	+	29	GGGTGCCAGTTGGGACAGGGTTGGCAGGG	43	exon1 of IT4var23/IT4var24 B, PfIT_040030600
4	1121158	-	30	GGGTTAAGGGTATAACTTTAGGGGTTAGGG	42	1.6 kb ups from IT4var23/IT4var24 B, PfIT_040030600
4	1130343	-	28	GGGCGTTTTTGGGCAGGGAAAACATGGG	43	
5	369201	-	25	GGGGGGGAATAATCCTATGGGGGGG	38	
5	369320	-	32	GGGGTAATGAAAAGGGGGGATAATCCTATGGG	38	
5	1049507	+	25	GGGGGGATATTCAAGGGGTTGAGGG	40	
5	1155750	+	19	GGGGGGGGGGGGGAAGGGG	70	
7	27480	+	30	GGGTTAAGGGTATAACTTTAGGGGTTAGGG	42	1.6 kb ups from *var44* B, PfIT_070005800
7	41318	+	33	GGGAGGGGGGGACTTACAGGTGGGGGTAAAGGG	43	exon1 of *var08*, PfIT_070005900
7	543522	+	29	GGGTGCGATAAGTCGGGGGGTTCTTGGGG	37	exon1 of *var15*, PfIT_070016900
7	557167	-	32	GGGATCAACATGGGAAGGACATATGGGAAGGG	40	exon1 *var20* B/A, PfIT_070017000
7	569681	-	31	GGGCCGGCGGGGGCAGGTCGTGGGTTTAGGG	44	exon1 *var64* A, PfIT_070017100
7	687763	+	33	GGGATAGGGAGAGAGATAGGGATAGAGATAGGG	42	
7	1057459	+	32	GGGAACCGTGTACAGGGCAGTTATAGGGGGGG	38	
8	110462	-	22	GGGAAAATTTTGGGGGGTTGGG	40	
8	1226799	+	20	GGGTGTGGGGGGTACTAGGG	43	
8	1229490	+	27	GGGTTAGGGTTTAAATTAGGGTTAGGG	42	
8	1229546	+	28	GGGTTAGGGTTTAATATTAGGGTTAGGG	41	
8	1229584	+	28	GGGTTAGGGTTTAATATTAGGGTTAGGG	41	
8	1229622	+	28	GGGTTAGGGTTTAATATTAGGGTTAGGG	41	
8	1229660	+	28	GGGTTAGGGTTTAATATTAGGGTTAGGG	41	
8	1229698	+	28	GGGTTAGGGTTTAATATTAGGGTTAGGG	41	
8	1229736	+	28	GGGTTAGGGTTTAATATTAGGGTTAGGG	41	
8	1229793	+	28	GGGTTAGGGTTTAATATTAGGGTTAGGG	41	
8	1229844	+	24	GGGTTTAGGGTTTAGGGTTTAGGG	48	
8	1229879	+	24	GGGTTTAGGGTTTAGGGTTTAGGG	48	
8	1229907	+	24	GGGTTTAGGGTTTAGGGTTTAGGG	48	
8	1229942	+	22	GGGTTAGGGTTTAGGGTTAGGG	47	
8	1362401	+	25	GGGTGGAAGGGCCGGTTCCGGGGGG	40	exon1 of *var61* B, PfIT_080037400
8	1369006	-	30	GGGTTAAGGGTATAACTTTAGGGGTTAGGG	42	1.7 kB ups of *var61* B, PfIT_080037400
9	1323421	-	18	GGGGGGGAGGGTTTAGGG	45	
10	706302	+	20	GGGGGGGAAGGGAGGTAGGG	44	
10	838750	-	22	GGGGATGGGGATGGGGATGGGG	72	
10	1060637	-	25	GGGAAATGGGGGGTCCAAATATGGG	39	
10	1196731	+	29	GGGGATTGGGTTGATGGGAAAATGCAGGG	44	
10	1559051	-	31	GGGGTTCGTCGGGTTCTTCAAGGGGGGAGGG	44	exon1 of *var22* A, PfIT_100044000
10	1574046	-	30	GGGTTAAGGGTATACATTTAGGGGTTAGGG	42	1.6 kb ups of *var41* B, PfIT_100044100
11	6814	+	28	GGGCGTTTTTGGGTAGGGAAAACATGGG	43	
11	25797	-	24	GGGGGGACAGGGTTTCCGTTTGGG	39	exon1 *var54* B, PfIT_110005600
11	27505	-	31	GGGTTCGGGTGCTGGGGCTTTTTCCTCTGGG	40	exon1 *var54* B, PfIT_110005600
12	24013	+	30	GGGTTAAGGGTATAACTTTAGGGGTTAGGG	42	1.7 kb ups of *var45* B, PfIT_120005500
12	774207	+	26	GGGGGGTTTGGGCGAATTCTTCCGGG	37	exon1 of *var16* B/C, PfIT_120024500
12	784003	+	31	GGGTGGTTTGGGTGGGGGTAGTGGATTTGGG	41	exon1 of *var63* B/C, PfIT_120024600
12	789494	-	30	GGGTTAAGGGTATAACTTTAGGGGTTAGGG	42	1.7 kB ups of *var63* B, PfIT_120024600
12	999261	+	25	GGGGTTGGGTTAGGGTCTATGAGGG	44	
12	1372560	+	14	GGGGGGGTGGGGGG	47	
12	1605134	+	22	GGGGGGGAAGGGGAATGTAGGG	43	
12	1770181	-	23	GGGGGGACAGGGGTTTGTGTGGG	41	exon1 of *var47* C, PfIT_120046200
12	2021013	+	22	GGGGGGAGTTGAAATGGGAGGG	39	
13	17714	+	30	GGGTTAAGGGTATAACTTTAGGGGTTAGGG	42	1.7 kb ups of *var14* B, PfIT_130005200
13	33351	+	29	GGGTCAAAGGGTTGATCCGCAGGGGGGGG	40	exon1 of *var09* A, PfIT_130005300
13	2923407	-	30	GGGTTAAGGGTATAACGTTAAGGGTTAGGG	40	1.7 kB ups of *var12* B, PfIT_130077800
14	50151	-	25	GGGGGGATAAGTCGGGTTGAGGGGG	41	exon1 of *var29* B, PfIT_140006100
14	1243062	-	14	GGGGGGGGGGGGG	47	
00_4	17034	+	30	GGGTTAAGGGTATAACTTTAGGGGTTAGGG	42	1.7 kb ups of *var35* B, PfIT_000009500

A.1.0.3 Neighboring genes to *var*-genes



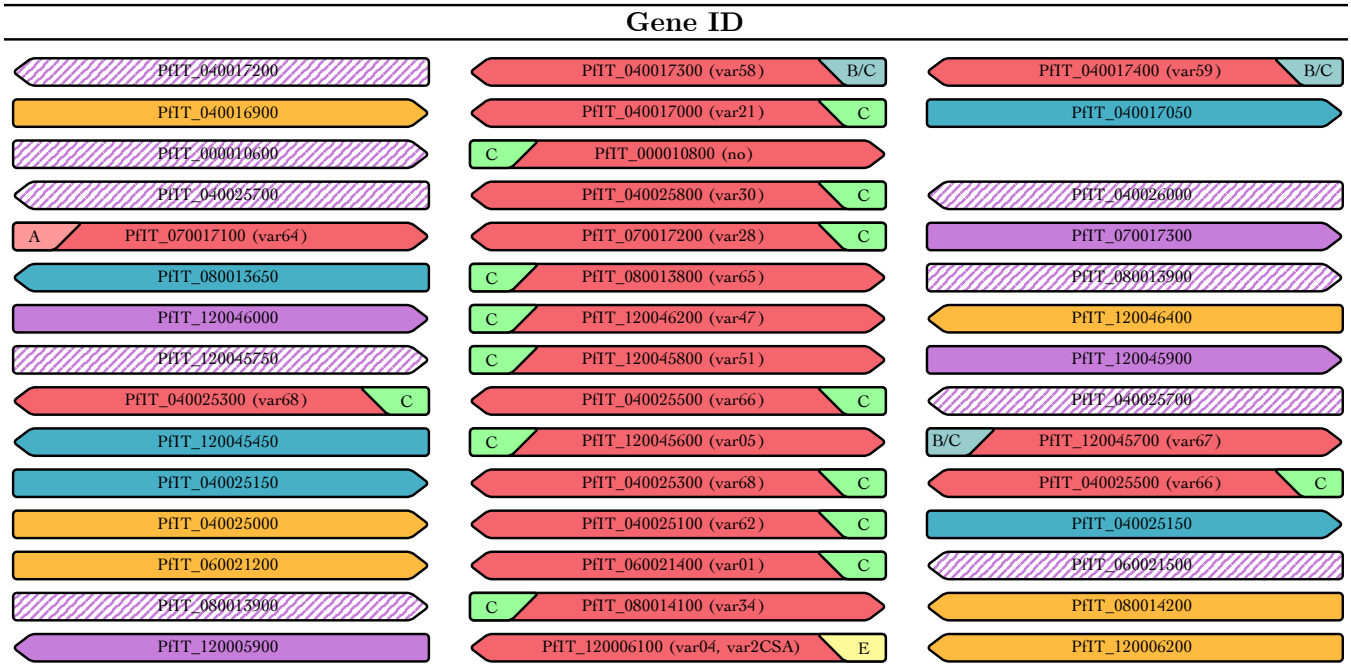


Figure A.2: Genomic *Var* gene orientation of the IT4/FCR3 isolate. The first column *Group* denotes the *var* group, the three following columns show the *var* gene of interest in the middle, and the genes located genomically before in the left column genomically afterwards in the right column. The color of the arrow indicates the select gene families: = *var*, = *rifin*, = *ruf* and all other genes are . Hatched arrows indicate pseudogenes . Arrows pointing right for genes located on the '+'-strand and pointing left for genes on the '-'-strand.

A.2 Material and Methods

Listing A.1: Samples used for *var* orientation analysis

```
IT4-P5-HBMEC_P1-EPCR_1.bam, IT4-P5-HBMEC_P1-EPCR_2.bam, IT4-SLI-var04_230520.bam, IT
4-SLI-var16_04.bam, IT4-SLI-var19-K2-01.bam, IT4-SLI-var19-K2-02.bam, IT4-SLI-var19-
K2-03.bam, IT4-SLI-var19-K2-P5_230531.bam, IT4-SLI-var19-K2-P5_230604.bam, IT4-SLI-
var19-K2-unpanned_230601.bam, IT4-SLI-var66-120422.bam, IT4-SLI-var66-170622.bam, IT
4_1.bam, IT4_2.bam, IT4_3.bam, IT4_BioID-Pos1.bam, IT4_BioID-Pos2.bam, IT4_BioID-
Pos3.bam, SLI-var04-P4-HBEC_231204.bam, SLI-var04-P4_HBEC_231206.bam, SLI-var04-
P4_HBEC_231208.bam, SLI-var04_221212.bam, SLI-var04_231123.bam, SLI-var04_231223.bam
, SLI-var08-P4-ICAM1_241020.bam, SLI-var08-P4-ICAM_231221.bam, SLI-var08-P4-ICA
M_240101.bam, SLI-var08-P5-ICAM1-P4-EPCR_240525.bam, SLI-var08_231123.bam, SLI-
var08_231202.bam, SLI-var08_231206.bam, SLI-var08_P4-ICAM_231219.bam, SLI-
var09_231108.bam, SLI-var09_231202.bam, SLI-var09_231204.bam, SLI-var09_231206.bam,
SLI-var09_231219.bam, SLI-var19-K2_P5_230614.bam, SLI-var19-K2_P5_231121.bam, SLI-
var20-c32_x1.bam, SLI-var31_241206.bam, SLI-var46_251206.bam, var02_1.bam, var02_2.
bam, var02_3.bam, var03_1.bam, var03_2.bam, var03_3.bam, var04_1.bam, var04_2.bam,
var08_1.bam, var08_2.bam, var08_3.bam, var16_1.bam, var16_2.bam, var16_3.bam,
var19_1.bam, var19_2.bam, var20_1.bam, var20_2.bam, var20_3.bam
```

Listing A.2: **Sequence: var27-20**. Recombined *var* gene from *var20* and *var27* in IT4var20-HA^{endo}

```
>>var27-var20b
1       ATGGTGGAGTTAGCAAAAATGGGGCCCAAGGAGGCTGCAGGTGGGGATGATATTGAGGAT
61      GAAAGTGCCAAACATATGTTTGATAGGATAGGAAAAGATGTGTACGATAAAGTAAAAGAG
121     GAAGCTAAAGAACGTGGTAAAGGCTTGCAAGGACGTTTGTCAGAAGCAAAATTTGAGAAA
181     AATGAAAGCGATCCACAAACACCAGAAGATCCATGCGATCTTGATCATAAATATCATACA
241     AATGTAACTACTAATGTAATTAATCCGTGCGCTGATAGATCTGACGTGCGTTTTTCCGAT
301     GAATATGGAGGTCAATGTACACATAATAGAATAAAAGATAGTCAACAGGGTGATAATAAA
361     GGTGCATGTGCTCCATATAGGCGATTGCATGTATGCGATCAAAATTTAGAACAGATAGAG
421     CCTATAAAAATAACAAATACTCATAATTTATTGGTAGATGTGTGTATGGCAGCAAAATTT
481     GAAGGACAATCAATAACACAAGATTATCCAAAATATCAAGCAACATATGGTGATTCTCCT
541     TCTCAAATATGTACTATGCTGGCACGAAGTTTTGCGGACATAGGGGACATTGTCAGAGGA
601     AGAGATTTGTATTTAGGTAATCCACAAGAAATAAAACAAAGACAACAATTAGAAAATAAT
661     TTGAAAACAATTTTCGGGAAAATATATGAAAAATTGAATGGCGCAGAAGCACGCTACGGA
721     AATGATCCGGAATTTTTTAAATTACGAGAAGATTGGTGGACTGCTAATCGAGAAACAGTA
781     TGGAAAGCCATCACATGTAACGCTTGGGGTAATACATATTTTCATGCAACGTGCAATAGA
841     GGAGAACGAACTAAAGGTTACTGCCGGTGTAACGACGACCAAGTTCCCACATATTTTGAT
901     TATGTGCCGCAGTATCTTCGCTGGTTCGAGGAATGGGCAGAAGATTTTTGTAGGAAAAAA
961     AATAAAAAAATAAAAGATGTTAAAAGAAATTGTCGTGGAAAAGATAAAGAGGATAAGGAT
1021    CGATATTGTAGCCGTAATGGCTACGATTGCGAAAAAACTAAACGAGCGATTGGTAAGTTG
1081    CGTTATGGTAAGCAATGCATTAGCTGTTTGTATGCATGTAATCCTTACGTTGATTGGATA
1141    AATAACCAAAAAGAACAATTTGACAAACAGAAAAAAAAATATGATGAAGAAATAAAAAAA
1201    TATGAAAATGGAGCATCAGGTGGTAGTAGGCAAAAACGGGATGCAGGTGGTACAACTACT
1261    ACTAATTATGATGGATATGAAAAAAAATTTTATGACGAACTTAATAAAAGTGAATATAGA
1321    ACCGTTGATAAATTTTTGGAAAAATTAAGTAATGAAGAAATATGCACAAAAGTTAAAGAC
1381    GAAGAAGGAGGAACAATTGATTTTAAAAACGTTAATAGTGATAGTACTAGTGGTGCTAGT
1441    GGCACTAATGTTGAAAGTCAAGGAACATTTTATCGTTCAAAATATTGCCAACCCTGCCCT
1501    TATTGTGGAGTGAAAAAGGTAAATAATGGTGGTAGTAGTAATGAATGGGAAGAGAAAAAT
1561    AATGGCAAGTGCAAGAGTGGAAAACTTTATGAGCCTAAACCCGACAAAGAAGGTACTACT
1621    ATTACAATCCTTAAAAGTGGTAAAGGACATGATGATATTGAAGAAAAATTAAACAAATTT
1681    TGTGATGAAAAAAATGGTGATACAATAAATAGTGGTGGTAGTGGTACGGGTGGTAGTGGT
1741    GGTGGTAACAGTGGTAGACAGGAATTGTATGAAGAATGGAAATGTTATAAAGGTGAAGAT
1801    GTAGTGAAAGTTGGACACGATGAGGATGACGAGGAGGATTATGAAAATGTAAAAAATGCA
1861    GGCGGATTATGTATATTAAAAAACCAAAAAAAGAATAAAGAAGAAGGTGGAAATACGTCT
```

1921 GAAAAGGAGCCTGATGAAATCCAAAAGACATTCAATCCTTTTTTTTACTATTGGGTTGCA

1981 CATATGTTAAAAGATTCCATACATTGGAAAAAAAAACTTCAGAGATGTTTACAAAATGGT

2041 AACAGAATAAAATGTGGAAACAATAAATGTAATAATGATTGTGAATGTTTTAAAAGATGG

2101 ATTACACAAAAAAAAGACGAATGGGGGAAAATAGTACAACATTTTAAAACGCAAAATATT

2161 AAAGGTAGAGGAGGTAGTGACAATACGGCAGAATTAATCCCATTTGATCACGATTATGTT

2221 CTTCAATACAATTTGCAAGAAGAATTTTTGAAAGGCGATTCCGAAGACGCTTCCGAAGAA

2281 AAATCCGAAAATAGTCTGGATGCAGAGGAGGCAGAGGAACTAAAACACCTTCGCGAAATC

2341 ATTGAAAGTGAAGACAATAATCAAGAAGCATCTGTTGGTGGTGGCGTCACTGAACAAAAA

2401 AATATAATGGATAAATTGCTCAACTACGAAAAAGACGAAGCCGATTTATGCCTAGAAATT

2461 CACGAAGATGAGGAAGAGGAAAAAGAAAAAGGAGACGGAAACGAATGTATCGAAGAGGGC

2521 GAAAATTTTCGTTATAATCCATGTAGTGGCGAAAGTGGTAACAAACGATACCCCGTTCTT

2581 GCGAACAAAGTAGCGTATCAAATGCATCACAAGGCAAAGACACAATTGGCTAGTCGTGCT

2641 GGTAGAAGTGCGTTGAGAGGTGATATATCCTTAGCGCAATTTAAAAATGGTCGTAACGGA

2701 AGTACATTGAAAGGACAAATTTGCAAAATTAACGAAAACTATTCCAATGATAGTCGTGGT

2761 AATAGTGGTGGACCATGTACAGGCAAAGATGGAGATCACGGAGGTGTGCGCATGAGAATA

2821 GGAACGGAATGGTCAAATATTGAAGGAAAAAAACAAACGTCATACAAAAACGTCTTTTTA

2881 CCTCCCCGACGAGAACACATGTGTACATCCAATTTAGAAAATTTAGATGTTGGTAGTGTC

2941 ACTAAAAATGATAAGGCTAGCCACTCATTATTGGGAGATGTTCAGCTCGCAGCAAAAACT

3001 GATGCAGCTGAGATAATAAAACGCTATAAAGATCAAAATAATATACAACTAACTGATCCA

3061 ATACAACAAAAAGACCAGGAGGCTATGTGTCGAGCTGTACGTTATAGTTTTGCCGATTTA

3121 GGAGACATTATTCGAGGAAGAGATATGTGGGATGAGGATAAGAGCTCAACAGACATGGAA

3181 ACACGTTTGATAACCGTATTTAAAAACATTAAAGAAAAACATGATGGAATCAAAGACAAC

3241 CCTAAATATACCGGTGATGAAAGCAAAAAGCCCGCATATAAAAAATTACGAGCAGATTGG

3301 TGGGAAGCAAATAGACATCAAGTGTGGAGAGCCATGAAATGCGCAACAAAAGGCATCATA

3361 TGTCCTGGTATGCCAGTTGACGATTATATCCCCCAACGTTTACGCTGGATGACTGAATGG

3421 GCTGAATGGTATTGTAAAGCGCAATCACAGGAGTATGACAAGTTAAAAAAAATCTGTGCA

3481 GATTGTATGAGTAAGGGTGATGGAAAATGTACGCAAGGTGATGTCGATTGTGGAAAGTGC

3541 AAAGCAGCATGTGATAAATATAAAGAGGAAATAGAAAAATGGAATGAACAATGGAGAAAA

3601 ATATCAGATAAATACAATCTATTATACCTACAAGCAAAAACTACTTCTACTAATCCTGGC

3661 CGTACTGTTCTTGGTGATGACGATCCCGACTATCAACAAATGGTAGATTTTTTGACCCCA

3721 ATACACAAAGCAAGTATTGCCGCACGTGTTCTTGTTAAACGTGCTGCTGGTAGTCCCACT

3781 GAGATCGCCGCCGCCGCCCCGATCACCCCCTACAGTACTGCTGCCGGATATATACACCAG

3841 GAAATAGGATATGGGGGGTGCCAGGAACAAACACAATTTTGTGAAAAAAAACATGGTGCA

3901 ACATCAACTAGTACCACGAAAGAAAACAAAGAATACACCTTTAAACAACCTCCGCCGGAG

3961 TATGCTACAGCGTGTGATTGCATAAATAGGTCGCAAACAGAGGAGCCGAAGAAAAAGGAA

4021 GAAAATGTAGAGAGTGCCTGCAAAATAGTGGAGAAAATACTTGAGGGTAAGAATGGAAGG

4081 ACTACAGTAGGTGAATGTAATCCAAAAGAGAGTTATCCTGATTGGGATTGCAAAAACAAT

4141 ATTGACATTAGTCATGATGGTGCTTGTATGCCTCCAAGGAGACAAAAACTATGTTTATAT

4201 TATATAGCACATGAGAGTCAAACAGAAAATATAAAAACAGACGATAATTTGAAAGATGCT

4261 TTTATTAAAACTGCAGCAGCAGAAACTTTTCTTTCATGGCAATATTATAAGAGTAAGAAT

4321 GATAGTGAAGCTAAAATATTAGATAGAGGCCTTATTCCATCCCAATTTTTAAGATCCATG

4381 ATGTACACGTTTGGAGATTATAGAGATATATGTTTGAACACAGATATATCTAAAAAACAA

4441 AATGATGTAGCTAAGGCAAAAGATAAAATAGGTAAATTTTTCTCAAAAGATGGCAGCAAA

4501 TCTCCTAGTGGCTTATCACGCCAAGAATGGTGGAAAACAAATGGTCCAGAGATTTGGAAA

4561 GGAATGTTATGTGCCTTAACAAAATACGTCACAGATACCGATAACAAAAGAAAAATCAAA

4621 AACGACTACTCATACGATAAAGTCAACCAATCCCAAAATGGCAACCCTTCCCTTGAAGAG

4681 TTTGCTGCTAAACCTCAATTTCTACGTTGGATGATCGAATGGGGAGAAGAGTTTTGTGCT

4741 GAACGTCAGAAGAAGGAAAATATCATAAAAGATGCATGTAATGAAATAAATTCTACACAA

4801 CAGTGTAATGATGCGAAACATCGTTGTAATCAAGCATGTAGAGCATATCAAGAATATGTT

4861 GAAAATAAAAAAAAAGAATTTTCGGGACAAACAAATAACTTTGTTCTAAAGGCAAATGTT

4921 CAGCCCCAAGATCCAGAATATAAAGGATATGAATATAAAGACGGCGTACAACCGATACAG

4981 GGGAATGAGTATTTACTGCAAAAATGTGATAATAATAAATGTTCTTGCATGGATGGAAAT

5041 GTACTTTCCGTCTCTCCAAAAGAAAAACCTTTTGGAAAATATGCCCATAAATATCCTGAG

5101 AAATGTGATTGTTATCAAGGAAAACATGTACCTAGCATACCACCTCCCCCCCCACCTGTA

5161 CAACCACAACCGGAAGCACCAACAGTAACAGTAGACGTTTGCAGCATAGTAAAAACACTA

5221 TTTAAAGACACAAACAATTTTTCCGACGCTTGTGGTCTAAAATACGGCAAAACCGCACCA

5281 TCCAGTTGGAAATGTATACCAAGTGACACAAAAAGTGGTGCTGGTGCCACCACCGGCAAA

5341 AGTGGTAGTGATAGTGGTAGTATTTGTATCCCACCCAGGAGGCGAAAACTATACCTACAC

5401 AAAATAGAAGGCGTCGACACCACCGTGTCAAGTGATGGAGAAACCACCACACCGATCACA

5461 CACGACGCGTTACGTGAGGCATTTATTCAAACTGCTGCTGTGGAAACTTTTTTCTTATGG

5521 CATAGATATAAAAAAATAAAAGAAAAGGAAAGACAGGAGGAACTACAAAATGGAACACTT

5581 TTATTACCACCTGCCCAAAAAGTGTCACCGGAGGACAACCCAGAACATCCCCAAAAGAAA

5641 TTAAAAGAAGGAAAAATCCCTGAGGAGTTTAAAAGACAAATGTTCTATACTTTAGGGGAT

5701 TATAGAGATTTATGTGTGGGTGTTAAAGACGACGTGGCTCAGGCGTTAGAAGCTAGTGGT

5761 GATAACAAAAGTGGCGACAAAAATATAAAAGATATATCGGAGAAAATAAAAAGTGTTATT

5821 GAAAAAAGTGGTGAACAAACTCCTCCTGGCCCCAAACCCGGTCAAACAACAACCAAACCA

5881 GAAGAGTGGTGGCAAAAAAATGGTGAACATATCTGGAATGCAATGATATGTGCTCTAACA

5941 CACAACACAGACACGCGACAAGTGGATGACCAAGTGAAAGGACAACTTTTCGAAAATGGA

6001 AAGAACACCCCCAAAAACTCCCAATACCAATACAAAAATGTCACAATTAGTAGTGTTTCT

6061 AGTAATGGTGGTCCTATTGGTAATATCAAACTGGAACAATTTGCTTCTAGACCTACATTT

6121 TTGCGCTGGTTAGAGGAATGGGGAGAAGAGTTTTGCCGTAAACAGTATCACAAGTTGGAA

6181 AGGATTAAGGAAGAATGTCACAAAGATGGTAATAGAAATTGTGATGATGATGGATTTGAA

6241 TGCAAAGAAATGTGTCCATGTAAGGATGGATCTTTTGAAACTTTGAAATGTCCCAGTTGT

6301 GCCAAATCTTGTAAGTCTTATAAAAAGTGGATAAGTAGGAAAAAAGACGAATTTACTAAA

6361 CAAAAAGGGGCATATGAAAAACAAAAAAAGGATGCCGAAGGTAATAATAATGATTATAAA

6421 GAATTTTCTAAAACACTAAGAAACTACAATGACGCTGCAGCATTTTTAAATAGCTTAAAA

6481 AACGGACCATGTTCTAAAAACGATGATGACAGTGTACAGGATGAAATAAAATTTGATGAT

6541 GAACGTAAGACATTTGGACATGAAACATATTGTAAACCATGTTCTAAAATTACAGTTAAA

6601 TGTAAGGAAAATAATCATTGCGATAATTCTAAACCAAATGATTGCCGAAATATAAATAGT

6661 ATTTCTGCAGAAGATATTGAAAAAAGGAGTAATTCTACTCAAGATGTTACTATGAGTGTC

6721 AGTGATAGCAATACAAATGGAAATAAATTTTATGATTTAAATGATTGTATAAAAGCAGGT

6781 ATATTTAAAGGTATTAGAGAAGATGTATGGAAATGTGGTGAATACTGTGGTGTAGATATA

6841 TGCACTCTGGAAAAAACCAATAATGAAGAAAGAGTCAGTGCGAAAGAAAATGATGGTAAA

6901 AACCAAATTATATTAATTAGAGTACTGTTTAAAAGATGGCTAGAAAGTTTTTTAGAAGAT

6961 TATAATAAAATTAATGACAAAATTTCACATTGTATGAAAAATGATAAAAAATCCCCATGT

7021 ATAAATGGATGTCAAAATAAATGTAATTGTGTAGAAAAATGGATAGAGAAGAAAAAAAGT

7081 GAATGGGGAAAGGTACGAGAACGTTACATCAATCAATATAGGGATAAGAATTCAAATGAA

7141 GCTTTCGAAGTGAAAAGTTTTTTGGAGACCTTGATACCTCAAATTCCTGTTGTAACTGAT

7201 AAAGGAAAGCATGACAGTTTAACTCAGTTAAAGAAGTTACTTAAATGTAATTGCTCTGAG

7261 AAGTCAGAAAATAGTAATGAGAAGGATGTTGTTCTATGTTTGCTTAAAAAGCTTGAAGAT

7321 AAAGCAAAAAATTGTAAAGACCAAGCTAGTGGCGAACCCTGTCCTCAAACCACATCAGAA

7381 AACCCTGATGATGAGGACATACTCCTTGAAGAGGAAAACCCAGTGGAAGCGCCAAACATT

7441 TGTCCGAAAGTGGAAGAACCAGAACCAGTGGTAGAAGAAGAAAAGTGTGACCTAGCAGAG

7501 GCACCATCAAAAGAATCATCAACAGAAGAAAATAGTGGTGAAGGCTCCAACTCTGAACAA

7561 ACCCCCGTTCTCAAGCCAGAAGAGGAACCTCCACCTCCTACTTCTTCTGAAACTGATACC

7621 CCTCCACCCGCGCCTCCAACAATACAACCCTCCCAAGCCGACCAACCAACAAACTCTATA

7681 AGTGACATATTATCATCTACCATCCCCTTTGGAATAGCTATTGCGTTAACTTCGATAGTG

7741 TTTTTATTTTTGAAGGTAATATATATAGTGGTATATATGTATATATATGCGTTTTGTGTA

7801 TATGTATGTACGGGTGTTTTGGGATGTATATATATGTATATATATGTTTGTATGTATATG

7861 TGTTTCTGTATATGTATCTGTTAGTATGTTTGGATATATATGTGTGTATATGTATGTGTT

7921 TTATATATATTTTATATATATGTATTTATATTAAAAAAGAAATATAAAAAAAAAATTATT

7981 AAAATAAAAAAAAAAAAAAAAAAAAAGGAGAAAAATATTTTAAAAATAATAAAAATTAAA

8041 ATAAAAATATAAATTTTGATAAAATAAAAAATGAAAAATATTATCAAAAAGAAATTAAAA

8101 AAAATTTTATATATAAAAAAAATGATTATAAAAAAAAATTTATTAGAAATAAAATAAAAA

8161 AAAATTTATTACATAAAAAAAAAAAAAGTTAAAAAAAAAATATATATCATAAAATAAAAA

8221 GAAAAGGGAAAAAATGTTAAAAAAAAAAATAAAATTAAAAAAAAAAAAAAAAAAAAAAAA

8281 AAAATTAAAAAAATTTTAAAAAAAAAATATATATCATAAAAAAAAAAAGAAATAAAAAAA

8341 TTTATTTAAATAAAATAAAAAAAAATTTAATGAAATAAAAAAAAATAAAAAAATTGAATT

8401 AAATAAAAAAAATAAAATAAAATTAATTACATGCACATATACACATACATATATATATAT

8461 ACCCATAACTACATTCATATATACGCATACATATATATATTATATATATATATACCCATA

8521 ACTACGTACACATATACACATACATATATATATATACCCATAACTACATACATACATA

8581 TACCTACACATACATATACACATATACATATATGTTCCTTTTTTTTTTAGAAAAAAACCAA

8641 ATCGTCGGTGGACTTGTTGCGTGTACTGAATATCCCGAAAGGAGAGTATGGAATGCCTAC

8701 ATTGAAATCAAGCAATCGTTATATCCCCTATGCTAGTGATCGATATAAAGGCAAAACATA

8761 CATTTATATGGAAGGAGATAGTGATAGTGGACACTACTACGAAGATACAACTGATGTTAC

8821 CTCTTCCGAAAGTGAGTATGAAGAATTGGATATTAATGATATATATGTACCAGGTAGTCC

8881 TAAATATAAAACGTTGATTGAAGTGGTACTAGAACCTAGTGGTAACAACACAACAGCTAG

8941 TGGTAAAAACACACCTAGTGATACACAAAATGATATACAAAATGATGGTATACCTAGTAG

9001 TAAAATTACAGATAATGAGTGGAATACATTGAAAGATGAATTTATATCACAATATCTACA

9061 AAGTGAACAACCAAATGATGTACCAAATGATTATACAAGTGGAAATAGTTCAACAAATAC

9121 CAATATTACTACCACGTCACGTCATAATGTGGAAGAAAAACCTTTTATTATGTCTATTCA

9181 TGATAGAAATTTATATACTGGAGAAGAAATTAATTATAATGTTAATATGGTTAATACTAT

9241 GGATGATATTCCAATTAATCGTGATAATAATGTTTATAGTGGTATAGATTTAATTAATGA

9301 CGCACTAAATGGTGATTATGACATTTACGATGAAGTATTGAAAAGAAAAGAAAATGAATT

9361 ATTTGGTACAAATCATGTGAAACAAACAAGTATACATAGTGTTGCCAAACCTGCACGTGA

9421 CGACCCCATCCACAACCAACTGGAACTATTCCATAAATGGCTAGATAGACATAGAGATAT

9481 GTGCGAAAAGTTGAAAAATCATCACGAACGATTAGCCAAATTGAAAGAAGAGTGGGAAAA

9541 TGAGACACATAGTGGTAACACTCACCCTAGTGATAGTAACAAAACGTTGAATACTGACGT

9601 TTCGATACAAATACATATGGATAATCCTAAACCTATAAATGAATTTACTAATATGGATAC

9661 TATCTTGGACGATCTGGATAAATATAATGAACCTTATTATGATGTGCAAGATGATATTTA

9721 TTATGATGTAAATGATCATGATACATCAACTGTGGATAGTAATGCTATGGATGTACCTAG

9781 TAAAGTACAAATTGAAATGGATGTAAATACCAAATTGGTGAAAGAGAAATATCCTATAGC

9841 AGATGTATGGGATATATAA

Listing A.3: **Sequence: var27-20**. Recombined *var* gene from *var20* and *var27* in IT4var20-HA^{endo}

```
>var27-20c
1       ATGGTGGAGTTAGCAAAAATGGGGCCCAAGGAGGCTGCAGGTGGGGATGATATTGAGGAT
61      GAAAGTGCCAAACATATGTTTGATAGGATAGGAAAAGATGTGTACGATAAAGTAAAAGAG
121     GAAGCTAAAGAACGTGGTAAAGGCTTGCAAGGACGTTTGTCAGAAGCAAAATTTGAGAAA
181     AATGAAAGCGATCCACAAACACCAGAAGATCCATGCGATCTTGATCATAAATATCATACA
241     AATGTAACTACTAATGTAATTAATCCGTGCGCTGATAGATCTGACGTGCGTTTTTCCGAT
301     GAATATGGAGGTCAATGTACACATAATAGAATAAAAGATAGTCAACAGGGTGATAATAAA
361     GGTGCATGTGCTCCATATAGGCGATTGCATGTATGCGATCAAAATTTAGAACAGATAGAG
421     CCTATAAAAATAACAAATACTCATAATTTATTGGTAGATGTGTGTATGGCAGCAAAATTT
481     GAAGGACAATCAATAACACAAGATTATCCAAAATATCAAGCAACATATGGTGATTCTCCT
541     TCTCAAATATGTACTATGCTGGCACGAAGTTTTGCGGACATAGGGGACATTGTCAGAGGA
601     AGAGATTTGTATTTAGGTAATCCACAAGAAATAAAACAAAGACAACAATTAGAAAATAAT
661     TTGAAAACAATTTTCGGGAAAATATATGAAAAATTGAATGGCGCAGAAGCACGCTACGGA
721     AATGATCCGGAATTTTTTAAATTACGAGAAGATTGGTGGACTGCTAATCGAGAAACAGTA
781     TGGAAAGCCATCACATGTAACGCTTGGGGTAATACATATTTTCATGCAACGTGCAATAGA
841     GGAGAACGAACTAAAGGTTACTGCCGGTGTAACGACGACCAAGTTCCCACATATTTTGAT
901     TATGTGCCGCAGTATCTTCGCTGGTTCGAGGAATGGGCAGAAGATTTTTGTAGGAAAAAA
961     AATAAAAAAATAAAAGATGTTAAAAGAAATTGTCGTGGAAAAGATAAAGAGGATAAGGAT
1021    CGATATTGTAGCCGTAATGGCTACGATTGCGAAAAAACTAAACGAGCGATTGGTAAGTTG
1081    CGTTATGGTAAGCAATGCATTAGCTGTTTGTATGCATGTAATCCTTACGTTGATTGGATA
1141    AATAACCAAAAAGAACAATTTGACAAACAGAAAAAAAAATATGATGAAGAAATAAAAAAA
1201    TATGAAAATGGAGCATCAGGTGGTAGTAGGCAAAAACGGGATGCAGGTGGTACAACTACT
1261    ACTAATTATGATGGATATGAAAAAAAATTTTATGACGAACTTAATAAAAGTGAATATAGA
1321    ACCGTTGATAAATTTTTGGAAAAATTAAGTAATGAAGAAATATGCACAAAAGTTAAAGAC
1381    GAAGAAGGAGGAACAATTGATTTTAAAAACGTTAATAGTGATAGTACTAGTGGTGCTAGT
1441    GGCACTAATGTTGAAAGTCAAGGAACATTTTATCGTTCAAAATATTGCCAACCCTGCCCT
1501    TATTGTGGAGTGAAAAAGGTAAATAATGGTGGTAGTAGTAATGAATGGGAAGAGAAAAAT
1561    AATGGCAAGTGCAAGAGTGGAAAACTTTATGAGCCTAAACCCGACAAAGAAGGTACTACT
1621    ATTACAATCCTTAAAAGTGGTAAAGGACATGATGATATTGAAGAAAAATTAAACAAATTT
1681    TGTGATGAAAAAAATGGTGATACAATAAATAGTGGTGGTAGTGGTACGGGTGGTAGTGGT
1741    GGTGGTAACAGTGGTAGACAGGAATTGTATGAAGAATGGAAATGTTATAAAGGTGAAGAT
1801    GTAGTGAAAGTTGGACACGATGAGGATGACGAGGAGGATTATGAAAATGTAAAAAATGCA
1861    GGCGGATTATGTATATTAAAAAACCAAAAAAAGAATAAAGAAGAAGGTGGAAATACGTCT
```

1921 GAAAAGGAGCCTGATGAAATCCAAAAGACATTCAATCCTTTTTTTTACTATTGGGTTGCA

1981 CATATGTTAAAAGATTCCATACATTGGAAAAAAAAACTTCAGAGATGTTTACAAAATGGT

2041 AACAGAATAAAATGTGGAAACAATAAATGTAATAATGATTGTGAATGTTTTAAAAGATGG

2101 ATTACACAAAAAAAAGACGAATGGGGGAAAATAGTACAACATTTTAAAACGCAAAATATT

2161 AAAGGTAGAGGAGGTAGTGACAATACGGCAGAATTAATCCCATTTGATCACGATTATGTT

2221 CTTCAATACAATTTGCAAGAAGAATTTTTGAAAGGCGATTCCGAAGACGCTTCCGAAGAA

2281 AAATCCGAAAATAGTCTGGATGCAGAGGAGGCAGAGGAACTAAAACACCTTCGCGAAATC

2341 ATTGAAAGTGAAGACAATAATCAAGAAGCATCTGTTGGTGGTGGCGTCACTGAACAAAAA

2401 AATATAATGGATAAATTGCTCAACTACGAAAAAGACGAAGCCGATTTATGCCTAGAAATT

2461 CACGAAGATGAGGAAGAGGAAAAAGAAAAAGGAGACGGAAACGAATGTATCGAAGAGGGC

2521 GAAAATTTTCGTTATAATCCATGTAGTGGCGAAAGTGGTAACAAACGATACCCCGTTCTT

2581 GCGAACAAAGTAGCGTATCAAATGCATCACAAGGCAAAGACACAATTGGCTAGTCGTGCT

2641 GGTAGAAGTGCGTTGAGAGGTGATATATCCTTAGCGCAATTTAAAAATGGTCGTAACGGA

2701 AGTACATTGAAAGGACAAATTTGCAAAATTAACGAAAACTATTCCAATGATAGTCGTGGT

2761 AATAGTGGTGGACCATGTACAGGCAAAGATGGAGATCACGGAGGTGTGCGCATGAAAATA

2821 GGAACACCATGGAAGCCTGGGAGACAGATACAAATGTCAGCCGAAGATATCTACATGCCA

2881 CCCCGACGTCAACATATGTGTACATCCAATTTGGAATATTTACAAACGAAAGATGGCCCA

2941 CTAAAACAGGGAGATGGCAAACTTGTTAATAATTCTTTTTTAGGAGATGTACTTCTATCA

3001 GCTAAAATGGATGCAGGCAAAATAATAGAACTGTATAAAAAACAGAATAACAAAAGTAAC

3061 CTAACTGATCCAGAGGATAATGAAAGTGCATGTAGAGCATTGCGCTATAGTTTTGCTGAT

3121 CTTGGAGACATTATTAGAGGAAGAGACCTGTGGGATAAAAACAGTGATGCTAAGAGATTA

3181 CAAACAAATTTGAAAGAAATATTTACTAAAATTAAAGAGGAACTTCCTGAAGACATCAAA

3241 AAAAAATATGATAAAGATGGCACGGATCATAAACTATTGAGAGAAGACTGGTGGGAGGCT

3301 AATAGACATCAAGTTTGGAGAGCTATGAAATGTGCAATAGAAAATGACAAAGATATGAAA

3361 TGTAATGGTATCCCCATAGAAGATTATATTCCGCAAAGATTAAGATGGATGACAGAATGG

3421 GCAGAATGGTTCTGCAAAGAACAGTCACGGTTGTATAACAAATTGGTAGCGGATTGTAAG

3481 AGTTGTAAGGGAAAAGCGAAATCATGTACACAAAAGGATGGTGACTGTACTAAATGCAAA

3541 GCAGCATGTGATAATTATAATAAGAAAATAAAACCATGGGAAGAACAATGGGAAAAAATA

3601 AAAAATAAATACGCACAATTATACAAAAAAGCATTAGATAGTGTTAATGGTAAGGAAGAA

3661 AGTAAAAAAAAAACTGCTAGTGATGCTAAAGACCAACAGGTTGTACATTTCTTGGCAGAA

3721 TTAATACGAAAAAGTGGTGGAGGTAAAGGTGGTAAAAATGTTAAAACCACTGTGTCCCCC

3781 ACCACCACCCCGAACACCCTCTACAGTTCCGCCGCAGGCTACATCCACCACGAATTGGGG

3841 AGGACCGTGGGATGTAACACGCAGAAGGAGTTTTGTTACAGCAAGAACGGTAAATACGCT

3901 TTTAAGGATCCTCCAAAAGGATATGAAGAGGCGTGTAAATGTAACGACAGAAATCCGAAA

3961 CCACAACCGGCACCAAAAAAAGAAGATGAAGATGCGTGCGATGTAGTTAAACCACTTTTG

4021 AAGGATAAGGGCGAAACAGATGATATAGATGGGTGCAATCAAAAATATAAAGCTGGAAAA
4081 GACAAATACCCTGGATGGGATTGTAATTCTCAGATTCATACAACACATAATGGAGCATGT
4141 ATGCCTCCTAGAAGACAAAAATTATGCGTAAGTGGTTTAACAAAAACAGATAGAATAAAA
4201 GCAATAGAATATATAAGAACAGAGTTTATTAAATCTGCAGCTATAGAAACACATTTTGCT
4261 TGGGATAGATATAAAGAGGATAATGGAGAAGCAGAAGCTGAATTAAAAAATGGAAATATT
4321 CCTGAAGGATTTAAAAGACAAATGTATTATACATTTGGTGATTATAGAGATATATTTTTC
4381 GGAAGAGATATTTCTACACATGCCTATATTTCAGGGGTATCGCCAAAAGTAATAACCATT
4441 TTAGAAAAGGAAAATGATGCAAAATACGCTGCTAAACAAAATTCAAACAACGAATTGCTT
4501 GACGACTGGTGGGATCAACATGGGAAGGACATATGGGAAGGGATGCTCTGTGCTTTAACA
4561 CATAAAATTTCAGATGAAGAAAAAAAAAAAGAAATCAAAAACAAGTACTCATACAAGAAA
4621 CTGAACGAGTCCCCCAAAGGCAGCAACAAAGTGGAAGATTTTGCTAAAAAACCTCAATTT
4681 TTGAGATGGTTTATTGAATGGGGCGATGAATTTTGTGCACAACGTGAAGAAAAGGAGGCT
4741 AAGGTAAAAGTATCTTGTAGTGATGCTAAGGATTATGATGGGTGTAAAAACACTAAGAGT
4801 AACGCTAGTTGTGTTAGCGCATGTAAAGTATATGAAGATTATATTACCAAGAAAAAAGTA
4861 GAATACACTAAGCAAAAAGGAAAATTTGATGCTGAAAAAATAACCGATAAAGAGGGATAT
4921 GAAGGTTTTTCAACTAAAGATGCTTCTGAATACTTGAAAAAAAAATGTTTGGATGATACA
4981 TGTAATTGTATGCAGAAAGTGAAAAATAACACCGAATATTGGAATACTCCTAATAAAACG
5041 TATACAAATAGTAATCTAGAAAAAAGGTGCGAGTGCCAACCACCACAAGAACCACCACCA
5101 GGCCCCGAAGGTGGCGCTCGTTCGGACAGCGGCCCACGTGACACCACACCACGACCTGCT
5161 GGTAGTGACGCCCGCTCCAACACCGTCCCCTCACCACCTCCACGACCTGCTGGTGACACC
5221 GTCCACGAAGTCGCGGAAGTCCAGGAGGAGGAGGAAGAAGACGAAGATGGCGACCTCCCG
5281 GAGGACCAGGACGAGGATGTGGAAGTCGCCGGCGCGGAAGAGGAGGAAGACCTCGACGTC
5341 GGTGTCGCTCGTATTCTACGAGGTCGGACCAACAGCCCAGACGAAGATGAAGATGAGGCC
5401 TCCGAAGAGGAGGACGACGACGATGACGACGCCCAGGACACCACAGAAGTCACGGGACAG
5461 GGGGAGGAGGAAACCGCAGAGGACCACCAGGACACCACGGAGGAAACCGTCGACCAGGAG
5521 AAAGCCGAGGAGGACAAGGACGGAGGGGGGGAGACACCACAAAAAGAGACACAACCAAAA
5581 GTGGAAGTAAATCCATGTGATATAGTAAAAACACTATTTACTACCACGGAGACTCTCAAA
5641 GAAGCCTGTCCAACCAAATATGTAAATGGCCGCGAAAAATTCCCCAATTGGAAGTGCATA
5701 AGTAGTGGTAGTGATGCTAGTGGTAGTATTTGTATCCCACCCAGGAGGCGAAAACTATAC
5761 CTACACAAAATAGAAGGCGTCGACACCACCGTGTCAAGTGATGGAGAAACCACCACACCG
5821 ATCACACACGACGCGTTACGTGAGGCATTTATTCAAACTGCTGCTGTGGAAACTTTTTTC
5881 TTATGGCATAGATATAAAAAAATAAAAGAAAAGGAAAGACAGGAGGAACTACAAAATGGA
5941 ACACTTTTATTACCACCTGCCCAAAAAGTGTCACCGGAGGACAACCCAGAACATCCCCAA
6001 AAGAAATTAAAAGAAGGAAAAATCCCTGAGGAGTTTAAAAGACAAATGTTCTATACTTTA
6061 GGGGATTATAGAGATTTATGTGTGGGTGTTAAAGACGACGTGGCTCAGGCGTTAGAAGCT

6121 AGTGGTGATAACAAAAGTGGCGACAAAAATATAAAAGATATATCGGAGAAAATAAAAAGT

6181 GTTATTGAAAAAAGTGGTGAACAAACTCCTCCTGGCCCCAAACCCGGTCAAACAACAACC

6241 AAACCAGAAGAGTGGTGGCAAAAAAATGGTGAACATATCTGGAATGCAATGATATGTGCT

6301 CTAACACACAACACAGACACGCGACAAGTGGATGACCAAGTGAAAGGACAACTTTTCGAA

6361 AATGGAAAGAACACCCCCAAAAACTCCCAATACCAATACAAAAATGTCACAATTAGTAGT

6421 GTTTCTAGTAATGGTGGTCCTATTGGTAATATCAAACTGGAACAATTTGCTTCTAGACCT

6481 ACATTTTTGCGCTGGTTAGAGGAATGGGGAGAAGAGTTTTGCCGTAAACAGTATCACAAG

6541 TTGGAAAGGATTAAGGAAGAATGTCACAAAGATGGTAATAGAAATTGTGATGATGATGGA

6601 TTTGAATGCAAAGAAATGTGTCCATGTAAGGATGGATCTTTTGAAACTTTGAAATGTCCC

6661 AGTTGTGCCAAATCTTGTAAGTCTTATAAAAAGTGGATAAGTAGGAAAAAAGACGAATTT

6721 ACTAAACAAAAAGGGGCATATGAAAAACAAAAAAAGGATGCCGAAGGTAATAATAATGAT

6781 TATAAAGAATTTTCTAAAACACTAAGAAACTACAATGACGCTGCAGCATTTTTAAATAGC

6841 TTAAAAAACGGACCATGTTCTAAAAACGATGATGACAGTGTACAGGATGAAATAAAATTT

6901 GATGATGAACGTAAGACATTTGGACATGAAACATATTGTAAACCATGTTCTAAAATTACA

6961 GTTAAATGTAAGGAAAATAATCATTGCGATAATTCTAAACCAAATGATTGCCGAAATATA

7021 AATAGTATTTCTGCAGAAGATATTGAAAAAAGGAGTAATTCTACTCAAGATGTTACTATG

7081 AGTGTCAGTGATAGCAATACAAATGGAAATAAATTTTATGATTTAAATGATTGTATAAAA

7141 GCAGGTATATTTAAAGGTATTAGAGAAGATGTATGGAAATGTGGTGAATACTGTGGTGTA

7201 GATATATGCACTCTGGAAAAAACCAATAATGAAGAAAGAGTCAGTGCGAAAGAAAATGAT

7261 GGTAAAAACCAAATTATATTAATTAGAGTACTGTTTAAAAGATGGCTAGAAAGTTTTTTA

7321 GAAGATTATAATAAAATTAATGACAAAATTTCACATTGTATGAAAAATGATAAAAAATCC

7381 CCATGTATAAATGGATGTCAAAATAAATGTAATTGTGTAGAAAAATGGATAGAGAAGAAA

7441 AAAAGTGAATGGGGAAAGGTACGAGAACGTTACATCAATCAATATAGGGATAAGAATTCA

7501 AATGAAGCTTTCGAAGTGAAAAGTTTTTTGGAGACCTTGATACCTCAAATTCCTGTTGTA

7561 ACTGATAAAGGAAAGCATGACAGTTTAACTCAGTTAAAGAAGTTACTTAAATGTAATTGC

7621 TCTGAGAAGTCAGAAAATAGTAATGAGAAGGATGTTGTTCTATGTTTGCTTAAAAAGCTT

7681 GAAGATAAAGCAAAAAATTGTAAAGACCAAGCTAGTGGCGAACCCTGTCCTCAAACCACA

7741 TCAGAAAACCCTGATGATGAGGACATACTCCTTGAAGAGGAAAACCCAGTGGAAGCGCCA

7801 AACATTTGTCCGAAAGTGGAAGAACCAGAACCAGTGGTAGAAGAAGAAAAGTGTGACCTA

7861 GCAGAGGCACCATCAAAAGAATCATCAACAGAAGAAAATAGTGGTGAAGGCTCCAACTCT

7921 GAACAAACCCCCGTTCTCAAGCCAGAAGAGGAACCTCCACCTCCTACTTCTTCTGAAACT

7981 GATACCCCTCCACCCGCGCCTCCAACAATACAACCCTCCCAAGCCGACCAACCAACAAAC

8041 TCTATAAGTGACATATTATCATCTACCATCCCCTTTGGAATAGCTATTGCGTTAACTTCG

8101 ATAGTGTTTTTATTTTTGAAGgtaatatatatagtggtatatatgtatatatatgcgttt

8161 tgtgtatatgtatgtacgggtgttttgggatgtatatatatgtatatatatgtttgtatg

8221 tatatgtgtttctgtatatgtatctgttagtatgtttggatatatatgtgtgtatatgta

8281 tgtgttttatatatatttatatatatgtatttatattaaaaaagaaatataaaaaaaaa

8341 attattaaaataaaaaaaaaaaaaaaaaaaaaggagaaaaatattttaaaaataataaaa

8401 attaaaataaaaatataaattttgataaaataaaaaatgaaaaatattatcaaaaagaaa

8461 ttaaaaaaaattttatatataaaaaaaatgattataaaaaaaaatttattagaaataaaa

8521 taaaaaaaaatttattacataaaaaaaaaaaaagttaaaaaaaaaatatatatcataaaa

8581 taaaaagaaaagggaaaaaatgttaaaaaaaaaaataaaattaaaaaaaaaaaaaaaaa

8641 aaaaaaaaaattaaaaaaattttaaaaaaaaaatatatatcataaaaaaaaaagaaata

8701 aaaaaatttatttaaataaaataaaaaaaaatttaatgaaataaaaaaaaataaaaaat

8761 tgaattaaataaaaaaaataaaataaaattaattacatgcacatatacacatacatatat

8821 atatatacccataactacattcatatatacgcatacatatatatattatatatatatata

8881 cccataactacgtacacatatacacatacatatatatatatacccataactacataca

8941 tacatatacctacacatacatatacacatatacatatatgttccttttttttagAAAAA

9001 AACCAAATCGTCGGTGGACTTGTTGCGTGTACTGAATATCCCGAAAGGAGAGTATGGAAT

9061 GCCTACATTGAAATCAAGCAATCGTTATATCCCCTATGCTAGTGATCGATATAAAGGCAA

9121 AACATACATTTATATGGAAGGAGATAGTGATAGTGGACACTACTACGAAGATACAACTGA

9181 TGTTACCTCTTCCGAAAGTGAGTATGAAGAATTGGATATTAATGATATATATGTACCAGG

9241 TAGTCCTAAATATAAAACGTTGATTGAAGTGGTACTAGAACCTAGTGGTAACAACACAAC

9301 AGCTAGTGGTAAAAACACACCTAGTGATACACAAAATGATATACAAAATGATGGTATACC

9361 TAGTAGTAAAATTACAGATAATGAGTGGAATACATTGAAAGATGAATTTATATCACAATA

9421 TCTACAAAGTGAACAACCAAATGATGTACCAAATGATTATACAAGTGGAAATAGTTCAAC

9481 AAATACCAATATTACTACCACGTCACGTCATAATGTGGAAGAAAAACCTTTTATTATGTC

9541 TATTCATGATAGAAATTTATATACTGGAGAAGAAATTAATTATAATGTTAATATGGTTAA

9601 TACTATGGATGATATTCCAATTAATCGTGATAATAATGTTTATAGTGGTATAGATTTAAT

9661 TAATGACGCACTAAATGGTGATTATGACATTTACGATGAAGTATTGAAAAGAAAAGAAAA

9721 TGAATTATTTGGTACAAATCATGTGAAACAAACAAGTATACATAGTGTTGCCAAACCTGC

9781 ACGTGACGACCCCATCCACAACCAACTGGAACTATTCCATAAATGGCTAGATAGACATAG

9841 AGATATGTGCGAAAAGTTGAAAAATCATCACGAACGATTAGCCAAATTGAAAGAAGAGTG

9901 GGAAAATGAGACACATAGTGGTAACACTCACCCTAGTGATAGTAACAAAACGTTGAATAC

9961 TGACGTTTCGATACAAATACATATGGATAATCCTAAACCTATAAATGAATTTACTAATAT

10021 GGATACTATCTTGGACGATCTGGATAAATATAATGAACCTTATTATGATGTGCAAGATGA

10081 TATTTATTATGATGTAAATGATCATGATACATCAACTGTGGATAGTAATGCTATGGATGT

10141 ACCTAGTAAAGTACAAATTGAAATGGATGTAAATACCAAATTGGTGAAAGAGAAATATCC

10201 TATAGCAGATGTATGGGATATATAA

A.3 Results

A.3.1 Genomics of SLI-transfectants

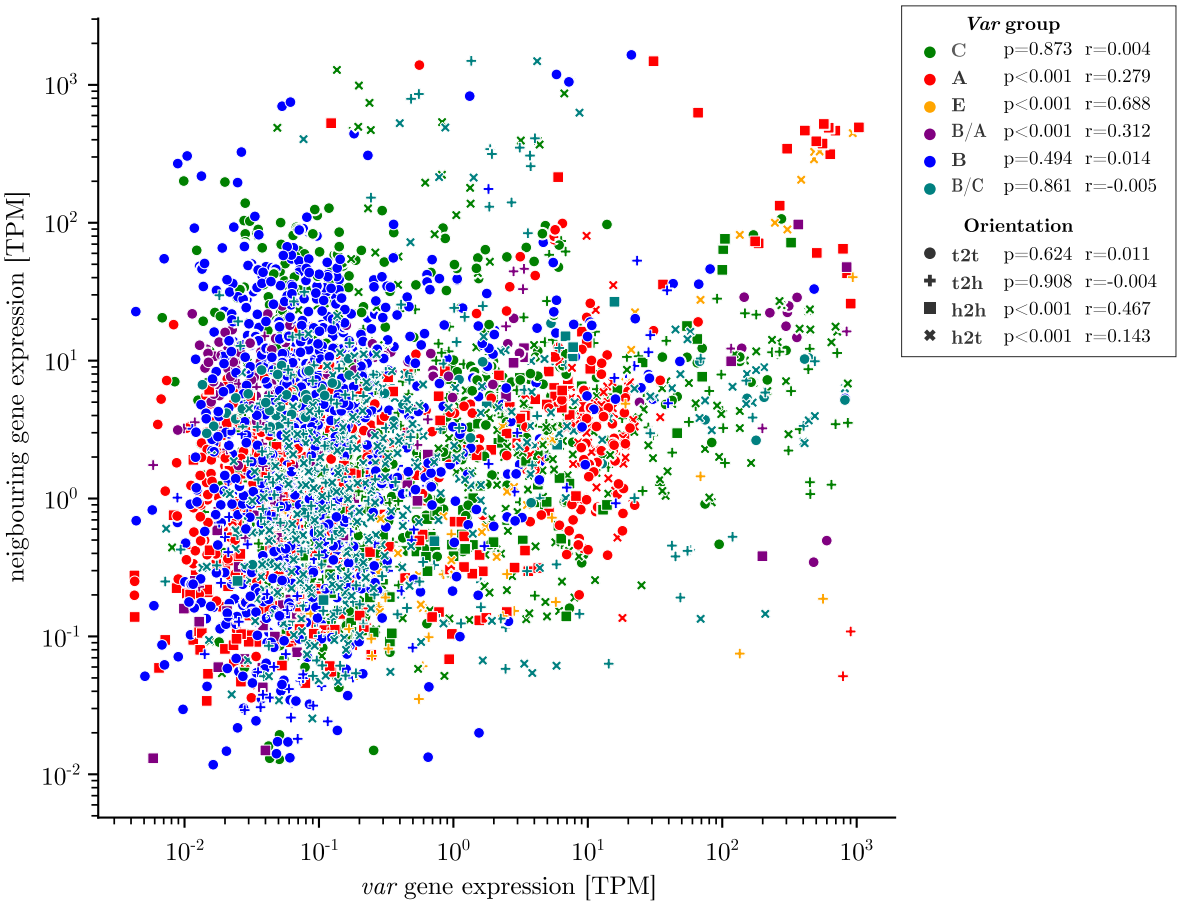


Figure A.3: ***Var* expression in relationship to neighbouring genes.** Scatterplot of *var* expression from RNA-seq data of 61 SLI-transfectants (see A.1). *Var* expression in TPM plotted on the x-axis, whilst expression of the neighbouring gene is plotted on the y-axis. Each *var* gene is depicted as two marker, once each in relationship to the upstream downstream neighbour. Pearson correlation coefficients (r) and corresponding two-tailed p-values are provided in the legend for each group and orientation type. Possible orientations: t2t = tail-to-tail; t2h = tail-to-head; h2h = head-to-head; h2t = head-to-tail.

IT4var08-HA^{endo}

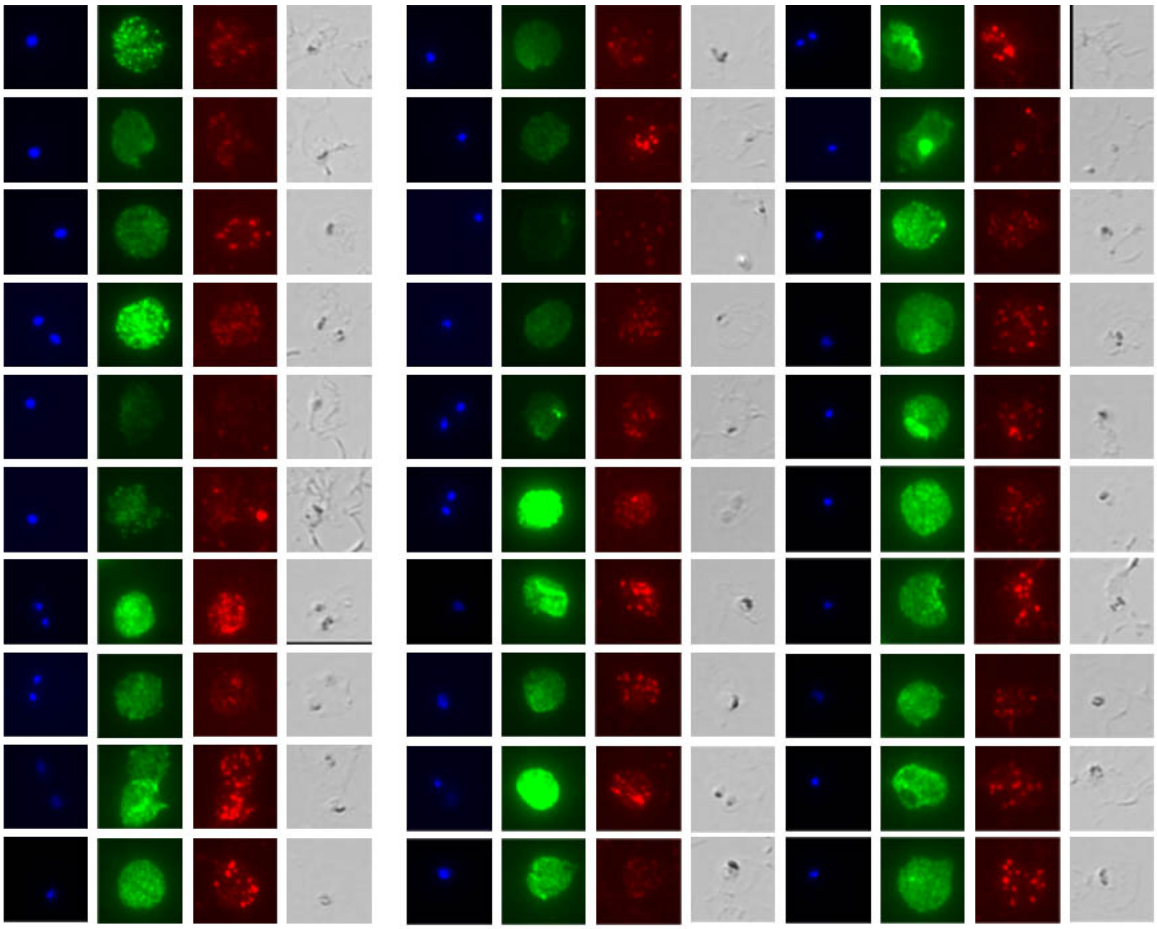


Figure A.4: **IFA of IT4var08-HA^{endo}**. Fluorescence microscopy images of acetone fixed parasites with α-HA to detect the HA-tagged *var08* (red) and α-KAHRP (green) to check for knobs and deletion of chromosome 2. Nuclei stained with Hoechst (blue) ; DIC: differential interference contrast.

Table A.2: Filtered list of DESeq2 results of Tab. A.3. Listed are all genes that are significantly differentially expressed ($p_{adj} \leq 0.05$ and fold change (fc) ≥ 2) between IT4var08-HA^{endo}-LC and IT4var08-HA^{endo}-P5-EPCR, located directly upstream or downstream of a significantly regulated *var* gene.

PfEMP1 -PF_ID	PfEMP1 – log_2FC	PfEMP1 – p_{adj}	*var* name	*var* group	N Pf_ID	N description	gene orientation	N – log_2FC	N – p_{adj}
PfIT_090005100	4.8895	1.83e-18	IT4var02	A	PfIT_090005200	rifin	h2h	8.6506	6.30E-09
PfIT_060036700	5.3233	7.18e-22	IT4var07	A	PfIT_060036600	rifin	h2h	8.4922	3.29E-09
PfIT_120045200	4.1732	1.87e-31	IT4var39	B/C	PfIT_120045100	acidic terminal segments, variant surface antigen of PfEMP1, putative	h2h	7.9984	1.55E-07
PfIT_080013800	6.4720	5.22e-37	IT4var65	C	PfIT_080013650	Plasmodium RNA of unknown function RUF6	h2h	6.6772	2.98E-11
PfIT_070017200	4.4329	3.27e-36	IT4var28	C	PfIT_070017300	rifin	h2h	5.9180	2.48E-13
PfIT_100044000	4.5908	1.74e-16	IT4var22	A	PfIT_100043900	rifin	h2h	5.8083	1.25E-08
PfIT_080037400	4.9643	1.54e-14	IT4var61	B	PfIT_080037300	rifin	t2h	4.3007	2.36E-06
PfIT_120006100	4.9607	4.88e-12	IT4var04 (var2CSA)	E	PfIT_120006200	hypothetical protein	h2t	3.8058	1.63E-03
PfIT_120024600	3.3667	1.29e-10	IT4var63	B/C	PfIT_120024700	erythrocyte membrane protein 1 (PfEMP1), pseudogene	h2t	3.0837	1.70E-06
PfIT_110005600	2.4460	3.55e-4	IT4var54	B	PfIT_110005700	rifin	t2t	3.0791	3.36E-03
PfIT_070005900	2.2863	2.01e-3	IT4var08	A	PfIT_070006000	rifin	h2h	2.4225	1.91E-04
PfIT_040025800	2.8489	1.03e-12	IT4var30	C	PfIT_040025700	rifin	t2h	1.9907	5.84E-04
PfIT_040025500	4.5556	4.68e-18	IT4var66	C	PfIT_040025700	rifin	h2t	1.9907	5.84E-04
PfIT_030029700	2.2005	1.60e-5	IT4var18	A	PfIT_030029600	rifin	h2h	1.7321	2.27E-02
PfIT_130077800	6.2471	5.84e-71	IT4var12	B	PfIT_130077700	rifin	t2t	1.1979	4.73E-02
PfIT_120005500	1.4722	4.35e-3	IT4var45	B	PfIT_120005600	rifin	t2t	1.1874	4.24E-02
PfIT_080014100	5.0199	1.17e-17	IT4var34	C	PfIT_080014200	asparagine-rich antigen Pfa55-14	t2t	1.1340	5.94E-03
PfIT_040025100	5.6832	1.72e-26	IT4var62	C	PfIT_040025000	conserved Plasmodium protein, unknown function	t2t	-1.3372	2.83E-02
PfIT_060021400	4.7417	9.26e-12	IT4var01	C	PfIT_060021200	conserved Plasmodium protein, unknown function	t2t	-2.2058	2.06E-04

Table A.3: Expression of *Pf*EMP1 in the IT4var08-HA^{endo} lines. Expression counts in [TPM]; LC, long term culture; Date: Date of sampling

	IT4var08-HA^{endo}			**IT4var08-HA^{endo} -LC**					**IT4var08-HA^{endo} -P4-ICAM1**					**IT4var08-HA^{endo} -P4-ICAM1-P4-EPCR**		
Replicate	1	2	3	1	2	3	4	5	1	2	3	4	5	1	2	3
Date	NA	NA	NA	23/11/23	23/12/02	23/12/06	24/01/26	24/10/20	23/12/19	23/12/21	24/01/01	24/04/04	24/10/20	24/03/30	24/04/08	24/05/25
IT4var01	0.000	0.000	0.012	0.021	0.008	0.139	0.032	0.028	0.057	0.043	0.096	0.121	0.320	0.069	0.038	0.036
IT4var02	0.006	0.008	0.006	0.112	0.077	0.082	0.163	0.103	0.250	0.269	0.302	0.151	0.209	0.154	0.178	0.168
IT4var03	0.029	0.000	0.006	0.057	0.000	0.333	0.094	0.125	0.182	0.214	0.156	0.073	0.143	0.081	0.067	0.042
IT4var04 (var2CSA)	0.076	0.131	0.041	0.087	0.161	0.853	0.746	8.879	0.273	0.278	0.998	15.311	12.612	8.077	18.559	22.100
IT4var05	0.010	0.000	0.013	0.140	0.134	0.424	0.119	0.105	0.320	0.244	0.358	0.176	0.128	0.156	0.194	0.122
IT4var06	0.011	0.000	0.000	0.006	0.018	0.056	0.032	0.012	0.034	0.034	0.048	0.028	0.022	0.023	0.011	0.017
IT4var07	0.001	0.000	0.007	0.141	0.102	0.020	0.144	0.213	0.496	0.503	0.473	0.225	0.231	0.201	0.169	0.133
IT4var08	95.250	93.029	96.399	80.631	77.615	54.018	72.764	65.059	31.288	30.652	36.302	32.519	34.195	36.346	28.760	24.556
IT4var09	0.005	0.010	0.000	0.021	0.020	0.244	0.013	0.009	0.033	0.034	0.023	0.006	0.008	0.013	0.013	0.007
IT4var10	0.014	0.000	0.004	0.237	0.228	0.247	0.391	0.300	1.453	1.469	1.179	0.630	1.125	0.107	0.078	0.104
IT4var11	0.021	0.000	0.011	0.057	0.048	0.029	0.084	0.060	0.148	0.150	0.140	0.057	0.116	0.083	0.050	0.060
IT4var12	0.017	0.000	0.012	0.080	0.130	0.254	0.222	0.137	3.378	3.915	2.256	0.720	1.135	8.633	7.665	11.406
IT4var13	0.032	0.030	0.006	0.166	0.190	0.740	0.162	0.040	0.241	0.251	0.198	0.070	0.054	0.096	0.050	0.061
IT4var14	0.037	0.071	0.016	0.186	0.393	0.754	0.141	0.044	0.220	0.211	0.131	0.051	0.062	0.060	0.056	0.068
IT4var15	0.018	0.033	0.014	0.137	0.160	0.222	0.259	0.206	1.474	1.520	1.164	0.270	0.287	0.428	0.364	0.338
IT4var16	0.014	0.034	0.016	0.142	0.150	0.172	0.306	0.213	9.024	9.867	8.004	7.566	7.528	1.270	1.158	1.762
IT4var17	0.019	0.019	0.004	0.077	0.059	0.095	0.054	0.046	0.032	0.031	0.036	0.027	0.031	0.018	0.010	0.008
IT4var18	0.047	0.033	0.013	0.078	0.139	0.493	0.202	0.155	0.324	0.353	0.268	0.202	0.176	0.415	0.551	0.443
IT4var19, IT4var32b	0.006	0.012	0.004	0.092	0.037	0.000	0.088	0.069	0.128	0.135	0.103	0.040	0.058	0.131	0.056	0.073
IT4var20	0.007	0.000	0.000	0.043	0.081	0.070	0.066	0.059	0.142	0.161	0.172	0.095	0.040	0.133	0.092	0.058
IT4var21	0.012	0.020	0.021	0.038	0.006	0.251	0.087	0.109	0.177	0.167	0.245	0.501	0.267	0.127	0.146	0.095
IT4var22	0.002	0.000	0.004	0.069	0.042	0.095	0.070	0.076	0.133	0.196	0.130	0.060	0.052	0.128	0.100	0.081
IT4var23, IT4var24	0.012	0.014	0.010	0.010	0.046	0.000	0.085	0.072	0.129	0.165	0.134	0.039	0.082	0.070	0.073	0.085
IT4var25	0.051	0.021	0.024	0.182	0.118	0.197	0.191	0.164	0.498	0.534	0.474	0.189	0.248	0.219	0.173	0.226
IT4var26	0.003	0.028	0.010	0.029	0.057	0.069	0.092	0.044	0.060	0.065	0.055	0.025	0.042	0.041	0.016	0.026
IT4var27	0.014	0.019	0.009	0.059	0.054	0.116	0.056	0.060	0.310	0.270	0.358	0.290	0.434	0.105	0.082	0.080
IT4var28	0.020	0.027	0.010	0.205	0.267	0.397	0.365	0.324	3.296	3.417	2.861	1.616	2.812	0.746	1.240	1.093
IT4var29	0.009	0.069	0.015	0.078	0.171	0.139	0.369	0.368	1.430	1.405	1.162	0.409	0.479	0.539	0.363	0.454
IT4var30	0.000	0.013	0.016	0.157	0.078	0.168	0.150	0.169	0.251	0.231	0.287	0.576	0.458	0.269	0.355	0.268
IT4var31	0.007	0.000	0.010	0.143	0.089	0.054	0.161	0.144	0.561	0.671	0.452	0.161	0.185	0.272	0.146	0.190
IT4var32a	0.003	0.000	0.000	0.031	0.027	0.056	0.009	0.020	0.541	0.501	0.303	0.049	0.077	2.498	1.319	1.144
IT4var33	0.018	0.015	0.019	0.077	0.126	0.219	0.152	0.147	0.397	0.480	0.367	0.187	0.248	0.237	0.144	0.191
IT4var34	0.256	0.447	0.224	2.891	2.212	2.599	3.464	4.886	6.823	6.508	8.578	8.110	6.936	9.447	7.105	5.117
IT4var35	0.023	0.015	0.024	0.062	0.024	0.256	0.089	0.063	0.093	0.086	0.087	0.040	0.097	0.044	0.029	0.033
IT4var39	0.028	0.028	0.017	0.080	0.076	0.106	0.178	0.228	0.393	0.371	0.357	0.350	0.255	0.299	0.365	0.373
IT4var40	0.000	0.000	0.000	0.000	0.000	0.000	0.000	0.000	0.000	0.000	0.000	0.000	0.000	0.000	0.000	0.000
IT4var41	0.000	0.000	0.001	0.048	0.060	0.060	0.061	0.035	1.256	1.361	0.840	0.416	0.490	0.145	0.102	0.097
IT4var44	0.012	0.006	0.012	0.055	0.096	0.042	0.140	0.170	0.366	0.357	0.306	0.303	0.751	0.327	0.316	0.499
IT4var45	0.059	0.083	0.016	0.137	0.108	0.483	0.211	0.197	0.279	0.282	0.244	0.116	0.258	0.127	0.095	0.132
IT4var46	0.011	0.009	0.002	0.075	0.087	0.231	0.129	0.077	0.102	0.098	0.103	0.062	0.100	0.064	0.033	0.042
IT4var47	0.014	0.021	0.011	0.092	0.062	0.309	0.143	0.137	0.232	0.233	0.293	0.144	0.151	0.132	0.108	0.082
IT4var51	0.010	0.013	0.009	0.032	0.090	0.193	0.248	0.243	0.366	0.418	0.449	0.166	0.372	0.327	0.249	0.188
IT4var54	0.013	0.068	0.003	0.019	0.022	0.237	0.050	0.056	0.058	0.050	0.054	0.038	0.156	0.037	0.017	0.016
IT4var58	0.018	0.041	0.019	0.145	0.248	0.273	0.568	0.316	7.623	8.102	6.242	5.693	4.768	0.917	0.956	0.998
IT4var59	0.002	0.027	0.019	0.077	0.073	0.169	0.090	0.074	0.098	0.091	0.197	0.200	0.132	0.089	0.135	0.085
IT4var60	0.003	0.000	0.002	0.022	0.009	0.079	0.060	0.101	0.070	0.064	0.082	0.033	0.025	0.043	0.053	0.037
IT4var61	0.000	0.000	0.002	0.551	0.708	0.271	0.824	0.899	1.966	1.906	1.217	0.140	0.264	0.395	0.398	0.382
IT4var62	0.026	0.071	0.013	0.040	0.047	0.195	0.125	0.072	0.215	0.205	0.322	0.221	0.165	0.276	0.151	0.117
IT4var63	0.033	0.020	0.009	0.047	0.110	0.134	0.068	0.046	0.158	0.195	0.194	0.238	0.113	0.088	0.058	0.064
IT4var64	0.009	0.000	0.002	0.052	0.009	0.105	0.095	0.081	0.289	0.312	0.294	0.158	0.077	0.191	0.124	0.074
IT4var65	0.046	0.026	0.027	0.652	0.473	0.581	2.115	2.139	5.062	4.901	5.480	5.767	5.136	8.838	8.249	7.686
IT4var66	1.257	1.738	0.946	5.890	4.598	4.966	8.399	10.323	13.478	12.436	12.275	14.013	14.601	14.750	17.576	16.938
IT4var67	0.030	0.030	0.012	0.491	0.699	0.320	0.722	1.011	2.788	2.787	2.349	0.651	0.782	1.049	1.127	1.155
IT4var68	0.026	0.035	0.014	0.117	0.029	0.413	0.070	0.135	0.161	0.207	0.229	0.263	0.215	0.207	0.178	0.158
PfIT_000010800	0.002	0.000	0.000	0.018	0.031	0.000	0.005	0.013	0.061	0.044	0.059	0.091	0.031	0.154	0.118	0.053
VAR1CSA	2.352	3.688	1.883	4.815	9.295	26.973	4.277	1.143	0.782	0.551	0.512	0.350	0.261	0.310	0.184	0.180

Table A.4: Expression of *Pf*EMP1 in IT4var19-K2-HA^{endo} before and after binding enrichment over CHO-K1-EPCR (IT4var19-K2-HA^{endo}-P5-EPCR). Expression counts in [TPM]; Date; Date of sampling.

	IT4var19-K2-HA^{endo}				**IT4var19-K2-HA^{endo}-P5-EPCR**			
Replicate	**1**	**2**	**3**	**4**	**1**	**2**	**3**	**4**
Date	22/11/14	22/20/11	22/12/09	23/06/01	23/05/31	23/06/04	23/06/14	23/11/21
IT4var01	0.030	0.017	0.035	0.041	0.042	0.000	0.028	0.000
IT4var02	0.066	0.082	0.056	0.042	0.067	0.116	0.015	0.142
IT4var03	0.054	0.044	0.000	0.000	0.037	0.000	0.125	0.233
IT4var04 (var2CSA)	0.124	0.137	0.166	0.111	0.056	0.087	0.111	0.179
IT4var05	0.071	0.024	0.032	0.043	0.049	0.027	0.026	0.123
IT4var06	0.244	0.120	0.020	0.192	0.247	0.239	0.184	0.343
IT4var07	0.040	0.013	0.000	0.033	0.027	0.030	0.037	0.070
IT4var08	0.047	0.028	0.183	0.069	0.116	0.024	0.102	0.092
IT4var09	0.029	0.016	0.123	0.040	0.013	0.037	0.073	0.021
IT4var10	0.040	0.092	0.018	0.097	0.054	0.030	0.037	0.095
IT4var11	0.082	0.058	0.080	0.059	0.040	0.022	0.043	0.038
IT4var12	0.114	0.141	0.078	0.115	0.078	0.065	0.116	0.136
IT4var13	0.083	0.058	0.298	0.071	0.108	0.066	0.260	0.162
IT4var14	0.067	0.112	0.584	0.171	0.196	0.120	0.384	0.247
IT4var15	0.067	0.111	0.076	0.090	0.084	0.063	0.072	0.073
IT4var16	0.104	0.057	0.135	0.230	0.095	0.037	0.110	0.043
IT4var17	0.019	0.032	0.022	0.097	0.085	0.081	0.071	0.021
IT4var18	0.079	0.110	0.150	0.067	0.079	0.031	0.177	0.144
IT4var19, IT4var32b	358.897	360.278	145.577	312.413	305.399	305.133	226.047	298.126
IT4var20	0.052	0.125	0.064	0.038	0.045	0.018	0.018	0.061
IT4var21	0.142	0.045	0.031	0.082	0.046	0.026	0.025	0.029
IT4var22	0.004	0.014	0.058	0.017	0.012	0.000	0.016	0.055
IT4var23, IT4var24	0.014	0.046	0.032	0.028	0.077	0.000	0.026	0.061
IT4var25	0.137	0.072	0.066	0.117	0.099	0.177	0.161	0.094
IT4var26	0.105	0.046	0.095	0.169	0.124	0.079	0.039	0.091
IT4var27	0.084	0.093	0.064	0.076	0.058	0.035	0.026	0.041
IT4var28	0.222	0.092	0.300	0.141	0.190	0.079	0.129	0.090
IT4var29	0.105	0.046	0.063	0.085	0.019	0.053	0.026	0.091
IT4var30	0.115	0.045	0.092	0.219	0.102	0.051	0.050	0.059
IT4var31	0.044	0.060	0.033	0.162	0.000	0.055	0.000	0.031
IT4var32a	1.119	0.649	0.419	0.986	1.056	1.016	1.289	1.529
IT4var33	0.117	0.073	0.150	0.030	0.040	0.083	0.055	0.127
IT4var34	3.658	2.039	1.227	1.925	1.346	1.436	1.067	1.869
IT4var35	0.176	0.073	0.234	0.179	0.101	0.056	0.055	0.096
IT4var39	0.100	0.071	0.194	0.058	0.078	0.054	0.026	0.155
IT4var40	0.000	0.000	0.000	0.000	0.000	0.000	0.000	0.000
IT4var41	0.053	0.048	0.088	0.049	0.013	0.018	0.027	0.042
IT4var44	0.190	0.056	0.076	0.136	0.138	0.021	0.073	0.073
IT4var45	0.104	0.230	0.205	0.056	0.133	0.066	0.245	0.030
IT4var46	0.066	0.132	0.251	0.000	0.097	0.042	0.140	0.029
IT4var47	0.069	0.138	0.141	0.056	0.038	0.052	0.064	0.090
IT4var51	0.143	0.065	0.177	0.131	0.027	0.025	0.072	0.056
IT4var54	0.082	0.158	0.062	0.055	0.075	0.155	0.228	0.044
IT4var58	0.144	0.137	0.156	0.292	0.141	0.104	0.102	0.164
IT4var59	0.163	0.079	0.124	0.083	0.056	0.039	0.101	0.118
IT4var60	0.000	0.000	0.024	0.000	0.014	0.000	0.000	0.000
IT4var61	0.044	0.000	0.000	0.029	0.060	0.000	0.000	0.032
IT4var62	0.128	0.094	0.049	0.116	0.058	0.148	0.053	0.077
IT4var63	0.081	0.089	0.214	0.055	0.157	0.076	0.100	0.088
IT4var64	0.021	0.009	0.024	0.043	0.043	0.060	0.039	0.057
IT4var65	0.253	0.065	0.088	0.105	0.142	0.086	0.097	0.028
IT4var66	310.987	18.014	7.736	14.053	2.448	2.543	1.191	0.151
IT4var67	0.246	0.214	0.349	0.137	0.143	0.023	0.296	0.120
IT4var68	0.178	0.197	0.162	0.000	0.000	0.202	0.066	0.103
PfIT_000010800	0.000	0.000	0.000	0.026	0.000	0.000	0.000	0.000
VAR1CSA	12.616	11.327	11.720	11.069	10.243	9.685	13.095	15.684

Table A.5: Expression of *Pf*EMP1 in the IT4var20-HA^{endo} lines. Expression counts in [TPM]; c32, single clone nr. 32; P4-EPCR = enriched four times over CHO-K1-EPCR cells, Date, Date of sampling

var-names	Pf-ID	IT4var20-HA^{endo}			IT4var20-HA^{endo}-c32			IT4var20-HA^{endo}-c32-P4-EPCR		
		1	2	3	1	2	3	1	2	3
IT4var01	PfIT_060021400	0.443	0.037	0.526	0.052	0.038	0.133	0.063	0.015	0.030
IT4var02	PfIT_090005100	8.159	0.614	2.852	0.072	0.000	0.072	0.057	0.093	0.024
IT4var03	PfIT_140006400	4.279	0.391	1.352	0.118	0.000	0.117	0.000	0.081	0.000
IT4var04 (var2CSA)	PfIT_120006100	2.830	0.843	1.628	0.167	0.155	0.220	1.086	1.491	1.679
IT4var05	PfIT_120045600	2.959	0.246	0.896	0.062	0.053	0.109	0.000	0.086	0.159
IT4var06	PfIT_020027600	0.080	0.066	0.177	0.033	0.017	0.227	0.000	0.265	0.040
IT4var07	PfIT_060036700	9.338	0.931	3.410	0.012	0.015	0.088	0.000	0.127	0.024
IT4var08	PfIT_070005900	6.448	0.455	2.181	0.074	0.000	0.148	0.023	0.204	0.088
IT4var09	PfIT_130005300	0.934	0.188	0.261	0.072	0.028	0.172	0.014	0.185	0.015
IT4var10	PfIT_140085700	0.229	0.015	0.089	0.041	0.000	0.244	0.011	0.174	0.036
IT4var11	PfIT_050005500	0.358	0.053	0.278	0.017	0.110	0.255	0.000	0.290	0.017
IT4var12	PfIT_130077800	4.192	0.228	1.067	0.116	0.043	0.473	0.126	0.266	0.144
IT4var13	PfIT_070016600	1.415	0.479	0.871	0.077	0.033	0.172	0.024	0.271	0.137
IT4var14	PfIT_130005200	1.052	0.361	0.649	0.062	0.071	0.304	0.047	0.305	0.000
IT4var15	PfIT_070016900	8.670	0.783	4.200	0.399	0.147	0.414	0.177	0.563	0.374
IT4var16	PfIT_120024500	12.803	0.541	5.317	0.079	0.056	0.022	0.027	0.238	0.147
IT4var17	PfIT_020005200	0.340	0.035	0.294	0.028	0.009	0.376	0.000	0.137	0.093
IT4var18	PfIT_030029700	5.142	0.944	1.913	0.091	0.054	0.281	0.086	0.200	0.173
IT4var19, IT4var32b	PfIT_010005000	0.986	0.135	0.461	0.024	0.031	0.153	0.011	0.112	0.037
IT4var20	PfIT_070017000	367.940	116.553	841.753	198.901	105.631	151.000	113.774	161.966	115.817
IT4var21	PfIT_040017000	1.936	0.221	1.774	0.217	0.051	0.133	0.046	0.132	0.151
IT4var22	PfIT_100044000	3.466	0.287	1.145	0.062	0.032	0.056	0.012	0.077	0.013
IT4var23, IT4var24	PfIT_040030600	0.708	0.051	0.569	0.000	0.000	0.092	0.000	0.159	0.042
IT4var25	PfIT_050038500	4.644	0.276	1.656	0.084	0.054	0.410	0.060	0.217	0.054
IT4var26	PfIT_120060400	0.331	0.025	0.293	0.041	0.026	0.488	0.000	0.368	0.062
IT4var27	PfIT_070016700	208.957	69.073	488.469	402.685	214.842	298.877	224.742	317.747	231.457
IT4var28	PfIT_070017200	13.879	1.988	6.047	0.213	0.000	0.288	0.029	0.157	0.238
IT4var29	PfIT_140006100	15.771	0.509	2.987	0.092	0.000	0.366	0.038	0.368	0.125
IT4var30	PfIT_040025800	3.671	0.419	1.856	0.198	0.102	0.340	0.056	0.183	0.141
IT4var31	PfIT_140006200	7.278	0.596	2.379	0.042	0.000	0.159	0.070	0.142	0.076
IT4var32a	PfIT_060036800	0.610	0.020	0.219	0.016	0.021	0.024	0.000	0.051	0.000
IT4var33	PfIT_040005400	2.472	0.228	1.171	0.021	0.124	0.193	0.040	0.155	0.044
IT4var34	PfIT_080014100	35.862	9.217	42.343	4.645	1.465	5.038	5.887	6.184	6.637
IT4var35	PfIT_000009500	0.990	0.054	0.576	1.482	0.801	2.122	1.105	1.385	0.789
IT4var39	PfIT_120045200	5.918	0.468	2.615	0.146	0.094	0.374	0.079	0.215	0.085
IT4var40	PfIT_030005100	0.000	0.000	0.000	0.000	0.000	0.000	0.000	0.000	0.000
IT4var41	PfIT_100044100	1.541	0.009	0.327	0.007	0.018	0.234	0.013	0.125	0.007
IT4var44	PfIT_070005800	0.521	0.031	0.423	0.016	0.042	0.159	0.000	0.186	0.067
IT4var45	PfIT_120005500	1.639	0.152	0.467	0.061	0.026	0.395	0.000	0.220	0.093
IT4var46	PfIT_030029800	0.895	0.089	0.211	0.052	0.033	0.223	0.000	0.120	0.033
IT4var47	PfIT_120046200	6.114	0.681	2.500	0.141	0.026	0.091	0.038	0.198	0.103
IT4var51	PfIT_120045800	10.287	1.207	4.035	0.019	0.061	0.085	0.107	0.098	0.174
IT4var54	PfIT_110005600	0.108	0.025	0.115	0.020	0.000	0.716	0.000	0.380	0.102
IT4var58	PfIT_040017300	7.003	0.452	1.598	0.221	0.103	0.030	0.047	0.176	0.062
IT4var59	PfIT_040017400	1.066	0.149	0.801	0.119	0.026	0.298	0.038	0.082	0.173
IT4var60	PfIT_120060300	2.494	0.694	1.200	0.046	0.000	0.046	0.015	0.048	0.016
IT4var61	PfIT_080037400	0.389	0.027	0.061	0.021	0.000	0.191	0.000	0.066	0.000
IT4var62	PfIT_040025100	2.330	0.507	1.737	0.208	0.054	0.281	0.020	0.054	0.106
IT4var63	PfIT_120024600	1.014	0.135	1.057	0.079	0.025	0.295	0.019	0.162	0.161
IT4var64	PfIT_070017100	66.119	6.019	30.815	0.123	0.000	0.196	0.000	0.238	0.322
IT4var65	PfIT_080013800	25.551	3.281	14.040	0.209	0.098	0.398	0.152	0.744	0.523
IT4var66	PfIT_040025500	98.425	38.397	123.405	39.157	17.646	32.275	21.693	40.996	34.617
IT4var67	PfIT_120045700	3.819	0.190	1.032	0.188	0.092	0.134	0.059	0.167	0.165
IT4var68	PfIT_040025300	1.343	0.390	1.332	0.174	0.134	0.416	0.098	0.197	0.035
PfIT_000010800	PfIT_000010800	0.101	0.023	0.161	0.000	0.012	0.000	0.000	0.019	0.000
VAR1CSA	PfIT_050037800	19.016	16.917	34.580	15.326	8.359	19.030	7.140	12.471	8.513

Blue — : Reads in the R1F2 orientation (read pair pointing away from each other). Dashed - - - : Proposed gene recombination sites. C1–C3 :

Table A.6: Differential gene expression between IT4var19-K2-HA^{endo} and IT4var19-K2-HA^{endo}-P5-EPCR. Top output of DEseq2 sorted by p_{adj}. Full data available on NCBI's Gene Expression Omnibus. Accession number GSE267413

Pf_ID	**Transcript Product Description**	**base mean**	**$\log_2$ FC**	**p_{value}**	**p_{adj}**
PfIT_140007400	Glycophorin-binding protein, putative	23.97	2.94	4.48×10^{-6}	2.40×10^{-2}
PfIT_140084700	EMP1-trafficking protein	332.20	3.73	1.39×10^{-5}	3.73×10^{-2}
PfIT_140085300	Plasmodium exported protein (PHISTa), unknown function	85.83	1.52	5.54×10^{-5}	9.89×10^{-2}
PfIT_040025700	rifin	29.28	−2.24	4.59×10^{-4}	5.38×10^{-1}
PfIT_140083100	EMP1-trafficking protein	69.11	2.51	5.02×10^{-4}	5.38×10^{-1}
PfIT_030006400	Plasmodium exported protein (hyp1), unknown function	541.17	−1.48	6.76×10^{-3}	9.99×10^{-1}
PfIT_050038100	rifin	3.61	3.72	7.56×10^{-3}	9.99×10^{-1}
PfIT_030029500	rifin	32.59	1.31	7.82×10^{-3}	9.99×10^{-1}
PfIT_110011500	conserved Plasmodium protein, unknown function	29.45	1.26	8.52×10^{-3}	9.99×10^{-1}
PfIT_020026200	Plasmodium exported protein, unknown function	27.43	1.33	8.83×10^{-3}	9.99×10^{-1}
PfIT_050020400	conserved Plasmodium protein, unknown function	6.57	2.32	9.18×10^{-3}	9.99×10^{-1}
PfIT_140066500	FYVE and coiled-coil domain-containing protein	83.83	−1.24	1.26×10^{-2}	9.99×10^{-1}
PfIT_090014700	SET domain protein, putative	34.41	1.11	1.30×10^{-2}	9.99×10^{-1}
PfIT_050007300	conserved protein, unknown function	60.82	0.88	1.54×10^{-2}	9.99×10^{-1}
PfIT_030010000	conserved Plasmodium protein, unknown function	1653.03	0.54	1.65×10^{-2}	9.99×10^{-1}
PfIT_100015300	protein ARV1, putative	8.10	1.98	1.79×10^{-2}	9.99×10^{-1}
PfIT_130074700	conserved Plasmodium protein, unknown function	98.82	0.84	1.80×10^{-2}	9.99×10^{-1}
PfIT_050038200	rifin	9.94	1.80	1.88×10^{-2}	9.99×10^{-1}
PfIT_090018100	protease, putative	55.77	0.90	1.97×10^{-2}	9.99×10^{-1}
PfIT_130069200	hypothetical protein	123.98	0.88	2.10×10^{-2}	9.99×10^{-1}
PfIT_110031500	protein phosphatase, putative	458.43	−1.00	2.19×10^{-2}	9.99×10^{-1}
PfIT_010005200	stevor	8.96	−2.74	2.27×10^{-2}	9.99×10^{-1}

Pf_ID	Transcript Product Description	base mean	$\log_2$ FC	p_{value}	p_{adj}
PfIT_040029600	Plasmodium exported protein (hyp6), unknown function	18.52	1.16	2.35×10^{-2}	9.99×10^{-1}
PfIT_100012500	conserved Plasmodium membrane protein, unknown function	476.05	−0.73	2.39×10^{-2}	9.99×10^{-1}
PfIT_120045800	erythrocyte membrane protein 1, PfEMP1	8.35	−1.66	2.53×10^{-2}	9.99×10^{-1}
PfIT_040025800	erythrocyte membrane protein 1, PfEMP1	44.41	−1.04	2.58×10^{-2}	9.99×10^{-1}
PfIT_100026300	conserved Plasmodium membrane protein, unknown function	130.84	0.71	2.62×10^{-2}	9.99×10^{-1}
PfIT_120013900	conserved Plasmodium protein, unknown function	32.51	1.30	2.64×10^{-2}	9.99×10^{-1}
PfIT_090010900	conserved Plasmodium protein, unknown function	44.65	0.77	2.67×10^{-2}	9.99×10^{-1}
PfIT_120014500	conserved Plasmodium protein, unknown function	26.95	1.07	2.73×10^{-2}	9.99×10^{-1}
PfIT_120049800	conserved Plasmodium protein, unknown function	28.50	1.04	2.78×10^{-2}	9.99×10^{-1}
PfIT_050031500	nucleolar Jumonji domain interacting protein, putative	448.36	−0.76	2.90×10^{-2}	9.99×10^{-1}
PfIT_130074300	glycosylphosphatidylinositol anchor attachment 1 protein, putative	100.08	0.97	3.08×10^{-2}	9.99×10^{-1}
PfIT_050022300	conserved Plasmodium protein, unknown function	24.31	1.35	3.16×10^{-2}	9.99×10^{-1}
PfIT_120048500	conserved Plasmodium protein, unknown function	6.07	1.83	3.18×10^{-2}	9.99×10^{-1}
PfIT_110017600	conserved Plasmodium protein, unknown function	123.09	−0.62	3.21×10^{-2}	9.99×10^{-1}
PfIT_090034300	conserved Plasmodium protein, unknown function	4.55	2.70	3.28×10^{-2}	9.99×10^{-1}
PfIT_060033300	amino acid transporter, putative	983.90	−0.59	3.31×10^{-2}	9.99×10^{-1}
PfIT_110049900	bicoid-interacting protein BIN3, putative	10.64	1.85	3.33×10^{-2}	9.99×10^{-1}
PfIT_030023100	conserved Plasmodium protein, unknown function	666.70	−0.93	3.37×10^{-2}	9.99×10^{-1}
PfIT_060034300	ribosome biogenesis protein YTM1, putative	251.30	0.57	3.38×10^{-2}	9.99×10^{-1}
PfIT_110048000	conserved Plasmodium protein, unknown function	1055.21	−0.84	3.39×10^{-2}	9.99×10^{-1}

Pf_ID	Transcript Product Description	base mean	$\log_2$ FC	p_{value}	p_{adj}
PfIT_020006400	PHISTb domain-containing RESA-like protein 1	106.67	0.96	3.40×10^{-2}	9.99×10^{-1}
PfIT_140020500	DnaJ protein, putative	408.80	−0.79	3.62×10^{-2}	9.99×10^{-1}
PfIT_030027300	iron-sulfur assembly protein, putative	50.33	1.03	3.66×10^{-2}	9.99×10^{-1}
PfIT_070031900	eukaryotic translation initiation factor 2 alpha subunit, putative	3208.52	−0.74	3.85×10^{-2}	9.99×10^{-1}
PfIT_010013100	conserved Plasmodium protein, unknown function	38.73	1.00	3.95×10^{-2}	9.99×10^{-1}
PfIT_140077300	exported protein 2	2645.29	−0.63	4.04×10^{-2}	9.99×10^{-1}
PfIT_080014400	histone acetyltransferase subunit NuA4, putative	217.16	−0.85	4.06×10^{-2}	9.99×10^{-1}
PfIT_080023000	conserved protein, unknown function	102.03	−0.78	4.11×10^{-2}	9.99×10^{-1}
PfIT_020019300	conserved Plasmodium membrane protein, unknown function	1115.01	−0.82	4.19×10^{-2}	9.99×10^{-1}
PfIT_140056400	serine/threonine protein kinase, putative	268.65	−0.83	4.27×10^{-2}	9.99×10^{-1}
PfIT_050011850	histone deacetylase, putative, pseudogene	3.97	2.51	4.28×10^{-2}	9.99×10^{-1}
PfIT_050015600	conserved Plasmodium protein, unknown function	152.41	0.60	4.41×10^{-2}	9.99×10^{-1}
PfIT_120015700	conserved Plasmodium protein, unknown function	68.52	0.75	4.42×10^{-2}	9.99×10^{-1}
PfIT_080026900	conserved Plasmodium protein, unknown function	21.76	1.37	4.64×10^{-2}	9.99×10^{-1}
PfIT_140016200	conserved Plasmodium protein, unknown function	177.78	−0.70	4.79×10^{-2}	9.99×10^{-1}
PfIT_140032100	conserved Plasmodium protein, unknown function	291.22	0.56	4.80×10^{-2}	9.99×10^{-1}
PfIT_060016300	conserved protein, unknown function	2.01	3.63	4.93×10^{-2}	9.99×10^{-1}
PfIT_130020100	ubiquitin-like protein, putative	18.14	1.21	5.00×10^{-2}	9.99×10^{-1}

Table A.7: **Differential gene expression between IT4var08-HA^{endo}-LC and IT4var08-HA^{endo}-P5-EPCR**. Top output of DESeq2 sorted by p_{adj}.

Pf_ID	Transcript description	base mean	$\log_2$ FC	p_{value}	p_{adj}
PfIT_120024500	PfEMP1	11 793.20	7.34	5.83×10^{-146}	3.16×10^{-142}
PfIT_040017300	PfEMP1	7401.65	8.04	3.94×10^{-106}	1.07×10^{-102}
PfIT_130077800	PfEMP1	3427.20	6.25	3.23×10^{-74}	5.84×10^{-71}
PfIT_140006100	PfEMP1	1179.46	6.78	9.16×10^{-69}	1.24×10^{-65}
PfIT_100044100	PfEMP1	1411.51	5.41	8.15×10^{-57}	8.83×10^{-54}
PfIT_070016900	PfEMP1	1543.90	4.66	3.93×10^{-53}	3.55×10^{-50}
PfIT_140085700	PfEMP1	2104.96	4.97	2.13×10^{-45}	1.65×10^{-42}
PfIT_120045700	PfEMP1	2609.52	4.89	6.04×10^{-45}	4.09×10^{-42}
PfIT_120045800	PfEMP1	382.21	5.74	3.53×10^{-43}	2.12×10^{-40}
PfIT_080013800	PfEMP1	4470.51	6.47	9.63×10^{-40}	5.22×10^{-37}
PfIT_070017200	PfEMP1	2867.26	4.43	6.65×10^{-39}	3.27×10^{-36}
PfIT_070017100	PfEMP1	366.25	5.13	7.75×10^{-39}	3.50×10^{-36}
PfIT_060036800	PfEMP1	568.03	4.19	4.49×10^{-35}	1.87×10^{-32}
PfIT_120045200	PfEMP1	345.89	4.17	4.83×10^{-34}	1.87×10^{-31}
PfIT_040025100	PfEMP1	231.37	5.68	4.77×10^{-29}	1.72×10^{-26}
PfIT_140006200	PfEMP1	431.39	5.72	1.39×10^{-26}	4.72×10^{-24}
PfIT_070035100	Plasmodium exported protein (PHISTb), unknown function	393.06	7.05	2.48×10^{-26}	7.91×10^{-24}
PfIT_060036700	PfEMP1	757.80	5.32	2.39×10^{-24}	7.18×10^{-22}
PfIT_050038500	PfEMP1	505.64	3.57	3.63×10^{-24}	1.03×10^{-21}
PfIT_070016700	PfEMP1	444.21	3.52	2.10×10^{-23}	5.69×10^{-21}
PfIT_040017000	PfEMP1	194.51	5.11	7.62×10^{-23}	1.96×10^{-20}
PfIT_040030600	PfEMP1	138.75	4.25	8.13×10^{-23}	2.00×10^{-20}
PfIT_000007700	exported protein family 4	141.76	4.24	9.30×10^{-23}	2.19×10^{-20}
PfIT_070017600	acidic terminal segments, variant surface antigen of PfEMP1, putative	219.04	5.83	5.42×10^{-22}	1.22×10^{-19}
PfIT_130077100	rifin	113.07	4.92	2.70×10^{-21}	5.85×10^{-19}
PfIT_100042800	Alpha/beta hydrolase family/Serine aminopeptidase, S33, putative	108.29	4.22	4.20×10^{-21}	8.75×10^{-19}
PfIT_050038200	rifin	106.82	5.29	5.51×10^{-21}	1.10×10^{-18}
PfIT_090005100	PfEMP1	424.34	4.89	9.48×10^{-21}	1.83×10^{-18}
PfIT_030007200	erythrocyte membrane protein 1 (PfEMP1), pseudogene	17 002.90	4.86	1.49×10^{-20}	2.79×10^{-18}
PfIT_040025500	PfEMP1	11 843.27	4.56	2.59×10^{-20}	4.68×10^{-18}

Pf_ID	Transcript Product Description	base mean	$\log_2$ FC	p_{value}	p_{adj}
PfIT_040005400	PfEMP1	408.05	3.24	3.29×10^{-20}	5.74×10^{-18}
PfIT_080014100	PfEMP1	7495.73	5.02	6.92×10^{-20}	1.17×10^{-17}
PfIT_070005800	PfEMP1	428.65	3.13	3.25×10^{-19}	5.33×10^{-17}
PfIT_040017600	rifin	401.52	4.80	5.91×10^{-19}	9.42×10^{-17}
PfIT_070017400	Pfmc-2TM Maurer's cleft two transmembrane protein	202.03	5.84	9.58×10^{-19}	1.48×10^{-16}
PfIT_120059000	Plasmodium exported protein (PHIST), unknown function	75.99	5.25	1.01×10^{-18}	1.53×10^{-16}
PfIT_100044000	PfEMP1	235.38	4.59	1.19×10^{-18}	1.74×10^{-16}
PfIT_120058300	gametocyte erythrocyte cytosolic protein	111.82	4.11	3.75×10^{-17}	5.34×10^{-15}
PfIT_140006400	PfEMP1	113.45	5.32	4.27×10^{-17}	5.93×10^{-15}
PfIT_130005500	rifin	114.16	6.97	9.26×10^{-17}	1.25×10^{-14}
PfIT_080037400	PfEMP1	1480.24	4.96	1.16×10^{-16}	1.54×10^{-14}
PfIT_110006100	exported protein family 4	76.31	3.82	1.83×10^{-16}	2.37×10^{-14}
PfIT_050037600	rifin	99.19	5.56	3.64×10^{-16}	4.58×10^{-14}
PfIT_070017300	rifin	96.85	5.92	2.01×10^{-15}	2.48×10^{-13}
PfIT_070017000	PfEMP1	224.14	3.89	2.21×10^{-15}	2.66×10^{-13}
PfIT_040025800	PfEMP1	305.51	2.85	8.75×10^{-15}	1.03×10^{-12}
PfIT_060034950	erythrocyte membrane protein 1 (PfEMP1), pseudogene	103.04	5.89	1.13×10^{-14}	1.30×10^{-12}
PfIT_070017500	exported protein family 1	84.50	5.12	1.29×10^{-14}	1.46×10^{-12}
PfIT_000009800	stevor	208.22	5.06	2.70×10^{-14}	2.99×10^{-12}
PfIT_120006100	PfEMP1	770.30	4.96	4.51×10^{-14}	4.88×10^{-12}
PfIT_060035100	exported protein family 1	82.16	6.07	7.92×10^{-14}	8.41×10^{-12}
PfIT_060021400	PfEMP1	83.78	4.74	8.89×10^{-14}	9.26×10^{-12}
PfIT_000010800	PfEMP1	50.86	4.51	2.30×10^{-13}	2.35×10^{-11}
PfIT_080013650	Plasmodium RNA of unknown function RUF6	65.51	6.68	2.97×10^{-13}	2.98×10^{-11}
PfIT_140006700	stevor	104.39	6.76	6.38×10^{-13}	6.18×10^{-11}
PfIT_050037700	rifin	192.40	5.16	6.39×10^{-13}	6.18×10^{-11}
PfIT_040029600	Plasmodium exported protein (hyp6), unknown function	101.65	2.99	8.65×10^{-13}	8.22×10^{-11}
PfIT_020006500	DnaJ protein, putative	1078.20	2.33	8.94×10^{-13}	8.34×10^{-11}
PfIT_120024600	PfEMP1	214.42	3.37	1.41×10^{-12}	1.29×10^{-10}
PfIT_040006300	acyl-CoA synthetase	90.25	3.01	2.09×10^{-12}	1.89×10^{-10}

Pf_ID	Transcript Product Description	base mean	$\log_2$ FC	p_{value}	p_{adj}
PfIT_040017700	erythrocyte membrane protein 1 (PfEMP1), pseudogene	1591.03	4.75	6.20×10^{-12}	5.51×10^{-10}
PfIT_110051300	tubulin–tyrosine ligase, putative	80.36	−4.59	1.20×10^{-11}	1.05×10^{-9}
PfIT_110006300	Pfmc-2TM Maurer's cleft two transmembrane protein	88.39	5.53	1.52×10^{-11}	1.31×10^{-9}
PfIT_120060300	PfEMP1	86.32	4.30	2.01×10^{-11}	1.70×10^{-9}
PfIT_060036600	rifin	58.96	8.49	3.95×10^{-11}	3.29×10^{-9}
PfIT_090005200	rifin	33.74	8.65	7.67×10^{-11}	6.30×10^{-9}
PfIT_100043900	rifin	33.70	5.81	1.55×10^{-10}	1.25×10^{-8}
PfIT_010005000	PfEMP1	196.08	4.00	1.62×10^{-10}	1.29×10^{-8}
PfIT_140085500	rifin	41.25	4.40	1.82×10^{-10}	1.43×10^{-8}
PfIT_040029900	Plasmodium exported protein (PHISTa), unknown function	29.43	4.19	4.40×10^{-10}	3.41×10^{-8}
PfIT_120046200	PfEMP1	316.50	2.18	5.95×10^{-10}	4.54×10^{-8}
PfIT_140006800	rifin	73.77	7.96	7.17×10^{-10}	5.40×10^{-8}
PfIT_120006300	acyl-CoA synthetase	1272.55	1.81	1.09×10^{-9}	8.06×10^{-8}
PfIT_120045100	acidic terminal segments, variant surface antigen of PfEMP1, putative	21.46	8.00	2.12×10^{-9}	1.55×10^{-7}
PfIT_140083600	Plasmodium exported protein (PHISTb), unknown function	1134.34	5.29	4.05×10^{-9}	2.93×10^{-7}
PfIT_110043400	RNA-binding protein, putative	3997.62	2.17	6.01×10^{-9}	4.29×10^{-7}
PfIT_010017100	Pfmc-2TM Maurer's cleft two transmembrane protein	304.47	3.85	1.20×10^{-8}	8.45×10^{-7}
PfIT_040029700	Plasmodium exported protein (hyp15), unknown function	51.52	3.02	1.39×10^{-8}	9.65×10^{-7}
PfIT_050005900	rifin	24.14	4.22	1.74×10^{-8}	1.20×10^{-6}
PfIT_120024700	erythrocyte membrane protein 1 (PfEMP1), pseudogene	44.25	3.08	2.51×10^{-8}	1.70×10^{-6}
PfIT_140006600	rifin	40.54	6.08	2.88×10^{-8}	1.92×10^{-6}
PfIT_140084500	Plasmodium exported protein, unknown function	21.76	5.16	3.48×10^{-8}	2.30×10^{-6}
PfIT_080037300	rifin	125.69	4.30	3.62×10^{-8}	2.36×10^{-6}
PfIT_130005200	PfEMP1	330.04	1.86	6.79×10^{-8}	4.38×10^{-6}
PfIT_040006100	Plasmodium exported protein, unknown function, pseudogene	232.08	3.00	9.98×10^{-8}	6.36×10^{-6}
PfIT_030007000	cytoadherence linked asexual protein 3.2	294.74	2.51	1.02×10^{-7}	6.41×10^{-6}
PfIT_110011700	nucleic acid binding protein, putative	352.00	−2.25	1.48×10^{-7}	9.21×10^{-6}

Pf_ID	Transcript Product Description	base mean	$\log_2$ FC	p_{value}	p_{adj}
PfIT_060014300	histone H3	692.82	−2.33	2.20×10^{-7}	1.35×10^{-5}
PfIT_030029700	PfEMP1	588.93	2.20	2.64×10^{-7}	1.60×10^{-5}
PfIT_080037200	stevor	27.60	4.41	2.68×10^{-7}	1.61×10^{-5}
PfIT_080036300	cytoadherence linked asexual protein 8	371.24	−2.50	3.97×10^{-7}	2.36×10^{-5}
PfIT_030015200	parasite-infected erythrocyte surface protein	871.27	−2.43	4.07×10^{-7}	2.40×10^{-5}
PfIT_020012200	serine repeat antigen 6	1442.42	−2.46	5.40×10^{-7}	3.15×10^{-5}
PfIT_140083100	EMP1-trafficking protein	624.35	6.91	6.65×10^{-7}	3.83×10^{-5}
PfIT_140074800	derlin-1	127.22	−2.10	9.01×10^{-7}	5.14×10^{-5}
PfIT_140077600	diacylglycerol kinase, putative	467.03	−2.08	1.05×10^{-6}	5.92×10^{-5}
PfIT_030028900	Pfmc-2TM Maurer's cleft two transmembrane protein	88.21	4.42	1.14×10^{-6}	6.39×10^{-5}
PfIT_130076800	Plasmodium exported protein, unknown function	62.37	3.51	1.27×10^{-6}	7.02×10^{-5}
PfIT_060031900	HECT-domain (ubiquitin-transferase), putative	2345.00	−2.89	1.39×10^{-6}	7.61×10^{-5}
PfIT_030028800	exported protein family 1	12.53	7.22	1.47×10^{-6}	7.97×10^{-5}
PfIT_050027800	inner membrane complex protein	85.01	−2.28	1.51×10^{-6}	8.09×10^{-5}
PfIT_030026000	UDP-N-acetylglucosamine–dolichyl-phosphate N-acetylglucosaminephosphotransferase, putative	110.23	−2.05	1.60×10^{-6}	8.50×10^{-5}
PfIT_110044600	conserved Plasmodium protein, unknown function	402.67	−2.51	2.18×10^{-6}	1.14×10^{-4}
PfIT_140084200	Plasmodium exported protein (hyp13), unknown function	81.61	2.48	2.25×10^{-6}	1.17×10^{-4}
PfIT_130029000	glideosome associated protein with multiple membrane spans 1	1204.78	−2.47	2.44×10^{-6}	1.26×10^{-4}
PfIT_040028000	glideosome associated protein with multiple membrane spans 2	248.20	−2.05	2.51×10^{-6}	1.28×10^{-4}
PfIT_060019500	cdc2-related protein kinase 5	365.22	−2.10	2.72×10^{-6}	1.38×10^{-4}
PfIT_120040100	V-type K+-independent H+-translocating inorganic pyrophosphatase	415.90	−2.39	2.79×10^{-6}	1.40×10^{-4}
PfIT_130005600	rifin	12.21	7.19	2.83×10^{-6}	1.40×10^{-4}
PfIT_050007000	rhoptry-associated protein 2	927.16	−2.41	2.96×10^{-6}	1.46×10^{-4}

Pf_ID	Transcript Product Description	base mean	$\log_2$ FC	p_{value}	p_{adj}
PfIT_140013400	glideosome associated protein with multiple membrane spans 3	1303.31	−2.42	3.59×10^{-6}	1.75×10^{-4}
PfIT_070006000	rifin	2223.11	2.42	3.95×10^{-6}	1.91×10^{-4}
PfIT_000009700	rifin	19.21	4.83	4.17×10^{-6}	2.00×10^{-4}
PfIT_030011200	FAD-dependent glycerol-3-phosphate dehydrogenase, putative	246.35	−1.85	4.28×10^{-6}	2.04×10^{-4}
PfIT_060021200	conserved Plasmodium protein, unknown function	101.87	−2.21	4.37×10^{-6}	2.06×10^{-4}
PfIT_020012100	serine repeat antigen 7	374.65	−2.19	5.04×10^{-6}	2.34×10^{-4}
PfIT_120058800	Plasmodium RESA N-terminal, putative	40.42	2.61	5.06×10^{-6}	2.34×10^{-4}
PfIT_140045900	ubiquinol-cytochrome c reductase iron-sulfur subunit, putative	284.04	−1.97	6.33×10^{-6}	2.90×10^{-4}
PfIT_140021000	serine/threonine protein phosphatase PP1	1168.89	−1.76	6.42×10^{-6}	2.92×10^{-4}
PfIT_050013300	SET domain protein, putative	1027.72	−2.49	6.55×10^{-6}	2.96×10^{-4}
PfIT_040008600	SET domain protein, putative	170.72	−2.30	6.76×10^{-6}	3.00×10^{-4}
PfIT_100041200	dynamin-like protein	267.00	−2.17	6.78×10^{-6}	3.00×10^{-4}
PfIT_100005800	alpha/beta hydrolase, putative	1341.27	−2.46	6.82×10^{-6}	3.00×10^{-4}
PfIT_080005300	stevor	29.58	4.08	7.16×10^{-6}	3.12×10^{-4}
PfIT_140016000	conserved Plasmodium membrane protein, unknown function	555.63	−1.96	7.53×10^{-6}	3.26×10^{-4}
PfIT_090034000	high molecular weight rhoptry protein 2	5318.14	−2.55	7.75×10^{-6}	3.33×10^{-4}
PfIT_080036600	histidine-rich protein II	1865.35	3.18	8.10×10^{-6}	3.46×10^{-4}
PfIT_080022700	rhoptry neck protein 5	1732.58	−2.61	8.28×10^{-6}	3.50×10^{-4}
PfIT_080020500	conserved Plasmodium protein, unknown function	241.13	−2.23	8.40×10^{-6}	3.53×10^{-4}
PfIT_060022300	malate dehydrogenase	92.97	−1.92	8.48×10^{-6}	3.53×10^{-4}
PfIT_050020900	glideosome-associated protein 40, putative	2602.79	−2.45	8.65×10^{-6}	3.55×10^{-4}
PfIT_110005600	PfEMP1	55.77	2.45	8.65×10^{-6}	3.55×10^{-4}
PfIT_130044000	conserved Plasmodium protein, unknown function	295.68	−1.84	8.95×10^{-6}	3.62×10^{-4}
PfIT_120026500	inner membrane complex protein 1h, putative	44.34	−2.60	8.96×10^{-6}	3.62×10^{-4}
PfIT_090019000	conserved Plasmodium protein, unknown function	226.11	−2.32	9.39×10^{-6}	3.77×10^{-4}

Pf_ID	Transcript Product Description	base mean	$\log_2$ FC	p_{value}	p_{adj}
PfIT_100032800	conserved Plasmodium protein, unknown function	88.47	−2.12	9.89×10^{-6}	3.89×10^{-4}
PfIT_130037500	conserved Plasmodium protein, unknown function	574.09	−2.01	9.96×10^{-6}	3.89×10^{-4}
PfIT_100040500	acetyl-CoA transporter, putative	139.43	−1.84	9.98×10^{-6}	3.89×10^{-4}
PfIT_090020200	conserved Plasmodium protein, unknown function	339.17	1.58	9.99×10^{-6}	3.89×10^{-4}
PfIT_130026800	3',5'-cyclic nucleotide phosphodiesterase, putative	789.48	−2.43	1.02×10^{-5}	3.94×10^{-4}
PfIT_110013100	succinyl-CoA synthetase alpha subunit, putative	338.38	−1.64	1.04×10^{-5}	3.99×10^{-4}
PfIT_070034800	EMP1-trafficking protein	944.84	2.94	1.09×10^{-5}	4.17×10^{-4}
PfIT_040023800	conserved Plasmodium protein, unknown function	173.95	−2.63	1.13×10^{-5}	4.25×10^{-4}
PfIT_020012300	serine repeat antigen 7	8086.94	−2.42	1.13×10^{-5}	4.25×10^{-4}
PfIT_100033700	RAP protein, putative	288.64	−1.99	1.15×10^{-5}	4.28×10^{-4}
PfIT_140071300	conserved Plasmodium protein, unknown function	130.25	−1.87	1.17×10^{-5}	4.32×10^{-4}
PfIT_090021800	conserved Plasmodium membrane protein, unknown function	31.51	−2.74	1.19×10^{-5}	4.37×10^{-4}
PfIT_140078800	protein disulfide-isomerase	288.62	−2.30	1.21×10^{-5}	4.40×10^{-4}
PfIT_030029800	PfEMP1	219.55	1.46	1.21×10^{-5}	4.40×10^{-4}
PfIT_060017400	apicoplast ribosomal protein L18 precursor, putative	317.55	−2.08	1.28×10^{-5}	4.55×10^{-4}
PfIT_120045600	PfEMP1	444.46	1.72	1.28×10^{-5}	4.55×10^{-4}
PfIT_120028200	cAMP-dependent protein kinase regulatory subunit	4850.35	−2.24	1.28×10^{-5}	4.55×10^{-4}
PfIT_090022600	glideosome-associated protein 50	2024.19	−2.28	1.29×10^{-5}	4.55×10^{-4}
PfIT_140058400	rhoptry neck protein 2	1440.18	−2.60	1.36×10^{-5}	4.79×10^{-4}
PfIT_030016100	phosphatidylinositol 3- and 4-kinase, putative	649.39	−2.23	1.45×10^{-5}	5.03×10^{-4}
PfIT_140053000	centrin-2	833.13	−2.23	1.45×10^{-5}	5.03×10^{-4}
PfIT_110015000	mitochondrial ribosomal protein L11 precursor, putative	148.21	−2.14	1.49×10^{-5}	5.15×10^{-4}
PfIT_100023600	conserved Plasmodium membrane protein, unknown function	527.19	−1.81	1.56×10^{-5}	5.34×10^{-4}
PfIT_100025900	schizont egress antigen-1	3637.66	−2.09	1.59×10^{-5}	5.41×10^{-4}

Pf_ID	Transcript Product Description	base mean	$\log_2$ FC	p_{value}	p_{adj}
PfIT_140029800	serine/threonine protein phosphatase 7	1548.23	−2.45	1.62×10^{-5}	5.47×10^{-4}
PfIT_140041700	NAD(P)H-dependent glutamate synthase, putative	1113.47	−2.27	1.63×10^{-5}	5.47×10^{-4}
PfIT_070035800	stevor	6.72	6.33	1.64×10^{-5}	5.49×10^{-4}
PfIT_050012100	rhomboid protease ROM4	1217.41	−2.41	1.66×10^{-5}	5.52×10^{-4}
PfIT_090037000	profilin, putative	1788.63	−2.09	1.69×10^{-5}	5.57×10^{-4}
PfIT_120032600	cyclin	1314.25	−1.90	1.71×10^{-5}	5.57×10^{-4}
PfIT_060008000	transcription factor with AP2 domain(s)	913.28	−2.37	1.71×10^{-5}	5.57×10^{-4}
PfIT_120025500	cell cycle associated protein, putative	164.59	−2.47	1.72×10^{-5}	5.57×10^{-4}
PfIT_130069400	6-cysteine protein	414.60	−2.17	1.82×10^{-5}	5.84×10^{-4}
PfIT_040025700	rifin	149.11	1.99	1.82×10^{-5}	5.84×10^{-4}
PfIT_120007800	mitochondrial phosphate carrier protein	215.35	−1.73	1.93×10^{-5}	6.16×10^{-4}
PfIT_140085200	rifin	10.14	6.92	1.97×10^{-5}	6.24×10^{-4}
PfIT_130050700	conserved Plasmodium protein, unknown function	863.75	−1.48	2.00×10^{-5}	6.28×10^{-4}
PfIT_120026100	histone-lysine N-methyltransferase, H3 lysine-4 specific	425.75	−1.84	2.01×10^{-5}	6.28×10^{-4}
PfIT_140040800	conserved Plasmodium membrane protein, unknown function	258.84	−2.55	2.04×10^{-5}	6.35×10^{-4}
PfIT_050032200	DNA replication licensing factor MCM3, putative	1681.16	−1.73	2.07×10^{-5}	6.40×10^{-4}
PfIT_100033800	conserved Plasmodium protein, unknown function	1543.11	−2.28	2.10×10^{-5}	6.46×10^{-4}
PfIT_080034300	prolyl 4-hydroxylase subunit alpha, putative	214.03	−2.08	2.27×10^{-5}	6.92×10^{-4}
PfIT_070008500	conserved Plasmodium protein, unknown function	645.30	−2.20	2.27×10^{-5}	6.92×10^{-4}
PfIT_050035400	conserved Plasmodium membrane protein, unknown function	240.66	−2.60	2.31×10^{-5}	6.98×10^{-4}
PfIT_140043000	cGMP-dependent protein kinase	544.27	−2.17	2.32×10^{-5}	6.98×10^{-4}
PfIT_020012400	serine repeat antigen 7	603.06	−2.17	2.34×10^{-5}	7.01×10^{-4}
PfIT_120020700	conserved Plasmodium protein, unknown function	302.42	−1.80	2.37×10^{-5}	7.02×10^{-4}
PfIT_050014000	single-stranded DNA-binding protein	373.61	−2.01	2.37×10^{-5}	7.02×10^{-4}

Pf_ID	Transcript Product Description	base mean	$\log_2$ FC	p_{value}	p_{adj}
PfIT_020026500	Pfmc-2TM Maurer's cleft two transmembrane protein	9.30	6.79	2.46×10^{-5}	7.25×10^{-4}
PfIT_100010000	conserved Plasmodium protein, unknown function	114.98	−2.05	2.49×10^{-5}	7.29×10^{-4}
PfIT_070014000	Cg1 protein	467.96	−1.51	2.56×10^{-5}	7.47×10^{-4}
PfIT_030017200	glycogen synthase kinase 3	859.19	−1.48	2.58×10^{-5}	7.48×10^{-4}
PfIT_100012700	tubulin beta chain	1088.90	−1.43	2.63×10^{-5}	7.58×10^{-4}
PfIT_130018800	conserved Plasmodium membrane protein, unknown function	236.00	−2.35	2.65×10^{-5}	7.58×10^{-4}
PfIT_100016300	cytochrome b-c1 complex subunit 7, putative	154.52	−1.99	2.74×10^{-5}	7.78×10^{-4}
PfIT_090010100	high molecular weight rhoptry protein 3	14 786.19	−2.39	2.76×10^{-5}	7.78×10^{-4}
PfIT_040020800	histone acetyltransferase, putative	1708.94	−1.52	2.77×10^{-5}	7.78×10^{-4}
PfIT_080008500	filament assembling protein, putative	985.21	−2.38	2.77×10^{-5}	7.78×10^{-4}
PfIT_130013900	tyrosine recombinase	272.38	−1.51	2.81×10^{-5}	7.82×10^{-4}
PfIT_140043600	ribonucleoside-diphosphate reductase, large subunit, putative	1406.74	−1.39	2.82×10^{-5}	7.82×10^{-4}
PfIT_080011400	ferlin, putative	337.29	−2.19	2.92×10^{-5}	8.06×10^{-4}
PfIT_100022300	serine/threonine protein phosphatase 8, putative	1127.18	−2.22	2.96×10^{-5}	8.15×10^{-4}
PfIT_140033300	ubiquinol-cytochrome c reductase hinge protein, putative	175.75	−1.91	3.02×10^{-5}	8.25×10^{-4}
PfIT_100039100	S-antigen	29 807.24	−2.32	3.11×10^{-5}	8.46×10^{-4}
PfIT_110037900	LEM3/CDC50 family protein, putative	182.82	−2.38	3.14×10^{-5}	8.49×10^{-4}
PfIT_090032300	cytochrome c oxidase subunit 5B, putative	180.76	−1.77	3.21×10^{-5}	8.62×10^{-4}
PfIT_130067000	cytochrome c oxidase subunit 2, putative	191.40	−1.82	3.22×10^{-5}	8.62×10^{-4}
PfIT_020027600	PfEMP1	74.94	1.82	3.23×10^{-5}	8.62×10^{-4}
PfIT_120050800	conserved Plasmodium protein, unknown function	134.73	−2.24	3.29×10^{-5}	8.75×10^{-4}
PfIT_110046000	phd finger protein, putative	195.00	−2.30	3.32×10^{-5}	8.77×10^{-4}
PfIT_100032600	conserved Plasmodium protein, unknown function	149.52	−1.81	3.39×10^{-5}	8.92×10^{-4}
PfIT_030024200	kinesin-8, putative	476.37	−1.77	3.43×10^{-5}	8.95×10^{-4}
PfIT_020012700	serine repeat antigen 7	487.85	−2.22	3.46×10^{-5}	8.95×10^{-4}

Pf_ID	Transcript Product Description	base mean	$\log_2$ FC	p_{value}	p_{adj}
PfIT_130048400	conserved Plasmodium protein, unknown function	265.36	−2.40	3.46×10^{-5}	8.95×10^{-4}
PfIT_110046500	conserved Plasmodium membrane protein, unknown function	316.99	−1.97	3.47×10^{-5}	8.95×10^{-4}
PfIT_130018100	conserved Plasmodium protein, unknown function	1219.99	−2.25	3.58×10^{-5}	9.19×10^{-4}
PfIT_100024300	conserved Plasmodium protein, unknown function	130.80	−2.45	3.67×10^{-5}	9.38×10^{-4}
PfIT_090008000	conserved Plasmodium membrane protein, unknown function	1083.32	−2.25	3.73×10^{-5}	9.48×10^{-4}
PfIT_100035700	conserved Plasmodium protein, unknown function	197.33	−2.54	3.79×10^{-5}	9.57×10^{-4}
PfIT_000007500	rifin	11.44	5.14	3.82×10^{-5}	9.57×10^{-4}
PfIT_130061700	ubiquitin-conjugating enzyme, putative	410.64	−2.20	3.82×10^{-5}	9.57×10^{-4}
PfIT_040020500	glutamyl-tRNA(Gln) amidotransferase subunit A	285.35	−1.49	3.87×10^{-5}	9.64×10^{-4}
PfIT_120058500	Plasmodium exported protein, unknown function	37.85	2.35	3.88×10^{-5}	9.64×10^{-4}
PfIT_110020300	rhoptry neck protein 4	2664.69	−2.39	3.91×10^{-5}	9.67×10^{-4}
PfIT_060021800	conserved Plasmodium membrane protein, unknown function	1819.47	−2.29	3.97×10^{-5}	9.77×10^{-4}
PfIT_060007700	centrosomal protein CEP76, putative	528.21	−2.06	3.99×10^{-5}	9.78×10^{-4}
PfIT_030023800	P-type ATPase, putative	468.51	−2.11	4.02×10^{-5}	9.79×10^{-4}
PfIT_030023300	conserved Plasmodium protein, unknown function	1084.35	−2.46	4.03×10^{-5}	9.79×10^{-4}
PfIT_070033500	conserved Plasmodium protein, unknown function	127.63	−1.71	4.06×10^{-5}	9.83×10^{-4}
PfIT_140058100	calcineurin subunit B	173.28	−2.44	4.13×10^{-5}	9.93×10^{-4}
PfIT_110035700	serpentine receptor, putative	86.80	−1.98	4.15×10^{-5}	9.95×10^{-4}
PfIT_070012200	rhoptry-associated membrane antigen	12 283.12	−2.53	4.28×10^{-5}	1.01×10^{-3}
PfIT_060017800	transcription factor with AP2 domain(s)	1361.62	−2.17	4.29×10^{-5}	1.01×10^{-3}
PfIT_120051400	actin I	8773.51	−2.07	4.29×10^{-5}	1.01×10^{-3}
PfIT_130017900	2-oxoisovalerate dehydrogenase subunit alpha, mitochondrial, putative	295.05	−2.00	4.29×10^{-5}	1.01×10^{-3}

Pf_ID	Transcript Product Description	base mean	$\log_2$ FC	p_{value}	p_{adj}
PfIT_000011300	erythrocyte membrane protein 1 (PfEMP1), pseudogene	16.26	3.37	4.40×10^{-5}	1.03×10^{-3}
PfIT_110023000	myosin light chain B	1539.88	−2.40	4.47×10^{-5}	1.04×10^{-3}
PfIT_130067100	conserved Plasmodium protein, unknown function	6028.70	−2.20	4.53×10^{-5}	1.05×10^{-3}
PfIT_030027100	diacylglycerol O-acyltransferase	193.63	−1.50	4.56×10^{-5}	1.05×10^{-3}
PfIT_130046100	mitochondrial pyruvate carrier protein 1, putative	41.66	−2.17	4.57×10^{-5}	1.05×10^{-3}
PfIT_020008900	conserved Plasmodium protein, unknown function	872.37	−2.17	4.61×10^{-5}	1.06×10^{-3}
PfIT_120041800	conserved Plasmodium protein, unknown function	339.07	−2.43	4.64×10^{-5}	1.06×10^{-3}
PfIT_120034300	conserved Plasmodium protein, unknown function	389.31	−2.13	4.70×10^{-5}	1.07×10^{-3}
PfIT_120033700	merozoite surface protein 9	19 407.64	−2.40	4.74×10^{-5}	1.07×10^{-3}
PfIT_110015100	actin-like protein, putative	173.75	−1.89	4.80×10^{-5}	1.08×10^{-3}
PfIT_090024400	regulator of chromosome condensation, putative	2007.68	−2.48	4.87×10^{-5}	1.09×10^{-3}
PfIT_090040500	cytoadherence linked asexual protein 9	2777.69	−2.45	4.92×10^{-5}	1.10×10^{-3}
PfIT_140059600	conserved Plasmodium protein, unknown function	172.99	−2.30	4.97×10^{-5}	1.11×10^{-3}
PfIT_020021300	conserved Plasmodium membrane protein, unknown function	134.66	−2.41	5.06×10^{-5}	1.12×10^{-3}
PfIT_130027800	palmitoyltransferase, putative	521.39	−2.21	5.10×10^{-5}	1.13×10^{-3}
PfIT_090039600	cAMP-dependent protein kinase catalytic subunit	1575.71	−2.17	5.11×10^{-5}	1.13×10^{-3}
PfIT_090025100	conserved Plasmodium protein, unknown function	188.84	−1.65	5.16×10^{-5}	1.13×10^{-3}
PfIT_140017000	rhoptry-associated protein 1	5897.35	−2.27	5.16×10^{-5}	1.13×10^{-3}
PfIT_140010200	selenoprotein	127.86	−2.14	5.24×10^{-5}	1.14×10^{-3}
PfIT_040013100	flap endonuclease 1	208.04	−1.81	5.25×10^{-5}	1.14×10^{-3}
PfIT_030007300	cytoadherence linked asexual protein 3.1	12 427.09	−2.34	5.31×10^{-5}	1.15×10^{-3}
PfIT_040012400	conserved Plasmodium protein, unknown function	3320.85	−2.24	5.39×10^{-5}	1.16×10^{-3}
PfIT_080015900	cullin-1, putative	302.99	−1.96	5.42×10^{-5}	1.16×10^{-3}

Pf_ID	Transcript Product Description	base mean	$\log_2$ FC	p_{value}	p_{adj}
PfIT_070034300	conserved Plasmodium protein, unknown function	706.72	−2.44	5.48×10^{-5}	1.17×10^{-3}
PfIT_090035400	conserved Plasmodium membrane protein, unknown function	190.64	−1.46	5.50×10^{-5}	1.17×10^{-3}
PfIT_140055500	conserved Plasmodium protein, unknown function	623.46	−2.29	5.65×10^{-5}	1.20×10^{-3}
PfIT_140069700	DNA-directed RNA polymerase III subunit RPC4, putative	619.22	1.24	5.68×10^{-5}	1.20×10^{-3}
PfIT_010010100	ras-related protein Rab-5C	103.34	−1.44	5.72×10^{-5}	1.20×10^{-3}
PfIT_140082500	Plasmodium exported protein (PHISTb), unknown function	887.72	−2.36	5.74×10^{-5}	1.20×10^{-3}
PfIT_080007400	transcription factor with AP2 domain(s)	723.01	−2.42	5.77×10^{-5}	1.20×10^{-3}
PfIT_130033600	conserved Plasmodium protein, unknown function	1000.65	−1.80	5.79×10^{-5}	1.20×10^{-3}
PfIT_140063900	vacuolar protein sorting-associated protein 4	181.51	−1.86	5.85×10^{-5}	1.21×10^{-3}
PfIT_120057300	rhoptry neck protein 3	854.36	−2.35	5.89×10^{-5}	1.21×10^{-3}
PfIT_100034100	conserved Plasmodium protein, unknown function	908.96	−2.24	6.28×10^{-5}	1.28×10^{-3}
PfIT_140010100	conserved Plasmodium protein, unknown function	116.22	−2.15	6.28×10^{-5}	1.28×10^{-3}
PfIT_100026900	4-hydroxy-3-methylbut-2-en-1-yl diphosphate synthase	230.19	−1.71	6.33×10^{-5}	1.29×10^{-3}
PfIT_140008700	conserved Plasmodium protein, unknown function	441.11	−1.97	6.42×10^{-5}	1.30×10^{-3}
PfIT_080036700	Plasmodium RESA N-terminal, putative	21.85	2.35	6.42×10^{-5}	1.30×10^{-3}
PfIT_070021900	conserved Plasmodium protein, unknown function	400.70	−2.35	6.52×10^{-5}	1.31×10^{-3}
PfIT_080022600	conserved Plasmodium protein, unknown function	2418.81	−2.63	6.60×10^{-5}	1.32×10^{-3}
PfIT_070010200	origin recognition complex subunit 2, putative	982.29	−1.80	6.66×10^{-5}	1.33×10^{-3}
PfIT_070026400	rhoptry-associated leucine zipper-like protein 1	5914.57	−2.56	6.72×10^{-5}	1.34×10^{-3}
PfIT_100017800	conserved Plasmodium protein, unknown function	1952.39	−2.53	6.79×10^{-5}	1.35×10^{-3}
PfIT_050033600	palmitoyltransferase	808.60	−2.47	6.81×10^{-5}	1.35×10^{-3}

Pf_ID	Transcript Product Description	base mean	$\log_2$ FC	p_{value}	p_{adj}
PfIT_110037800	conserved Plasmodium protein, unknown function	2796.32	−1.82	6.88×10^{-5}	1.35×10^{-3}
PfIT_000005900	erythrocyte binding like protein 1	3760.42	−2.38	7.03×10^{-5}	1.38×10^{-3}
PfIT_120033400	NIMA related kinase 1	844.69	−1.65	7.12×10^{-5}	1.39×10^{-3}
PfIT_030026200	protein kinase, putative	538.08	−2.25	7.23×10^{-5}	1.41×10^{-3}
PfIT_130013100	conserved Plasmodium membrane protein, unknown function	844.62	−2.25	7.24×10^{-5}	1.41×10^{-3}
PfIT_040009400	dipeptidyl aminopeptidase 3	1867.30	−2.59	7.29×10^{-5}	1.41×10^{-3}
PfIT_120020300	thioredoxin peroxidase 2	57.49	−1.94	7.33×10^{-5}	1.41×10^{-3}
PfIT_110037400	aquaglyceroporin	847.83	−1.79	7.38×10^{-5}	1.42×10^{-3}
PfIT_120037700	conserved Plasmodium protein, unknown function	263.62	−2.50	7.70×10^{-5}	1.47×10^{-3}
PfIT_130030700	conserved Plasmodium protein, unknown function	1148.53	−2.33	7.74×10^{-5}	1.48×10^{-3}
PfIT_100039000	probable protein, unknown function	538.15	−2.26	7.93×10^{-5}	1.51×10^{-3}
PfIT_130035800	conserved Plasmodium protein, unknown function	434.02	−1.85	7.98×10^{-5}	1.51×10^{-3}
PfIT_030025900	conserved Plasmodium protein, unknown function	444.05	−2.27	8.05×10^{-5}	1.52×10^{-3}
PfIT_100029500	conserved Plasmodium membrane protein, unknown function	556.16	−2.26	8.09×10^{-5}	1.52×10^{-3}
PfIT_130026000	conserved Plasmodium protein, unknown function	611.54	−2.12	8.11×10^{-5}	1.52×10^{-3}
PfIT_090007200	serine/threonine protein kinase, FIKK family	74.46	1.69	8.25×10^{-5}	1.54×10^{-3}
PfIT_030010800	conserved Plasmodium protein, unknown function	74.20	−1.67	8.35×10^{-5}	1.55×10^{-3}
PfIT_040027900	asparagine-rich protein	426.85	−2.20	8.36×10^{-5}	1.55×10^{-3}
PfIT_090009600	copper-transporting ATPase	1280.68	−1.66	8.41×10^{-5}	1.55×10^{-3}
PfIT_120029200	conserved Plasmodium protein, unknown function	2269.27	−2.33	8.47×10^{-5}	1.56×10^{-3}
PfIT_110042900	guanylyl cyclase	432.34	−2.16	8.58×10^{-5}	1.57×10^{-3}
PfIT_140044100	succinyl-CoA ligase, putative	103.46	−1.78	8.63×10^{-5}	1.57×10^{-3}
PfIT_080008700	DNA repair and recombination protein RAD54, putative	865.12	−1.68	8.64×10^{-5}	1.57×10^{-3}
PfIT_120039800	conserved Plasmodium protein, unknown function	534.00	−1.88	8.67×10^{-5}	1.58×10^{-3}
PfIT_140055600	hypothetical protein	976.62	−2.07	8.72×10^{-5}	1.58×10^{-3}

Pf_ID	Transcript Product Description	base mean	$\log_2$ FC	p_{value}	p_{adj}
PfIT_130043000	conserved Plasmodium protein, unknown function	424.32	−2.36	8.81×10^{-5}	1.59×10^{-3}
PfIT_130017300	conserved Plasmodium protein, unknown function	317.84	−2.30	9.09×10^{-5}	1.63×10^{-3}
PfIT_120006200	hypothetical protein	14.03	3.81	9.11×10^{-5}	1.63×10^{-3}
PfIT_140070200	conserved Plasmodium membrane protein, unknown function	1268.40	−2.49	9.20×10^{-5}	1.64×10^{-3}
PfIT_020011700	merozoite surface protein 4	1933.17	−2.33	9.23×10^{-5}	1.64×10^{-3}
PfIT_130077500	rifin	22.19	3.04	9.25×10^{-5}	1.64×10^{-3}
PfIT_060017300	rhoptry protein ROP14	1634.57	−2.53	9.27×10^{-5}	1.64×10^{-3}
PfIT_060030200	Sec14 domain containing protein	241.13	−1.96	9.28×10^{-5}	1.64×10^{-3}
PfIT_010007600	conserved Plasmodium membrane protein, unknown function	172.81	−2.59	9.42×10^{-5}	1.66×10^{-3}
PfIT_080010800	serine/threonine protein kinase, FIKK family	96.16	−2.27	9.60×10^{-5}	1.68×10^{-3}
PfIT_100039600	duffy binding-like merozoite surface protein	2652.22	−2.22	9.66×10^{-5}	1.69×10^{-3}
PfIT_060011700	conserved Plasmodium protein, unknown function	406.78	−2.56	9.80×10^{-5}	1.71×10^{-3}
PfIT_050034500	conserved Plasmodium protein, unknown function	1654.79	−1.68	9.84×10^{-5}	1.71×10^{-3}
PfIT_090020300	conserved Plasmodium protein, unknown function	103.88	−1.75	9.89×10^{-5}	1.71×10^{-3}
PfIT_030011300	conserved Plasmodium protein, unknown function	248.75	−1.96	9.89×10^{-5}	1.71×10^{-3}
PfIT_130066800	conserved Plasmodium protein, unknown function	676.90	−2.24	9.96×10^{-5}	1.71×10^{-3}
PfIT_040012300	conserved Plasmodium protein, unknown function	1946.08	−2.10	1.00×10^{-4}	1.72×10^{-3}
PfIT_020025300	cytoadherence linked asexual protein 2	35.60	−2.65	1.00×10^{-4}	1.72×10^{-3}
PfIT_130044200	serine/threonine protein kinase, putative	215.50	−1.68	1.01×10^{-4}	1.72×10^{-3}
PfIT_080025700	2-oxoglutarate dehydrogenase E1 component	407.50	−1.45	1.02×10^{-4}	1.74×10^{-3}
PfIT_100039200	glutamate-rich protein	2715.11	−2.13	1.03×10^{-4}	1.74×10^{-3}
PfIT_030012500	conserved Plasmodium protein, unknown function	1438.63	−1.52	1.03×10^{-4}	1.74×10^{-3}

Pf_ID	Transcript Product Description	base mean	$\log_2$ FC	p_{value}	p_{adj}
PfIT_060033100	phospholipase, putative	407.95	−1.97	1.04×10^{-4}	1.75×10^{-3}
PfIT_140017300	conserved Plasmodium protein, unknown function	153.74	−2.14	1.05×10^{-4}	1.75×10^{-3}
PfIT_040010600	apical sushi protein	2225.44	−2.47	1.05×10^{-4}	1.75×10^{-3}
PfIT_100030000	conserved Plasmodium protein, unknown function	1410.03	−2.21	1.05×10^{-4}	1.75×10^{-3}
PfIT_040015300	ribosome biogenesis GTPase A, putative	1309.37	−1.72	1.05×10^{-4}	1.75×10^{-3}
PfIT_140038700	conserved Plasmodium protein, unknown function	139.40	−1.88	1.06×10^{-4}	1.75×10^{-3}
PfIT_020017400	Leu/Phe-tRNA protein transferase, putative	729.18	−2.05	1.06×10^{-4}	1.75×10^{-3}
PfIT_120030600	small subunit rRNA processing factor, putative	599.16	1.19	1.07×10^{-4}	1.75×10^{-3}
PfIT_050006300	serine/threonine protein kinase, FIKK family	141.07	−2.33	1.07×10^{-4}	1.75×10^{-3}
PfIT_070028000	conserved Plasmodium protein, unknown function	712.67	−1.72	1.07×10^{-4}	1.75×10^{-3}
PfIT_020019400	rhoptry neck protein 6	7331.30	−2.58	1.08×10^{-4}	1.75×10^{-3}
PfIT_100031700	centrin-3	183.26	−1.85	1.08×10^{-4}	1.75×10^{-3}
PfIT_010010300	centrin-1	280.10	−1.67	1.08×10^{-4}	1.75×10^{-3}
PfIT_060036100	Plasmodium exported protein, unknown function	11.66	5.16	1.08×10^{-4}	1.75×10^{-3}
PfIT_100011900	conserved Plasmodium protein, unknown function	150.78	1.37	1.08×10^{-4}	1.75×10^{-3}
PfIT_030019700	conserved Plasmodium membrane protein, unknown function	167.81	−2.09	1.09×10^{-4}	1.75×10^{-3}
PfIT_130067300	conserved Plasmodium protein, unknown function	66.75	−1.84	1.11×10^{-4}	1.78×10^{-3}
PfIT_110017300	conserved Plasmodium protein, unknown function	97.21	−2.42	1.12×10^{-4}	1.79×10^{-3}
PfIT_000012000	rifin	63.59	−1.74	1.13×10^{-4}	1.79×10^{-3}
PfIT_100024400	cytoplasmic dynein intermediate chain, putative	157.66	−1.84	1.13×10^{-4}	1.79×10^{-3}
PfIT_080031400	dehydrodolichyl diphosphate synthetase, putative	128.30	−2.00	1.14×10^{-4}	1.80×10^{-3}
PfIT_130061500	conserved Plasmodium protein, unknown function	544.04	−1.94	1.15×10^{-4}	1.82×10^{-3}

Pf_ID	Transcript Product Description	base mean	$\log_2$ FC	p_{value}	p_{adj}
PfIT_120043500	sphingomyelin phosphodiesterase, putative	389.01	−2.13	1.16×10^{-4}	1.82×10^{-3}
PfIT_020021600	ATP synthase F1, alpha subunit	308.85	−1.36	1.16×10^{-4}	1.82×10^{-3}
PfIT_120026900	conserved Plasmodium protein, unknown function	232.00	−1.48	1.16×10^{-4}	1.82×10^{-3}
PfIT_140040200	conserved Plasmodium protein, unknown function	270.46	−1.68	1.17×10^{-4}	1.83×10^{-3}
PfIT_100007300	conserved Plasmodium protein, unknown function	30.76	−2.09	1.17×10^{-4}	1.83×10^{-3}
PfIT_050010200	conserved protein, unknown function	69.29	−2.04	1.18×10^{-4}	1.83×10^{-3}
PfIT_090028800	thiamine pyrophosphokinase	139.89	−1.97	1.19×10^{-4}	1.84×10^{-3}
PfIT_120017100	DNA replication licensing factor MCM5, putative	1014.53	−1.64	1.20×10^{-4}	1.85×10^{-3}
PfIT_140017400	ankyrin-repeat protein, putative	188.26	−2.26	1.22×10^{-4}	1.88×10^{-3}
PfIT_050027700	50S ribosomal protein L17, apicoplast, putative	90.79	−1.95	1.23×10^{-4}	1.89×10^{-3}
PfIT_140084100	Plasmodium exported protein (PHISTa), unknown function	83.20	2.34	1.24×10^{-4}	1.89×10^{-3}
PfIT_100038600	ADP-ribosylation factor, putative	141.15	−2.07	1.24×10^{-4}	1.89×10^{-3}
PfIT_100037800	ubiquitin-conjugating enzyme, putative	226.28	−1.62	1.24×10^{-4}	1.89×10^{-3}
PfIT_110025600	tyrosine kinase-like protein	305.86	−2.19	1.25×10^{-4}	1.89×10^{-3}
PfIT_070010300	DNA replication licensing factor MCM7	1571.61	−1.66	1.26×10^{-4}	1.90×10^{-3}
PfIT_120027800	glideosome-associated protein 45	2209.97	−2.11	1.26×10^{-4}	1.90×10^{-3}
PfIT_100018900	conserved Plasmodium protein, unknown function	2078.62	−2.54	1.27×10^{-4}	1.91×10^{-3}
PfIT_060016200	leucine-rich repeat protein	882.95	−2.11	1.29×10^{-4}	1.93×10^{-3}
PfIT_030021000	conserved Plasmodium protein, unknown function	329.02	−1.42	1.29×10^{-4}	1.93×10^{-3}
PfIT_090012800	P1 nuclease, putative	188.04	−1.66	1.29×10^{-4}	1.93×10^{-3}
PfIT_100032200	zinc finger, C3HC4 type, putative	75.41	−2.15	1.30×10^{-4}	1.93×10^{-3}
PfIT_130027500	conserved Plasmodium protein, unknown function	655.34	−1.53	1.30×10^{-4}	1.93×10^{-3}
PfIT_050010700	conserved Plasmodium protein, unknown function	268.03	−1.78	1.32×10^{-4}	1.94×10^{-3}
PfIT_060011600	spindle assembly abnormal protein 6, putative	546.10	−1.98	1.33×10^{-4}	1.94×10^{-3}

Pf_ID	Transcript Product Description	base mean	$\log_2$ FC	p_{value}	p_{adj}
PfIT_050016300	stearoyl-CoA desaturase	367.06	−1.97	1.33×10^{-4}	1.94×10^{-3}
PfIT_040016600	conserved Plasmodium protein, unknown function	253.60	−1.48	1.33×10^{-4}	1.94×10^{-3}
PfIT_140046800	conserved Plasmodium protein, unknown function	181.01	−2.50	1.33×10^{-4}	1.94×10^{-3}
PfIT_020011500	merozoite surface protein 2	7643.11	−2.28	1.33×10^{-4}	1.94×10^{-3}
PfIT_090007500	serine repeat antigen 7	455.52	−1.39	1.33×10^{-4}	1.94×10^{-3}
PfIT_140038600	conserved Plasmodium protein, unknown function	416.66	−2.02	1.34×10^{-4}	1.95×10^{-3}
PfIT_120006500	Plasmodium exported protein (PHISTc), unknown function	506.03	1.13	1.36×10^{-4}	1.97×10^{-3}
PfIT_140074700	zinc finger protein, putative	412.94	−1.71	1.36×10^{-4}	1.97×10^{-3}
PfIT_060024900	conserved Plasmodium protein, unknown function	1011.43	−2.49	1.38×10^{-4}	1.99×10^{-3}
PfIT_130025400	ATP-dependent Clp protease adaptor protein ClpS, putative	72.16	−1.66	1.39×10^{-4}	1.99×10^{-3}
PfIT_040009500	conserved Plasmodium protein, unknown function	240.14	−2.31	1.39×10^{-4}	1.99×10^{-3}
PfIT_100035100	MORN repeat-containing protein 1	481.74	−1.71	1.41×10^{-4}	2.01×10^{-3}
PfIT_140049100	conserved Plasmodium protein, unknown function	253.86	−1.96	1.41×10^{-4}	2.01×10^{-3}
PfIT_020015200	conserved Plasmodium protein, unknown function	762.17	−2.20	1.41×10^{-4}	2.01×10^{-3}
PfIT_070005900	PfEMP1	56 525.96	2.29	1.42×10^{-4}	2.01×10^{-3}
PfIT_070019500	conserved Plasmodium protein, unknown function	372.24	−1.76	1.43×10^{-4}	2.02×10^{-3}
PfIT_110038900	conserved Plasmodium protein, unknown function	727.13	−1.97	1.44×10^{-4}	2.02×10^{-3}
PfIT_130031300	conserved Plasmodium protein, unknown function	198.52	−1.94	1.44×10^{-4}	2.02×10^{-3}
PfIT_090034900	merozoite surface protein 1	33 906.91	−2.46	1.44×10^{-4}	2.02×10^{-3}
PfIT_140058200	sortilin	793.11	−1.13	1.46×10^{-4}	2.04×10^{-3}
PfIT_130036700	CPW-WPC family protein	250.21	−2.48	1.46×10^{-4}	2.04×10^{-3}
PfIT_120015700	conserved Plasmodium protein, unknown function	44.96	1.83	1.47×10^{-4}	2.04×10^{-3}
PfIT_040019300	armadillo-domain containing rhoptry protein	1509.03	−2.41	1.49×10^{-4}	2.07×10^{-3}
PfIT_010014100	kinesin-8, putative	398.10	−2.21	1.50×10^{-4}	2.07×10^{-3}

Pf_ID	Transcript Product Description	base mean	$\log_2$ FC	p_{value}	p_{adj}
PfIT_140032200	conserved Plasmodium protein, unknown function	326.53	−1.88	1.55×10^{-4}	2.14×10^{-3}
PfIT_050038100	rifin	137.49	5.80	1.57×10^{-4}	2.16×10^{-3}
PfIT_070022600	mitochondrial ribosomal protein S8 precursor, putative	254.97	−1.28	1.58×10^{-4}	2.17×10^{-3}
PfIT_140011000	mitochondrial ribosomal protein L16 precursor, putative	67.17	−1.73	1.59×10^{-4}	2.17×10^{-3}
PfIT_140075500	shewanella-like protein phosphatase 1, putative	320.41	−2.12	1.59×10^{-4}	2.17×10^{-3}
PfIT_010009300	conserved Plasmodium protein, unknown function	408.42	−2.01	1.59×10^{-4}	2.17×10^{-3}
PfIT_140067000	inner membrane complex sub-compartment protein 3	161.39	−2.28	1.60×10^{-4}	2.18×10^{-3}
PfIT_050023100	zinc finger protein, putative	286.40	−1.96	1.64×10^{-4}	2.23×10^{-3}
PfIT_060009600	nucleoside diphosphate kinase, putative	139.10	−1.69	1.65×10^{-4}	2.23×10^{-3}
PfIT_100007800	inner membrane complex protein 1c, putative	3296.47	−2.05	1.66×10^{-4}	2.24×10^{-3}
PfIT_140042000	conserved Plasmodium protein, unknown function	1284.60	−2.34	1.67×10^{-4}	2.25×10^{-3}
PfIT_100038400	conserved Plasmodium protein, unknown function	305.92	−1.34	1.69×10^{-4}	2.27×10^{-3}
PfIT_110016900	conserved protein, unknown function	145.80	1.44	1.70×10^{-4}	2.27×10^{-3}
PfIT_070032500	zinc finger, C3HC4 type, putative	849.51	−1.76	1.70×10^{-4}	2.27×10^{-3}
PfIT_130040400	merozoite surface protein 7	3631.33	−2.10	1.70×10^{-4}	2.27×10^{-3}
PfIT_090020900	conserved Plasmodium protein, unknown function	41.20	−2.58	1.71×10^{-4}	2.28×10^{-3}
PfIT_030008000	HAD superfamily protein, putative	2343.13	−1.86	1.74×10^{-4}	2.31×10^{-3}
PfIT_130036900	protein tyrosine phosphatase-like protein, putative	117.43	−1.94	1.78×10^{-4}	2.36×10^{-3}
PfIT_020022000	calcium-dependent protein kinase 1	637.93	−2.42	1.79×10^{-4}	2.36×10^{-3}
PfIT_050010100	conserved Plasmodium protein, unknown function	705.74	−1.48	1.80×10^{-4}	2.36×10^{-3}
PfIT_110051100	sporozoite asparagine-rich protein	36.97	−2.92	1.80×10^{-4}	2.36×10^{-3}
PfIT_090031000	conserved Plasmodium protein, unknown function	407.15	−1.84	1.82×10^{-4}	2.39×10^{-3}
PfIT_090013300	conserved Plasmodium protein, unknown function	795.42	−2.25	1.83×10^{-4}	2.39×10^{-3}

Pf_ID	Transcript Product Description	base mean	$\log_2$ FC	p_{value}	p_{adj}
PfIT_140022800	metacaspase-like protein	591.15	−2.24	1.84×10^{-4}	2.40×10^{-3}
PfIT_050031000	inner membrane complex protein 1g, putative	1865.79	−2.12	1.85×10^{-4}	2.41×10^{-3}
PfIT_120053000	dipeptidyl aminopeptidase 2	140.53	−2.15	1.86×10^{-4}	2.41×10^{-3}
PfIT_020022400	conserved Plasmodium protein, unknown function	414.99	−1.36	1.86×10^{-4}	2.41×10^{-3}
PfIT_130047100	inner membrane complex protein 1k, putative	115.08	−2.52	1.87×10^{-4}	2.42×10^{-3}
PfIT_130026400	conserved Plasmodium protein, unknown function	957.13	−2.43	1.88×10^{-4}	2.42×10^{-3}
PfIT_120037500	CG2-related protein, putative	1441.01	−2.25	1.88×10^{-4}	2.42×10^{-3}
PfIT_040009600	6-cysteine protein	687.53	−2.08	1.88×10^{-4}	2.42×10^{-3}
PfIT_010009100	conserved Plasmodium protein, unknown function	887.05	−1.92	1.90×10^{-4}	2.44×10^{-3}
PfIT_100015000	inner membrane complex sub-compartment protein 1	111.61	−1.66	1.92×10^{-4}	2.45×10^{-3}
PfIT_080022800	conserved Plasmodium protein, unknown function	72.10	−1.91	1.93×10^{-4}	2.46×10^{-3}
PfIT_110007000	Plasmodium exported protein (PHISTb), unknown function	184.96	1.66	1.94×10^{-4}	2.46×10^{-3}
PfIT_110019200	conserved Plasmodium protein, unknown function	299.96	−2.08	1.96×10^{-4}	2.49×10^{-3}
PfIT_050036200	conserved Plasmodium protein, unknown function	311.39	−2.22	2.01×10^{-4}	2.53×10^{-3}
PfIT_080007200	conserved Plasmodium protein, unknown function	4569.97	1.43	2.02×10^{-4}	2.53×10^{-3}
PfIT_050015200	conserved Plasmodium protein, unknown function	85.49	−1.96	2.02×10^{-4}	2.53×10^{-3}
PfIT_030016600	conserved protein, unknown function	238.35	−1.72	2.02×10^{-4}	2.53×10^{-3}
PfIT_100035300	OTU-like cysteine protease, putative	913.44	−2.27	2.02×10^{-4}	2.53×10^{-3}
PfIT_110019900	peptidyl-prolyl cis-trans isomerase	625.56	−1.13	2.03×10^{-4}	2.53×10^{-3}
PfIT_130009100	chromosome condensation protein, putative	323.35	−1.64	2.06×10^{-4}	2.57×10^{-3}
PfIT_040013200	sporozoite invasion-associated protein 1	68.75	−2.24	2.09×10^{-4}	2.58×10^{-3}
PfIT_090036800	conserved Plasmodium protein, unknown function	512.10	−2.17	2.09×10^{-4}	2.58×10^{-3}

Pf_ID	Transcript Product Description	base mean	$\log_2$ FC	p_{value}	p_{adj}
PfIT_110034300	conserved Plasmodium protein, unknown function	193.51	1.45	2.09×10^{-4}	2.58×10^{-3}
PfIT_140083300	Plasmodium exported protein (hyp15), unknown function	49.98	7.20	2.09×10^{-4}	2.58×10^{-3}
PfIT_030008900	inner membrane complex protein 1e, putative	460.33	−2.12	2.09×10^{-4}	2.58×10^{-3}
PfIT_120058400	Plasmodium exported protein (PHISTa), unknown function	342.34	1.53	2.09×10^{-4}	2.58×10^{-3}
PfIT_060024200	merozoite surface protein 10	209.49	−2.11	2.12×10^{-4}	2.60×10^{-3}
PfIT_110049400	serine/threonine protein kinase, putative	2566.67	−2.58	2.12×10^{-4}	2.60×10^{-3}
PfIT_090023900	protein disulfide isomerase	255.86	−1.78	2.13×10^{-4}	2.61×10^{-3}
PfIT_120052900	conserved Plasmodium protein, unknown function	114.65	−2.20	2.15×10^{-4}	2.62×10^{-3}
PfIT_080008100	serine/threonine protein phosphatase 2B catalytic subunit A	809.94	−2.21	2.16×10^{-4}	2.63×10^{-3}
PfIT_140054900	conserved Plasmodium protein, unknown function	1814.98	−1.53	2.17×10^{-4}	2.63×10^{-3}
PfIT_070027500	conserved Plasmodium protein, unknown function	520.63	−2.15	2.17×10^{-4}	2.63×10^{-3}
PfIT_010008600	cyclase-associated protein	434.15	−2.21	2.23×10^{-4}	2.69×10^{-3}
PfIT_080011300	conserved Plasmodium membrane protein, unknown function	131.11	−2.43	2.23×10^{-4}	2.69×10^{-3}
PfIT_140056900	conserved Plasmodium protein, unknown function	115.68	−1.97	2.24×10^{-4}	2.69×10^{-3}
PfIT_140064700	conserved Plasmodium protein, unknown function	505.21	−2.06	2.24×10^{-4}	2.69×10^{-3}
PfIT_130068200	conserved Plasmodium protein, unknown function	45.81	−2.09	2.26×10^{-4}	2.71×10^{-3}
PfIT_120040500	serine hydroxymethyltransferase	436.26	−1.45	2.29×10^{-4}	2.73×10^{-3}
PfIT_060018900	conserved Plasmodium membrane protein, unknown function	385.94	−1.94	2.32×10^{-4}	2.77×10^{-3}
PfIT_120048800	vacuolar-sorting protein SNF7, putative	143.98	−2.26	2.33×10^{-4}	2.78×10^{-3}
PfIT_130023700	chromosome segregation protein, putative	876.55	−1.54	2.34×10^{-4}	2.78×10^{-3}
PfIT_140077400	inorganic anion exchanger, inorganic anion antiporter	649.87	−1.32	2.35×10^{-4}	2.79×10^{-3}
PfIT_050008800	actin-depolymerizing factor 1	1617.99	−1.88	2.36×10^{-4}	2.79×10^{-3}

Pf_ID	Transcript Product Description	base mean	$\log_2$ FC	p_{value}	p_{adj}
PfIT_050013200	6-cysteine protein	552.62	−2.31	2.36×10^{-4}	2.79×10^{-3}
PfIT_110041200	conserved Plasmodium protein, unknown function	338.23	−1.93	2.37×10^{-4}	2.79×10^{-3}
PfIT_100024000	autophagy-related protein 8	154.33	−1.87	2.38×10^{-4}	2.79×10^{-3}
PfIT_080015200	protein phosphatase PPM5, putative	2566.28	−2.09	2.39×10^{-4}	2.80×10^{-3}
PfIT_080030200	translation initiation factor IF-3	36.73	−2.06	2.40×10^{-4}	2.81×10^{-3}
PfIT_140064900	spindle assembly abnormal protein 4, putative	391.43	−1.46	2.41×10^{-4}	2.81×10^{-3}
PfIT_100011300	rhoGAP GTPase, putative	489.77	−2.33	2.44×10^{-4}	2.85×10^{-3}
PfIT_050036000	formin 1	288.98	−2.15	2.48×10^{-4}	2.88×10^{-3}
PfIT_100039800	probable protein, unknown function	3268.02	−2.38	2.48×10^{-4}	2.88×10^{-3}
PfIT_140042600	conserved Plasmodium protein, unknown function	1141.69	−2.35	2.49×10^{-4}	2.88×10^{-3}
PfIT_110028100	structural maintenance of chromosomes protein 5, putative	204.84	−1.85	2.51×10^{-4}	2.90×10^{-3}
PfIT_120009000	transporter, putative	493.44	−1.46	2.52×10^{-4}	2.90×10^{-3}
PfIT_130027900	conserved Plasmodium protein, unknown function	101.11	−2.54	2.55×10^{-4}	2.92×10^{-3}
PfIT_130031200	conserved Plasmodium protein, unknown function	526.46	−1.89	2.55×10^{-4}	2.92×10^{-3}
PfIT_110012700	conserved Plasmodium protein, unknown function	484.27	−2.14	2.55×10^{-4}	2.92×10^{-3}
PfIT_120033800	conserved Plasmodium protein, unknown function	362.35	−1.84	2.56×10^{-4}	2.93×10^{-3}
PfIT_110040700	conserved Plasmodium protein, unknown function	829.72	−2.33	2.57×10^{-4}	2.93×10^{-3}
PfIT_140039100	protein-L-isoaspartate(D-aspartate) O-methyltransferase, putative	102.44	−1.51	2.59×10^{-4}	2.95×10^{-3}
PfIT_090021900	conserved Plasmodium membrane protein, unknown function	132.71	−2.29	2.62×10^{-4}	2.97×10^{-3}
PfIT_130015300	conserved Plasmodium protein, unknown function	109.54	−2.44	2.63×10^{-4}	2.98×10^{-3}
PfIT_140015900	DNA damage-inducible protein 1, putative	333.17	−1.97	2.64×10^{-4}	2.98×10^{-3}
PfIT_110033400	conserved Plasmodium protein, unknown function	570.17	−2.28	2.66×10^{-4}	3.00×10^{-3}
PfIT_110040500	conserved Plasmodium protein, unknown function	715.28	−1.67	2.75×10^{-4}	3.10×10^{-3}

Pf_ID	Transcript Product Description	base mean	$\log_2$ FC	p_{value}	p_{adj}
PfIT_090012300	conserved Plasmodium protein, unknown function	272.35	−2.17	2.76×10^{-4}	3.10×10^{-3}
PfIT_130046800	inner membrane complex suture component, putative	147.61	−1.92	2.76×10^{-4}	3.10×10^{-3}
PfIT_050031400	ADP-ribosylation factor GTPase-activating protein, putative	348.12	−1.67	2.79×10^{-4}	3.12×10^{-3}
PfIT_110020400	serine esterase, putative	2114.78	−2.22	2.80×10^{-4}	3.12×10^{-3}
PfIT_060015600	conserved Plasmodium protein, unknown function	504.76	−2.17	2.80×10^{-4}	3.12×10^{-3}
PfIT_100021300	enoyl-CoA hydratase-related protein, putative	52.24	−1.98	2.80×10^{-4}	3.12×10^{-3}
PfIT_140046100	conserved Plasmodium protein, unknown function	97.04	−2.01	2.81×10^{-4}	3.12×10^{-3}
PfIT_070012100	conserved Plasmodium protein, unknown function	393.51	−1.82	2.81×10^{-4}	3.12×10^{-3}
PfIT_050009900	2-oxoisovalerate dehydrogenase subunit beta, mitochondrial, putative	191.91	−1.57	2.86×10^{-4}	3.16×10^{-3}
PfIT_010008300	novel putative transporter 1	315.43	−1.95	2.91×10^{-4}	3.21×10^{-3}
PfIT_130049100	conserved Plasmodium protein, unknown function	952.05	−2.22	2.92×10^{-4}	3.22×10^{-3}
PfIT_120026400	conserved Plasmodium protein, unknown function	436.59	−1.69	2.98×10^{-4}	3.27×10^{-3}
PfIT_090025000	ADP-ribosylation factor, putative	597.62	−2.29	2.99×10^{-4}	3.28×10^{-3}
PfIT_020012600	serine repeat antigen 7	101.33	−2.11	3.01×10^{-4}	3.29×10^{-3}
PfIT_060023500	conserved Plasmodium protein, unknown function	178.53	−1.99	3.02×10^{-4}	3.29×10^{-3}
PfIT_140073000	large ribosomal subunit assembling protein, putative	352.64	1.21	3.02×10^{-4}	3.29×10^{-3}
PfIT_110031200	autophagy-related protein 23, putative	4542.12	−2.27	3.03×10^{-4}	3.29×10^{-3}
PfIT_060022700	phosphatidylinositol N-acetylglucosaminyltransferase subunit GPI1	142.55	−1.84	3.04×10^{-4}	3.29×10^{-3}
PfIT_130053900	conserved Plasmodium protein, unknown function	212.37	−2.42	3.08×10^{-4}	3.34×10^{-3}
PfIT_110005700	rifin	19.80	3.08	3.11×10^{-4}	3.36×10^{-3}
PfIT_010012100	photosensitized INA-labeled protein PHIL1, putative	1868.77	−2.28	3.12×10^{-4}	3.36×10^{-3}

Pf_ID	Transcript Product Description	base mean	$\log_2$ FC	p_{value}	p_{adj}
PfIT_040027800	conserved Plasmodium protein, unknown function	882.36	−2.36	3.14×10^{-4}	3.38×10^{-3}
PfIT_050034900	conserved Plasmodium protein, unknown function	892.20	−1.49	3.18×10^{-4}	3.41×10^{-3}
PfIT_120032700	cyclin related protein, putative	713.17	−1.58	3.18×10^{-4}	3.41×10^{-3}
PfIT_090019600	type II NADH:ubiquinone oxidoreductase	273.41	−1.85	3.19×10^{-4}	3.42×10^{-3}
PfIT_040019000	conserved protein, unknown function	255.68	−1.82	3.22×10^{-4}	3.44×10^{-3}
PfIT_130077600	stevor	13.95	4.42	3.25×10^{-4}	3.47×10^{-3}
PfIT_130036600	signal peptidase 21 kDa subunit	172.17	−1.69	3.26×10^{-4}	3.47×10^{-3}
PfIT_080015800	conserved Plasmodium protein, unknown function	167.22	−2.24	3.32×10^{-4}	3.51×10^{-3}
PfIT_080021300	conserved Plasmodium protein, unknown function	74.12	1.65	3.32×10^{-4}	3.51×10^{-3}
PfIT_080026000	conserved Plasmodium protein, unknown function	299.24	−1.76	3.32×10^{-4}	3.51×10^{-3}
PfIT_070006200	rifin	8.90	5.74	3.34×10^{-4}	3.53×10^{-3}
PfIT_120056400	coronin	4751.68	−2.17	3.35×10^{-4}	3.53×10^{-3}
PfIT_020014300	transporter, putative	466.01	−2.10	3.36×10^{-4}	3.54×10^{-3}
PfIT_060020100	kinetochore protein NDC80, putative	409.80	−1.60	3.39×10^{-4}	3.56×10^{-3}
PfIT_020022600	conserved Plasmodium membrane protein, unknown function	42.47	−2.42	3.41×10^{-4}	3.57×10^{-3}
PfIT_100018000	GDP-L-fucose synthase	61.67	−1.97	3.43×10^{-4}	3.58×10^{-3}
PfIT_070034400	conserved Plasmodium protein, unknown function	1235.52	−1.77	3.48×10^{-4}	3.63×10^{-3}
PfIT_140037800	conserved Plasmodium protein, unknown function	1820.73	−2.30	3.49×10^{-4}	3.63×10^{-3}
PfIT_100007200	conserved Plasmodium protein, unknown function	490.02	−2.31	3.53×10^{-4}	3.66×10^{-3}
PfIT_030021100	inorganic pyrophosphatase, putative	645.33	−1.53	3.56×10^{-4}	3.69×10^{-3}
PfIT_120054700	cutA, putative	89.32	−1.73	3.57×10^{-4}	3.70×10^{-3}
PfIT_130062200	serine/threonine protein kinase, putative	2019.04	−2.67	3.62×10^{-4}	3.73×10^{-3}
PfIT_010009900	conserved Plasmodium protein, unknown function	108.45	−1.94	3.62×10^{-4}	3.73×10^{-3}
PfIT_060018700	conserved Plasmodium protein, unknown function	288.19	−2.47	3.62×10^{-4}	3.73×10^{-3}
PfIT_050019200	ATP-dependent DNA helicase UvrD	217.75	−1.44	3.63×10^{-4}	3.73×10^{-3}

Pf_ID	Transcript Product Description	base mean	$\log_2$ FC	p_{value}	p_{adj}
PfIT_100023200	conserved Plasmodium protein, unknown function	769.68	−2.41	3.66×10^{-4}	3.76×10^{-3}
PfIT_050006900	rhoptry-associated protein 3	923.36	−2.47	3.67×10^{-4}	3.76×10^{-3}
PfIT_030013600	conserved protein, unknown function	111.16	−1.81	3.68×10^{-4}	3.76×10^{-3}
PfIT_130011100	conserved Plasmodium protein, unknown function	126.77	−2.49	3.68×10^{-4}	3.76×10^{-3}
PfIT_030022000	cdc2-related protein kinase 4	1698.92	−1.80	3.69×10^{-4}	3.76×10^{-3}
PfIT_110035100	conserved Plasmodium protein, unknown function	239.71	−1.71	3.73×10^{-4}	3.79×10^{-3}
PfIT_140020600	26S proteasome regulatory subunit RPN13, putative	322.40	−1.29	3.74×10^{-4}	3.79×10^{-3}
PfIT_090034200	G2 protein, putative	74.59	−1.92	3.75×10^{-4}	3.80×10^{-3}
PfIT_100023700	conserved Plasmodium protein, unknown function	273.38	−1.94	3.78×10^{-4}	3.82×10^{-3}
PfIT_090040200	Plasmodium exported protein, unknown function	314.87	−1.48	3.79×10^{-4}	3.82×10^{-3}
PfIT_140018600	p1/s1 nuclease, putative	161.83	−1.97	3.79×10^{-4}	3.82×10^{-3}
PfIT_070006900	Plasmodium exported protein (hyp12), unknown function	825.62	1.69	3.80×10^{-4}	3.82×10^{-3}
PfIT_120012400	conserved Plasmodium protein, unknown function	1865.08	−1.63	3.82×10^{-4}	3.83×10^{-3}
PfIT_140026900	tetratricopeptide repeat family protein, putative	334.46	−2.04	3.83×10^{-4}	3.83×10^{-3}
PfIT_140047700	serine/threonine protein kinase, putative	288.96	−2.01	3.87×10^{-4}	3.87×10^{-3}
PfIT_040023700	conserved Plasmodium protein, unknown function	209.74	−1.54	3.96×10^{-4}	3.95×10^{-3}
PfIT_140067800	conserved Plasmodium protein, unknown function	385.23	−1.64	3.99×10^{-4}	3.97×10^{-3}
PfIT_020016400	conserved Plasmodium protein, unknown function	162.82	−1.55	4.00×10^{-4}	3.98×10^{-3}
PfIT_070019600	calcium/calmodulin-dependent protein kinase, putative	60.33	−2.03	4.02×10^{-4}	3.98×10^{-3}
PfIT_140046600	conserved Plasmodium protein, unknown function	566.81	−1.78	4.05×10^{-4}	4.01×10^{-3}
PfIT_120049200	double C2-like domain-containing protein	793.88	−1.88	4.06×10^{-4}	4.01×10^{-3}
PfIT_060024500	DnaJ protein, putative	80.44	−1.79	4.07×10^{-4}	4.02×10^{-3}

Pf_ID	Transcript Product Description	base mean	$\log_2$ FC	p_{value}	p_{adj}
PfIT_050020600	conserved Plasmodium protein, unknown function	719.06	−2.38	4.08×10^{-4}	4.02×10^{-3}
PfIT_110050500	conserved Plasmodium protein, unknown function	39.84	−2.19	4.09×10^{-4}	4.02×10^{-3}
PfIT_080033500	folate transporter 1	145.87	−2.01	4.10×10^{-4}	4.02×10^{-3}
PfIT_040028300	cysteine-rich protective antigen	1502.53	−2.18	4.10×10^{-4}	4.02×10^{-3}
PfIT_060017600	conserved Plasmodium protein, unknown function	612.51	−2.10	4.14×10^{-4}	4.05×10^{-3}
PfIT_140041600	conserved Plasmodium protein, unknown function	312.92	−2.49	4.17×10^{-4}	4.07×10^{-3}
PfIT_050014100	conserved Plasmodium protein, unknown function	2661.01	−2.08	4.20×10^{-4}	4.09×10^{-3}
PfIT_110028900	ethanolamine kinase	733.12	−1.60	4.22×10^{-4}	4.10×10^{-3}
PfIT_040029300	Plasmodium exported protein (PHISTa), unknown function	2169.96	1.23	4.23×10^{-4}	4.11×10^{-3}
PfIT_130039900	MSP7-like protein	52.45	−2.12	4.26×10^{-4}	4.12×10^{-3}
PfIT_030008200	palmitoyltransferase	141.68	−2.34	4.26×10^{-4}	4.12×10^{-3}
PfIT_120027700	transcription factor with AP2 domain(s)	53.36	1.88	4.28×10^{-4}	4.13×10^{-3}
PfIT_090041400	lysophospholipase, putative	202.27	1.33	4.31×10^{-4}	4.15×10^{-3}
PfIT_010012200	LCCL domain-containing protein	394.46	−2.65	4.38×10^{-4}	4.21×10^{-3}
PfIT_130037400	conserved Plasmodium membrane protein, unknown function	205.43	−2.23	4.39×10^{-4}	4.21×10^{-3}
PfIT_090013000	conserved Plasmodium protein, unknown function	275.66	−1.99	4.40×10^{-4}	4.22×10^{-3}
PfIT_090031800	fumarate hydratase, putative	290.88	−1.91	4.41×10^{-4}	4.22×10^{-3}
PfIT_110047400	DnaJ protein, putative	201.33	−2.04	4.44×10^{-4}	4.24×10^{-3}
PfIT_100018100	conserved Plasmodium protein, unknown function	1322.77	−2.24	4.45×10^{-4}	4.24×10^{-3}
PfIT_120034800	myosin D	1949.58	−2.19	4.46×10^{-4}	4.25×10^{-3}
PfIT_080026500	ribosomal RNA small subunit methyltransferase NEP1, putative	255.93	1.16	4.48×10^{-4}	4.26×10^{-3}
PfIT_140020000	30S ribosomal protein S9, putative	162.44	−1.66	4.50×10^{-4}	4.27×10^{-3}
PfIT_110044200	carbonic anhydrase	30.01	−2.45	4.52×10^{-4}	4.28×10^{-3}
PfIT_120005500	PfEMP1	348.90	1.47	4.60×10^{-4}	4.35×10^{-3}
PfIT_030012900	conserved Plasmodium protein, unknown function	799.00	−2.21	4.62×10^{-4}	4.35×10^{-3}
PfIT_130050900	inner membrane complex protein	495.14	−1.95	4.63×10^{-4}	4.36×10^{-3}

Pf_ID	Transcript Product Description	base mean	$\log_2$ FC	p_{value}	p_{adj}
PfIT_140024000	Cyclic nucleotide-binding domain containing protein, putative	1147.73	−2.25	4.64×10^{-4}	4.36×10^{-3}
PfIT_030025500	signal peptidase complex subunit 2, putative	296.99	−1.58	4.68×10^{-4}	4.40×10^{-3}
PfIT_100008800	conserved Plasmodium membrane protein, unknown function	374.20	−1.60	4.76×10^{-4}	4.46×10^{-3}
PfIT_020012500	serine repeat antigen 7	460.83	−1.98	4.80×10^{-4}	4.48×10^{-3}
PfIT_060020500	conserved Plasmodium protein, unknown function	213.16	−1.42	4.80×10^{-4}	4.48×10^{-3}
PfIT_070033600	conserved Plasmodium protein, unknown function	29.33	−2.64	4.81×10^{-4}	4.48×10^{-3}
PfIT_140043700	conserved Plasmodium protein, unknown function	292.02	−2.48	4.82×10^{-4}	4.48×10^{-3}
PfIT_090014200	subpellicular microtubule protein 1, putative	113.60	−2.09	4.84×10^{-4}	4.50×10^{-3}
PfIT_130049600	conserved protein, unknown function	661.75	−1.81	4.85×10^{-4}	4.50×10^{-3}
PfIT_090008300	conserved Plasmodium protein, unknown function	2989.75	−2.29	4.94×10^{-4}	4.56×10^{-3}
PfIT_120051600	myosin A tail domain interacting protein	2221.07	−2.10	4.94×10^{-4}	4.56×10^{-3}
PfIT_100039500	merozoite surface protein	356.76	−2.13	4.97×10^{-4}	4.59×10^{-3}
PfIT_130056900	glycerol kinase	325.14	−2.22	5.00×10^{-4}	4.59×10^{-3}
PfIT_100039900	merozoite surface protein	623.64	−2.11	5.00×10^{-4}	4.59×10^{-3}
PfIT_090035900	selenoprotein	37.17	1.73	5.02×10^{-4}	4.60×10^{-3}
PfIT_100016200	conserved Plasmodium protein, unknown function	1293.99	−2.32	5.03×10^{-4}	4.60×10^{-3}
PfIT_130005300	PfEMP1	56.65	1.47	5.03×10^{-4}	4.60×10^{-3}
PfIT_090029100	conserved Plasmodium protein, unknown function	439.82	−1.93	5.06×10^{-4}	4.60×10^{-3}
PfIT_090032100	conserved Plasmodium protein, unknown function	767.76	−1.66	5.06×10^{-4}	4.60×10^{-3}
PfIT_070020100	drug/metabolite exporter, drug/metabolite transporter	148.30	−1.27	5.06×10^{-4}	4.60×10^{-3}
PfIT_100013700	tubulin–tyrosine ligase, putative	518.28	−2.30	5.07×10^{-4}	4.61×10^{-3}
PfIT_110033800	conserved Plasmodium protein, unknown function	629.52	−2.54	5.10×10^{-4}	4.61×10^{-3}
PfIT_140077700	conserved Plasmodium membrane protein, unknown function	122.61	−1.85	5.11×10^{-4}	4.61×10^{-3}

Pf_ID	Transcript Product Description	base mean	$\log_2$ FC	p_{value}	p_{adj}
PfIT_130060600	RAP protein, putative	27.75	1.91	5.11×10^{-4}	4.61×10^{-3}
PfIT_100040200	probable protein, unknown function	1968.26	−2.21	5.11×10^{-4}	4.61×10^{-3}
PfIT_070020200	zinc transporter, putative	243.58	−1.51	5.12×10^{-4}	4.61×10^{-3}
PfIT_110032000	protein disulfide isomerase, putative	153.61	−1.88	5.21×10^{-4}	4.69×10^{-3}
PfIT_070009400	serine/threonine protein kinase, putative	1375.71	−2.08	5.24×10^{-4}	4.71×10^{-3}
PfIT_100026200	conserved Plasmodium protein, unknown function	472.29	1.19	5.26×10^{-4}	4.71×10^{-3}
PfIT_080007900	adenylyl cyclase beta	1326.26	−1.96	5.27×10^{-4}	4.71×10^{-3}
PfIT_060027900	conserved Plasmodium protein, unknown function	81.94	−1.44	5.28×10^{-4}	4.72×10^{-3}
PfIT_060016700	6-cysteine protein	702.73	−2.00	5.33×10^{-4}	4.75×10^{-3}
PfIT_120014900	cGMP-specific phosphodiesterase	164.72	−2.58	5.36×10^{-4}	4.76×10^{-3}
PfIT_030013500	conserved Plasmodium protein, unknown function	412.67	−1.94	5.37×10^{-4}	4.76×10^{-3}
PfIT_080020800	vacuolar protein sorting-associated protein 9, putative	2813.61	−1.72	5.37×10^{-4}	4.76×10^{-3}
PfIT_140047300	conserved Plasmodium protein, unknown function	147.22	−2.43	5.37×10^{-4}	4.76×10^{-3}
PfIT_090018700	conserved Plasmodium protein, unknown function	2233.19	−2.20	5.41×10^{-4}	4.79×10^{-3}
PfIT_070011000	conserved Plasmodium protein, unknown function	218.95	−1.48	5.43×10^{-4}	4.80×10^{-3}
PfIT_020013200	acyl carrier protein	52.28	−1.64	5.45×10^{-4}	4.81×10^{-3}
PfIT_130045000	conserved Plasmodium protein, unknown function	1167.12	−1.60	5.50×10^{-4}	4.84×10^{-3}
PfIT_070022400	exported serine/threonine protein kinase	313.51	−1.56	5.50×10^{-4}	4.84×10^{-3}
PfIT_030028200	Rh5 interacting protein	2433.99	−2.31	5.51×10^{-4}	4.84×10^{-3}
PfIT_030015800	conserved Plasmodium protein, unknown function	17.30	−3.10	5.52×10^{-4}	4.84×10^{-3}
PfIT_120008900	conserved Plasmodium protein, unknown function	131.68	−1.40	5.54×10^{-4}	4.85×10^{-3}
PfIT_110027500	leucine-rich repeat protein	138.12	−1.61	5.56×10^{-4}	4.86×10^{-3}
PfIT_070029600	conserved Plasmodium protein, unknown function	1121.75	−2.22	5.57×10^{-4}	4.86×10^{-3}
PfIT_130029400	conserved Plasmodium membrane protein, unknown function	130.82	−1.64	5.62×10^{-4}	4.89×10^{-3}

Pf_ID	Transcript Product Description	base mean	$\log_2$ FC	p_{value}	p_{adj}
PfIT_130047900	myosin A	7734.04	−2.19	5.68×10^{-4}	4.93×10^{-3}
PfIT_110008800	conserved Plasmodium protein, unknown function	206.97	−1.21	5.68×10^{-4}	4.93×10^{-3}
PfIT_120054600	conserved Plasmodium protein, unknown function	86.29	−1.91	5.72×10^{-4}	4.95×10^{-3}
PfIT_010006600	vacuolar protein sorting-associated protein 51, putative	85.09	−1.69	5.76×10^{-4}	4.97×10^{-3}
PfIT_080016500	conserved Plasmodium protein, unknown function	358.94	−1.95	5.77×10^{-4}	4.97×10^{-3}
PfIT_100039400	merozoite surface protein 6	5903.65	−2.05	5.77×10^{-4}	4.97×10^{-3}
PfIT_120014700	zinc finger transcription factor, putative	1265.25	−1.56	5.78×10^{-4}	4.97×10^{-3}
PfIT_140036600	plasmepsin IX	496.33	−2.06	5.78×10^{-4}	4.97×10^{-3}
PfIT_100011400	RING zinc finger protein, putative	327.82	−2.62	5.82×10^{-4}	4.99×10^{-3}
PfIT_110026200	serine/threonine protein kinase, putative	49.69	−2.23	5.87×10^{-4}	5.03×10^{-3}
PfIT_130037900	apurinic/apyrimidinic endonuclease Apn1, putative	420.14	−1.43	5.89×10^{-4}	5.03×10^{-3}
PfIT_100021200	rhoptry neck protein 12	430.47	−2.22	5.90×10^{-4}	5.03×10^{-3}
PfIT_110017000	DNA helicase, putative	74.01	−1.38	5.91×10^{-4}	5.03×10^{-3}
PfIT_120028100	conserved Plasmodium protein, unknown function	111.54	−2.10	5.91×10^{-4}	5.03×10^{-3}
PfIT_100023300	conserved Plasmodium protein, unknown function	36.00	−2.54	5.92×10^{-4}	5.03×10^{-3}
PfIT_130012700	DNA-directed RNA polymerase alpha chain, putative	515.24	−1.05	5.93×10^{-4}	5.03×10^{-3}
PfIT_070009200	conserved Plasmodium membrane protein, unknown function	2492.62	−1.55	5.94×10^{-4}	5.03×10^{-3}
PfIT_130051200	kinetochore protein SPC25, putative	167.09	−1.18	5.97×10^{-4}	5.05×10^{-3}
PfIT_100032700	merozoite TRAP-like protein	1785.36	−1.89	6.02×10^{-4}	5.08×10^{-3}
PfIT_100007600	conserved Plasmodium protein, unknown function	645.93	−2.25	6.02×10^{-4}	5.08×10^{-3}
PfIT_140015700	aldo-keto reductase, putative	881.31	−1.21	6.08×10^{-4}	5.12×10^{-3}
PfIT_130023200	small ribosomal subunit nuclear export protein, putative	971.95	1.17	6.13×10^{-4}	5.15×10^{-3}
PfIT_020020400	palmitoyltransferase, putative	19.04	−2.93	6.14×10^{-4}	5.15×10^{-3}
PfIT_030026500	microtubule and actin binding protein, putative	505.12	−1.92	6.16×10^{-4}	5.16×10^{-3}

Pf_ID	Transcript Product Description	base mean	$\log_2$ FC	p_{value}	p_{adj}
PfIT_020007700	palmitoyltransferase, putative	36.64	−1.69	6.20×10^{-4}	5.19×10^{-3}
PfIT_120011500	IMP-specific 5'-nucleotidase, putative	110.65	−2.12	6.23×10^{-4}	5.21×10^{-3}
PfIT_140079600	conserved Plasmodium protein, unknown function	567.42	−2.15	6.26×10^{-4}	5.22×10^{-3}
PfIT_050009700	ATP-dependent helicase, putative	167.30	−1.47	6.28×10^{-4}	5.23×10^{-3}
PfIT_040023000	regulator of chromosome condensation, putative	1224.15	−1.92	6.30×10^{-4}	5.24×10^{-3}
PfIT_130011300	conserved Plasmodium protein, unknown function	60.33	−1.51	6.32×10^{-4}	5.24×10^{-3}
PfIT_130032700	conserved Plasmodium protein, unknown function	330.76	−1.90	6.34×10^{-4}	5.26×10^{-3}
PfIT_120032400	conserved Plasmodium protein, unknown function	123.40	−2.10	6.41×10^{-4}	5.30×10^{-3}
PfIT_140032900	ABC transporter G family member 2	35.58	−2.15	6.43×10^{-4}	5.31×10^{-3}
PfIT_090022000	conserved Plasmodium protein, unknown function	286.49	−2.29	6.49×10^{-4}	5.36×10^{-3}
PfIT_060019300	GPI-anchored wall transfer protein 1, putative	97.98	−1.41	6.51×10^{-4}	5.36×10^{-3}
PfIT_100025100	conserved Plasmodium protein, unknown function	171.81	−1.56	6.52×10^{-4}	5.37×10^{-3}
PfIT_060018100	conserved Plasmodium protein, unknown function	267.24	−1.90	6.55×10^{-4}	5.38×10^{-3}
PfIT_120049000	ubiquitin-conjugating enzyme E2, putative	2403.06	−2.23	6.58×10^{-4}	5.40×10^{-3}
PfIT_070023700	LEM3/CDC50 family protein, putative	301.11	−1.49	6.59×10^{-4}	5.40×10^{-3}
PfIT_120029300	BRO1 domain-containing protein, putative	207.50	−2.41	6.62×10^{-4}	5.41×10^{-3}
PfIT_050022000	transcription factor with AP2 domain(s)	737.52	−1.79	6.67×10^{-4}	5.45×10^{-3}
PfIT_130015900	RNA-binding protein, putative	3408.93	−2.02	6.69×10^{-4}	5.46×10^{-3}
PfIT_090034800	leucine-rich repeat protein	465.07	−2.72	6.72×10^{-4}	5.47×10^{-3}
PfIT_120059200	stevor	8.72	4.85	6.78×10^{-4}	5.51×10^{-3}
PfIT_100029900	conserved Plasmodium protein, unknown function	29.91	−2.36	6.78×10^{-4}	5.51×10^{-3}
PfIT_100021600	conserved Plasmodium protein, unknown function	1278.30	−2.20	6.87×10^{-4}	5.56×10^{-3}

Pf_ID	Transcript Product Description	base mean	$\log_2$ FC	p_{value}	p_{adj}
PfIT_140083800	Plasmodium exported protein (PHISTa), unknown function	14.10	2.55	6.87×10^{-4}	5.56×10^{-3}
PfIT_070023600	conserved Plasmodium protein, unknown function	667.13	−1.67	6.99×10^{-4}	5.64×10^{-3}
PfIT_090025200	conserved Plasmodium protein, unknown function	725.83	−1.99	6.99×10^{-4}	5.64×10^{-3}
PfIT_040011900	transcription factor, putative	395.82	1.08	7.11×10^{-4}	5.73×10^{-3}
PfIT_010008700	conserved Plasmodium protein, unknown function	193.21	−1.92	7.12×10^{-4}	5.73×10^{-3}
PfIT_100032900	inner membrane complex protein 1m, putative	207.81	−2.27	7.14×10^{-4}	5.73×10^{-3}
PfIT_050015600	conserved Plasmodium protein, unknown function	120.46	1.66	7.17×10^{-4}	5.75×10^{-3}
PfIT_030015700	conserved Plasmodium protein, unknown function	57.61	−1.60	7.18×10^{-4}	5.75×10^{-3}
PfIT_040008300	conserved Plasmodium protein, unknown function	65.01	−2.22	7.19×10^{-4}	5.75×10^{-3}
PfIT_060028300	anaphase-promoting complex subunit 11, putative	124.99	−1.61	7.26×10^{-4}	5.80×10^{-3}
PfIT_020017100	secreted protein with altered thrombospondin repeat domain	924.67	−1.97	7.27×10^{-4}	5.80×10^{-3}
PfIT_130031800	conserved Plasmodium protein, unknown function	108.95	−1.27	7.30×10^{-4}	5.81×10^{-3}
PfIT_120044600	ATP-dependent zinc metalloprotease FTSH 1	770.05	−1.05	7.37×10^{-4}	5.85×10^{-3}
PfIT_020011800	conserved Plasmodium protein, unknown function	2543.81	−2.28	7.37×10^{-4}	5.85×10^{-3}
PfIT_020017300	multidrug efflux pump, putative	163.47	−1.50	7.39×10^{-4}	5.85×10^{-3}
PfIT_040008700	conserved Plasmodium protein, unknown function	225.93	−2.10	7.39×10^{-4}	5.85×10^{-3}
PfIT_020011600	merozoite surface protein 5	637.14	−2.12	7.50×10^{-4}	5.92×10^{-3}
PfIT_120035100	thioredoxin-like associated protein 1, putative	114.97	−2.12	7.50×10^{-4}	5.92×10^{-3}
PfIT_080014200	asparagine-rich antigen Pfa55-14	394.53	1.13	7.54×10^{-4}	5.94×10^{-3}
PfIT_060032100	choline/ethanolaminephosphotransferase, putative	4297.76	−2.05	7.56×10^{-4}	5.95×10^{-3}
PfIT_110030200	kelch protein, putative	2640.18	−2.25	7.58×10^{-4}	5.96×10^{-3}
PfIT_140074200	rab GTPase activator, putative	1597.93	−1.47	7.70×10^{-4}	6.03×10^{-3}

Pf_ID	Transcript Product Description	base mean	$\log_2$ FC	p_{value}	p_{adj}
PfIT_140033000	conserved Plasmodium protein, unknown function	137.18	−1.95	7.70×10^{-4}	6.03×10^{-3}
PfIT_030010400	AP endonuclease (DNA-[apurinic or apyrimidinic site] lyase), putative	475.14	−1.56	7.74×10^{-4}	6.05×10^{-3}
PfIT_070014800	conserved Plasmodium membrane protein, unknown function	215.50	−1.86	7.77×10^{-4}	6.07×10^{-3}
PfIT_060015500	conserved Plasmodium protein, unknown function	39.77	−2.32	7.79×10^{-4}	6.07×10^{-3}
PfIT_000007200	Plasmodium RESA N-terminal, putative	42.86	2.00	7.80×10^{-4}	6.08×10^{-3}
PfIT_140037300	cytochrome c oxidase subunit 2, putative	96.58	−1.52	7.85×10^{-4}	6.11×10^{-3}
PfIT_020007800	repetitive organellar protein, putative	1644.91	−2.25	7.88×10^{-4}	6.12×10^{-3}
PfIT_120010300	probable protein, unknown function	292.24	−2.03	7.89×10^{-4}	6.12×10^{-3}
PfIT_080018100	conserved Plasmodium protein, unknown function	463.88	−2.01	7.91×10^{-4}	6.12×10^{-3}
PfIT_120041700	protein-S-isoprenylcysteine O-methyltransferase, putative	90.07	−1.89	7.93×10^{-4}	6.13×10^{-3}
PfIT_130046000	ras-related protein Rab-11B	129.88	−1.67	7.97×10^{-4}	6.16×10^{-3}
PfIT_130043900	conserved Plasmodium protein, unknown function	1344.33	−2.29	8.01×10^{-4}	6.18×10^{-3}
PfIT_100039300	merozoite surface protein 3	7522.95	−2.17	8.04×10^{-4}	6.19×10^{-3}
PfIT_110045600	phosphatidylinositol N-acetylglucosaminyltransferase subunit H, putative	244.46	−1.46	8.13×10^{-4}	6.25×10^{-3}
PfIT_110038000	apical membrane antigen 1	4330.59	−2.23	8.14×10^{-4}	6.25×10^{-3}
PfIT_090016300	conserved Plasmodium protein, unknown function	72.12	−1.70	8.17×10^{-4}	6.27×10^{-3}
PfIT_080013300	plasmepsin X	2339.37	−2.06	8.22×10^{-4}	6.29×10^{-3}
PfIT_090036900	protein MAM3, putative	1408.91	−2.19	8.45×10^{-4}	6.47×10^{-3}
PfIT_020012800	conserved Plasmodium protein, unknown function	773.08	−1.51	8.48×10^{-4}	6.47×10^{-3}
PfIT_100018800	conserved Plasmodium protein, unknown function	38.87	−2.05	8.59×10^{-4}	6.56×10^{-3}
PfIT_120029500	conserved Plasmodium protein, unknown function	583.16	1.13	8.62×10^{-4}	6.57×10^{-3}
PfIT_050014300	chromosome condensation protein, putative	953.90	−1.52	8.76×10^{-4}	6.66×10^{-3}

Pf_ID	Transcript Product Description	base mean	$\log_2$ FC	p_{value}	p_{adj}
PfIT_130057000	inner membrane complex protein 1f, putative	4218.40	−1.93	8.78×10^{-4}	6.67×10^{-3}
PfIT_140050600	calmodulin-like protein	48.37	−1.88	8.84×10^{-4}	6.70×10^{-3}
PfIT_090036700	adenylate kinase-like protein 2	111.02	−1.66	8.88×10^{-4}	6.73×10^{-3}
PfIT_130055600	conserved Plasmodium protein, unknown function	931.13	0.91	8.89×10^{-4}	6.73×10^{-3}
PfIT_140061700	conserved Plasmodium protein, unknown function	605.29	−1.57	8.97×10^{-4}	6.77×10^{-3}
PfIT_100008400	WD repeat-containing protein, putative	708.74	−1.31	9.15×10^{-4}	6.90×10^{-3}
PfIT_050009400	AN1-like zinc finger family protein	105.45	−2.31	9.19×10^{-4}	6.92×10^{-3}
PfIT_130069000	conserved Plasmodium protein, unknown function	155.36	−1.41	9.33×10^{-4}	7.02×10^{-3}
PfIT_080033800	conserved Plasmodium protein, unknown function	270.56	−1.90	9.34×10^{-4}	7.02×10^{-3}
PfIT_060026450	conserved Plasmodium protein, unknown function	78.54	−1.45	9.40×10^{-4}	7.05×10^{-3}
PfIT_110045500	conserved Plasmodium protein, unknown function	314.43	−1.69	9.49×10^{-4}	7.11×10^{-3}
PfIT_140065100	exonuclease V, mitochondrial, putative	85.05	−1.65	9.54×10^{-4}	7.14×10^{-3}
PfIT_120058600	hypothetical protein	29.12	1.77	9.62×10^{-4}	7.18×10^{-3}
PfIT_090032500	cytochrome c oxidase subunit 6B, putative	270.87	−1.34	9.63×10^{-4}	7.19×10^{-3}
PfIT_050013700	guanidine nucleotide exchange factor	1007.75	−1.80	9.66×10^{-4}	7.20×10^{-3}
PfIT_080029300	GTP-binding protein, putative	135.74	−1.61	9.76×10^{-4}	7.26×10^{-3}
PfIT_130052300	WD repeat-containing protein 92, putative	27.40	−1.78	9.77×10^{-4}	7.26×10^{-3}
PfIT_110049200	conserved Plasmodium protein, unknown function	153.23	−2.21	9.83×10^{-4}	7.28×10^{-3}
PfIT_080027900	conserved Plasmodium protein, unknown function	4124.81	−2.13	9.83×10^{-4}	7.28×10^{-3}
PfIT_110016500	conserved Plasmodium protein, unknown function	2157.61	−1.63	9.87×10^{-4}	7.30×10^{-3}
PfIT_020020500	DEAD/DEAH box helicase, putative	131.61	−1.50	9.91×10^{-4}	7.32×10^{-3}
PfIT_140030000	conserved Plasmodium protein, unknown function	207.97	−1.74	9.98×10^{-4}	7.36×10^{-3}
PfIT_090024700	CS domain protein, putative	247.70	−1.49	9.99×10^{-4}	7.36×10^{-3}

Pf_ID	Transcript Product Description	base mean	$\log_2$ FC	p_{value}	p_{adj}
PfIT_050027300	conserved Plasmodium protein, unknown function	326.11	−1.63	1.00×10^{-3}	7.36×10^{-3}
PfIT_140029100	conserved Plasmodium protein, unknown function	169.22	−1.76	1.00×10^{-3}	7.36×10^{-3}
PfIT_130066200	polyadenylate-binding protein, putative	583.08	−1.30	1.00×10^{-3}	7.36×10^{-3}
PfIT_070035200	erythrocyte binding antigen-175	15 558.24	−2.26	1.01×10^{-3}	7.36×10^{-3}
PfIT_050010600	UDP-N-acetyl glucosamine:UMP antiporter	61.10	−2.58	1.01×10^{-3}	7.36×10^{-3}
PfIT_120058200	Plasmodium exported protein, unknown function	5.37	5.00	1.01×10^{-3}	7.36×10^{-3}
PfIT_140041300	conserved Plasmodium protein, unknown function	14.68	−2.66	1.01×10^{-3}	7.37×10^{-3}
PfIT_130068100	conserved Plasmodium protein, unknown function	301.91	−1.39	1.01×10^{-3}	7.38×10^{-3}
PfIT_120048700	conserved Plasmodium protein, unknown function	382.51	−2.44	1.02×10^{-3}	7.41×10^{-3}
PfIT_120049500	RNA polymerase II transcription factor B subunit 2, putative	650.40	1.10	1.02×10^{-3}	7.41×10^{-3}
PfIT_110009900	conserved Plasmodium protein, unknown function	230.46	−1.67	1.02×10^{-3}	7.41×10^{-3}
PfIT_130021500	ADP-ribosylation factor, putative	142.07	−1.86	1.03×10^{-3}	7.46×10^{-3}
PfIT_110042500	conserved Plasmodium protein, unknown function	373.85	−2.06	1.03×10^{-3}	7.46×10^{-3}
PfIT_050012700	subtilisin-like protease 1	1869.97	−2.15	1.04×10^{-3}	7.51×10^{-3}
PfIT_130036800	conserved Plasmodium protein, unknown function	462.68	−2.15	1.05×10^{-3}	7.55×10^{-3}
PfIT_110044900	conserved Plasmodium protein, unknown function	2322.84	0.88	1.05×10^{-3}	7.56×10^{-3}
PfIT_020022500	replication factor C subunit 2, putative	186.00	−1.36	1.06×10^{-3}	7.60×10^{-3}
PfIT_140008400	conserved Plasmodium protein, unknown function	295.86	−2.21	1.06×10^{-3}	7.60×10^{-3}
PfIT_130009200	DNA ligase I	104.67	−1.94	1.07×10^{-3}	7.68×10^{-3}
PfIT_010009800	conserved Plasmodium protein, unknown function	149.89	−1.56	1.08×10^{-3}	7.74×10^{-3}
PfIT_000007300	stevor	4.06	5.59	1.08×10^{-3}	7.75×10^{-3}
PfIT_110042000	apicoplast ribosomal protein S14p/S29e precursor, putative	130.17	−1.57	1.09×10^{-3}	7.82×10^{-3}

Pf_ID	Transcript Product Description	base mean	$\log_2$ FC	p_{value}	p_{adj}
PfIT_130014600	H/ACA ribonucleoprotein complex subunit 1, putative	723.55	1.13	1.10×10^{-3}	7.85×10^{-3}
PfIT_080033700	GPI-anchored micronemal antigen	1243.30	−2.13	1.10×10^{-3}	7.85×10^{-3}
PfIT_130013000	tripartite motif protein, putative	212.36	−2.48	1.10×10^{-3}	7.85×10^{-3}
PfIT_130053800	TBC domain protein, putative	190.77	−1.68	1.10×10^{-3}	7.85×10^{-3}
PfIT_060034600	conserved Plasmodium protein, unknown function	57.10	−1.94	1.11×10^{-3}	7.86×10^{-3}
PfIT_050023400	SWIB/MDM2 domain-containing protein, putative	161.46	−1.81	1.11×10^{-3}	7.90×10^{-3}
PfIT_010007700	StAR-related lipid transfer protein	1114.98	−2.07	1.12×10^{-3}	7.90×10^{-3}
PfIT_050011300	conserved Plasmodium protein, unknown function	159.30	1.18	1.12×10^{-3}	7.90×10^{-3}
PfIT_050009000	myosin B	1287.66	−1.96	1.13×10^{-3}	8.00×10^{-3}
PfIT_140021700	conserved Plasmodium protein, unknown function	105.21	−1.72	1.14×10^{-3}	8.05×10^{-3}
PfIT_110017400	conserved Plasmodium protein, unknown function	190.12	−1.96	1.14×10^{-3}	8.05×10^{-3}
PfIT_140031700	conserved Plasmodium protein, unknown function	427.07	−2.14	1.14×10^{-3}	8.05×10^{-3}
PfIT_110033200	GPI-anchor transamidase	56.39	−1.77	1.15×10^{-3}	8.06×10^{-3}
PfIT_120035300	subpellicular microtubule protein 2, putative	75.91	−2.02	1.15×10^{-3}	8.08×10^{-3}
PfIT_110030300	kelch protein, putative	3162.28	−2.23	1.15×10^{-3}	8.08×10^{-3}
PfIT_090013200	conserved Plasmodium protein, unknown function	91.43	−1.97	1.16×10^{-3}	8.10×10^{-3}
PfIT_110032100	CRAL/TRIO domain-containing protein, putative	493.91	−1.79	1.18×10^{-3}	8.23×10^{-3}
PfIT_010014500	UMP-CMP kinase, putative	707.47	−1.51	1.19×10^{-3}	8.28×10^{-3}
PfIT_100032300	rRNA-processing protein EBP2, putative	780.69	1.10	1.19×10^{-3}	8.28×10^{-3}
PfIT_100018300	conserved protein, unknown function	904.37	−1.51	1.19×10^{-3}	8.32×10^{-3}
PfIT_140079000	conserved Plasmodium protein, unknown function	201.41	−1.07	1.20×10^{-3}	8.32×10^{-3}
PfIT_130022400	DNA replication licensing factor MCM4	1272.24	−1.47	1.20×10^{-3}	8.32×10^{-3}
PfIT_130033500	conserved Plasmodium protein, unknown function	531.58	−1.41	1.20×10^{-3}	8.32×10^{-3}

Pf_ID	Transcript Product Description	base mean	$\log_2$ FC	p_{value}	p_{adj}
PfIT_040015600	conserved Plasmodium protein, unknown function	484.79	1.97	1.20×10^{-3}	8.32×10^{-3}
PfIT_070013600	Cg8 protein	156.86	−1.26	1.20×10^{-3}	8.32×10^{-3}
PfIT_040024100	apical merozoite protein	299.17	−2.10	1.20×10^{-3}	8.32×10^{-3}
PfIT_140006900	rifin	54.30	5.65	1.21×10^{-3}	8.35×10^{-3}
PfIT_140028400	copper transporter, putative	152.94	−1.82	1.23×10^{-3}	8.46×10^{-3}
PfIT_070018100	negative elongation factor A, putative	265.83	−2.02	1.23×10^{-3}	8.46×10^{-3}
PfIT_130036300	protein kinase, putative	171.38	−1.90	1.23×10^{-3}	8.48×10^{-3}
PfIT_040016500	DNA polymerase alpha catalytic subunit A	453.40	−1.30	1.25×10^{-3}	8.60×10^{-3}
PfIT_130024000	conserved Plasmodium protein, unknown function	267.62	−1.84	1.26×10^{-3}	8.67×10^{-3}
PfIT_140009700	conserved Plasmodium protein, unknown function	1041.15	−1.36	1.27×10^{-3}	8.68×10^{-3}
PfIT_090019400	GINS complex subunit Psf3, putative	98.28	−1.47	1.28×10^{-3}	8.77×10^{-3}
PfIT_030018400	conserved Plasmodium protein, unknown function	160.92	−1.11	1.29×10^{-3}	8.81×10^{-3}
PfIT_130063400	patatin-like phospholipase, putative	189.00	−1.47	1.29×10^{-3}	8.81×10^{-3}
PfIT_120038600	homocysteine S-methyltransferase, putative	79.64	−1.79	1.29×10^{-3}	8.82×10^{-3}
PfIT_080009500	methionine aminopeptidase 1c, putative	153.99	−1.39	1.31×10^{-3}	8.94×10^{-3}
PfIT_040023300	conserved Plasmodium protein, unknown function	66.09	−1.34	1.32×10^{-3}	8.96×10^{-3}
PfIT_090038500	conserved Plasmodium protein, unknown function	71.77	−2.01	1.32×10^{-3}	8.99×10^{-3}
PfIT_110029500	conserved Plasmodium protein, unknown function	107.45	−1.54	1.32×10^{-3}	8.99×10^{-3}
PfIT_040019500	conserved Plasmodium protein, unknown function	61.50	1.44	1.33×10^{-3}	9.02×10^{-3}
PfIT_040028600	reticulocyte binding protein homologue 5	594.47	−2.21	1.34×10^{-3}	9.08×10^{-3}
PfIT_130052400	DNA topoisomerase 3, putative	179.22	−1.50	1.34×10^{-3}	9.09×10^{-3}
PfIT_130070800	DNA topoisomerase VI, b subunit, putative	332.35	−1.80	1.35×10^{-3}	9.11×10^{-3}
PfIT_140055800	crossover junction endonuclease MUS81, putative	234.88	−1.67	1.36×10^{-3}	9.14×10^{-3}

Pf_ID	Transcript Product Description	base mean	$\log_2$ FC	p_{value}	p_{adj}
PfIT_080021400	conserved Plasmodium protein, unknown function	121.60	−1.82	1.36×10^{-3}	9.14×10^{-3}
PfIT_130006400	erythrocyte binding antigen-140	3882.83	−2.12	1.36×10^{-3}	9.16×10^{-3}
PfIT_120055500	vacuolar protein sorting-associated protein 26, putative	304.59	−0.95	1.37×10^{-3}	9.18×10^{-3}
PfIT_080021200	vacuolar protein sorting-associated protein 2, putative	105.56	−1.63	1.37×10^{-3}	9.18×10^{-3}
PfIT_110047300	transcription factor with AP2 domain(s)	976.77	−1.97	1.37×10^{-3}	9.18×10^{-3}
PfIT_140053100	conserved Plasmodium protein, unknown function	217.33	−1.48	1.37×10^{-3}	9.18×10^{-3}
PfIT_060024100	conserved Plasmodium protein, unknown function	67.27	−1.95	1.37×10^{-3}	9.18×10^{-3}
PfIT_040020900	repressor of RNA polymerase III transcription MAF1, putative	124.83	−1.79	1.39×10^{-3}	9.26×10^{-3}
PfIT_110051700	conserved Plasmodium protein, unknown function	41.19	−1.66	1.39×10^{-3}	9.26×10^{-3}
PfIT_140076500	conserved Plasmodium protein, unknown function	129.74	1.09	1.41×10^{-3}	9.37×10^{-3}
PfIT_140069100	cytochrome c1 precursor, putative	303.56	−1.44	1.41×10^{-3}	9.40×10^{-3}
PfIT_060029800	conserved Plasmodium protein, unknown function	469.18	1.41	1.41×10^{-3}	9.40×10^{-3}
PfIT_120052700	serine/threonine protein kinase, putative	67.49	−2.07	1.42×10^{-3}	9.41×10^{-3}
PfIT_110020800	folate transporter 2	151.00	−1.39	1.42×10^{-3}	9.41×10^{-3}
PfIT_040009900	ag-1 blood stage membrane protein homologue	837.44	−2.00	1.43×10^{-3}	9.49×10^{-3}
PfIT_130008900	conserved Plasmodium protein, unknown function	822.29	−1.21	1.44×10^{-3}	9.50×10^{-3}
PfIT_140023900	cysteine protease ATG4, putative	269.19	−1.69	1.44×10^{-3}	9.51×10^{-3}
PfIT_060029000	conserved Plasmodium protein, unknown function	59.96	−1.61	1.44×10^{-3}	9.51×10^{-3}
PfIT_030013100	conserved Plasmodium protein, unknown function	245.88	−1.98	1.45×10^{-3}	9.54×10^{-3}
PfIT_130027300	adenosine-diphosphatase, putative	347.63	−1.54	1.46×10^{-3}	9.60×10^{-3}
PfIT_040023900	conserved Plasmodium membrane protein, unknown function	245.93	1.01	1.47×10^{-3}	9.63×10^{-3}
PfIT_110019100	glycerol-3-phosphate dehydrogenase, putative	87.72	−1.48	1.48×10^{-3}	9.70×10^{-3}

Pf_ID	Transcript Product Description	base mean	$\log_2$ FC	p_{value}	p_{adj}
PfIT_080036900	stevor	7.90	5.56	1.49×10^{-3}	9.74×10^{-3}
PfIT_130054400	nucleoside diphosphate hydrolase, putative	104.07	−1.80	1.50×10^{-3}	9.79×10^{-3}
PfIT_100015900	heme oxygenase	315.60	−1.35	1.51×10^{-3}	9.85×10^{-3}
PfIT_040011100	conserved Plasmodium protein, unknown function	14 641.30	0.91	1.51×10^{-3}	9.85×10^{-3}
PfIT_070008100	conserved Plasmodium protein, unknown function	559.57	−1.15	1.51×10^{-3}	9.88×10^{-3}
PfIT_140024400	DNA replication licensing factor MCM2	988.32	−1.43	1.52×10^{-3}	9.91×10^{-3}
PfIT_040015400	conserved Plasmodium protein, unknown function	1649.38	−1.37	1.52×10^{-3}	9.92×10^{-3}
PfIT_130017200	malonyl CoA-acyl carrier protein transacylase precursor	24.06	−2.16	1.54×10^{-3}	1.00×10^{-2}
PfIT_130055500	small nuclear ribonucleoprotein E, putative	275.71	1.00	1.55×10^{-3}	1.01×10^{-2}
PfIT_130018900	conserved Plasmodium protein, unknown function	103.84	−2.20	1.57×10^{-3}	1.02×10^{-2}
PfIT_070010000	conserved Plasmodium protein, unknown function	169.60	−2.02	1.58×10^{-3}	1.03×10^{-2}
PfIT_080029700	lipase maturation factor, putative	31.63	−1.68	1.59×10^{-3}	1.03×10^{-2}
PfIT_010006000	erythrocyte binding antigen-181	2337.41	−2.30	1.60×10^{-3}	1.03×10^{-2}
PfIT_020016100	dolichol-linked oligosaccharide biosynthesis enzyme, putative	32.16	−1.86	1.60×10^{-3}	1.03×10^{-2}
PfIT_140027600	mannose-1-phosphate guanyltransferase, putative	114.95	−1.39	1.60×10^{-3}	1.03×10^{-2}
PfIT_120010400	conserved Plasmodium protein, unknown function	278.03	−1.49	1.60×10^{-3}	1.03×10^{-2}
PfIT_090041300	Plasmodium exported protein (PHISTc), unknown function	1079.67	1.80	1.60×10^{-3}	1.03×10^{-2}
PfIT_130052200	conserved Plasmodium protein, unknown function	97.97	−1.82	1.62×10^{-3}	1.04×10^{-2}
PfIT_110008300	CCR4-NOT transcription complex subunit 1, putative	1993.85	−1.17	1.62×10^{-3}	1.04×10^{-2}
PfIT_030018800	co-chaperone p23	154.90	−1.52	1.64×10^{-3}	1.05×10^{-2}
PfIT_140029600	ankyrin, putative	333.09	−2.00	1.64×10^{-3}	1.05×10^{-2}
PfIT_030016200	protein kinase, putative	305.30	−2.05	1.65×10^{-3}	1.05×10^{-2}

Pf_ID	Transcript Product Description	base mean	$\log_2$ FC	p_{value}	p_{adj}
PfIT_130008800	conserved Plasmodium protein, unknown function	148.68	−1.98	1.65×10^{-3}	1.05×10^{-2}
PfIT_140025800	ATP-dependent rRNA helicase SPB4, putative	1358.76	0.91	1.65×10^{-3}	1.06×10^{-2}
PfIT_130054900	conserved Plasmodium protein, unknown function	277.53	−1.15	1.67×10^{-3}	1.06×10^{-2}
PfIT_060016400	conserved Plasmodium protein, unknown function	29.66	−1.77	1.67×10^{-3}	1.06×10^{-2}
PfIT_120044400	DNA gyrase subunit B	118.34	−1.32	1.67×10^{-3}	1.06×10^{-2}
PfIT_050006800	interspersed repeat antigen	17 043.02	0.95	1.70×10^{-3}	1.08×10^{-2}
PfIT_070032000	conserved Plasmodium membrane protein, unknown function	270.92	−1.41	1.70×10^{-3}	1.08×10^{-2}
PfIT_140029000	ERAD-associated E3 ubiquitin-protein ligase HRD1	99.48	−1.65	1.70×10^{-3}	1.08×10^{-2}
PfIT_020005200	PfEMP1	69.73	1.58	1.71×10^{-3}	1.08×10^{-2}
PfIT_020016000	GAF domain-related protein, putative	82.72	−1.77	1.72×10^{-3}	1.09×10^{-2}
PfIT_060028800	sphingomyelin synthase 1, putative	124.89	−2.06	1.72×10^{-3}	1.09×10^{-2}
PfIT_140085300	Plasmodium exported protein (PHISTa), unknown function	84.66	1.39	1.72×10^{-3}	1.09×10^{-2}
PfIT_130036500	conserved Plasmodium protein, unknown function	953.57	1.01	1.73×10^{-3}	1.09×10^{-2}
PfIT_090010500	conserved Plasmodium protein, unknown function	286.60	1.09	1.73×10^{-3}	1.09×10^{-2}
PfIT_100025600	ATP-dependent RNA helicase ROK1, putative	629.54	1.14	1.74×10^{-3}	1.10×10^{-2}
PfIT_140012500	RNA-binding protein, putative	2627.34	0.90	1.75×10^{-3}	1.10×10^{-2}
PfIT_140020300	conserved Plasmodium protein, unknown function	1617.35	−2.18	1.75×10^{-3}	1.10×10^{-2}
PfIT_130063100	U3 small nucleolar RNA-associated protein 21, putative	1571.78	1.34	1.77×10^{-3}	1.11×10^{-2}
PfIT_060017900	myosin E, putative	5948.42	−2.06	1.78×10^{-3}	1.11×10^{-2}
PfIT_060034000	secreted ookinete protein, putative	9.99	−2.78	1.80×10^{-3}	1.12×10^{-2}
PfIT_090008100	DEAD/DEAH box helicase, putative	9424.37	0.84	1.81×10^{-3}	1.13×10^{-2}
PfIT_010009500	conserved Plasmodium protein, unknown function	51.26	−1.56	1.82×10^{-3}	1.13×10^{-2}
PfIT_120020200	conserved Plasmodium membrane protein, unknown function	177.46	−1.17	1.82×10^{-3}	1.13×10^{-2}
PfIT_140071800	potassium channel	13.46	2.56	1.84×10^{-3}	1.14×10^{-2}

Pf_ID	Transcript Product Description	base mean	$\log_2$ FC	p_{value}	p_{adj}
PfIT_060007400	cation/H+ antiporter	88.15	−1.14	1.84×10^{-3}	1.14×10^{-2}
PfIT_140021300	ubiquitin carboxyl-terminal hydrolase, putative	561.44	1.27	1.84×10^{-3}	1.14×10^{-2}
PfIT_100026700	kelch protein, putative	2417.71	0.97	1.84×10^{-3}	1.14×10^{-2}
PfIT_080019100	conserved Plasmodium protein, unknown function	119.02	1.47	1.85×10^{-3}	1.14×10^{-2}
PfIT_130043700	conserved Plasmodium protein, unknown function	64.21	−1.26	1.85×10^{-3}	1.15×10^{-2}
PfIT_140076200	conserved Plasmodium protein, unknown function	117.92	−1.72	1.86×10^{-3}	1.15×10^{-2}
PfIT_140045500	copper transporter	303.31	−1.38	1.86×10^{-3}	1.15×10^{-2}
PfIT_130041500	conserved Plasmodium protein, unknown function	367.05	−0.98	1.86×10^{-3}	1.15×10^{-2}
PfIT_020019200	conserved Plasmodium protein, unknown function	367.14	−1.83	1.87×10^{-3}	1.15×10^{-2}
PfIT_070015600	conserved Plasmodium protein, unknown function	1880.97	1.12	1.88×10^{-3}	1.16×10^{-2}
PfIT_080036100	Plasmodium exported protein, unknown function	361.74	2.65	1.89×10^{-3}	1.16×10^{-2}
PfIT_110021700	conserved Plasmodium protein, unknown function	396.94	−1.61	1.89×10^{-3}	1.16×10^{-2}
PfIT_100038500	translation initiation factor IF-3, putative	163.78	−1.69	1.90×10^{-3}	1.17×10^{-2}
PfIT_070029100	kinesin-19, putative	705.19	−2.01	1.91×10^{-3}	1.17×10^{-2}
PfIT_060015100	succinate dehydrogenase subunit 3, putative	22.78	−2.04	1.91×10^{-3}	1.17×10^{-2}
PfIT_040023400	conserved Plasmodium protein, unknown function	16.00	−2.19	1.92×10^{-3}	1.17×10^{-2}
PfIT_100020000	conserved Plasmodium protein, unknown function	259.51	−2.14	1.92×10^{-3}	1.17×10^{-2}
PfIT_050012500	conserved Plasmodium protein, unknown function	581.54	−2.45	1.96×10^{-3}	1.19×10^{-2}
PfIT_080016800	RNA-binding protein, putative	285.43	−1.30	2.00×10^{-3}	1.21×10^{-2}
PfIT_140046000	CCAAT-binding transcription factor, putative	179.01	−1.65	2.00×10^{-3}	1.21×10^{-2}
PfIT_060018000	thiamin-phosphate pyrophosphorylase, putative	698.85	−1.65	2.00×10^{-3}	1.21×10^{-2}
PfIT_030012300	conserved protein, unknown function	126.16	−1.43	2.00×10^{-3}	1.22×10^{-2}

Pf_ID	Transcript Product Description	base mean	$\log_2$ FC	p_{value}	p_{adj}
PfIT_140058900	SNARE protein, putative	116.03	−1.57	2.01×10^{-3}	1.22×10^{-2}
PfIT_130060000	60S ribosomal protein L7-2, putative	272.92	1.29	2.02×10^{-3}	1.22×10^{-2}
PfIT_130023300	conserved Plasmodium membrane protein, unknown function	372.93	0.97	2.02×10^{-3}	1.22×10^{-2}
PfIT_120014800	cytosolic iron-sulfur protein assembly protein 1, putative	955.38	−1.96	2.03×10^{-3}	1.23×10^{-2}
PfIT_100027500	HORMA domain protein, putative	110.64	−1.15	2.06×10^{-3}	1.24×10^{-2}
PfIT_100035200	conserved Plasmodium protein, unknown function	223.43	−1.63	2.07×10^{-3}	1.25×10^{-2}
PfIT_030024800	protein phosphatase inhibitor 2	197.54	−1.00	2.07×10^{-3}	1.25×10^{-2}
PfIT_120008300	conserved Plasmodium protein, unknown function	962.10	0.98	2.09×10^{-3}	1.25×10^{-2}
PfIT_020008200	conserved Plasmodium protein, unknown function	175.56	−1.47	2.11×10^{-3}	1.26×10^{-2}
PfIT_090007100	serine/threonine protein kinase, FIKK family	1435.20	1.17	2.11×10^{-3}	1.26×10^{-2}
PfIT_130060500	DNA replication licensing factor MCM6	1131.41	−1.31	2.11×10^{-3}	1.26×10^{-2}
PfIT_050027600	conserved Plasmodium protein, unknown function	1209.46	−1.74	2.12×10^{-3}	1.26×10^{-2}
PfIT_060017700	syntaxin binding protein, putative	369.13	−1.01	2.12×10^{-3}	1.26×10^{-2}
PfIT_010010200	2-C-methyl-D-erythritol 4-phosphate cytidylyltransferase, putative	158.31	−1.59	2.12×10^{-3}	1.26×10^{-2}
PfIT_020011900	iron-sulfur assembly protein, putative	35.06	−1.91	2.12×10^{-3}	1.26×10^{-2}
PfIT_100042500	RESA-like protein with PHIST and DnaJ domains	1256.35	0.90	2.12×10^{-3}	1.26×10^{-2}
PfIT_090018400	conserved Plasmodium protein, unknown function	633.83	−1.97	2.13×10^{-3}	1.26×10^{-2}
PfIT_040006700	reticulocyte binding protein homologue 1	6172.07	−2.25	2.13×10^{-3}	1.26×10^{-2}
PfIT_130050600	conserved Plasmodium protein, unknown function	35.92	−1.83	2.15×10^{-3}	1.28×10^{-2}
PfIT_140047400	cytoplasmic tRNA 2-thiolation protein 2, putative	241.05	1.02	2.15×10^{-3}	1.28×10^{-2}
PfIT_120034600	conserved Plasmodium protein, unknown function	638.45	−1.10	2.16×10^{-3}	1.28×10^{-2}
PfIT_130040300	MSP7-like protein	21.18	−2.42	2.16×10^{-3}	1.28×10^{-2}

Pf_ID	Transcript Product Description	base mean	$\log_2$ FC	p_{value}	p_{adj}
PfIT_060021900	conserved Plasmodium protein, unknown function	111.96	−1.72	2.17×10^{-3}	1.28×10^{-2}
PfIT_030020900	mitochondrial ribosomal protein L27 precursor, putative	343.31	−1.82	2.17×10^{-3}	1.28×10^{-2}
PfIT_140055100	conserved Plasmodium protein, unknown function	190.31	0.95	2.18×10^{-3}	1.28×10^{-2}
PfIT_120011400	shewanella-like protein phosphatase 2	804.12	−1.91	2.19×10^{-3}	1.29×10^{-2}
PfIT_140015100	conserved Plasmodium protein, unknown function	743.87	0.85	2.20×10^{-3}	1.30×10^{-2}
PfIT_030012400	conserved Plasmodium protein, unknown function	196.34	−1.38	2.20×10^{-3}	1.30×10^{-2}
PfIT_050037000	Plasmodium exported protein (PHISTb), unknown function	9233.43	2.58	2.22×10^{-3}	1.31×10^{-2}
PfIT_030015400	eukaryotic translation initiation factor 3 subunit K, putative	559.62	1.09	2.28×10^{-3}	1.34×10^{-2}
PfIT_080030500	protein KRI1, putative	2815.97	0.88	2.30×10^{-3}	1.35×10^{-2}
PfIT_090041100	ring-exported protein 4	252.09	2.13	2.31×10^{-3}	1.35×10^{-2}
PfIT_040009300	conserved Plasmodium membrane protein, unknown function	2050.08	2.19	2.33×10^{-3}	1.36×10^{-2}
PfIT_120011700	conserved Plasmodium protein, unknown function	2989.46	−1.99	2.33×10^{-3}	1.36×10^{-2}
PfIT_120057500	conserved Plasmodium protein, unknown function	900.40	2.21	2.35×10^{-3}	1.37×10^{-2}
PfIT_120051100	conserved Plasmodium protein, unknown function	121.82	1.22	2.36×10^{-3}	1.38×10^{-2}
PfIT_080011500	glycosyltransferase family 28 protein, putative	14.88	−2.69	2.37×10^{-3}	1.38×10^{-2}
PfIT_060030000	conserved Plasmodium protein, unknown function	35.45	1.40	2.37×10^{-3}	1.38×10^{-2}
PfIT_140011300	conserved Plasmodium protein, unknown function	126.51	−2.18	2.37×10^{-3}	1.38×10^{-2}
PfIT_090015700	phosphatidylinositol N-acetylglucosaminyltransferase, putative	160.99	−2.01	2.38×10^{-3}	1.38×10^{-2}
PfIT_090015800	conserved Plasmodium protein, unknown function	3448.53	−2.27	2.40×10^{-3}	1.39×10^{-2}
PfIT_040019200	conserved Plasmodium protein, unknown function	342.53	−2.47	2.40×10^{-3}	1.39×10^{-2}
PfIT_120022200	DNA-binding chaperone, putative	8160.30	1.02	2.40×10^{-3}	1.39×10^{-2}

Pf_ID	Transcript Product Description	base mean	$\log_2$ FC	p_{value}	p_{adj}
PfIT_070021500	conserved Plasmodium protein, unknown function	356.46	−1.45	2.41×10^{-3}	1.39×10^{-2}
PfIT_140013200	ATP-dependent Clp protease, putative	391.32	−1.35	2.45×10^{-3}	1.42×10^{-2}
PfIT_130013800	conserved Plasmodium protein, unknown function	371.70	−1.17	2.48×10^{-3}	1.43×10^{-2}
PfIT_110051800	mitochondrial ATP synthase delta subunit, putative	85.45	−1.28	2.48×10^{-3}	1.43×10^{-2}
PfIT_030019600	conserved Plasmodium protein, unknown function	72.63	−2.13	2.49×10^{-3}	1.43×10^{-2}
PfIT_080027100	mediator of RNA polymerase II transcription subunit 7, putative	133.87	1.28	2.49×10^{-3}	1.43×10^{-2}
PfIT_130064400	conserved Plasmodium protein, unknown function	1098.60	0.82	2.49×10^{-3}	1.43×10^{-2}
PfIT_030023500	trophozoite stage antigen	191.50	−1.98	2.50×10^{-3}	1.43×10^{-2}
PfIT_090010200	conserved Plasmodium protein, unknown function	143.40	−1.91	2.50×10^{-3}	1.43×10^{-2}
PfIT_100009300	U3 small nucleolar RNA-associated protein 25, putative	1075.97	0.95	2.51×10^{-3}	1.43×10^{-2}
PfIT_100030700	conserved Plasmodium protein, unknown function	18 253.14	−2.33	2.51×10^{-3}	1.43×10^{-2}
PfIT_110049800	conserved protein, unknown function	37.89	−1.84	2.51×10^{-3}	1.44×10^{-2}
PfIT_000009900	acyl-CoA synthetase	26.38	−1.57	2.52×10^{-3}	1.44×10^{-2}
PfIT_120018700	conserved Plasmodium protein, unknown function	21.67	−2.66	2.52×10^{-3}	1.44×10^{-2}
PfIT_110029600	vacuolar membrane protein-related, putative	58.25	−1.55	2.52×10^{-3}	1.44×10^{-2}
PfIT_020026000	Pfmc-2TM Maurer's cleft two transmembrane protein	3.42	5.35	2.52×10^{-3}	1.44×10^{-2}
PfIT_140082000	conserved Plasmodium protein, unknown function	74.58	−1.89	2.53×10^{-3}	1.44×10^{-2}
PfIT_020021000	conserved Plasmodium protein, unknown function	159.59	−0.99	2.53×10^{-3}	1.44×10^{-2}
PfIT_090039200	transcription factor with AP2 domain(s), putative	163.45	−1.25	2.54×10^{-3}	1.44×10^{-2}
PfIT_140038000	ATP-specific succinyl-CoA synthetase beta subunit, putative	202.11	−1.16	2.55×10^{-3}	1.44×10^{-2}
PfIT_040005600	rifin	10.05	2.95	2.56×10^{-3}	1.45×10^{-2}
PfIT_110049600	dynamin-like protein	1169.66	−1.42	2.57×10^{-3}	1.45×10^{-2}

Pf_ID	Transcript Product Description	base mean	$\log_2$ FC	p_{value}	p_{adj}
PfIT_110025300	palmitoyltransferase, putative	112.78	−1.64	2.57×10^{-3}	1.45×10^{-2}
PfIT_120053100	nucleolar rRNA processing protein, putative	659.01	1.22	2.58×10^{-3}	1.46×10^{-2}
PfIT_110027000	conserved Plasmodium protein, unknown function	53.14	−1.77	2.59×10^{-3}	1.46×10^{-2}
PfIT_140017600	conserved Plasmodium protein, unknown function	2810.52	−2.23	2.61×10^{-3}	1.47×10^{-2}
PfIT_130024700	conserved Plasmodium protein, unknown function	1683.61	−1.19	2.61×10^{-3}	1.47×10^{-2}
PfIT_000023600:rRNA	rRNA	277.80	−1.16	2.62×10^{-3}	1.47×10^{-2}
PfIT_050008400	50S ribosomal protein L28, apicoplast, putative	503.17	−1.51	2.62×10^{-3}	1.47×10^{-2}
PfIT_060034300	ribosome biogenesis protein YTM1, putative	197.16	1.23	2.64×10^{-3}	1.48×10^{-2}
PfIT_010012800	conserved protein, unknown function	1096.09	1.07	2.65×10^{-3}	1.48×10^{-2}
PfIT_110041700	apical exonemal protein	382.73	−1.79	2.66×10^{-3}	1.49×10^{-2}
PfIT_080024800	conserved Plasmodium protein, unknown function	189.49	−1.34	2.66×10^{-3}	1.49×10^{-2}
PfIT_050030600	G-protein coupled receptor, putative	42.74	−1.98	2.68×10^{-3}	1.49×10^{-2}
PfIT_100034700	calmodulin, putative	160.01	−1.58	2.69×10^{-3}	1.50×10^{-2}
PfIT_120012900	RNA-binding protein, putative	141.19	−1.86	2.70×10^{-3}	1.51×10^{-2}
PfIT_140064100	large ribosomal subunit nuclear export factor, putative	2268.06	0.95	2.72×10^{-3}	1.51×10^{-2}
PfIT_130010700	membrane integral peptidase, M50 family, putative	23.45	−1.91	2.73×10^{-3}	1.52×10^{-2}
PfIT_020010600	conserved Plasmodium protein, unknown function	155.59	−1.15	2.74×10^{-3}	1.52×10^{-2}
PfIT_130007300	early transcribed membrane protein 13	44.45	−2.44	2.75×10^{-3}	1.53×10^{-2}
PfIT_090031700	zinc finger protein, putative	107.69	−2.15	2.76×10^{-3}	1.53×10^{-2}
PfIT_110031000	conserved Plasmodium protein, unknown function	1919.60	0.85	2.76×10^{-3}	1.53×10^{-2}
PfIT_130044700	conserved Plasmodium protein, unknown function	90.49	−1.57	2.77×10^{-3}	1.53×10^{-2}
PfIT_130043300	conserved Plasmodium membrane protein, unknown function	235.72	−1.28	2.78×10^{-3}	1.54×10^{-2}
PfIT_110025700	WD repeat-containing protein, putative	9.88	−2.76	2.78×10^{-3}	1.54×10^{-2}

Pf_ID	Transcript Product Description	base mean	$\log_2$ FC	p_{value}	p_{adj}
PfIT_100017600	conserved Plasmodium protein, unknown function	661.74	−1.38	2.80×10^{-3}	1.54×10^{-2}
PfIT_130064000	zinc finger protein, putative	195.71	−1.63	2.82×10^{-3}	1.55×10^{-2}
PfIT_050037100	lysine-rich membrane-associated PHISTb protein	2604.14	2.46	2.83×10^{-3}	1.56×10^{-2}
PfIT_130045600	nucleolar complex protein 2, putative	3605.69	1.09	2.83×10^{-3}	1.56×10^{-2}
PfIT_010016100	glutamic acid-rich protein	42 525.38	2.32	2.85×10^{-3}	1.56×10^{-2}
PfIT_030020800	microneme associated antigen	309.87	−2.06	2.88×10^{-3}	1.58×10^{-2}
PfIT_050011700	conserved Plasmodium protein, unknown function	9.84	−2.58	2.89×10^{-3}	1.58×10^{-2}
PfIT_020007900	protein kinase, putative	776.03	−1.78	2.89×10^{-3}	1.58×10^{-2}
PfIT_020026700	exported protein family 4	21.02	2.26	2.90×10^{-3}	1.58×10^{-2}
PfIT_080024100	BRIX domain, putative	385.06	1.01	2.90×10^{-3}	1.58×10^{-2}
PfIT_140027900	conserved Plasmodium protein, unknown function	60.70	−1.39	2.90×10^{-3}	1.58×10^{-2}
PfIT_140033400	conserved Plasmodium protein, unknown function	305.36	−1.09	2.91×10^{-3}	1.59×10^{-2}
PfIT_060018400	conserved protein, unknown function	446.18	1.45	2.93×10^{-3}	1.60×10^{-2}
PfIT_090008400	alpha tubulin 2	529.39	−1.51	2.97×10^{-3}	1.62×10^{-2}
PfIT_090037400	apicoplast ribosomal protein S6, putative	33.31	−1.46	2.99×10^{-3}	1.63×10^{-2}
PfIT_110014700	conserved Plasmodium protein, unknown function	654.73	0.97	3.02×10^{-3}	1.64×10^{-2}
PfIT_130040100	MSP7-like protein	174.32	−1.36	3.03×10^{-3}	1.64×10^{-2}
PfIT_040020200	RING zinc finger protein, putative	146.89	−2.07	3.05×10^{-3}	1.65×10^{-2}
PfIT_110017600	conserved Plasmodium protein, unknown function	137.49	1.30	3.05×10^{-3}	1.65×10^{-2}
PfIT_110009400	calcium/calmodulin-dependent protein kinase, putative	1486.63	−1.70	3.06×10^{-3}	1.66×10^{-2}
PfIT_120050400	kinesin-13, putative	105.88	−1.33	3.09×10^{-3}	1.67×10^{-2}
PfIT_140050000	conserved Plasmodium protein, unknown function	68.99	−1.25	3.10×10^{-3}	1.67×10^{-2}
PfIT_110017700	UDP-galactose transporter, putative	158.44	−1.32	3.13×10^{-3}	1.69×10^{-2}
PfIT_120047900	protein geranylgeranyltransferase type II, alpha subunit, putative	221.00	1.52	3.13×10^{-3}	1.69×10^{-2}
PfIT_120027000	conserved Plasmodium membrane protein, unknown function	2780.10	1.11	3.14×10^{-3}	1.69×10^{-2}

Pf_ID	Transcript Product Description	base mean	$\log_2$ FC	p_{value}	p_{adj}
PfIT_100027000	CDGSH iron-sulfur domain-containing protein, putative	56.89	−1.47	3.15×10^{-3}	1.70×10^{-2}
PfIT_130029100	vacuolar protein sorting-associated protein 52, putative	412.75	1.01	3.16×10^{-3}	1.70×10^{-2}
PfIT_070028300	conserved Plasmodium protein, unknown function	3829.87	0.90	3.17×10^{-3}	1.70×10^{-2}
PfIT_130053300	conserved Plasmodium protein, unknown function	62.32	−1.78	3.17×10^{-3}	1.70×10^{-2}
PfIT_130049900	lipoyl synthase	68.93	−1.66	3.18×10^{-3}	1.70×10^{-2}
PfIT_030025600	ATP-dependent RNA helicase DDX6	176.16	−1.43	3.19×10^{-3}	1.71×10^{-2}
PfIT_130076100	Plasmodium exported protein (PHISTc), unknown function	1751.83	2.55	3.26×10^{-3}	1.74×10^{-2}
PfIT_110015200	conserved Plasmodium protein, unknown function	43.93	−1.57	3.27×10^{-3}	1.75×10^{-2}
PfIT_020021200	autophagy-related protein 11, putative	7485.95	−2.11	3.28×10^{-3}	1.75×10^{-2}
PfIT_050005500	PfEMP1	264.52	1.16	3.28×10^{-3}	1.75×10^{-2}
PfIT_130035000	apicoplast calcium binding protein 1	201.96	−2.14	3.28×10^{-3}	1.75×10^{-2}
PfIT_050033500	conserved Plasmodium protein, unknown function	233.38	−2.26	3.30×10^{-3}	1.75×10^{-2}
PfIT_110042300	conserved Plasmodium protein, unknown function	282.13	−2.27	3.32×10^{-3}	1.76×10^{-2}
PfIT_130010200	conserved Plasmodium protein, unknown function	80.15	−1.61	3.33×10^{-3}	1.77×10^{-2}
PfIT_040011600	conserved Plasmodium protein, unknown function	142.83	1.27	3.34×10^{-3}	1.77×10^{-2}
PfIT_130031900	conserved Plasmodium protein, unknown function	565.54	−1.19	3.38×10^{-3}	1.79×10^{-2}
PfIT_020027200	rifin	8.31	3.62	3.38×10^{-3}	1.79×10^{-2}
PfIT_130017800	conserved Plasmodium protein, unknown function	148.22	−2.00	3.43×10^{-3}	1.82×10^{-2}
PfIT_140015800	conserved Plasmodium protein, unknown function	144.67	−1.64	3.46×10^{-3}	1.83×10^{-2}
PfIT_090006900	serine/threonine protein kinase, FIKK family	426.85	−1.71	3.46×10^{-3}	1.83×10^{-2}
PfIT_030026100	conserved Plasmodium protein, unknown function	146.21	−1.96	3.47×10^{-3}	1.83×10^{-2}
PfIT_040028700	reticulocyte binding protein homologue 4	623.42	−2.18	3.49×10^{-3}	1.84×10^{-2}

Pf_ID	Transcript Product Description	base mean	$\log_2$ FC	p_{value}	p_{adj}
PfIT_040022000	conserved Plasmodium protein, unknown function	78.56	−1.58	3.50×10^{-3}	1.84×10^{-2}
PfIT_110029200	hypothetical protein	1309.49	−1.29	3.51×10^{-3}	1.84×10^{-2}
PfIT_120056500	thymidylate kinase	116.38	−1.10	3.53×10^{-3}	1.85×10^{-2}
PfIT_120035400	ATP-dependent protease subunit ClpQ	93.87	−1.30	3.54×10^{-3}	1.86×10^{-2}
PfIT_050036400	conserved Plasmodium protein, unknown function	109.52	−1.39	3.60×10^{-3}	1.89×10^{-2}
PfIT_010005900	alpha/beta hydrolase fold/Alpha/beta hydrolase family/Serine aminopeptidase, S33, putative	20.89	−2.00	3.61×10^{-3}	1.89×10^{-2}
PfIT_060011200	RING zinc finger protein, putative	56.06	−1.19	3.63×10^{-3}	1.90×10^{-2}
PfIT_090032000	dynein light chain, putative	22.25	−1.94	3.64×10^{-3}	1.90×10^{-2}
PfIT_140022400	dimethyladenosine transferase, putative	541.07	1.09	3.66×10^{-3}	1.91×10^{-2}
PfIT_120020500	peptidyl-prolyl cis-trans isomerase	57.20	−1.48	3.66×10^{-3}	1.91×10^{-2}
PfIT_130032800	conserved Plasmodium protein, unknown function	49.66	−2.25	3.67×10^{-3}	1.91×10^{-2}
PfIT_050012600	conserved Plasmodium protein, unknown function	147.10	−1.80	3.68×10^{-3}	1.92×10^{-2}
PfIT_120015000	porphobilinogen deaminase	40.20	−2.07	3.70×10^{-3}	1.92×10^{-2}
PfIT_040028750	erythrocyte binding antigen-165, pseudogene	423.85	−1.71	3.71×10^{-3}	1.93×10^{-2}
PfIT_080024600	conserved Plasmodium protein, unknown function	692.67	−1.56	3.72×10^{-3}	1.93×10^{-2}
PfIT_140046500	conserved Plasmodium protein, unknown function	162.69	−1.68	3.74×10^{-3}	1.94×10^{-2}
PfIT_080036500	Plasmodium exported protein (PHISTa), unknown function, pseudogene	32.31	1.79	3.76×10^{-3}	1.95×10^{-2}
PfIT_120012600	conserved Plasmodium protein, unknown function	29.59	−2.17	3.79×10^{-3}	1.96×10^{-2}
PfIT_140036500	serine/threonine protein phosphatase 2A activator	133.34	−1.40	3.79×10^{-3}	1.96×10^{-2}
PfIT_090029900	protein phosphatase-beta	41.05	−1.38	3.80×10^{-3}	1.96×10^{-2}
PfIT_120036400	amino acid transporter, putative	696.53	−1.88	3.80×10^{-3}	1.96×10^{-2}
PfIT_130066900	iron-sulfur assembly protein, putative	39.78	−1.64	3.81×10^{-3}	1.96×10^{-2}

Pf_ID	Transcript Product Description	base mean	$\log_2$ FC	p_{value}	p_{adj}
PfIT_120021900	cell traversal protein for ookinetes and sporozoites	85.70	−2.36	3.85×10^{-3}	1.98×10^{-2}
PfIT_140083200	Plasmodium exported protein (hyp6), unknown function	68.50	5.98	3.86×10^{-3}	1.99×10^{-2}
PfIT_040014100	conserved Plasmodium protein, unknown function	129.54	−1.28	3.87×10^{-3}	1.99×10^{-2}
PfIT_010006900	zinc-carboxypeptidase, putative	1373.80	−1.24	3.90×10^{-3}	2.00×10^{-2}
PfIT_120054800	leucine-rich repeat protein	107.52	−1.56	3.91×10^{-3}	2.01×10^{-2}
PfIT_020006700	erythrocyte membrane protein 3	6002.47	2.57	3.92×10^{-3}	2.01×10^{-2}
PfIT_090040600	ring-exported protein 1	75 735.36	1.25	3.92×10^{-3}	2.01×10^{-2}
PfIT_120027100	tRNA-splicing ligase RtcB, putative	132.01	1.15	3.93×10^{-3}	2.01×10^{-2}
PfIT_070027600	conserved Plasmodium protein, unknown function	6197.19	0.92	3.94×10^{-3}	2.01×10^{-2}
PfIT_110040400	3-oxo-5-alpha-steroid 4-dehydrogenase, putative	689.34	−1.02	3.94×10^{-3}	2.01×10^{-2}
PfIT_080031300	SPRY domain, putative	153.70	−1.14	3.99×10^{-3}	2.04×10^{-2}
PfIT_060028500	N-acetylglucosaminylphosphatidylinositol deacetylase, putative	43.85	−1.74	4.04×10^{-3}	2.06×10^{-2}
PfIT_080035000	sporozoite invasion-associated protein 2	16.58	1.98	4.05×10^{-3}	2.06×10^{-2}
PfIT_120023300	thrombospondin-related apical membrane protein	170.06	−1.84	4.06×10^{-3}	2.07×10^{-2}
PfIT_060023900	conserved Plasmodium protein, unknown function	22.18	−1.60	4.09×10^{-3}	2.08×10^{-2}
PfIT_070022800	conserved Plasmodium protein, unknown function	288.22	−1.51	4.11×10^{-3}	2.08×10^{-2}
PfIT_100025400	conserved Plasmodium membrane protein, unknown function	72.77	−1.50	4.11×10^{-3}	2.08×10^{-2}
PfIT_090023000	conserved Plasmodium protein, unknown function	47.33	−1.56	4.11×10^{-3}	2.08×10^{-2}
PfIT_030008800	inner membrane complex protein 1a, putative	56.10	−1.30	4.11×10^{-3}	2.08×10^{-2}
PfIT_100030600	conserved Plasmodium protein, unknown function	15.36	−2.27	4.14×10^{-3}	2.09×10^{-2}
PfIT_100025300	conserved Plasmodium protein, unknown function	252.10	−1.38	4.16×10^{-3}	2.11×10^{-2}
PfIT_140062100	conserved Plasmodium protein, unknown function	220.60	−1.51	4.17×10^{-3}	2.11×10^{-2}

Pf_ID	Transcript Product Description	base mean	$\log_2$ FC	p_{value}	p_{adj}
PfIT_090022100	conserved Plasmodium protein, unknown function	341.22	−1.33	4.19×10^{-3}	2.11×10^{-2}
PfIT_050007200	chromosome assembly factor 1	765.68	−1.29	4.20×10^{-3}	2.12×10^{-2}
PfIT_120022500	snoRNA-associated small subunit rRNA processing protein, putative	3051.15	0.92	4.20×10^{-3}	2.12×10^{-2}
PfIT_060006500	conserved Plasmodium protein, unknown function	979.48	0.81	4.22×10^{-3}	2.12×10^{-2}
PfIT_130048800	conserved Plasmodium protein, unknown function	108.04	−1.16	4.22×10^{-3}	2.12×10^{-2}
PfIT_030020100	conserved Plasmodium protein, unknown function	114.62	−1.36	4.24×10^{-3}	2.13×10^{-2}
PfIT_120008000	peptidyl-prolyl cis-trans isomerase	110.39	−1.09	4.28×10^{-3}	2.15×10^{-2}
PfIT_140033700	conserved Plasmodium protein, unknown function	256.76	−1.28	4.28×10^{-3}	2.15×10^{-2}
PfIT_080029000	conserved Plasmodium protein, unknown function	149.33	−1.87	4.29×10^{-3}	2.15×10^{-2}
PfIT_120042500	periodic tryptophan protein 1, putative	826.41	0.88	4.32×10^{-3}	2.16×10^{-2}
PfIT_100031100	U3 small nucleolar ribonucleoprotein protein MPP10, putative	3115.37	0.89	4.33×10^{-3}	2.16×10^{-2}
PfIT_130015800	ras-related protein Rab-5B	386.14	−1.33	4.33×10^{-3}	2.16×10^{-2}
PfIT_070029000	kelch protein, putative	638.40	−1.65	4.33×10^{-3}	2.16×10^{-2}
PfIT_100005200	Plasmodium exported protein (hyp12), unknown function	242.51	2.18	4.34×10^{-3}	2.17×10^{-2}
PfIT_070032600	alpha/beta hydrolase, putative	50.14	−1.30	4.37×10^{-3}	2.18×10^{-2}
PfIT_120015500	syntaxin, Qa-SNARE family	155.51	−1.17	4.42×10^{-3}	2.20×10^{-2}
PfIT_040008800	transcription factor with AP2 domain(s), putative	60.86	−1.78	4.42×10^{-3}	2.20×10^{-2}
PfIT_020020700	conserved Plasmodium protein, unknown function	255.49	1.21	4.43×10^{-3}	2.20×10^{-2}
PfIT_140026200	conserved Plasmodium protein, unknown function	18.32	−2.05	4.48×10^{-3}	2.22×10^{-2}
PfIT_040016400	conserved Plasmodium protein, unknown function	151.23	−1.23	4.48×10^{-3}	2.22×10^{-2}
PfIT_110034100	phosphatidylinositol-4-phosphate 5-kinase, putative	107.82	−1.62	4.52×10^{-3}	2.24×10^{-2}
PfIT_060018600	conserved Plasmodium protein, unknown function	31.62	−2.01	4.54×10^{-3}	2.25×10^{-2}

Pf_ID	Transcript Product Description	base mean	$\log_2$ FC	p_{value}	p_{adj}
PfIT_140049400	serine/threonine protein kinase	103.22	−1.73	4.55×10^{-3}	2.25×10^{-2}
PfIT_020014800	conserved Plasmodium protein, unknown function	986.20	−1.25	4.55×10^{-3}	2.25×10^{-2}
PfIT_140031800	DEAD/DEAH box helicase, putative	264.87	−1.60	4.56×10^{-3}	2.25×10^{-2}
PfIT_110041100	conserved Plasmodium protein, unknown function	4244.11	0.79	4.58×10^{-3}	2.26×10^{-2}
PfIT_000023900	cytochrome c oxidase subunit 1	129.20	−1.39	4.59×10^{-3}	2.26×10^{-2}
PfIT_070033800	dynein heavy chain, putative	150.47	−1.48	4.59×10^{-3}	2.26×10^{-2}
PfIT_140021900	RNA-binding protein Nova-1, putative	214.61	−1.13	4.59×10^{-3}	2.26×10^{-2}
PfIT_140079900	nucleoporin NUP116/NSP116, putative	232.14	1.38	4.61×10^{-3}	2.27×10^{-2}
PfIT_030029600	rifin	34.90	1.73	4.62×10^{-3}	2.27×10^{-2}
PfIT_080023100	zinc finger protein, putative	788.85	−1.94	4.64×10^{-3}	2.27×10^{-2}
PfIT_130074100	DNA repair endonuclease, putative	142.11	−1.29	4.66×10^{-3}	2.28×10^{-2}
PfIT_090020400	glycolipid transfer protein, putative	15.38	−1.83	4.66×10^{-3}	2.28×10^{-2}
PfIT_100032400	nucleolar preribosomal assembly protein, putative	962.94	1.04	4.67×10^{-3}	2.29×10^{-2}
PfIT_080031900	ATP-dependent RNA helicase DBP10, putative	3885.11	1.04	4.73×10^{-3}	2.31×10^{-2}
PfIT_100028500	conserved Plasmodium protein, unknown function	46.51	−1.58	4.73×10^{-3}	2.31×10^{-2}
PfIT_080016600	conserved Plasmodium protein, unknown function	55.24	−1.67	4.75×10^{-3}	2.32×10^{-2}
PfIT_090041000	ring-exported protein 3	14 132.16	0.99	4.78×10^{-3}	2.33×10^{-2}
PfIT_140073900	conserved Plasmodium protein, unknown function	573.25	1.20	4.78×10^{-3}	2.33×10^{-2}
PfIT_110028500	conserved Plasmodium protein, unknown function	318.20	−1.42	4.79×10^{-3}	2.33×10^{-2}
PfIT_130075000	U2 small nuclear ribonucleoprotein A', putative	158.43	1.14	4.79×10^{-3}	2.33×10^{-2}
PfIT_130049800	U6 snRNA phosphodiesterase, putative	49.70	−1.88	4.80×10^{-3}	2.33×10^{-2}
PfIT_030016900	E3 ubiquitin-protein ligase, putative	143.71	−1.48	4.81×10^{-3}	2.33×10^{-2}
PfIT_100026600	citrate synthase, mitochondrial precursor, putative	641.08	−1.64	4.83×10^{-3}	2.34×10^{-2}
PfIT_060036000	cytoadherence linked asexual protein 2	4.71	−4.57	4.85×10^{-3}	2.35×10^{-2}

Pf_ID	Transcript Product Description	base mean	$\log_2$ FC	p_{value}	p_{adj}
PfIT_010013100	conserved Plasmodium protein, unknown function	72.02	−1.24	4.87×10^{-3}	2.35×10^{-2}
PfIT_100042900	serine/threonine protein kinase, FIKK family	1963.02	2.20	4.88×10^{-3}	2.36×10^{-2}
PfIT_110016700	conserved Plasmodium protein, unknown function	47.21	−1.52	4.90×10^{-3}	2.37×10^{-2}
PfIT_090025600	conserved Plasmodium protein, unknown function	36.86	1.41	4.92×10^{-3}	2.38×10^{-2}
PfIT_110044800	conserved Plasmodium protein, unknown function	158.03	−1.84	4.94×10^{-3}	2.38×10^{-2}
PfIT_110030100	conserved Plasmodium protein, unknown function	48.55	−1.47	4.95×10^{-3}	2.38×10^{-2}
PfIT_140055400	gamete egress and sporozoite traversal protein, putative	68.13	−1.96	4.96×10^{-3}	2.39×10^{-2}
PfIT_030028700	erythrocyte membrane protein 1 (PfEMP1), exon 2, pseudogene	8.04	3.91	4.99×10^{-3}	2.40×10^{-2}
PfIT_060019800	conserved Plasmodium protein, unknown function	600.66	−0.79	5.01×10^{-3}	2.41×10^{-2}
PfIT_140062000	ferlin, putative	211.54	−1.96	5.02×10^{-3}	2.41×10^{-2}
PfIT_060025100	mRNA binding Pumilio-homology domain protein, putative	1152.19	1.07	5.02×10^{-3}	2.41×10^{-2}
PfIT_040019100	GTP-binding protein, putative	444.79	−1.64	5.05×10^{-3}	2.42×10^{-2}
PfIT_050033750	conserved Plasmodium protein, unknown function	579.08	0.81	5.05×10^{-3}	2.42×10^{-2}
PfIT_100016100	conserved Plasmodium protein, unknown function	335.60	−1.46	5.09×10^{-3}	2.43×10^{-2}
PfIT_050030900	conserved Plasmodium protein, unknown function	322.71	−1.58	5.10×10^{-3}	2.44×10^{-2}
PfIT_020021400	conserved Plasmodium protein, unknown function	78.30	−1.27	5.15×10^{-3}	2.46×10^{-2}
PfIT_080026600	clp1-related protein, putative	550.61	1.02	5.19×10^{-3}	2.48×10^{-2}
PfIT_050030400	structural maintenance of chromosomes protein 6, putative	856.47	−1.00	5.22×10^{-3}	2.49×10^{-2}
PfIT_040011400	conserved Plasmodium protein, unknown function	102.38	−1.45	5.24×10^{-3}	2.50×10^{-2}
PfIT_140070800	conserved Plasmodium membrane protein, unknown function	766.96	−1.22	5.25×10^{-3}	2.50×10^{-2}
PfIT_070030600	conserved Plasmodium protein, unknown function	69.25	−1.45	5.29×10^{-3}	2.51×10^{-2}

Pf_ID	Transcript Product Description	base mean	$\log_2$ FC	p_{value}	p_{adj}
PfIT_040028800	surface-associated interspersed protein 4.2 (SURFIN 4.2)	65.76	1.35	5.30×10^{-3}	2.52×10^{-2}
PfIT_140043300	histidine triad protein, putative	174.51	0.97	5.31×10^{-3}	2.52×10^{-2}
PfIT_060008600	glyoxalase I	103.37	−1.25	5.32×10^{-3}	2.52×10^{-2}
PfIT_080033600	conserved Plasmodium protein, unknown function	125.97	−1.69	5.37×10^{-3}	2.55×10^{-2}
PfIT_110021200	conserved Plasmodium protein, unknown function	70.62	−1.64	5.39×10^{-3}	2.55×10^{-2}
PfIT_040019400	arsenical pump-driving ATPase, putative	227.63	0.95	5.42×10^{-3}	2.56×10^{-2}
PfIT_130006500	Plasmodium exported protein (hyp8), unknown function	6794.82	1.74	5.51×10^{-3}	2.60×10^{-2}
PfIT_070032100	actin-like protein, putative	39.18	−1.51	5.53×10^{-3}	2.61×10^{-2}
PfIT_030008300	spindle pole body protein, putative	265.13	−1.22	5.64×10^{-3}	2.66×10^{-2}
PfIT_110050700	CCAAT-box DNA binding protein subunit B	1398.81	−2.06	5.66×10^{-3}	2.67×10^{-2}
PfIT_140021600	uracil-DNA glycosylase	108.86	−1.27	5.66×10^{-3}	2.67×10^{-2}
PfIT_070015100	conserved Plasmodium protein, unknown function	2734.72	−1.03	5.67×10^{-3}	2.67×10^{-2}
PfIT_110006800	Plasmodium exported protein, unknown function	236.67	1.43	5.67×10^{-3}	2.67×10^{-2}
PfIT_120022100:tRNA	tRNA Proline	21.86	1.77	5.68×10^{-3}	2.67×10^{-2}
PfIT_120041600	S-adenosyl-methyltransferase, putative	180.24	−0.96	5.73×10^{-3}	2.69×10^{-2}
PfIT_110011000	conserved Plasmodium protein, unknown function	11.63	−2.17	5.77×10^{-3}	2.70×10^{-2}
PfIT_130024600	N2,N2-dimethylguanosine tRNA methyltransferase, putative	1443.52	1.00	5.79×10^{-3}	2.71×10^{-2}
PfIT_130046900	GPI mannosyltransferase 3	49.95	−1.85	5.81×10^{-3}	2.72×10^{-2}
PfIT_140039700	chromatin assembly factor 1 P55 subunit, putative	92.05	−1.15	5.82×10^{-3}	2.72×10^{-2}
PfIT_110050000	conserved Plasmodium protein, unknown function	348.82	1.11	5.84×10^{-3}	2.73×10^{-2}
PfIT_090038300	gamma-tubulin complex component, putative	177.44	−0.90	5.85×10^{-3}	2.73×10^{-2}
PfIT_100041400	enhancer of rudimentary homolog, putative	244.39	1.41	5.86×10^{-3}	2.73×10^{-2}

Pf_ID	Transcript Product Description	base mean	$\log_2$ FC	p_{value}	p_{adj}
PfIT_070031500	conserved Plasmodium protein, unknown function	30.00	1.97	5.89×10^{-3}	2.74×10^{-2}
PfIT_020010500	conserved Plasmodium protein, unknown function	635.90	0.99	5.90×10^{-3}	2.75×10^{-2}
PfIT_100024800	histone acetyltransferase, putative	1629.52	0.88	5.92×10^{-3}	2.75×10^{-2}
PfIT_080010200	conserved Plasmodium protein, unknown function	79.79	−1.72	5.97×10^{-3}	2.77×10^{-2}
PfIT_140056600	conserved Plasmodium protein, unknown function	79.20	1.19	6.02×10^{-3}	2.80×10^{-2}
PfIT_100006900	conserved Plasmodium protein, unknown function	282.73	−0.95	6.03×10^{-3}	2.80×10^{-2}
PfIT_120021800	male development gene 1	137.53	−1.24	6.05×10^{-3}	2.81×10^{-2}
PfIT_020022900	ATP-dependent rRNA helicase RRP3, putative	1140.13	1.10	6.09×10^{-3}	2.82×10^{-2}
PfIT_080010300	gamete release protein, putative	847.29	−1.80	6.09×10^{-3}	2.82×10^{-2}
PfIT_040025000	conserved Plasmodium protein, unknown function	339.94	−1.34	6.11×10^{-3}	2.83×10^{-2}
PfIT_120048300	syntaxin, Qa-SNARE family	72.26	−1.44	6.15×10^{-3}	2.84×10^{-2}
PfIT_110024000	conserved Plasmodium protein, unknown function	94.90	−1.44	6.17×10^{-3}	2.85×10^{-2}
PfIT_020019100	serine/threonine protein kinase, putative	2626.26	−1.79	6.22×10^{-3}	2.87×10^{-2}
PfIT_090011800	conserved Plasmodium protein, unknown function	165.32	0.90	6.27×10^{-3}	2.89×10^{-2}
PfIT_050008600	conserved Plasmodium protein, unknown function	168.28	−1.06	6.28×10^{-3}	2.89×10^{-2}
PfIT_080023600	BEM46-like protein, putative	492.70	−1.77	6.28×10^{-3}	2.89×10^{-2}
PfIT_140071700	conserved Plasmodium protein, unknown function	758.78	1.03	6.34×10^{-3}	2.91×10^{-2}
PfIT_140023200	conserved Plasmodium protein, unknown function	134.95	−1.24	6.35×10^{-3}	2.91×10^{-2}
PfIT_120008600	origin recognition complex subunit 1	661.40	−0.99	6.35×10^{-3}	2.91×10^{-2}
PfIT_010006300	conserved Plasmodium protein, unknown function	47.04	−1.32	6.35×10^{-3}	2.91×10^{-2}
PfIT_100027900	conserved Plasmodium protein, unknown function	193.73	−2.17	6.37×10^{-3}	2.92×10^{-2}
PfIT_100040300	conserved Plasmodium protein, unknown function	57.15	−1.36	6.37×10^{-3}	2.92×10^{-2}

Pf_ID	Transcript Product Description	base mean	$\log_2$ FC	p_{value}	p_{adj}
PfIT_140071600	tRNA 3'-trailer sequence RNase, putative	517.60	1.22	6.38×10^{-3}	2.92×10^{-2}
PfIT_130066300	protein arginine N-methyltransferase 5, putative	374.09	1.02	6.39×10^{-3}	2.92×10^{-2}
PfIT_050030700	WD repeat-containing protein, putative	440.84	1.11	6.39×10^{-3}	2.92×10^{-2}
PfIT_120037600	conserved Plasmodium protein, unknown function	240.33	−1.84	6.40×10^{-3}	2.92×10^{-2}
PfIT_140007400	Glycophorin-binding protein, putative	9.47	−2.82	6.41×10^{-3}	2.92×10^{-2}
PfIT_140063300	conserved protein, unknown function	258.66	1.48	6.47×10^{-3}	2.95×10^{-2}
PfIT_030008500	lipoamide acyltransferase component of branched-chain alpha-keto acid dehydrogenase complex	283.71	−0.93	6.55×10^{-3}	2.98×10^{-2}
PfIT_020020900	vacuolar protein sorting-associated protein 45, putative	87.16	−1.27	6.57×10^{-3}	2.98×10^{-2}
PfIT_040021900	memo-like protein	230.35	−1.13	6.57×10^{-3}	2.98×10^{-2}
PfIT_130016200	protein ISD11, putative	118.81	1.15	6.59×10^{-3}	2.99×10^{-2}
PfIT_120041300	conserved Plasmodium protein, unknown function	540.44	0.82	6.60×10^{-3}	2.99×10^{-2}
PfIT_140032300	conserved Plasmodium protein, unknown function	401.66	1.14	6.63×10^{-3}	3.00×10^{-2}
PfIT_070014400	conserved Plasmodium protein, unknown function	53.45	−1.21	6.64×10^{-3}	3.00×10^{-2}
PfIT_110016100	conserved Plasmodium protein, unknown function	114.86	1.16	6.64×10^{-3}	3.00×10^{-2}
PfIT_090032400	phosphatidylserine decarboxylase	871.24	−0.94	6.66×10^{-3}	3.01×10^{-2}
PfIT_070033200	60S ribosomal export protein NMD3, putative	1132.02	1.05	6.66×10^{-3}	3.01×10^{-2}
PfIT_070006700	rifin	6.95	3.82	6.67×10^{-3}	3.01×10^{-2}
PfIT_110047100	conserved Plasmodium protein, unknown function	44.61	−2.52	6.67×10^{-3}	3.01×10^{-2}
PfIT_070020600	conserved Plasmodium protein, unknown function	2026.96	−0.96	6.67×10^{-3}	3.01×10^{-2}
PfIT_010007300	actin-related protein	96.70	−1.51	6.68×10^{-3}	3.01×10^{-2}
PfIT_130059700	large subunit rRNA methyltransferase, putative	6602.03	0.89	6.69×10^{-3}	3.01×10^{-2}
PfIT_140082300	early transcribed membrane protein 14.2	26.52	2.03	6.72×10^{-3}	3.02×10^{-2}

Pf_ID	Transcript Product Description	base mean	$\log_2$ FC	p_{value}	p_{adj}
PfIT_030019300	conserved Plasmodium protein, unknown function	646.26	0.94	6.74×10^{-3}	3.02×10^{-2}
PfIT_040022100	conserved Plasmodium protein, unknown function	34.21	−1.89	6.74×10^{-3}	3.02×10^{-2}
PfIT_140011100	rRNA biogenesis protein RRP5, putative	716.87	0.80	6.76×10^{-3}	3.03×10^{-2}
PfIT_130018600	peptidyl-prolyl cis-trans isomerase, putative	35.96	−1.37	6.79×10^{-3}	3.04×10^{-2}
PfIT_140058300	ribosome biogenesis protein TSR1, putative	1529.56	0.85	6.83×10^{-3}	3.06×10^{-2}
PfIT_090037200	peptide release factor, putative	131.58	−1.33	6.86×10^{-3}	3.07×10^{-2}
PfIT_060013000	conserved Plasmodium protein, unknown function	95.26	−1.38	6.86×10^{-3}	3.07×10^{-2}
PfIT_080010400	conserved Plasmodium protein, unknown function	572.98	−2.13	6.88×10^{-3}	3.07×10^{-2}
PfIT_060009500	cyclin dependent kinase binding protein, putative	71.51	−1.60	6.90×10^{-3}	3.08×10^{-2}
PfIT_130071400	conserved Plasmodium protein, unknown function	165.47	−1.13	6.90×10^{-3}	3.08×10^{-2}
PfIT_060031700	ribonuclease P protein subunit p29, putative	623.49	0.89	6.91×10^{-3}	3.08×10^{-2}
PfIT_080024000	conserved Plasmodium protein, unknown function	2862.59	0.83	6.92×10^{-3}	3.08×10^{-2}
PfIT_120036000	conserved Plasmodium protein, unknown function	240.96	−1.29	6.93×10^{-3}	3.08×10^{-2}
PfIT_040012600	conserved Plasmodium protein, unknown function	332.57	−1.87	6.94×10^{-3}	3.08×10^{-2}
PfIT_090018200	conserved Plasmodium protein, unknown function	215.43	−1.36	6.95×10^{-3}	3.09×10^{-2}
PfIT_140012400	ribosome biogenesis protein BOP1, putative	4584.57	0.80	6.97×10^{-3}	3.09×10^{-2}
PfIT_010009200	DNA binding protein, putative	73.07	−1.39	6.99×10^{-3}	3.10×10^{-2}
PfIT_120052000	signal recognition particle receptor, beta subunit	311.08	−0.84	7.04×10^{-3}	3.12×10^{-2}
PfIT_140075800	conserved Plasmodium protein, unknown function	39.25	1.34	7.10×10^{-3}	3.14×10^{-2}
PfIT_100027100	conserved Plasmodium membrane protein, unknown function	323.72	−1.63	7.13×10^{-3}	3.15×10^{-2}

Pf_ID	Transcript Product Description	base mean	$\log_2$ FC	p_{value}	p_{adj}
PfIT_070027300	conserved Plasmodium protein, unknown function	5.95	−4.06	7.13×10^{-3}	3.15×10^{-2}
PfIT_040007000	stevor	2.57	4.93	7.14×10^{-3}	3.15×10^{-2}
PfIT_120031900	ataxin-3, putative	241.63	−1.19	7.14×10^{-3}	3.15×10^{-2}
PfIT_060015300	conserved Plasmodium protein, unknown function	105.12	−1.19	7.15×10^{-3}	3.15×10^{-2}
PfIT_140021800	DNA-directed RNA polymerases I and III subunit RPAC2, putative	159.77	0.98	7.17×10^{-3}	3.16×10^{-2}
PfIT_100014200	DNA2/NAM7 helicase, putative	2014.63	0.90	7.18×10^{-3}	3.16×10^{-2}
PfIT_080022900	high mobility group protein B2	1688.23	−0.92	7.26×10^{-3}	3.19×10^{-2}
PfIT_140084700	EMP1-trafficking protein	1006.10	2.41	7.26×10^{-3}	3.19×10^{-2}
PfIT_050023800	WD repeat-containing protein 26, putative	285.55	−1.07	7.28×10^{-3}	3.19×10^{-2}
PfIT_080019600	conserved Plasmodium protein, unknown function	65.15	−1.90	7.29×10^{-3}	3.20×10^{-2}
PfIT_120036300	conserved Plasmodium protein, unknown function	99.83	−1.63	7.32×10^{-3}	3.21×10^{-2}
PfIT_090030900	monocarboxylate transporter, putative	156.08	−0.98	7.36×10^{-3}	3.22×10^{-2}
PfIT_030011400	conserved Plasmodium protein, unknown function	50.03	−1.29	7.41×10^{-3}	3.24×10^{-2}
PfIT_060009200	conserved Plasmodium protein, unknown function	90.40	−1.23	7.45×10^{-3}	3.25×10^{-2}
PfIT_110037100	amino acid transporter, putative	21.72	−1.78	7.46×10^{-3}	3.26×10^{-2}
PfIT_110043900	adrenodoxin reductase, putative	253.56	−1.63	7.48×10^{-3}	3.26×10^{-2}
PfIT_090039100	conserved Plasmodium protein, unknown function	30.80	−1.88	7.52×10^{-3}	3.28×10^{-2}
PfIT_140062400	transcription factor with AP2 domain(s)	435.57	−1.31	7.52×10^{-3}	3.28×10^{-2}
PfIT_120007100	XPA binding protein 1, putative	881.23	0.97	7.54×10^{-3}	3.28×10^{-2}
PfIT_040006600	surface-associated interspersed protein 4.1 (SURFIN 4.1)	969.92	−2.04	7.55×10^{-3}	3.29×10^{-2}
PfIT_080008800	AAA family ATPase, putative	1171.48	−1.28	7.59×10^{-3}	3.30×10^{-2}
PfIT_110043600	transcription factor with AP2 domain(s)	1536.38	2.04	7.65×10^{-3}	3.32×10^{-2}
PfIT_110024800	tRNA nucleotidyltransferase, putative	690.90	0.74	7.67×10^{-3}	3.33×10^{-2}
PfIT_090010800	vacuolar protein sorting-associated protein 46, putative	120.70	−1.36	7.68×10^{-3}	3.33×10^{-2}

Pf_ID	Transcript Product Description	base mean	$\log_2$ FC	p_{value}	p_{adj}
PfIT_110034600	60S ribosomal protein L38	2134.19	1.08	7.69×10^{-3}	3.33×10^{-2}
PfIT_050035300	phosphoenolpyruvate/phosphate translocator	143.03	−1.47	7.69×10^{-3}	3.33×10^{-2}
PfIT_130039300	conserved Plasmodium protein, unknown function	45.83	−1.55	7.71×10^{-3}	3.33×10^{-2}
PfIT_140041400	cytochrome c oxidase assembly protein, putative	139.18	−1.39	7.71×10^{-3}	3.33×10^{-2}
PfIT_140081800	bromodomain protein, putative	1052.42	0.83	7.73×10^{-3}	3.34×10^{-2}
PfIT_130008000	conserved Plasmodium protein, unknown function	88.18	1.16	7.74×10^{-3}	3.34×10^{-2}
PfIT_060015000	SNARE associated Golgi protein, putative	17.29	−1.92	7.77×10^{-3}	3.35×10^{-2}
PfIT_120015400	50S ribosomal protein L1, apicoplast, putative	116.89	−1.14	7.77×10^{-3}	3.35×10^{-2}
PfIT_070035000	Plasmodium exported protein, unknown function	286.95	1.01	7.78×10^{-3}	3.35×10^{-2}
PfIT_100030500	cell division cycle protein 20 homolog, putative	26.20	−1.71	7.79×10^{-3}	3.35×10^{-2}
PfIT_110030600	autophagy-related protein 7, putative	220.74	−1.28	7.81×10^{-3}	3.35×10^{-2}
PfIT_040020700	DNA helicase MCM9, putative	281.86	−1.19	7.81×10^{-3}	3.35×10^{-2}
PfIT_050033900	nucleolar preribosomal GTPase, putative	439.47	1.06	7.83×10^{-3}	3.36×10^{-2}
PfIT_140014800	transcription factor with AP2 domain(s), putative	2086.53	1.01	7.83×10^{-3}	3.36×10^{-2}
PfIT_090023700	PPPDE peptidase, putative	364.22	−1.71	7.88×10^{-3}	3.37×10^{-2}
PfIT_140017700	conserved Plasmodium membrane protein, unknown function	534.63	−2.14	7.89×10^{-3}	3.38×10^{-2}
PfIT_130063800	conserved Plasmodium protein, unknown function	71.65	−1.67	7.89×10^{-3}	3.38×10^{-2}
PfIT_130033300	conserved Plasmodium protein, unknown function	166.07	−1.08	7.90×10^{-3}	3.38×10^{-2}
PfIT_120043800	protein kinase 2	131.20	−1.23	7.91×10^{-3}	3.38×10^{-2}
PfIT_120030500	conserved Plasmodium protein, unknown function	280.19	1.07	7.94×10^{-3}	3.39×10^{-2}
PfIT_120038200	conserved Plasmodium protein, unknown function	165.27	−1.53	7.95×10^{-3}	3.39×10^{-2}
PfIT_140035300	conserved Plasmodium protein, unknown function	398.01	−0.94	7.95×10^{-3}	3.39×10^{-2}

Pf_ID	Transcript Product Description	base mean	$\log_2$ FC	p_{value}	p_{adj}
PfIT_070009300	phosphoinositide-binding protein, putative	587.98	−1.11	7.98×10^{-3}	3.40×10^{-2}
PfIT_040023600	protein transport protein GOT1, putative	63.93	−1.39	7.99×10^{-3}	3.40×10^{-2}
PfIT_120013500	conserved Plasmodium protein, unknown function	753.88	0.81	8.12×10^{-3}	3.45×10^{-2}
PfIT_050024500	cytochrome c oxidase assembly protein (heme A: farnesyltransferase), putative	105.90	−1.09	8.15×10^{-3}	3.46×10^{-2}
PfIT_030026900	RNA triphosphatase	1170.00	0.96	8.15×10^{-3}	3.46×10^{-2}
PfIT_140036900	conserved Plasmodium protein, unknown function	20.53	−1.89	8.18×10^{-3}	3.47×10^{-2}
PfIT_110043500	conserved Plasmodium protein, unknown function	86.48	1.12	8.19×10^{-3}	3.47×10^{-2}
PfIT_040022400	conserved Plasmodium protein, unknown function	176.98	−1.25	8.24×10^{-3}	3.49×10^{-2}
PfIT_110037200	pre-mRNA-splicing factor 38A, putative	887.39	0.78	8.25×10^{-3}	3.49×10^{-2}
PfIT_020005600	rifin	8.50	3.13	8.25×10^{-3}	3.49×10^{-2}
PfIT_040018600	calmodulin-like protein	17.31	−1.85	8.26×10^{-3}	3.49×10^{-2}
PfIT_130006600	surface-associated interspersed protein	50.04	1.43	8.26×10^{-3}	3.49×10^{-2}
PfIT_100021700	conserved Plasmodium protein, unknown function	7467.81	0.80	8.32×10^{-3}	3.51×10^{-2}
PfIT_140035500	apicoplast ribosomal protein L15 precursor, putative	510.51	−0.92	8.33×10^{-3}	3.51×10^{-2}
PfIT_060033600	cullin-like protein, putative	1704.60	0.78	8.34×10^{-3}	3.51×10^{-2}
PfIT_020013300	ribosome-recycling factor	511.26	−1.04	8.35×10^{-3}	3.51×10^{-2}
PfIT_140028600	mitochondrial ribosomal protein L21 precursor, putative	256.39	−1.38	8.37×10^{-3}	3.52×10^{-2}
PfIT_030020200	conserved Plasmodium protein, unknown function	73.34	−1.06	8.40×10^{-3}	3.53×10^{-2}
PfIT_090015600	DNA primase large subunit, putative	117.90	−1.62	8.45×10^{-3}	3.55×10^{-2}
PfIT_070010600	40S ribosomal protein S29, putative	1399.93	1.14	8.48×10^{-3}	3.56×10^{-2}
PfIT_130062900	DNA helicase, putative	375.43	−1.09	8.49×10^{-3}	3.56×10^{-2}
PfIT_100035600	protein phosphatase inhibitor 3	138.37	−0.96	8.50×10^{-3}	3.56×10^{-2}
PfIT_110051400	conserved Plasmodium protein, unknown function	1165.47	−1.15	8.51×10^{-3}	3.56×10^{-2}

Pf_ID	Transcript Product Description	base mean	$\log_2$ FC	p_{value}	p_{adj}
PfIT_110045100	conserved Plasmodium protein, unknown function	69.37	−1.33	8.54×10^{-3}	3.57×10^{-2}
PfIT_000006600	Plasmodium RESA N-terminal, putative	400.33	0.86	8.54×10^{-3}	3.57×10^{-2}
PfIT_100017400	conserved Plasmodium protein, unknown function	253.10	−1.49	8.58×10^{-3}	3.58×10^{-2}
PfIT_120052400	conserved Plasmodium protein, unknown function	105.38	1.04	8.58×10^{-3}	3.58×10^{-2}
PfIT_050017400	CDK-activating kinase assembly factor	173.64	1.06	8.68×10^{-3}	3.62×10^{-2}
PfIT_010007400	parasite-infected erythrocyte surface protein	207.55	−0.82	8.75×10^{-3}	3.64×10^{-2}
PfIT_140076450	conserved Plasmodium protein, unknown function	496.55	0.86	8.76×10^{-3}	3.65×10^{-2}
PfIT_050007900	conserved Plasmodium protein, unknown function	30.08	1.91	8.80×10^{-3}	3.66×10^{-2}
PfIT_020006800	knob-associated histidine-rich protein	48 433.33	2.04	8.81×10^{-3}	3.66×10^{-2}
PfIT_090009400	bacterial histone-like protein	48.32	−1.74	8.85×10^{-3}	3.68×10^{-2}
PfIT_090026800	conserved Plasmodium protein, unknown function	42.42	−1.79	8.89×10^{-3}	3.69×10^{-2}
PfIT_140035000	peptide chain release factor 1, putative	131.26	−1.08	8.90×10^{-3}	3.69×10^{-2}
PfIT_120019300	conserved Plasmodium protein, unknown function	76.31	−1.37	8.91×10^{-3}	3.69×10^{-2}
PfIT_080018800	GDP-mannose 4,6-dehydratase	108.32	−1.26	8.96×10^{-3}	3.71×10^{-2}
PfIT_140028100	mitochondrial import inner membrane translocase subunit TIM8, putative	53.26	1.17	8.97×10^{-3}	3.71×10^{-2}
PfIT_080019300	ATPase, putative	948.59	0.73	9.06×10^{-3}	3.74×10^{-2}
PfIT_140044200	trafficking protein particle complex subunit 5, putative	222.07	1.08	9.08×10^{-3}	3.75×10^{-2}
PfIT_090036300	conserved Plasmodium protein, unknown function	130.21	−1.48	9.08×10^{-3}	3.75×10^{-2}
PfIT_130009300	CorA-like Mg2+ transporter protein, putative	119.91	−1.50	9.08×10^{-3}	3.75×10^{-2}
PfIT_120008700	conserved Plasmodium protein, unknown function	567.00	1.06	9.10×10^{-3}	3.75×10^{-2}
PfIT_000006000	serine/threonine protein kinase, FIKK family	251.49	−1.78	9.17×10^{-3}	3.78×10^{-2}

Pf_ID	Transcript Product Description	base mean	$\log_2$ FC	p_{value}	p_{adj}
PfIT_080032500	conserved Plasmodium protein, unknown function	426.70	−1.01	9.19×10^{-3}	3.78×10^{-2}
PfIT_090013100	conserved Plasmodium membrane protein, unknown function	95.77	−1.25	9.24×10^{-3}	3.80×10^{-2}
PfIT_090040900	Plasmodium exported protein (hyp11), unknown function	374.02	2.17	9.24×10^{-3}	3.80×10^{-2}
PfIT_070007300	small exported membrane protein 1	1181.89	1.98	9.27×10^{-3}	3.81×10^{-2}
PfIT_050021700	metabolite/drug transporter, putative	115.86	−1.24	9.31×10^{-3}	3.82×10^{-2}
PfIT_000023800	cytochrome b	144.76	−1.25	9.33×10^{-3}	3.82×10^{-2}
PfIT_090028300	thioredoxin reductase	312.94	−1.48	9.34×10^{-3}	3.83×10^{-2}
PfIT_060034100	DNA polymerase epsilon catalytic subunit A, putative	317.60	−1.01	9.37×10^{-3}	3.83×10^{-2}
PfIT_040012500	AAA family ATPase, putative	965.15	−1.85	9.38×10^{-3}	3.83×10^{-2}
PfIT_030009200	60S ribosomal protein L44	3161.36	1.13	9.40×10^{-3}	3.84×10^{-2}
PfIT_140067300	apicoplast ribosomal protein S10, putative	62.06	−1.80	9.40×10^{-3}	3.84×10^{-2}
PfIT_070012700	RAP protein, putative	266.77	−0.98	9.41×10^{-3}	3.84×10^{-2}
PfIT_080028600	lipoate-protein ligase B	89.01	1.34	9.42×10^{-3}	3.84×10^{-2}
PfIT_140078900	DNA-directed RNA polymerase, alpha subunit, putative	70.30	−1.18	9.43×10^{-3}	3.84×10^{-2}
PfIT_140036300	ADP-dependent DNA helicase RecQ	259.37	−0.83	9.43×10^{-3}	3.84×10^{-2}
PfIT_130048600	conserved Plasmodium protein, unknown function	995.09	−0.92	9.44×10^{-3}	3.84×10^{-2}
PfIT_140029900	conserved Plasmodium membrane protein, unknown function	25.01	−1.92	9.47×10^{-3}	3.85×10^{-2}
PfIT_140026400	conserved Plasmodium protein, unknown function	5995.55	0.80	9.49×10^{-3}	3.86×10^{-2}
PfIT_050011900	GTPase-activating protein, putative	307.28	−0.84	9.60×10^{-3}	3.89×10^{-2}
PfIT_100008700	conserved Plasmodium protein, unknown function	44.79	−1.94	9.60×10^{-3}	3.89×10^{-2}
PfIT_140012300	RING zinc finger protein, putative	369.46	−1.22	9.64×10^{-3}	3.90×10^{-2}
PfIT_090028000	cyclin-dependent kinases regulatory subunit, putative	61.72	−1.45	9.64×10^{-3}	3.90×10^{-2}
PfIT_060034700	ATP-dependent RNA helicase HAS1	1396.00	0.86	9.64×10^{-3}	3.90×10^{-2}
PfIT_120047800	conserved protein, unknown function	81.38	−1.23	9.68×10^{-3}	3.91×10^{-2}
PfIT_130020600	conserved Plasmodium protein, unknown function	75.47	−1.72	9.71×10^{-3}	3.92×10^{-2}

Pf_ID	Transcript Product Description	base mean	$\log_2$ FC	p_{value}	p_{adj}
PfIT_070009700	conserved Plasmodium protein, unknown function	239.82	−1.33	9.72×10^{-3}	3.93×10^{-2}
PfIT_140077000	conserved Plasmodium protein, unknown function	223.03	−1.04	9.76×10^{-3}	3.94×10^{-2}
PfIT_050018200	conserved Plasmodium protein, unknown function	197.17	−1.03	9.79×10^{-3}	3.94×10^{-2}
PfIT_050011400	60S ribosomal subunit protein L24-2, putative	646.31	0.84	9.79×10^{-3}	3.94×10^{-2}
PfIT_120033200	leucine-rich repeat protein	89.82	−1.26	9.79×10^{-3}	3.94×10^{-2}
PfIT_110006200	exported protein family 3	2.34	4.80	9.80×10^{-3}	3.94×10^{-2}
PfIT_030025700	histone H2A variant, putative	3146.12	−0.84	9.87×10^{-3}	3.97×10^{-2}
PfIT_060027000	ferredoxin–NADP reductase	281.55	1.06	9.88×10^{-3}	3.97×10^{-2}
PfIT_070021800	calcium-dependent protein kinase 4	2060.54	−1.38	9.92×10^{-3}	3.98×10^{-2}
PfIT_090014300	conserved Plasmodium protein, unknown function	174.63	−1.58	9.93×10^{-3}	3.98×10^{-2}
PfIT_040011300	conserved Plasmodium protein, unknown function	164.01	−1.56	9.96×10^{-3}	3.99×10^{-2}
PfIT_070011200	conserved Plasmodium protein, unknown function	283.71	−1.36	9.99×10^{-3}	4.00×10^{-2}
PfIT_140033200	conserved Plasmodium protein, unknown function	1555.79	0.80	1.00×10^{-2}	4.00×10^{-2}
PfIT_060014000	mitochondrial ribosomal protein L19 precursor, putative	99.20	−1.16	1.00×10^{-2}	4.02×10^{-2}
PfIT_110038800	conserved Plasmodium protein, unknown function	1148.05	0.99	1.01×10^{-2}	4.02×10^{-2}
PfIT_130010100	conserved Plasmodium protein, unknown function	369.49	−1.09	1.01×10^{-2}	4.03×10^{-2}
PfIT_130013300	carbamoyl phosphate synthetase	8220.96	0.91	1.01×10^{-2}	4.04×10^{-2}
PfIT_140038300	inner membrane complex suture component, putative	78.30	−1.59	1.02×10^{-2}	4.05×10^{-2}
PfIT_090035800	nucleolar protein Nop52, putative	5212.34	0.76	1.02×10^{-2}	4.06×10^{-2}
PfIT_070031000	conserved Plasmodium protein, unknown function	78.92	−1.32	1.02×10^{-2}	4.06×10^{-2}
PfIT_120015300	ABC transporter B family member 7, putative	123.45	−1.33	1.02×10^{-2}	4.06×10^{-2}
PfIT_120039500	protein TOC75, putative	175.14	−1.54	1.02×10^{-2}	4.06×10^{-2}
PfIT_140069300	conserved Plasmodium protein, unknown function	71.86	1.16	1.03×10^{-2}	4.07×10^{-2}

Pf_ID	Transcript Product Description	base mean	$\log_2$ FC	p_{value}	p_{adj}
PfIT_140008000	lysophospholipase, putative	380.24	1.26	1.03×10^{-2}	4.08×10^{-2}
PfIT_090029800	proline–tRNA ligase, putative	190.06	−1.33	1.03×10^{-2}	4.08×10^{-2}
PfIT_080027200	conserved Plasmodium membrane protein, unknown function	97.39	1.35	1.03×10^{-2}	4.09×10^{-2}
PfIT_140076700	phosphodiesterase delta, putative	26.27	−1.62	1.04×10^{-2}	4.10×10^{-2}
PfIT_110049900	bicoid-interacting protein BIN3, putative	24.65	−1.58	1.04×10^{-2}	4.10×10^{-2}
PfIT_130030900	mitochondrial fission 1 protein, putative	38.94	−1.42	1.04×10^{-2}	4.12×10^{-2}
PfIT_050006700	skeleton-binding protein 1	22 899.55	1.29	1.04×10^{-2}	4.13×10^{-2}
PfIT_130026900	phosphodiesterase gamma, putative	58.89	−1.46	1.05×10^{-2}	4.13×10^{-2}
PfIT_100036300	phosphatidylinositol N-acetylglucosaminyltransferase subunit A, putative	188.28	−1.17	1.05×10^{-2}	4.15×10^{-2}
PfIT_130050000	conserved Plasmodium protein, unknown function	153.83	1.03	1.05×10^{-2}	4.16×10^{-2}
PfIT_100019800	ribonucleotide reductase small subunit, putative	304.06	−1.22	1.06×10^{-2}	4.16×10^{-2}
PfIT_090031500	CS domain protein, putative	105.80	−0.94	1.06×10^{-2}	4.16×10^{-2}
PfIT_140033500	lipase, putative	5936.57	0.77	1.06×10^{-2}	4.17×10^{-2}
PfIT_080008600	mitogen-activated protein kinase organizer 1, putative	108.74	−1.03	1.07×10^{-2}	4.19×10^{-2}
PfIT_110039300	DNA-directed RNA polymerase I subunit RPA2, putative	2198.01	0.87	1.07×10^{-2}	4.19×10^{-2}
PfIT_110046900	methyltransferase, putative	622.75	1.09	1.07×10^{-2}	4.20×10^{-2}
PfIT_130028500	V-type proton ATPase subunit G, putative	417.09	1.08	1.07×10^{-2}	4.20×10^{-2}
PfIT_080020300	FAD-dependent monooxygenase, putative	84.79	−1.10	1.07×10^{-2}	4.21×10^{-2}
PfIT_090013800	conserved Plasmodium membrane protein, unknown function	26.17	−1.82	1.08×10^{-2}	4.23×10^{-2}
PfIT_100029300	conserved Plasmodium protein, unknown function	62.16	−1.32	1.08×10^{-2}	4.24×10^{-2}
PfIT_120005600	rifin	433.62	1.19	1.08×10^{-2}	4.24×10^{-2}
PfIT_110010900	exonuclease, putative	493.79	−0.84	1.09×10^{-2}	4.25×10^{-2}
PfIT_060035600	rifin	4.52	3.85	1.09×10^{-2}	4.25×10^{-2}
PfIT_010016800	DBL containing protein, unknown function	67.05	0.97	1.09×10^{-2}	4.25×10^{-2}

Pf_ID	Transcript Product Description	base mean	$\log_2$ FC	p_{value}	p_{adj}
PfIT_140051600	ATP-dependent RNA helicase MAK5, putative	2372.12	1.10	1.09×10^{-2}	4.25×10^{-2}
PfIT_130042700	conserved Plasmodium protein, unknown function	884.05	0.84	1.09×10^{-2}	4.25×10^{-2}
PfIT_130014500	HORMA domain protein, putative	448.86	−0.85	1.09×10^{-2}	4.26×10^{-2}
PfIT_050030500	conserved Plasmodium protein, unknown function	32.14	−1.82	1.09×10^{-2}	4.26×10^{-2}
PfIT_040019600	conserved Plasmodium protein, unknown function	116.26	−1.10	1.10×10^{-2}	4.26×10^{-2}
PfIT_110012200	conserved Plasmodium protein, unknown function	13.56	1.86	1.10×10^{-2}	4.28×10^{-2}
PfIT_050028800	conserved Plasmodium protein, unknown function	112.87	−0.98	1.10×10^{-2}	4.28×10^{-2}
PfIT_140052100	conserved Plasmodium protein, unknown function	2620.41	0.83	1.11×10^{-2}	4.30×10^{-2}
PfIT_090025700	conserved Plasmodium membrane protein, unknown function	863.51	1.06	1.11×10^{-2}	4.30×10^{-2}
PfIT_100023800	conserved Plasmodium protein, unknown function	491.35	−0.99	1.11×10^{-2}	4.30×10^{-2}
PfIT_130058500	Plasmodium exported protein, unknown function	2997.73	1.39	1.11×10^{-2}	4.31×10^{-2}
PfIT_120036200	conserved Plasmodium protein, unknown function	398.52	−1.63	1.11×10^{-2}	4.31×10^{-2}
PfIT_080015600	conserved Plasmodium protein, unknown function	51.42	1.66	1.12×10^{-2}	4.33×10^{-2}
PfIT_130036000	GPI transamidase subunit PIG-U, putative	73.46	−1.17	1.12×10^{-2}	4.34×10^{-2}
PfIT_090005500	rifin	12.33	2.74	1.12×10^{-2}	4.34×10^{-2}
PfIT_140032700	dynein-associated protein, putative	57.75	−1.41	1.14×10^{-2}	4.39×10^{-2}
PfIT_130063500	small subunit rRNA processing factor, putative	5286.38	0.76	1.14×10^{-2}	4.39×10^{-2}
PfIT_020011100	EPSP synthase (3-phosphoshikimate 1-carboxyvinyltransferase)/Shikimate kinase, putative	1506.53	1.07	1.14×10^{-2}	4.40×10^{-2}
PfIT_000009600	rifin	110.46	1.24	1.14×10^{-2}	4.40×10^{-2}
PfIT_060010800	probable protein, unknown function	195.37	−1.07	1.14×10^{-2}	4.40×10^{-2}
PfIT_130006900	EMP1-trafficking protein	2116.73	1.03	1.15×10^{-2}	4.41×10^{-2}
PfIT_080016100	ER membrane protein complex subunit 1, putative	460.04	0.89	1.15×10^{-2}	4.41×10^{-2}

Pf_ID	Transcript Product Description	base mean	$\log_2$ FC	p_{value}	p_{adj}
PfIT_030017800	conserved Plasmodium protein, unknown function	500.35	0.94	1.15×10^{-2}	4.43×10^{-2}
PfIT_050035900	CPW-WPC family protein	52.99	−1.26	1.16×10^{-2}	4.44×10^{-2}
PfIT_040010200	conserved Plasmodium protein, unknown function	181.37	1.10	1.16×10^{-2}	4.44×10^{-2}
PfIT_090021200	methyltransferase, putative	127.04	1.07	1.16×10^{-2}	4.44×10^{-2}
PfIT_070008800	conserved Plasmodium membrane protein, unknown function	2183.05	0.91	1.16×10^{-2}	4.44×10^{-2}
PfIT_050037500	rifin	2.27	4.76	1.16×10^{-2}	4.45×10^{-2}
PfIT_130070000	DNA-directed RNA polymerases I, II, and III subunit RPABC1, putative	1042.74	0.84	1.16×10^{-2}	4.45×10^{-2}
PfIT_050024900	conserved Plasmodium protein, unknown function	3140.71	0.90	1.17×10^{-2}	4.46×10^{-2}
PfIT_130074800	conserved Plasmodium protein, unknown function	984.14	0.94	1.17×10^{-2}	4.46×10^{-2}
PfIT_090034700	conserved Plasmodium protein, unknown function	308.28	−1.54	1.17×10^{-2}	4.46×10^{-2}
PfIT_140038800	leucine-rich repeat protein	38.28	−1.39	1.17×10^{-2}	4.46×10^{-2}
PfIT_100033100	WD repeat-containing protein, putative	341.58	1.05	1.17×10^{-2}	4.46×10^{-2}
PfIT_070018200	conserved Plasmodium protein, unknown function	3972.47	0.96	1.17×10^{-2}	4.47×10^{-2}
PfIT_080035300	Plasmodium exported protein (PHISTc), unknown function	8033.25	0.80	1.18×10^{-2}	4.48×10^{-2}
PfIT_020007500	octaprenyl pyrophosphate synthase	56.49	−1.21	1.18×10^{-2}	4.48×10^{-2}
PfIT_130032900	nicotinate-nucleotide adenylyltransferase	74.39	−1.19	1.18×10^{-2}	4.49×10^{-2}
PfIT_060015700	60S ribosomal protein L39	876.18	1.07	1.19×10^{-2}	4.51×10^{-2}
PfIT_120007300	conserved Plasmodium membrane protein, unknown function	8.41	−2.45	1.19×10^{-2}	4.51×10^{-2}
PfIT_110045000	conserved Plasmodium protein, unknown function	560.52	0.71	1.20×10^{-2}	4.53×10^{-2}
PfIT_120052200	DNA replication origin binding protein, putative	86.93	−1.29	1.20×10^{-2}	4.54×10^{-2}
PfIT_120033600	RNA pseudouridylate synthase, putative	176.78	−1.35	1.20×10^{-2}	4.54×10^{-2}
PfIT_130038700	conserved protein, unknown function	960.27	1.25	1.20×10^{-2}	4.54×10^{-2}

Pf_ID	Transcript Product Description	base mean	$\log_2$ FC	p_{value}	p_{adj}
PfIT_110024200	conserved Plasmodium protein, unknown function	1558.97	0.73	1.21×10^{-2}	4.58×10^{-2}
PfIT_100005600	alpha/beta hydrolase, putative	1879.88	1.29	1.21×10^{-2}	4.58×10^{-2}
PfIT_140060300	conserved Plasmodium protein, unknown function	1470.19	0.81	1.22×10^{-2}	4.60×10^{-2}
PfIT_060036500	rifin	3.09	5.21	1.23×10^{-2}	4.63×10^{-2}
PfIT_140053200	heme detoxification protein	82.94	−1.24	1.23×10^{-2}	4.63×10^{-2}
PfIT_010014300	replication factor c protein, putative	288.80	−1.05	1.23×10^{-2}	4.63×10^{-2}
PfIT_140048700	tRNA binding protein, putative	1383.42	0.74	1.23×10^{-2}	4.63×10^{-2}
PfIT_130054000	WD repeat-containing protein 16, putative	15.65	−2.12	1.23×10^{-2}	4.63×10^{-2}
PfIT_100043800	rifin	7.79	3.66	1.23×10^{-2}	4.64×10^{-2}
PfIT_060028000	conserved Plasmodium protein, unknown function	140.50	−0.98	1.23×10^{-2}	4.64×10^{-2}
PfIT_140020700	conserved Plasmodium protein, unknown function	743.04	0.94	1.24×10^{-2}	4.64×10^{-2}
PfIT_010013000	phosphatidate cytidylyltransferase, putative	115.47	−0.87	1.24×10^{-2}	4.64×10^{-2}
PfIT_130048200	transcription factor with AP2 domain(s)	334.84	0.97	1.24×10^{-2}	4.64×10^{-2}
PfIT_130050200	conserved Plasmodium protein, unknown function	1625.48	1.11	1.24×10^{-2}	4.64×10^{-2}
PfIT_030018500	conserved Plasmodium protein, unknown function	145.26	−1.10	1.24×10^{-2}	4.64×10^{-2}
PfIT_100036400	DER1-like protein, putative	221.30	−0.93	1.25×10^{-2}	4.68×10^{-2}
PfIT_140030200	conserved Plasmodium protein, unknown function	7959.59	0.99	1.25×10^{-2}	4.68×10^{-2}
PfIT_050028500	conserved Plasmodium protein, unknown function	76.71	−0.97	1.26×10^{-2}	4.69×10^{-2}
PfIT_130047800	sporozoite protein essential for cell traversal	129.26	−1.60	1.26×10^{-2}	4.70×10^{-2}
PfIT_130039000	histone H3-like centromeric protein CSE4	193.19	−1.23	1.26×10^{-2}	4.71×10^{-2}
PfIT_140076100	conserved Plasmodium protein, unknown function	180.26	−0.93	1.27×10^{-2}	4.72×10^{-2}
PfIT_130077700	rifin	418.28	1.20	1.27×10^{-2}	4.73×10^{-2}
PfIT_100026800	phospholipid scramblase, putative	409.20	−1.28	1.27×10^{-2}	4.73×10^{-2}

Pf_ID	Transcript Product Description	base mean	$\log_2$ FC	p_{value}	p_{adj}
PfIT_030019000	conserved Plasmodium protein, unknown function	55.97	−1.38	1.27×10^{-2}	4.73×10^{-2}
PfIT_120052100	RAC-beta serine/threonine protein kinase	100.19	−1.40	1.28×10^{-2}	4.75×10^{-2}
PfIT_110022700	haloacid dehalogenase-like hydrolase, putative	257.89	−1.25	1.28×10^{-2}	4.75×10^{-2}
PfIT_060022100	60S ribosomal protein L27a, putative	3203.17	1.09	1.28×10^{-2}	4.75×10^{-2}
PfIT_130023000	conserved Plasmodium protein, unknown function	115.26	0.92	1.28×10^{-2}	4.75×10^{-2}
PfIT_130027100	protein transport protein SFT2, putative	721.16	0.73	1.29×10^{-2}	4.77×10^{-2}
PfIT_090008600	60S ribosomal protein L32	5138.94	0.98	1.29×10^{-2}	4.77×10^{-2}
PfIT_060016900	nucleolar GTP-binding protein 1, putative	3784.68	0.97	1.29×10^{-2}	4.77×10^{-2}
PfIT_030007600	conserved Plasmodium protein, unknown function	310.87	0.79	1.29×10^{-2}	4.77×10^{-2}
PfIT_050033100	RNA helicase 1	1022.55	0.82	1.29×10^{-2}	4.77×10^{-2}
PfIT_140007200	rifin	2.15	4.68	1.29×10^{-2}	4.77×10^{-2}
PfIT_010017400	erythrocyte membrane protein 1 (PfEMP1), pseudogene	2.18	4.70	1.29×10^{-2}	4.77×10^{-2}
PfIT_130028600	acetyltransferase, GNAT family, putative	86.99	−0.95	1.29×10^{-2}	4.77×10^{-2}
PfIT_090018300	conserved Plasmodium protein, unknown function	393.32	−0.79	1.30×10^{-2}	4.78×10^{-2}
PfIT_120037200	dihydrolipoyl dehydrogenase, mitochondrial	81.73	−1.18	1.30×10^{-2}	4.78×10^{-2}
PfIT_130040900	conserved Plasmodium protein, unknown function	110.66	1.07	1.30×10^{-2}	4.78×10^{-2}
PfIT_140058700	DER1-like protein	14.41	−1.65	1.30×10^{-2}	4.78×10^{-2}
PfIT_090037300	palmitoyltransferase, putative	61.45	−1.54	1.30×10^{-2}	4.80×10^{-2}
PfIT_100017100	U3 small nucleolar RNA-associated protein 13, putative	1486.45	0.73	1.31×10^{-2}	4.80×10^{-2}
PfIT_140018100	conserved Plasmodium protein, unknown function	819.62	0.94	1.31×10^{-2}	4.80×10^{-2}
PfIT_090041200	virulence-associated protein 1	26.23	1.48	1.31×10^{-2}	4.80×10^{-2}
PfIT_030009800	elongation factor Ts	175.04	−0.83	1.31×10^{-2}	4.81×10^{-2}
PfIT_020012900	KRR1 small subunit processome component, putative	1137.86	0.76	1.31×10^{-2}	4.81×10^{-2}

Pf_ID	Transcript Product Description	base mean	$\log_2$ FC	p_{value}	p_{adj}
PfIT_090020600	sugar transporter, putative	936.66	−1.39	1.32×10^{-2}	4.82×10^{-2}
PfIT_140081500	cytochrome c oxidase assembly protein COX11, putative	83.40	−1.45	1.32×10^{-2}	4.84×10^{-2}
PfIT_140026000	glutathione S-transferase	272.98	1.03	1.32×10^{-2}	4.84×10^{-2}
PfIT_130034600	chromatin assembly factor 1 subunit, putative	203.76	−1.17	1.33×10^{-2}	4.84×10^{-2}
PfIT_050027400	transcription initiation factor TFIID subunit 10, putative	312.09	0.81	1.33×10^{-2}	4.84×10^{-2}
PfIT_130061800	phosphatase 2A regulatory subunit-related protein, putative	84.32	−1.13	1.33×10^{-2}	4.84×10^{-2}
PfIT_050029800	50S ribosomal protein L12, apicoplast, putative	180.86	−1.19	1.33×10^{-2}	4.86×10^{-2}
PfIT_130053400	GTPase, putative	84.54	−1.34	1.33×10^{-2}	4.86×10^{-2}
PfIT_060034200	conserved Plasmodium protein, unknown function	31.81	−1.99	1.35×10^{-2}	4.92×10^{-2}
PfIT_070020400	protein SDA1, putative	2033.89	0.89	1.35×10^{-2}	4.92×10^{-2}
PfIT_080006700	probable protein, unknown function	9.84	−2.91	1.36×10^{-2}	4.94×10^{-2}
PfIT_130045300	secreted ookinete protein, putative	225.78	0.90	1.37×10^{-2}	4.98×10^{-2}
PfIT_120029600	histone chaperone ASF1, putative	201.62	−1.26	1.37×10^{-2}	4.98×10^{-2}
PfIT_100021100	DNA polymerase delta catalytic subunit	398.63	−0.99	1.37×10^{-2}	4.99×10^{-2}
PfIT_140068500	conserved Plasmodium protein, unknown function	46.70	−1.31	1.38×10^{-2}	4.99×10^{-2}
PfIT_130038900	U3 small nucleolar RNA-associated protein 4, putative	1435.18	1.01	1.38×10^{-2}	4.99×10^{-2}
PfIT_130063600	conserved Plasmodium protein, unknown function	747.27	0.69	1.38×10^{-2}	5.00×10^{-2}
PfIT_100036800	RNA polymerase II-associated protein 1, putative	461.24	1.07	1.38×10^{-2}	5.00×10^{-2}
PfIT_110037700	conserved membrane protein, unknown function	2071.85	0.75	1.38×10^{-2}	5.00×10^{-2}

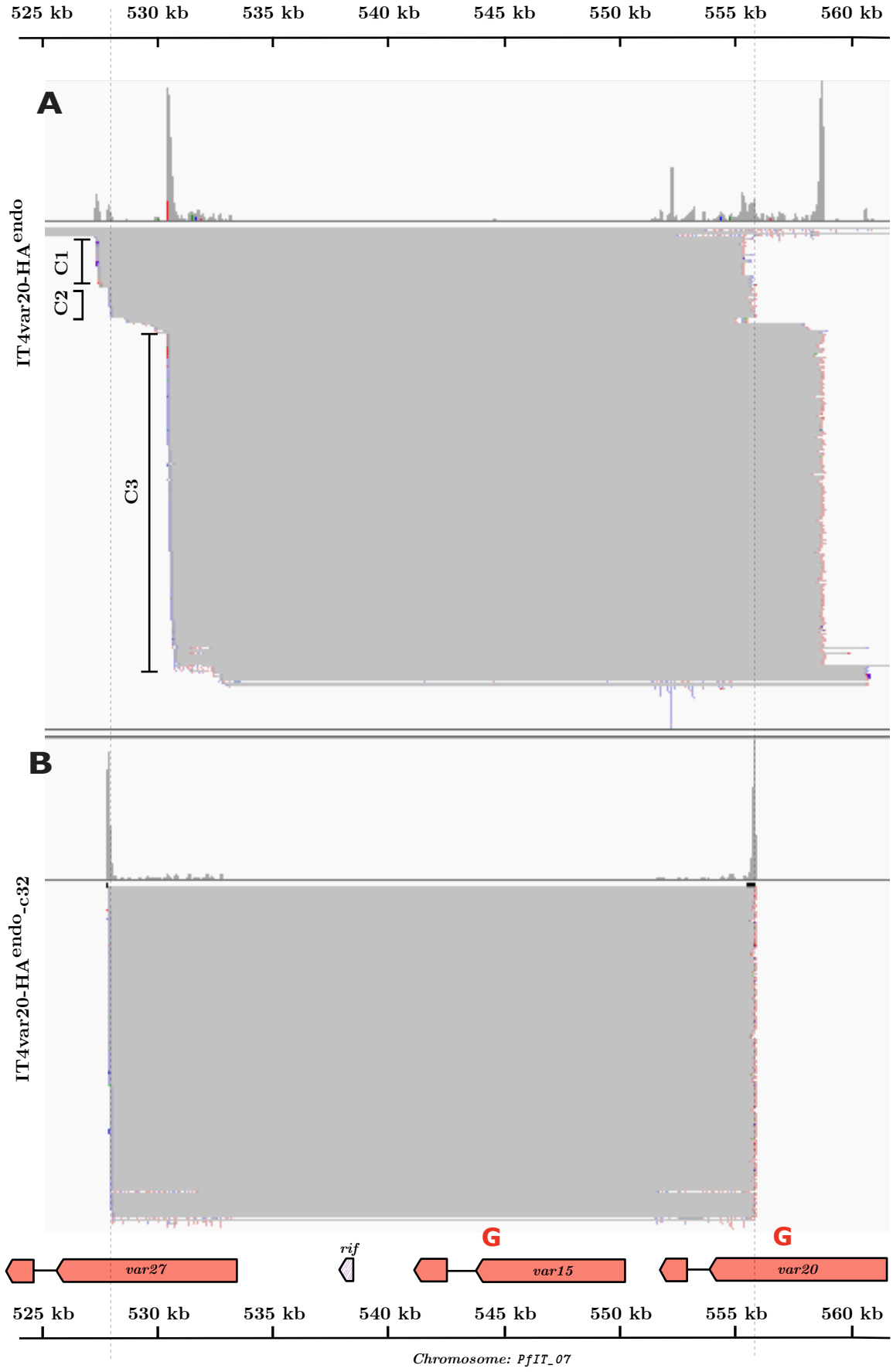


Figure A.5: **Coverage of R1F2 paired reads of IT4var20-HA^{endo} (top) and IT4var20-HA^{endo}-c32 (bottom) over the genomic region** `PfIT_07:522,286-562,099`. Red: reads mapping to +-strand, Blue: reads mapping to –strand. C1–C3 : Clusters of R1F2 paired-reads with inserts spanning from *var27* to the *var20* locus, G: Putative quadruplex forming sequence

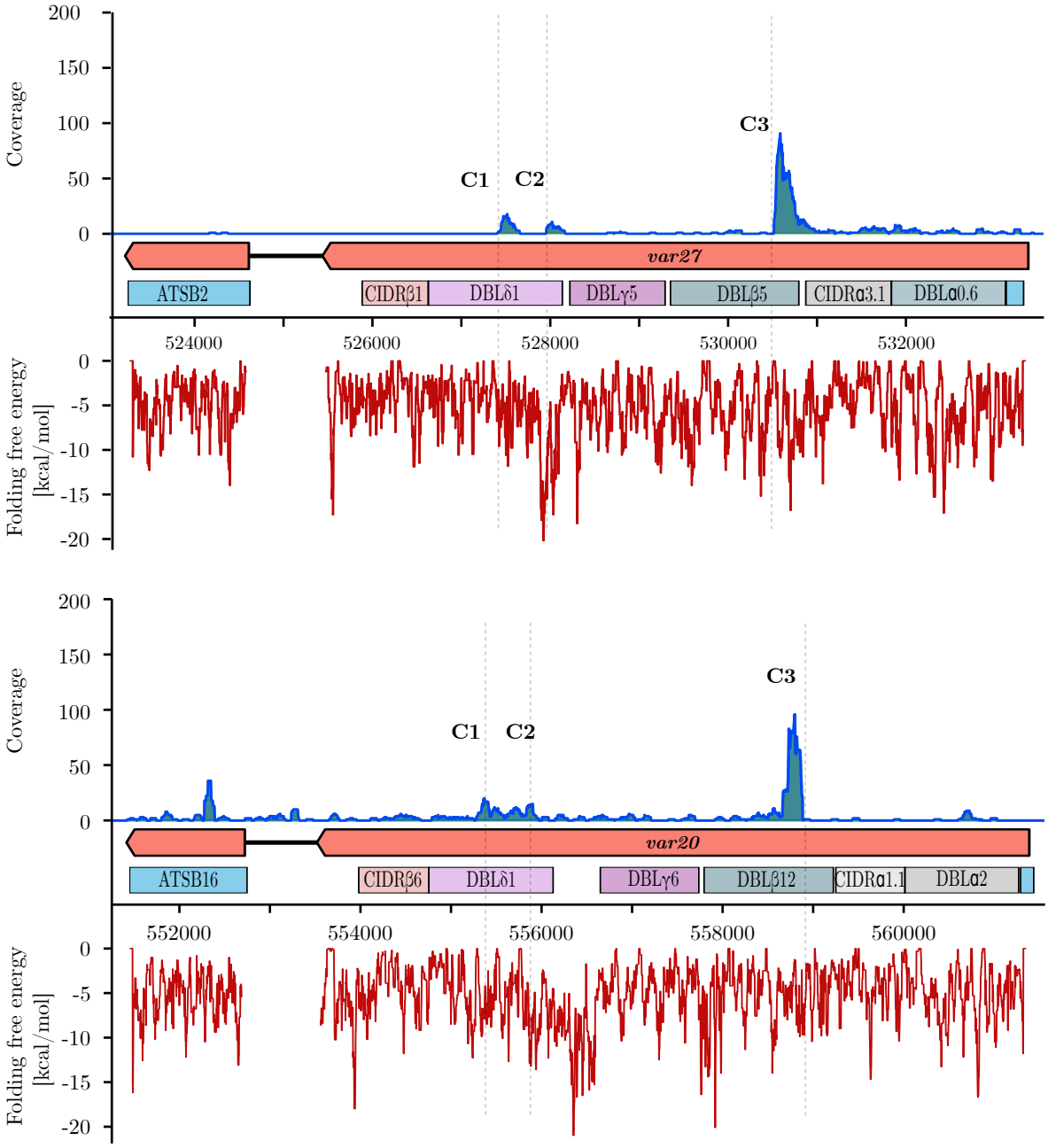


Figure A.6: **Folding free energy of *var27* (top) and *var20* (bottom) with coverage of disconcordant reads**. Blue — : R1F2 paired reads of IT4var20-HA^{endo} as indicators for possible recombination sites. Red — : Folding free energy. Calculations kindly provided by Prof. Thomas Lavstsen as published in [171].

A.3.2 Antimalaria peptides

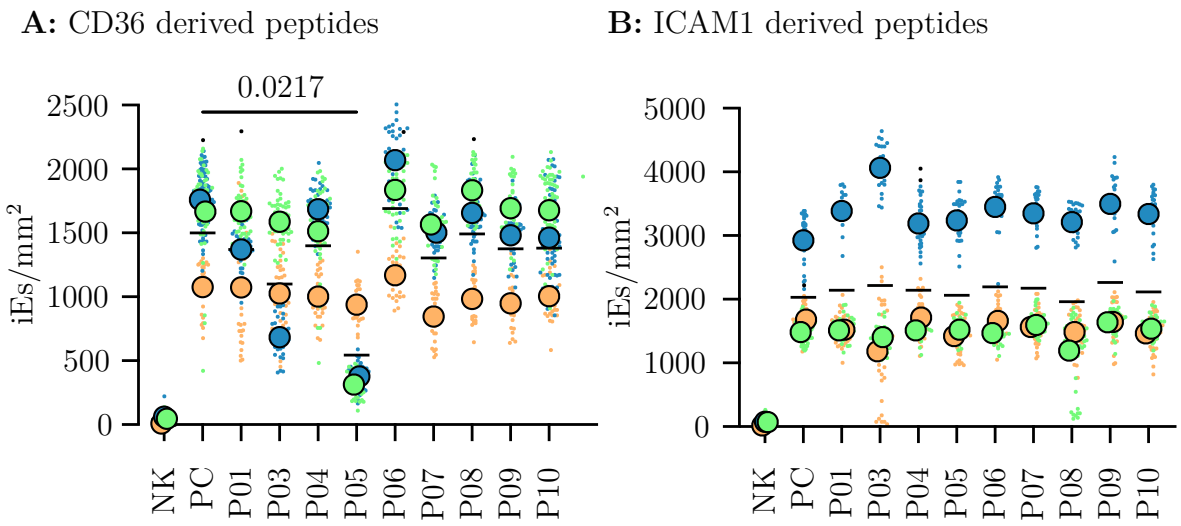


Figure A.7: **Effect of endothelial cell receptor derived peptides on binding of IT4var01-HA^{endo} iEs to transgenic CHO cells**. **A:** Inhibition of CD36 derived peptides CD36-PXX) on IT4var01-HA^{endo} cytoadhesion to CHO-CD36 cells with ICAM1-P10) as positive control (PC). **B:** Inhibition of ICAM1 derived peptides ICAM1-PXX) on IT4var01-HA^{endo} cytoadhesion to CHO-ICAM1 cells with CD36-P10) as PC. No peptides and CHO-GFP as negative control (NC). Statistic with non-parametric Kruskal-Wallis test for comparison of each peptide sample with PC.

Publications

61. Bachmann, A., Metwally, N. G., Allweier, J., Cronshagen, J., Del Pilar Martinez Tauler, M., Murk, A., Roth, L. K., Torabi, H., Wu, Y., Gutsmann, T. & Bruchhaus, I. CD36—A Host Receptor Necessary for Malaria Parasites to Establish and Maintain Infection. *Microorganisms* **10,** 2356. ISSN: 2076-2607. doi:10.3390/microorganisms10122356 (Nov. 29, 2022).

70. Allweier, J., Bartels, M., Torabi, H., Tauler, M. D. P. M., Metwally, N. G., Roeder, T., Gutsmann, T. & Bruchhaus, I. Cytoadhesion of *Plasmodium Falciparum* -Infected Red Blood Cells Changes the Expression of Cytokine-, Histone- and Antiviral Protein-Encoding Genes in Brain Endothelial Cells. *Molecular Microbiology* **122,** 948–967. doi:10.1111/mmi.15331 (Dec. 2024).

109. Cronshagen, J., Allweier, J., Mesén-Ramírez, P., Stäcker, J., Vaaben, A. V., Ramón-Zamorano, G., Naranjo-Prado, I., Ofori, S., Jansen, P. W., Hornebeck, J., Kieferle, F., Murk, A., Martin, E., Castro-Peña, C., Bártfai, R., Lavstsen, T., Bruchhaus, I. & Spielmann, T. *A System for Functional Studies of the Major Virulence Factor of Malaria Parasites* https://elifesciences.org/reviewed-preprints/103542v1. Pre-published.

190. Metwally, N. G., Tauler, M. D. P. M., Torabi, H., Allweier, J., Mohamed, S., Bessemoulin, M., Bouws, P., Alshikh, F., Wu, Y., Temori, M., Schell, T., Rakotonirinalalao, M., Honecker, B., Höhn, K., Jacobs, T., Heine, H. & Bruchhaus, I. Distinct Brain and Lung Endothelial miRNAmRNA Profiles after Exposure to Plasmodium Falciparum-Infected Red Blood Cells. *iScience* **27,** 111265. doi:10.1016/j.isci.2024.111265 (Nov. 15, 2024).

Bibliography

1. Nosten, F., Richard-Lenoble, D. & Danis, M. A Brief History of Malaria. *La Presse Médicale* **51,** 104130. ISSN: 07554982. doi:10.1016/j.lpm.2022.104130 (Sept. 2022).

2. WHO. *World Malaria Report 2025: Addressing the Threat of Antimalarial Drug Resistance* (WHO, Dec. 2025).

3. Oxford Economics Africa & Malaria No More UK. *The Malaria Dividend Report* (2024).

4. WHO. *World Malaria Report 2024: Addressing Inequity in the Global Malaria Response* (WHO, Sept. 2024).

5. Sarma, N., Patouillard, E., Cibulskis, R. E. & Arcand, J.-L. The Economic Burden of Malaria: Revisiting the Evidence. *The American Journal of Tropical Medicine and Hygiene* **101,** 1405–1415. ISSN: 0002-9637, 1476-1645. doi:10.4269/ajtmh.19-0386 (Dec. 4, 2019).

6. Smith, L. M., Motta, F. C., Chopra, G., Moch, J. K., Nerem, R. R., Cummins, B., Roche, K. E., Kelliher, C. M., Leman, A. R., Harer, J., Gedeon, T., Waters, N. C. & Haase, S. B. An Intrinsic Oscillator Drives the Blood Stage Cycle of the Malaria Parasite *Plasmodium Falciparum. Science* **368,** 754–759. ISSN: 0036-8075, 1095-9203. doi:10.1126/science.aba4357 (May 15, 2020).

7. Roberts, L. S., Janovy, J. & Schmidt, G. D. *Gerald D. Schmidt & Larry S. Roberts' Foundations of Parasitology* 8th ed. ISBN: 978-0-07-302827-9 (McGraw-Hill, Boston, 2009).

8. Kwiatkowski, D. & Nowak, M. Periodic and Chaotic Host-Parasite Interactions in Human Malaria. *Proceedings of the National Academy of Sciences* **88,** 5111–5113. ISSN: 0027-8424, 1091-6490. doi:10.1073/pnas.88.12.5111 (June 15, 1991).

9. Ahmed, M. A. & Cox-Singh, J. *P Lasmodium Knowlesi* – an Emerging Pathogen. *ISBT Science Series* **10,** 134–140. ISSN: 1751-2816, 1751-2824. doi:10.1111/voxs.12115 (Apr. 2015).

10. Cowman, A. F., Healer, J., Marapana, D. & Marsh, K. Malaria: Biology and Disease. *Cell* **167,** 610–624. ISSN: 00928674. doi:10.1016/j.cell.2016.07.055 (Oct. 2016).

11. WHO. *WHO Guidelines for Malaria, 30 November 2024* doi:10.2471/B09146 (World Health Organization, Nov. 29, 2024).

12. Taylor, C., Namaste, S. M. L., Lowell, J., Useem, J. & Yé, Y. Estimating the Fraction of Severe Malaria among Malaria-Positive Children: Analysis of Household Surveys in 19 Malaria-Endemic Countries in Africa. *The American Journal of Tropical Medicine and Hygiene* **104,** 1375–1382. ISSN: 1476-1645. doi:10.4269/ajtmh.20-1351 (Feb. 1, 2021).

13. Trampuz, A., Jereb, M., Muzlovic, I. & Prabhu, R. M. Clinical Review: Severe Malaria. *Critical Care (London, England)* **7,** 315–323. ISSN: 1364-8535. doi:10.1186/cc2183 (Aug. 2003).

14. Fried, M. & Duffy, P. E. Adherence of Plasmodium Falciparum to Chondroitin Sulfate A in the Human Placenta. *Science* **272,** 1502–1504. doi:10.1126/science.272.5267.1502 (June 7, 1996).

15. Salanti, A., Dahlbäck, M., Turner, L., Nielsen, M. A., Barfod, L., Magistrado, P., Jensen, A. T., Lavstsen, T., Ofori, M. F., Marsh, K., Hviid, L. & Theander, T. G. Evidence for the Involvement of VAR2CSA in Pregnancy-associated Malaria. *The Journal of Experimental Medicine* **200,** 1197–1203. ISSN: 1540-9538, 0022-1007. doi:10.1084/jem.20041579 (Nov. 1, 2004).

16. White, N. The Treatment of Malaria. *New England Journal of Medicine* **335,** 800–806. ISSN: 0028-4793, 1533-4406. doi:10.1056/NEJM199609123351107 (Sept. 12, 1996).

17. *World Malaria Report 2023* (ed WHO) ISBN: 978-92-4-008617-3 (2023).

18. Dondorp, A. M., Fanello, C. I., Hendriksen, I. C., Gomes, E., Seni, A., Chhaganlal, K. D., Bojang, K., Olaosebikan, R., Anunobi, N., Maitland, K., Kivaya, E., Agbenyega, T., Nguah, S. B., Evans, J., Gesase, S., Kahabuka, C., Mtove, G., Nadjm, B., Deen, J., Mwanga-Amumpaire, J., Nansumba, M., Karema, C., Umulisa, N., Uwimana, A.,

Mokuolu, O. A., Adedoyin, O. T., Johnson, W. B., Tshefu, A. K., Onyamboko, M. A., Sakulthaew, T., Ngum, W. P., Silamut, K., Stepniewska, K., Woodrow, C. J., Bethell, D., Wills, B., Oneko, M., Peto, T. E., Von Seidlein, L., Day, N. P. & White, N. J. Artesunate versus Quinine in the Treatment of Severe Falciparum Malaria in African Children (AQUAMAT): An Open-Label, Randomised Trial. *The Lancet* **376,** 1647–1657. ISSN: 01406736. doi:10.1016/S0140-6736(10)61924-1 (Nov. 2010).

19. Sinka, M. E., Bangs, M. J., Manguin, S., Rubio-Palis, Y., Chareonviriyaphap, T., Coetzee, M., Mbogo, C. M., Hemingway, J., Patil, A. P., Temperley, W. H., Gething, P. W., Kabaria, C. W., Burkot, T. R., Harbach, R. E. & Hay, S. I. A Global Map of Dominant Malaria Vectors. *Parasites & Vectors* **5,** 69. ISSN: 1756-3305. doi:10.1186/1756-3305-5-69 (Dec. 2012).

20. Gantz, V. M., Jasinskiene, N., Tatarenkova, O., Fazekas, A., Macias, V. M., Bier, E. & James, A. A. Highly Efficient Cas9-mediated Gene Drive for Population Modification of the Malaria Vector Mosquito *Anopheles Stephensi. Proceedings of the National Academy of Sciences* **112.** ISSN: 0027-8424, 1091-6490. doi:10.1073/pnas.1521077112 (Dec. 8, 2015).

21. El-Moamly, A. A. & El-Sweify, M. A. Malaria Vaccines: The 60-Year Journey of Hope and Final Success—Lessons Learned and Future Prospects. *Tropical Medicine and Health* **51,** 29. ISSN: 1349-4147. doi:10.1186/s41182-023-00516-w (May 17, 2023).

22. Hill, A. V. S. Vaccines against Malaria. *Philosophical Transactions of the Royal Society B: Biological Sciences* **366,** 2806–2814. ISSN: 0962-8436, 1471-2970. doi:10.1098/rstb.2011.0091 (Oct. 12, 2011).

23. Impouma, B., Adidja, A., Mboussou, F., Cabore, J. & Moeti, M. Malaria Vaccine Introduction in Africa: Progress and Challenges. *The Lancet,* S0140673624028411. ISSN: 01406736. doi:10.1016/S0140-6736(24)02841-1 (Jan. 2025).

24. Mouwenda, Y. D., Jochems, S. P., Van Unen, V., Betouke Ongwe, M. E., De Steenhuijsen Piters, W. A., Stam, K. A., Massinga Loembe, M., Sim, B. K. L., Esen, M., Hoffman, S. L., Kremsner, P. G., Fendel, R., Mordmüller, B. & Yazdanbakhsh, M. Immune Responses Associated with Protection Induced by Chemoattenuated Pf-

SPZ Vaccine in Malaria-Naive Europeans. *JCI Insight* **9,** e170210. ISSN: 2379-3708. doi:10.1172/jci.insight.170210 (May 8, 2024).

25. Mordmüller, B., Sulyok, M., Egger-Adam, D., Resende, M., De Jongh, W. A., Jensen, M. H., Smedegaard, H. H., Ditlev, S. B., Soegaard, M., Poulsen, L., Dyring, C., Calle, C. L., Knoblich, A., Ibáñez, J., Esen, M., Deloron, P., Ndam, N., Issifou, S., Houard, S., Howard, R. F., Reed, S. G., Leroy, O., Luty, A. J. F., Theander, T. G., Kremsner, P. G., Salanti, A. & Nielsen, M. A. First-in-Human, Randomized, Double-blind Clinical Trial of Differentially Adjuvanted PAMVAC, A Vaccine Candidate to Prevent Pregnancy-associated Malaria. *Clinical Infectious Diseases* **69,** 1509–1516. ISSN: 1058-4838, 1537-6591. doi:10.1093/cid/ciy1140 (Oct. 15, 2019).

26. Doritchamou, J., Nielsen, M. A., Chêne, A., Viebig, N. K., Lambert, L. E., Sander, A. F., Semblat, J.-P., Hundt, S., Orr-Gonzalez, S., Janitzek, C. M., Spiegel, A. J., Clemmensen, S. B., Thomas, M. L., Nason, M. C., Snow-Smith, M., Barnafo, E. K., Shiloach, J., Chen, B. B., Nadakal, S., Highsmith, K., Ouahes, T., Conteh, S., Sharma, A., Torano, H., Butler, B., Reiter, K., Rausch, K. M., Scaria, P. V., Anderson, C., Narum, D. L., Salanti, A., Fried, M., Theander, T. G., Gamain, B. & Duffy, P. E. Aotus Nancymaae Model Predicts Human Immune Response to the Placental Malaria Vaccine Candidate VAR2CSA. *Lab Animal* **52,** 315–323. ISSN: 0093-7355, 1548-4475. doi:10.1038/s41684-023-01274-2 (Dec. 2023).

27. Duffy, P. E. & Patrick Gorres, J. Malaria Vaccines since 2000: Progress, Priorities, Products. *npj Vaccines* **5,** 48. ISSN: 2059-0105. doi:10.1038/s41541-020-0196-3 (June 9, 2020).

28. Sturm, A., Amino, R., Van De Sand, C., Regen, T., Retzlaff, S., Rennenberg, A., Krueger, A., Pollok, J.-M., Menard, R. & Heussler, V. T. Manipulation of Host Hepatocytes by the Malaria Parasite for Delivery into Liver Sinusoids. *Science* **313,** 1287–1290. ISSN: 0036-8075, 1095-9203. doi:10.1126/science.1129720 (Sept. 2006).

29. Rowe, J. A., Claessens, A., Corrigan, R. A. & Arman, M. Adhesion of *Plasmodium Falciparum* -Infected Erythrocytes to Human Cells: Molecular Mechanisms and Therapeutic Implications. *Expert Reviews in Molecular Medicine* **11,** e16. ISSN: 1462-3994. doi:10.1017/S1462399409001082 (May 2009).

30. Berendt, A., Ferguson, D. & Newbold, C. Sequestration in Plasmodium Falciparum Malaria: Sticky Cells and Sticky Problems. *Parasitology Today* **6,** 247–254. ISSN: 01694758. doi:10.1016/0169-4758(90)90184-6 (Aug. 1990).

31. Dondorp, A. M., Lee, S. J., Faiz, M. A., Mishra, S., Price, R., Tjitra, E., Than, M., Htut, Y., Mohanty, S., Yunus, E. B., Rahman, R., Nosten, F., Anstey, N. M., Day, N. P. J. & White, N. J. The Relationship between Age and the Manifestations of and Mortality Associated with Severe Malaria. *Clinical Infectious Diseases* **47,** 151–157. ISSN: 1058-4838, 1537-6591. doi:10.1086/589287 (July 15, 2008).

32. Lubiana, P., Bouws, P., Roth, L. K., Dörpinghaus, M., Rehn, T., Brehmer, J., Wichers, J. S., Bachmann, A., Höhn, K., Roeder, T., Thye, T., Gutsmann, T., Burmester, T., Bruchhaus, I. & Metwally, N. G. Adhesion between P. Falciparum Infected Erythrocytes and Human Endothelial Receptors Follows Alternative Binding Dynamics under Flow and Febrile Conditions. *Scientific Reports* **10,** 4548. ISSN: 2045-2322. doi:10.1038/s41598-020-61388-2 (Mar. 11, 2020).

33. Warncke, J. D. & Beck, H.-P. Host Cytoskeleton Remodeling throughout the Blood Stages of Plasmodium Falciparum. *Microbiology and Molecular Biology Reviews* **83,** e00013–19. ISSN: 1092-2172, 1098-5557. doi:10.1128/MMBR.00013-19 (Nov. 20, 2019).

34. Cheng, Q., Cloonan, N., Fischer, K., Thompson, J., Waine, G., Lanzer, M. & Saul, A. Stevor and Rif Are Plasmodium Falciparum Multicopy Gene Families Which Potentially Encode Variant Antigens. *Molecular and Biochemical Parasitology* **97,** 161–176. ISSN: 01666851. doi:10.1016/S0166-6851(98)00144-3 (Nov. 1998).

35. Otto, T. D., Assefa, S. A., Böhme, U., Sanders, M. J., Kwiatkowski, D. P., Pf3k consortium, Berriman, M. & Newbold, C. Evolutionary Analysis of the Most Polymorphic Gene Family in Falciparum Malaria. *Wellcome Open Research* **4,** 193. ISSN: 2398-502X. doi:10.12688/wellcomeopenres.15590.1 (Dec. 3, 2019).

36. Gardner, M. J., Hall, N., Fung, E., White, O., Berriman, M., Hyman, R. W., Carlton, J. M., Pain, A., Nelson, K. E., Bowman, S., Paulsen, I. T., James, K., Eisen, J. A., Rutherford, K., Salzberg, S. L., Craig, A., Kyes, S., Chan, M.-S., Nene, V., Shallom, S. J., Suh, B., Peterson, J., Angiuoli, S., Pertea, M., Allen, J., Selengut, J., Haft, D., Mather, M. W., Vaidya, A. B., Martin, D. M. A., Fairlamb, A. H., Fraunholz,

M. J., Roos, D. S., Ralph, S. A., McFadden, G. I., Cummings, L. M., Subramanian, G. M., Mungall, C., Venter, J. C., Carucci, D. J., Hoffman, S. L., Newbold, C., Davis, R. W., Fraser, C. M. & Barrell, B. Genome Sequence of the Human Malaria Parasite Plasmodium Falciparum. *Nature* **419,** 498–511. ISSN: 0028-0836, 1476-4687. doi:10.1038/nature01097 (Oct. 2002).

37. Guizetti, J. & Scherf, A. Silence, Activate, Poise and Switch! Mechanisms of Antigenic Variation in *P Lasmodium Falciparum. Cellular Microbiology* **15,** 718–726. ISSN: 1462-5814, 1462-5822. doi:10.1111/cmi.12115 (May 2013).

38. Bachmann, A., Esser, C., Petter, M., Predehl, S., Von Kalckreuth, V., Schmiedel, S., Bruchhaus, I. & Tannich, E. Absence of Erythrocyte Sequestration and Lack of Multicopy Gene Family Expression in Plasmodium Falciparum from a Splenectomized Malaria Patient. *PLoS ONE* **4** (ed Heussler, V. T.) e7459. ISSN: 1932-6203. doi:10.1371/journal.pone.0007459 (Oct. 14, 2009).

39. Hadjimichael, E. & Deitsch, K. W. Variable Surface Antigen Expression, Virulence, and Persistent Infection by *Plasmodium Falciparum* Malaria Parasites. *Microbiology and Molecular Biology Reviews* **89** (ed Lodoen, M. B.) e00114–23. ISSN: 1092-2172, 1098-5557. doi:10.1128/mmbr.00114-23 (Mar. 27, 2025).

40. Florini, F., Visone, J. E., Hadjimichael, E., Malpotra, S., Nötzel, C., Kafsack, B. F. C. & Deitsch, K. W. scRNA-seq Reveals Transcriptional Plasticity of Var Gene Expression in Plasmodium Falciparum for Host Immune Avoidance. *Nature Microbiology.* ISSN: 2058-5276. doi:10.1038/s41564-025-02008-5 (May 16, 2025).

41. Volz, J. C., Bártfai, R., Petter, M., Langer, C., Josling, G. A., Tsuboi, T., Schwach, F., Baum, J., Rayner, J. C., Stunnenberg, H. G., Duffy, M. F. & Cowman, A. F. PfSET10, a Plasmodium Falciparum Methyltransferase, Maintains the Active Var Gene in a Poised State during Parasite Division. *Cell Host & Microbe* **11,** 7–18. ISSN: 19313128. doi:10.1016/j.chom.2011.11.011 (Jan. 2012).

42. Wichers-Misterek, J. S., Krumkamp, R., Held, J., Von Thien, H., Wittmann, I., Höppner, Y. D., Ruge, J. M., Moser, K., Dara, A., Strauss, J., Esen, M., Fendel, R., Sulyok, Z., Jeninga, M. D., Kremsner, P. G., Sim, B. K. L., Hoffman, S. L., Duffy, M. F., Otto, T. D., Gilberger, T.-W., Silva, J. C., Mordmüller, B., Petter, M. & Bachmann,

A. The Exception That Proves the Rule: Virulence Gene Expression at the Onset of Plasmodium Falciparum Blood Stage Infections. *PLOS Pathogens* **19** (ed Dzikowski, R.) e1011468. ISSN: 1553-7374. doi:10.1371/journal.ppat.1011468 (June 29, 2023).

43. Jing, Q., Cao, L., Zhang, L., Cheng, X., Gilbert, N., Dai, X., Sun, M., Liang, S. & Jiang, L. Plasmodium Falciparumvar Gene Is Activated by Its Antisense Long Noncoding RNA. *Frontiers in Microbiology* **9,** 3117. ISSN: 1664-302X. doi:10.3389/fmicb.2018.03117 (Dec. 18, 2018).

44. Amit-Avraham, I., Pozner, G., Eshar, S., Fastman, Y., Kolevzon, N., Yavin, E. & Dzikowski, R. Antisense Long Noncoding RNAs Regulate *Var* Gene Activation in the Malaria Parasite *Plasmodium Falciparum. Proceedings of the National Academy of Sciences* **112.** ISSN: 0027-8424, 1091-6490. doi:10.1073/pnas.1420855112 (Mar. 3, 2015).

45. Srivastava, S., Bhowmick, K., Chatterjee, S., Basha, J., Kundu, T. K. & Dhar, S. K. Histone H3K9 Acetylation Level Modulates Gene Expression and May Affect Parasite Growth in Human Malaria Parasite *Plasmodium Falciparum. The FEBS Journal* **281,** 5265–5278. ISSN: 1742-464X, 1742-4658. doi:10.1111/febs.13067 (Dec. 2014).

46. Su, X.-z., Heatwole, V. M., Wertheimer, S. P., Guinet, F., Herrfeldt, J. A., Peterson, D. S., Ravetch, J. A. & Wellems, T. E. The Large Diverse Gene Family Var Encodes Proteins Involved in Cytoadherence and Antigenic Variation of Plasmodium Falciparum-Infected Erythrocytes. *Cell* **82,** 89–100. ISSN: 00928674. doi:10.1016/0092-8674(95)90055-1 (July 1995).

47. Lavstsen, T., Salanti, A., Jensen, A. T., Arnot, D. E. & Theander, T. G. Sub-Grouping of Plasmodium Falciparum 3D7 Var Genes Based on Sequence Analysis of Coding and Non-Coding Regions. *Malaria Journal* **2,** 27. ISSN: 1475-2875. doi:10.1186/1475-2875-2-27 (Sept. 10, 2003).

48. Smith, J. D., Subramanian, G., Gamain, B., Baruch, D. I. & Miller, L. H. Classification of Adhesive Domains in the Plasmodium Falciparum Erythrocyte Membrane Protein 1 Family. *Molecular and Biochemical Parasitology* **110,** 293–310. ISSN: 01666851. doi:10.1016/S0166-6851(00)00279-6 (Oct. 2000).

49. Andradi-Brown, C., Wichers-Misterek, J. S., Von Thien, H., Höppner, Y. D., Scholz, J. A., Hansson, H., Filtenborg Hocke, E., Gilberger, T. W., Duffy, M. F., Lavstsen, T., Baum, J., Otto, T. D., Cunnington, A. J. & Bachmann, A. A Novel Computational Pipeline for Var Gene Expression Augments the Discovery of Changes in the Plasmodium Falciparum Transcriptome during Transition from in Vivo to Short-Term in Vitro Culture. *eLife* **12,** RP87726. ISSN: 2050-084X. doi:10.7554/eLife.87726 (Jan. 25, 2024).

50. Claessens, A., Hamilton, W. L., Kekre, M., Otto, T. D., Faizullabhoy, A., Rayner, J. C. & Kwiatkowski, D. Generation of Antigenic Diversity in Plasmodium Falciparum by Structured Rearrangement of Var Genes During Mitosis. *PLoS Genetics* **10** (ed Deitsch, K.) e1004812. ISSN: 1553-7404. doi:10.1371/journal.pgen.1004812 (Dec. 18, 2014).

51. Huckaby, A. C., Granum, C. S., Carey, M. A., Szlachta, K., Al-Barghouthi, B., Wang, Y.-H. & Guler, J. L. Complex DNA Structures Trigger Copy Number Variation across the *Plasmodium Falciparum* Genome. *Nucleic Acids Research* **47,** 1615–1627. ISSN: 0305-1048, 1362-4962. doi:10.1093/nar/gky1268 (Feb. 28, 2019).

52. Smargiasso, N., Gabelica, V., Damblon, C., Rosu, F., De Pauw, E., Teulade-Fichou, M.-P., Rowe, J. & Claessens, A. Putative DNA G-quadruplex Formation within the Promoters of Plasmodium Falciparum Var Genes. *BMC Genomics* **10,** 362. ISSN: 1471-2164. doi:10.1186/1471-2164-10-362 (2009).

53. Gage, H. L. & Merrick, C. J. Conserved Associations between G-quadruplex-forming DNA Motifs and Virulence Gene Families in Malaria Parasites. *BMC Genomics* **21,** 236. ISSN: 1471-2164. doi:10.1186/s12864-020-6625-x (Dec. 2020).

54. Kraemer, S. M., Kyes, S. A., Aggarwal, G., Springer, A. L., Nelson, S. O., Christodoulou, Z., Smith, L. M., Wang, W., Levin, E., Newbold, C. I., Myler, P. J. & Smith, J. D. Patterns of Gene Recombination Shape Var Gene Repertoires in Plasmodium Falciparum: Comparisons of Geographically Diverse Isolates. *BMC Genomics* **8,** 45. ISSN: 1471-2164. doi:10.1186/1471-2164-8-45 (Dec. 2007).

55. Barry, A. E., Leliwa-Sytek, A., Tavul, L., Imrie, H., Migot-Nabias, F., Brown, S. M., McVean, G. A. V. & Day, K. P. Population Genomics of the Immune Evasion (Var)

Genes of Plasmodium Falciparum. *PLoS Pathogens* **3** (ed Mackinnon, M. J.) e34. ISSN: 1553-7374. doi:10.1371/journal.ppat.0030034 (Mar. 16, 2007).

56. Freitas-Junior, L. H., Bottius, E., Pirrit, L. A., Deitsch, K. W., Scheidig, C., Guinet, F., Nehrbass, U., Wellems, T. E. & Scherf, A. Frequent Ectopic Recombination of Virulence Factor Genes in Telomeric Chromosome Clusters of P. Falciparum. *Nature* **407,** 1018–1022. ISSN: 0028-0836, 1476-4687. doi:10.1038/35039531 (Oct. 2000).

57. Helms, G., Dasanna, A. K., Schwarz, U. S. & Lanzer, M. Modeling Cytoadhesion of *Plasmodium Falciparum*- Infected Erythrocytes and Leukocytes—Common Principles and Distinctive Features. *FEBS Letters* **590,** 1955–1971. ISSN: 0014-5793, 1873-3468. doi:10.1002/1873-3468.12142 (July 2016).

58. Ho, M., Hickey, M. J., Murray, A. G., Andonegui, G. & Kubes, P. Visualization of *Plasmodium Falciparum*– Endothelium Interactions in Human Microvasculature. *The Journal of Experimental Medicine* **192,** 1205–1212. ISSN: 0022-1007, 1540-9538. doi:10.1084/jem.192.8.1205 (Oct. 16, 2000).

59. Yipp, B. G., Anand, S., Schollaardt, T., Patel, K. D., Looareesuwan, S. & Ho, M. Synergism of Multiple Adhesion Molecules in Mediating Cytoadherence of Plasmodium Falciparum-Infected Erythrocytes to Microvascular Endothelial Cells under Flow. *Blood* **96,** 2292–2298. ISSN: 0006-4971 (Sept. 15, 2000).

60. Hviid, L., Jensen, A. R. & Deitsch, K. W. PfEMP1 and Var Genes – Still of Key Importance in Plasmodium Falciparum Malaria Pathogenesis and Immunity. *Advances in Parasitology* **125,** 53–103. doi:10.1016/bs.apar.2024.02.001 (2024).

61. Bachmann, A., Metwally, N. G., Allweier, J., Cronshagen, J., Del Pilar Martinez Tauler, M., Murk, A., Roth, L. K., Torabi, H., Wu, Y., Gutsmann, T. & Bruchhaus, I. CD36—A Host Receptor Necessary for Malaria Parasites to Establish and Maintain Infection. *Microorganisms* **10,** 2356. ISSN: 2076-2607. doi:10.3390/microorganisms10122356 (Nov. 29, 2022).

62. Lim, Y. B., Thingna, J., Cao, J. & Lim, C. T. Single Molecule and Multiple Bond Characterization of Catch Bond Associated Cytoadhesion in Malaria. *Scientific Reports* **7,** 4208. ISSN: 2045-2322. doi:10.1038/s41598-017-04352-x (June 23, 2017).

63. Lim, Y. B., Thingna, J., Kong, F., Dao, M., Cao, J. & Lim, C. T. Temperature-Induced Catch-Slip to Slip Bond Transit in Plasmodium Falciparum-Infected Erythrocytes. *Biophysical Journal* **118,** 105–116. ISSN: 00063495. doi:10.1016/j.bpj.2019.11.016 (Jan. 2020).

64. Hsieh, F.-L., Turner, L., Bolla, J. R., Robinson, C. V., Lavstsen, T. & Higgins, M. K. The Structural Basis for CD36 Binding by the Malaria Parasite. *Nature Communications* **7,** 12837. ISSN: 2041-1723. doi:10.1038/ncomms12837 (Sept. 26, 2016).

65. Ochola, L. B., Siddondo, B. R., Ocholla, H., Nkya, S., Kimani, E. N., Williams, T. N., Makale, J. O., Liljander, A., Urban, B. C., Bull, P. C., Szestak, T., Marsh, K. & Craig, A. G. Specific Receptor Usage in Plasmodium Falciparum Cytoadherence Is Associated with Disease Outcome. *PLoS ONE* **6** (ed Sutherland, C. J.) e14741. ISSN: 1932-6203. doi:10.1371/journal.pone.0014741 (Mar. 3, 2011).

66. Ortolan, L. S., Avril, M., Xue, J., Seydel, K. B., Zheng, Y. & Smith, J. D. Plasmodium Falciparum Parasite Lines Expressing DC8 and Group a PfEMP1 Bind to Brain, Intestinal, and Kidney Endothelial Cells. *Frontiers in Cellular and Infection Microbiology* **Volume 12 - 2022.** ISSN: 2235-2988. doi:10.3389/fcimb.2022.813011 (2022).

67. Silverstein, R. L. & Febbraio, M. CD36, a Scavenger Receptor Involved in Immunity, Metabolism, Angiogenesis, and Behavior (2010).

68. Nolan, D. J., Ginsberg, M., Israely, E., Palikuqi, B., Poulos, M. G., James, D., Ding, B.-S., Schachterle, W., Liu, Y., Rosenwaks, Z., Butler, J. M., Xiang, J., Rafii, A., Shido, K., Rabbany, S. Y., Elemento, O. & Rafii, S. Molecular Signatures of Tissue-Specific Microvascular Endothelial Cell Heterogeneity in Organ Maintenance and Regeneration. *Developmental Cell* **26,** 204–219. ISSN: 1534-5807. doi:10.1016/j.devcel.2013.06.017 (July 2013).

69. Swerlick, R. A., Lee, K. H., Wick, T. M. & Lawley, T. J. Human Dermal Microvascular Endothelial but Not Human Umbilical Vein Endothelial Cells Express CD36 in Vivo and in Vitro. *The Journal of Immunology* **148,** 78–83. ISSN: 0022-1767, 1550-6606. doi:10.4049/jimmunol.148.1.78 (Jan. 1, 1992).

70. Allweier, J., Bartels, M., Torabi, H., Tauler, M. D. P. M., Metwally, N. G., Roeder, T., Gutsmann, T. & Bruchhaus, I. Cytoadhesion of *Plasmodium Falciparum* -Infected Red Blood Cells Changes the Expression of Cytokine-, Histone- and Antiviral Protein-Encoding Genes in Brain Endothelial Cells. *Molecular Microbiology* **122,** 948–967. doi:10.1111/mmi.15331 (Dec. 2024).

71. Schofield, L., Novakovic, S., Gerold, P., Schwarz, R. T., McConville, M. J. & Tachado, S. D. Glycosylphosphatidylinositol Toxin of Plasmodium Up-Regulates Intercellular Adhesion Molecule-1, Vascular Cell Adhesion Molecule-1, and E-selectin Expression in Vascular Endothelial Cells and Increases Leukocyte and Parasite Cytoadherence via Tyrosine Kinase-Dependent Signal Transduction. *The Journal of Immunology* **156,** 1886–1896. ISSN: 0022-1767, 1550-6606. doi:10.4049/jimmunol.156.5.1886 (Mar. 1, 1996).

72. Turner, G. D. H., Morrison, H. & Pukritayakamee, S. An Immunohistochemical Study of the Pathology of Fatal Malaria. **145** (1994).

73. Staunton, D. E., Dustin, M. L., Erickson, H. P. & Springer, T. A. The Arrangement of the Immunoglobulin-like Domains of ICAM-1 and the Binding Sites for LFA-1 and Rhinovirus. *Cell* **61,** 243–254. ISSN: 0092-8674. doi:10.1016/0092-8674(90)90805-O (Apr. 20, 1990).

74. Berendt, A. R., McDowall, A., Craig, A. G., Bates, P. A., Sternberg, M. J., Marsh, K., Newbold, C. I. & Hogg, N. The Binding Site on ICAM-1 for Plasmodium Falciparum-Infected Erythrocytes Overlaps, but Is Distinct from, the LFA-1-binding Site. *Cell* **68,** 71–81. ISSN: 00928674. doi:10.1016/0092-8674(92)90207-S (Jan. 1992).

75. Lennartz, F., Adams, Y., Bengtsson, A., Olsen, R. W., Turner, L., Ndam, N. T., Ecklu-Mensah, G., Moussiliou, A., Ofori, M. F., Gamain, B., Lusingu, J. P., Petersen, J. E., Wang, C. W., Nunes-Silva, S., Jespersen, J. S., Lau, C. K., Theander, T. G., Lavstsen, T., Hviid, L., Higgins, M. K. & Jensen, A. T. Structure-Guided Identification of a Family of Dual Receptor-Binding PfEMP1 That Is Associated with Cerebral Malaria. *Cell Host & Microbe* **21,** 403–414. ISSN: 19313128. doi:10.1016/j.chom.2017.02.009 (Mar. 2017).

76. Bengtsson, A., Joergensen, L., Rask, T. S., Olsen, R. W., Andersen, M. A., Turner, L., Theander, T. G., Hviid, L., Higgins, M. K., Craig, A., Brown, A. & Jensen, A. T. R. A Novel Domain Cassette Identifies *Plasmodium Falciparum* PfEMP1 Proteins Binding ICAM-1 and Is a Target of Cross-Reactive, Adhesion-Inhibitory Antibodies. *The Journal of Immunology* **190,** 240–249. ISSN: 0022-1767, 1550-6606. doi:10.4049/jimmunol.1202578 (Jan. 1, 2013).

77. Smith, J. D., Craig, A. G., Kriek, N., Hudson-Taylor, D., Kyes, S., Fagen, T., Pinches, R., Baruch, D. I., Newbold, C. I. & Miller, L. H. Identification of a *Plasmodium Falciparum* Intercellular Adhesion Molecule-1 Binding Domain: A Parasite Adhesion Trait Implicated in Cerebral Malaria. *Proceedings of the National Academy of Sciences* **97,** 1766–1771. ISSN: 0027-8424, 1091-6490. doi:10.1073/pnas.040545897 (Feb. 15, 2000).

78. Janes, J. H., Wang, C. P., Levin-Edens, E., Vigan-Womas, I., Guillotte, M., Melcher, M., Mercereau-Puijalon, O. & Smith, J. D. Investigating the Host Binding Signature on the Plasmodium Falciparum PfEMP1 Protein Family. *PLoS Pathogens* **7** (ed Deitsch, K.) e1002032. ISSN: 1553-7374. doi:10.1371/journal.ppat.1002032 (May 5, 2011).

79. Cronshagen, J. *Establishment of Cell Lines Expressing Erythrocyte Membrane Protein 1 (PfEMP1) Variants of Choice to Study Plasmodium Falciparum Cytoadherence Associated Functions* PhD thesis (Universität Hamburg, Hamburg, 2024).

80. Mackay, F., Loetscher, H., Stueber, D., Gehr, G. & Lesslauer, W. Tumor Necrosis Factor Alpha (TNF-alpha)-Induced Cell Adhesion to Human Endothelial Cells Is under Dominant Control of One TNF Receptor Type, TNF-R55. *The Journal of experimental medicine* **177,** 1277–1286. ISSN: 0022-1007, 1540-9538. doi:10.1084/jem.177.5.1277 (May 1, 1993).

81. Wajant, H. & Siegmund, D. TNFR1 and TNFR2 in the Control of the Life and Death Balance of Macrophages. *Frontiers in Cell and Developmental Biology* **7,** 91. ISSN: 2296-634X. doi:10.3389/fcell.2019.00091 (May 29, 2019).

82. Kwiatkowski, D., Sambou, I., Twumasi, P., Greenwood, B., Hill, A., Manogue, K., Cerami, A., Castracane, J. & Brewster, D. TNF Concentration in Fatal Cerebral,

Non-Fatal Cerebral, and Uncomplicated Plasmodium Falciparum Malaria. *The Lancet* **336,** 1201–1204. ISSN: 01406736. doi:10.1016/0140-6736(90)92827-5 (Nov. 1990).

83. Esser, C., Bachmann, A., Kuhn, D., Schuldt, K., Förster, B., Thiel, M., May, J., Koch-Nolte, F., Yáñez-Mó, M., Sánchez-Madrid, F., Schinkel, A. H., Jalkanen, S., Craig, A. G., Bruchhaus, I. & Horstmann, R. D. Evidence of Promiscuous Endothelial Binding by *P Lasmodium Falciparum* -infected Erythrocytes. *Cellular Microbiology* **16,** 701–708. ISSN: 1462-5814, 1462-5822. doi:10.1111/cmi.12270 (May 2014).

84. Moxon, C. A., Wassmer, S. C., Milner, D. A., Chisala, N. V., Taylor, T. E., Seydel, K. B., Molyneux, M. E., Faragher, B., Esmon, C. T., Downey, C., Toh, C.-H., Craig, A. G. & Heyderman, R. S. Loss of Endothelial Protein C Receptors Links Coagulation and Inflammation to Parasite Sequestration in Cerebral Malaria in African Children. *Blood* **122,** 842–851. ISSN: 0006-4971, 1528-0020. doi:10.1182/blood-2013-03-490219 (Aug. 1, 2013).

85. Turner, L., Lavstsen, T., Berger, S. S., Wang, C. W., Petersen, J. E. V., Avril, M., Brazier, A. J., Freeth, J., Jespersen, J. S., Nielsen, M. A., Magistrado, P., Lusingu, J., Smith, J. D., Higgins, M. K. & Theander, T. G. Severe Malaria Is Associated with Parasite Binding to Endothelial Protein C Receptor. *Nature* **498,** 502–505. ISSN: 0028-0836, 1476-4687. doi:10.1038/nature12216 (June 2013).

86. Lavstsen, T., Turner, L., Saguti, F., Magistrado, P., Rask, T. S., Jespersen, J. S., Wang, C. W., Berger, S. S., Baraka, V., Marquard, A. M., Seguin-Orlando, A., Willerslev, E., Gilbert, M. T. P., Lusingu, J. & Theander, T. G. *Plasmodium Falciparum* Erythrocyte Membrane Protein 1 Domain Cassettes 8 and 13 Are Associated with Severe Malaria in Children. *Proceedings of the National Academy of Sciences* **109.** ISSN: 0027-8424, 1091-6490. doi:10.1073/pnas.1120455109 (June 26, 2012).

87. Bernabeu, M., Danziger, S. A., Avril, M., Vaz, M., Babar, P. H., Brazier, A. J., Herricks, T., Maki, J. N., Pereira, L., Mascarenhas, A., Gomes, E., Chery, L., Aitchison, J. D., Rathod, P. K. & Smith, J. D. Severe Adult Malaria Is Associated with Specific PfEMP1 Adhesion Types and High Parasite Biomass. *Proceedings of the National Academy of Sciences* **113.** ISSN: 0027-8424, 1091-6490. doi:10.1073/pnas.1524294113 (June 7, 2016).

88. Rajan Raghavan, S. S., Turner, L., Jensen, R. W., Johansen, N. T., Jensen, D. S., Gourdon, P., Zhang, J., Wang, Y., Theander, T. G., Wang, K. & Lavstsen, T. Endothelial Protein C Receptor Binding Induces Conformational Changes to Severe Malaria-Associated Group A PfEMP1. *Structure* **31,** 1174–1183.e4. ISSN: 09692126. doi:10.1016/j.str.2023.07.011 (Oct. 2023).

89. Flens, M. J. & Zaman, G. J. R. Tissue Distribution of the Multidrug Resistance Protein. **148** (1996).

90. Neish, A. S., Williams, A. J., Palmer, H. J., Whitley, M. Z. & Collins, T. Functional Analysis of the Human Vascular Cell Adhesion Molecule 1 Promoter. *The Journal of experimental medicine* **176,** 1583–1593. ISSN: 0022-1007, 1540-9538. doi:10.1084/jem.176.6.1583 (Dec. 1, 1992).

91. Udomsangpetch, R., Reinhardt, P. H., Schollaardt, T., Elliott, J. F., Kubes, P. & Ho, M. Promiscuity of Clinical Plasmodium Falciparum Isolates for Multiple Adhesion Molecules under Flow Conditions. *The Journal of Immunology* **158,** 4358–4364. ISSN: 0022-1767, 1550-6606. doi:10.4049/jimmunol.158.9.4358 (May 1, 1997).

92. Ockenhouse, C. F., Tegoshi, T., Maeno, Y., Benjamin, C., Ho, M., Kan, K. E., Thway, Y., Win, K., Aikawa, M. & Lobb, R. R. Human Vascular Endothelial Cell Adhesion Receptors for Plasmodium Falciparum-Infected Erythrocytes: Roles for Endothelial Leukocyte Adhesion Molecule 1 and Vascular Cell Adhesion Molecule 1. *The Journal of Experimental Medicine* **176,** 1183–1189. ISSN: 0022-1007. doi:10.1084/jem.176.4.1183 (Oct. 1, 1992).

93. Sugiura, N., Clausen, T. M., Shioiri, T., Gustavsson, T., Watanabe, H. & Salanti, A. Molecular Dissection of Placental Malaria Protein VAR2CSA Interaction with a Chemo-Enzymatically Synthesized Chondroitin Sulfate Library. *Glycoconjugate Journal* **33,** 985–994. ISSN: 0282-0080, 1573-4986. doi:10.1007/s10719-016-9685-z (Dec. 2016).

94. Spliid, C. B., Toledo, A. G., Sanderson, P., Mao, Y., Gatto, F., Gustavsson, T., Choudhary, S., Saldanha, A. L., Vogelsang, R. P., Gögenur, I., Theander, T. G., Leach, F. E., Amster, I. J., Esko, J. D., Salanti, A. & Clausen, T. M. The Specificity of the Malarial VAR2CSA Protein for Chondroitin Sulfate Depends on 4-O-sulfation and

Ligand Accessibility. *Journal of Biological Chemistry* **297,** 101391. ISSN: 00219258. doi:10.1016/j.jbc.2021.101391 (Dec. 2021).

95. Rogerson, S. J., Chaiyaroj, S. C., Ng, K., Reeder, J. C. & Brown, G. V. Chondroitin Sulfate A Is a Cell Surface Receptor for Plasmodium Falciparum-Infected Erythrocytes. *The Journal of experimental medicine* **182,** 15–20. ISSN: 0022-1007, 1540-9538. doi:10.1084/jem.182.1.15 (July 1, 1995).

96. Esko, J. D., Stewart, T. E. & Taylor, W. H. Animal Cell Mutants Defective in Glycosaminoglycan Biosynthesis. *Proceedings of the National Academy of Sciences* **82,** 3197–3201. ISSN: 0027-8424, 1091-6490. doi:10.1073/pnas.82.10.3197 (May 1985).

97. Salanti, A., Staalsoe, T., Lavstsen, T., Jensen, A. T. R., Sowa, M. P. K., Arnot, D. E., Hviid, L. & Theander, T. G. Selective Upregulation of a Single Distinctly Structured *Var* Gene in Chondroitin Sulphate A-adhering *Plasmodium Falciparum* Involved in Pregnancy-associated Malaria. *Molecular Microbiology* **49,** 179–191. ISSN: 0950-382X, 1365-2958. doi:10.1046/j.1365-2958.2003.03570.x (July 2003).

98. Ma, R., Lian, T., Huang, R., Renn, J. P., Petersen, J. D., Zimmerberg, J., Duffy, P. E. & Tolia, N. H. Structural Basis for Placental Malaria Mediated by Plasmodium Falciparum VAR2CSA. *Nature Microbiology* **6,** 380–391. ISSN: 2058-5276. doi:10.1038/s41564-020-00858-9 (Jan. 15, 2021).

99. Medof, M. E., Walter, E. I., Rutgers, J. L., Knowles, D. M. & Nussenzweig, V. Identification of the Complement Decay-Accelerating Factor (DAF) on Epithelium and Glandular Cells and in Body Fluids. *The Journal of experimental medicine* **165,** 848–864. ISSN: 0022-1007, 1540-9538. doi:10.1084/jem.165.3.848 (Mar. 1, 1987).

100. Egan, E. S., Jiang, R. H. Y., Moechtar, M. A., Barteneva, N. S., Weekes, M. P., Nobre, L. V., Gygi, S. P., Paulo, J. A., Frantzreb, C., Tani, Y., Takahashi, J., Watanabe, S., Goldberg, J., Paul, A. S., Brugnara, C., Root, D. E., Wiegand, R. C., Doench, J. G. & Duraisingh, M. T. A Forward Genetic Screen Identifies Erythrocyte CD55 as Essential for *Plasmodium Falciparum* Invasion. *Science* **348,** 711–714. ISSN: 0036-8075, 1095-9203. doi:10.1126/science.aaa3526 (May 8, 2015).

101. Singethan, K. & Schneider-Schaulies, J. Tetraspanins: Small Transmembrane Proteins with Big Impact on Membrane Microdomain Structures. *Communicative & Integrative Biology* **1,** 11–13. ISSN: 1942-0889. doi:10.4161/cib.1.1.6406 (July 2008).

102. Barreiro, O., Yáñez-Mó, M., Sala-Valdés, M., Gutiérrez-López, M. D., Ovalle, S., Higginbottom, A., Monk, P. N., Cabañas, C. & Sánchez-Madrid, F. Endothelial Tetraspanin Microdomains Regulate Leukocyte Firm Adhesion during Extravasation. *Blood* **105,** 2852–2861. ISSN: 0006-4971, 1528-0020. doi:10.1182/blood-2004-09-3606 (Apr. 1, 2005).

103. Barreiro, O., Zamai, M., Yáñez-Mó, M., Tejera, E., López-Romero, P., Monk, P. N., Gratton, E., Caiolfa, V. R. & Sánchez-Madrid, F. Endothelial Adhesion Receptors Are Recruited to Adherent Leukocytes by Inclusion in Preformed Tetraspanin Nanoplatforms. *The Journal of Cell Biology* **183,** 527–542. ISSN: 1540-8140, 0021-9525. doi:10.1083/jcb.200805076 (Nov. 3, 2008).

104. Powner, D., Kopp, P. M., Monkley, S. J., Critchley, D. R. & Berditchevski, F. Tetraspanin CD9 in Cell Migration. *Biochemical Society Transactions* **39,** 563–567. ISSN: 0300-5127, 1470-8752. doi:10.1042/BST0390563 (Apr. 1, 2011).

105. Beckwith, K. A., Byrd, J. C. & Muthusamy, N. Tetraspanins as Therapeutic Targets in Hematological Malignancy: A Concise Review. *Frontiers in Physiology* **6.** ISSN: 1664-042X. doi:10.3389/fphys.2015.00091 (Mar. 23, 2015).

106. Jensen, J. B. & Trager, W. Plasmodium Falciparum in Culture: Establishment of Additional Strains. *The American Journal of Tropical Medicine and Hygiene* **27,** 743–746. ISSN: 0002-9637. doi:10.4269/ajtmh.1978.27.743 (July 1978).

107. Fernandez, V., Treutiger, C. J., Nash, G. B. & Wahlgren, M. Multiple Adhesive Phenotypes Linked to Rosetting Binding of Erythrocytes in Plasmodium Falciparum Malaria. *INFECT. IMMUN.* **66** (1998).

108. Kao, F. T. & Puck, T. T. Genetics of Somatic Mammalian Cells, VII. Induction and Isolation of Nutritional Mutants in Chinese Hamster Cells. *Proceedings of the National Academy of Sciences* **60,** 1275–1281. ISSN: 0027-8424, 1091-6490. doi:10.1073/pnas.60.4.1275 (Aug. 1968).

109. Cronshagen, J., Allweier, J., Mesén-Ramírez, P., Stäcker, J., Vaaben, A. V., Ramón-Zamorano, G., Naranjo-Prado, I., Ofori, S., Jansen, P. W., Hornebeck, J., Kieferle, F., Murk, A., Martin, E., Castro-Peña, C., Bártfai, R., Lavstsen, T., Bruchhaus, I. & Spielmann, T. *A System for Functional Studies of the Major Virulence Factor of Malaria Parasites* https://elifesciences.org/reviewed-preprints/103542v1. Pre-published.

110. Metwally, N. G., Tilly, A.-K., Lubiana, P., Roth, L. K., Dörpinghaus, M., Lorenzen, S., Schuldt, K., Witt, S., Bachmann, A., Tidow, H., Gutsmann, T., Burmester, T., Roeder, T., Tannich, E. & Bruchhaus, I. Characterisation of Plasmodium Falciparum Populations Selected on the Human Endothelial Receptors P-selectin, E-selectin, CD9 and CD151. *Scientific Reports* **7,** 4069. ISSN: 2045-2322. doi:10.1038/s41598-017-04241-3 (June 22, 2017).

111. Bedre, R. *Reneshbedre/Bioinfokit: Bioinformatics Data Analysis and Visualization Toolkit* version 2.0.9. Zenodo, Sept. 2022. doi:10.5281/zenodo.3964972.

112. Stirling, D. R., Swain-Bowden, M. J., Lucas, A. M., Carpenter, A. E., Cimini, B. A. & Goodman, A. CellProfiler 4: Improvements in Speed, Utility and Usability. *BMC Bioinformatics* **22,** 433. ISSN: 1471-2105. doi:10.1186/s12859-021-04344-9 (Dec. 2021).

113. Love, M. I., Huber, W. & Anders, S. Moderated Estimation of Fold Change and Dispersion for RNA-seq Data with DESeq2. *Genome Biology* **15,** 550. ISSN: 1474-760X. doi:10.1186/s13059-014-0550-8 (Dec. 5, 2014).

114. Andrews, S., Krueger, F., Segonds-Pichon, A., Biggins, L., Krueger, C. & Wingett, S. *FastQC: a quality control tool for high throughput sequence data* Babraham, UK, Jan. 2012.

115. Liao, Y., Smyth, G. K. & Shi, W. featureCounts: An Efficient General Purpose Program for Assigning Sequence Reads to Genomic Features. *Bioinformatics* **30,** 923–930. ISSN: 1367-4811, 1367-4803. doi:10.1093/bioinformatics/btt656 (Apr. 1, 2014).

116. Kim, D., Paggi, J. M., Park, C., Bennett, C. & Salzberg, S. L. Graph-Based Genome Alignment and Genotyping with HISAT2 and HISAT-genotype. *Nature Biotechnology*

37, 907–915. ISSN: 1087-0156, 1546-1696. doi:10.1038/s41587-019-0201-4 (Aug. 2019).

117. Ge, S. X., Son, E. W. & Yao, R. iDEP: An Integrated Web Application for Differential Expression and Pathway Analysis of RNA-Seq Data. *BMC Bioinformatics* **19,** 534. ISSN: 1471-2105. doi:10.1186/s12859-018-2486-6 (Dec. 2018).

118. Berg, S., Kutra, D., Kroeger, T., Straehle, C. N., Kausler, B. X., Haubold, C., Schiegg, M., Ales, J., Beier, T., Rudy, M., Eren, K., Cervantes, J. I., Xu, B., Beuttenmueller, F., Wolny, A., Zhang, C., Koethe, U., Hamprecht, F. A. & Kreshuk, A. Ilastik: Interactive Machine Learning for (Bio)Image Analysis. *Nature Methods* **16,** 1226–1232. ISSN: 1548-7091, 1548-7105. doi:10.1038/s41592-019-0582-9 (Dec. 2019).

119. Kikin, O., D'Antonio, L. & Bagga, P. S. QGRS Mapper: A Web-Based Server for Predicting G-quadruplexes in Nucleotide Sequences. *Nucleic Acids Research* **34,** W676–W682. ISSN: 0305-1048, 1362-4962. doi:10.1093/nar/gkl253 (Web Server July 1, 2006).

120. R Core Team. *R: A Language and Environment for Statistical Computing* manual (R Foundation for Statistical Computing, Vienna, Austria, 2021).

121. Danecek, P., Bonfield, J. K., Liddle, J., Marshall, J., Ohan, V., Pollard, M. O., Whitwham, A., Keane, T., McCarthy, S. A., Davies, R. M. & Li, H. Twelve Years of SAMtools and BCFtools. *GigaScience* **10,** giab008. ISSN: 2047-217X. doi:10.1093/gigascience/giab008 (Jan. 29, 2021).

122. Waskom, M. Seaborn: Statistical Data Visualization. *Journal of Open Source Software* **6,** 3021. ISSN: 2475-9066. doi:10.21105/joss.03021 (Apr. 6, 2021).

123. Prjibelski, A., Antipov, D., Meleshko, D., Lapidus, A. & Korobeynikov, A. Using SPAdes De Novo Assembler. *Current Protocols in Bioinformatics* **70,** e102. ISSN: 1934-3396, 1934-340X. doi:10.1002/cpbi.102 (June 2020).

124. Bruijning, M., Visser, M. D., Hallmann, C. A. & Jongejans, E. TRACKDEM : Automated Particle Tracking to Obtain Population Counts and Size Distributions from Videos in R. *Methods in Ecology and Evolution* **9** (ed Golding, N.) 965–973. ISSN: 2041-210X, 2041-210X. doi:10.1111/2041-210X.12975 (Apr. 2018).

125. Birnbaum, J., Flemming, S., Reichard, N., Soares, A. B., Mesén-Ramírez, P., Jonscher, E., Bergmann, B. & Spielmann, T. A Genetic System to Study Plasmodium Falciparum Protein Function. *Nature Methods* **14,** 450–456. ISSN: 1548-7091, 1548-7105. doi:10.1038/nmeth.4223 (Apr. 2017).

126. Trager, W. & Jensen, J. B. Human Malaria Parasites in Continuous Culture. *Science* **193,** 673–675. ISSN: 0036-8075, 1095-9203. doi:10.1126/science.781840 (Aug. 20, 1976).

127. Goodyer, I. D., Johnson, J., Eisenthal, R. & Hayes, D. J. Purification of Mature-Stage *Plasmodium Falciparum* by Gelatine Flotation. *Annals of Tropical Medicine & Parasitology* **88,** 209–211. ISSN: 0003-4983, 1364-8594. doi:10.1080/00034983.1994.11812859 (Jan. 1994).

128. Lambros, C. & Vanderberg, J. P. Synchronization of Plasmodium Falciparum Erythrocytic Stages in Culture. *The Journal of Parasitology* **65,** 418. ISSN: 00223395. doi:10.2307/3280287 (June 1979).

129. Thomas, J. A., Collins, C. R., Das, S., Hackett, F., Graindorge, A., Bell, D., Deu, E. & Blackman, M. J. Development and Application of a Simple Plaque Assay for the Human Malaria Parasite Plasmodium Falciparum. *PLOS ONE* **11** (ed Spielmann, T.) e0157873. ISSN: 1932-6203. doi:10.1371/journal.pone.0157873 (June 22, 2016).

130. Wu, Y., Bouws, P., Lorenzen, S., Bruchhaus, I. & Metwally, N. G. in *Parasite Genomics: Methods and Protocols* (eds de Pablos, L. M. & Sotillo, J.) 187–197 (Springer US, New York, NY, 2021). ISBN: 978-1-0716-1681-9. doi:10.1007/978-1-0716-1681-9_11.

131. Hughes, K. R., Biagini, G. A. & Craig, A. G. Continued Cytoadherence of Plasmodium Falciparum Infected Red Blood Cells after Antimalarial Treatment. *Molecular and Biochemical Parasitology* **169,** 71–78. ISSN: 01666851. doi:10.1016/j.molbiopara.2009.09.007 (Feb. 2010).

132. Smith, J. D., Chitnis, C. E., Craig, A. G., Roberts, D. J., Hudson-Taylor, D. E., Peterson, D. S., Pinches, R., Newbold, C. I. & Miller, L. H. Switches in Expression of Plasmodium Falciparum Var Genes Correlate with Changes in Antigenic and Cy-

toadherent Phenotypes of Infected Erythrocytes. *Cell* **82,** 101–110. ISSN: 00928674. doi:10.1016/0092-8674(95)90056-X (July 1995).

133. Ockenhouse, C. F., Ho, M., Tandon, N. N., Van Seventer, G. A., Shaw, S., White, N. J., Jamieson, G. A., Chulay, J. D. & Webster, H. K. Molecular Basis of Sequestration in Severe and Uncomplicated Plasmodium Falciparum Malaria: Differential Adhesion of Infected Erythrocytes to CD36 and ICAM-l. *Journal of Infectious Diseases* **164,** 163–169. ISSN: 0022-1899, 1537-6613. doi:10.1093/infdis/164.1.163 (July 1, 1991).

134. Avril, M., Tripathi, A. K., Brazier, A. J., Andisi, C., Janes, J. H., Soma, V. L., Sullivan, D. J., Bull, P. C., Stins, M. F. & Smith, J. D. A Restricted Subset of *Var* Genes Mediates Adherence of *Plasmodium Falciparum* -Infected Erythrocytes to Brain Endothelial Cells. *Proceedings of the National Academy of Sciences* **109.** ISSN: 0027-8424, 1091-6490. doi:10.1073/pnas.1120534109 (June 26, 2012).

135. Howell, D. P.-G., Levin, E. A., Springer, A. L., Kraemer, S. M., Phippard, D. J., Schief, W. R. & Smith, J. D. Mapping a Common Interaction Site Used by *Plasmodium Falciparum* Duffy Binding-like Domains to Bind Diverse Host Receptors. *Molecular Microbiology* **67,** 78–87. ISSN: 0950-382X, 1365-2958. doi:10.1111/j.1365-2958.2007.06019.x (Jan. 2008).

136. Frank, M., Dzikowski, R., Amulic, B. & Deitsch, K. Variable Switching Rates of Malaria Virulence Genes Are Associated with Chromosomal Position. *Molecular Microbiology* **64,** 1486–1498. ISSN: 0950-382X, 1365-2958. doi:10.1111/j.1365-2958.2007.05736.x (June 2007).

137. Brehmer, J. *Analyse Der Bindungseigenschaften Zwischen P. Falciparum Infizierten Erythrozyten Und Verschiedenen Endothelrezeptoren* PhD thesis (Universität Hamburg, Hamburg, 2021).

138. Bertin, G. I., Lavstsen, T., Guillonneau, F., Doritchamou, J., Wang, C. W., Jespersen, J. S., Ezimegnon, S., Fievet, N., Alao, M. J., Lalya, F., Massougbodji, A., Ndam, N. T., Theander, T. G. & Deloron, P. Expression of the Domain Cassette 8 Plasmodium Falciparum Erythrocyte Membrane Protein 1 Is Associated with Cerebral Malaria in Benin. *PLoS ONE* **8** (ed Snounou, G.) e68368. ISSN: 1932-6203. doi:10.1371/journal.pone.0068368 (July 29, 2013).

139. Wu, Y. *The Role of Human Endothelium and microRNAs as Active Participants in the Immune Response and Pathogenesis during Malaria* PhD thesis (Universität Hamburg, Hamburg, 2023).

140. Torabi, H. *Influence of Plasmodium Falciparum Infected Erythrocytes on the Gene Expression of Human Endothelial Cells* MA thesis (Universität Hamburg, Hamburg, 2022).

141. Nunes-Silva, S., Dechavanne, S., Moussiliou, A., Pstrąg, N., Semblat, J.-P., Gangnard, S., Tuikue-Ndam, N., Deloron, P., Chêne, A. & Gamain, B. Beninese Children with Cerebral Malaria Do Not Develop Humoral Immunity against the IT4-VAR19-DC8 PfEMP1 Variant Linked to EPCR and Brain Endothelial Binding. *Malaria Journal* **14,** 493. ISSN: 1475-2875. doi:10.1186/s12936-015-1008-5 (Dec. 2015).

142. Azasi, Y., Lindergard, G., Ghumra, A., Mu, J., Miller, L. H. & Rowe, J. A. Infected Erythrocytes Expressing DC13 PfEMP1 Differ from Recombinant Proteins in EPCR-binding Function. *Proceedings of the National Academy of Sciences* **115,** 1063–1068. ISSN: 0027-8424, 1091-6490. doi:10.1073/pnas.1712879115 (Jan. 30, 2018).

143. Smith, JosephD., Kyes, S., Craig, AlisterG., Fagan, T., Hudson-Taylor, D., Miller, LouisH., Baruch, DrorI. & Newbold, ChrisI. Analysis of Adhesive Domains from the A4VAR Plasmodium Falciparum Erythrocyte Membrane Protein-1 Identifies a CD36 Binding Domain. *Molecular and Biochemical Parasitology* **97,** 133–148. ISSN: 01666851. doi:10.1016/S0166-6851(98)00145-5 (Nov. 1998).

144. Robinson, B. A., Welch, T. L. & Smith, J. D. Widespread Functional Specialization of *Plasmodium Falciparum* Erythrocyte Membrane Protein 1 Family Members to Bind CD36 Analysed across a Parasite Genome. *Molecular Microbiology* **47,** 1265–1278. ISSN: 0950-382X, 1365-2958. doi:10.1046/j.1365-2958.2003.03378.x (Mar. 2003).

145. Dahlbäck, M., Jørgensen, L. M., Nielsen, M. A., Clausen, T. M., Ditlev, S. B., Resende, M., Pinto, V. V., Arnot, D. E., Theander, T. G. & Salanti, A. The Chondroitin Sulfate A-binding Site of the VAR2CSA Protein Involves Multiple N-terminal Domains. *Journal of Biological Chemistry* **286,** 15908–15917. ISSN: 00219258. doi:10.1074/jbc.M110.191510 (May 2011).

146. Andrews, K., Adams, Y., Viebig, N., Lanzer, M. & Schwartz-Albiez, R. Adherence of Plasmodium Falciparum Infected Erythrocytes to CHO-745 Cells and Inhibition of Binding by Protein A in the Presence of Human Serum. *International Journal for Parasitology* **35,** 1127–1134. ISSN: 00207519. doi:10.1016/j.ijpara.2005.05.007 (Sept. 2005).

147. Ruponen, M., Honkakoski, P., Tammi, M. & Urtti, A. Cell-surface Glycosaminoglycans Inhibit Cation-mediated Gene Transfer. *The Journal of Gene Medicine* **6,** 405–414. ISSN: 1099-498X, 1521-2254. doi:10.1002/jgm.522 (Apr. 2004).

148. Noble, R., Christodoulou, Z., Kyes, S., Pinches, R., Newbold, C. I. & Recker, M. The Antigenic Switching Network of Plasmodium Falciparum and Its Implications for the Immuno-Epidemiology of Malaria. *eLife* **2,** e01074. ISSN: 2050-084X. doi:10.7554/eLife.01074 (Sept. 17, 2013).

149. Recker, M., Buckee, C. O., Serazin, A., Kyes, S., Pinches, R., Christodoulou, Z., Springer, A. L., Gupta, S. & Newbold, C. I. Antigenic Variation in Plasmodium Falciparum Malaria Involves a Highly Structured Switching Pattern. *PLoS Pathogens* **7** (ed Kim, K.) e1001306. ISSN: 1553-7374. doi:10.1371/journal.ppat.1001306 (Mar. 3, 2011).

150. Magallón-Tejada, A., Machevo, S., Cisteró, P., Lavstsen, T., Aide, P., Rubio, M., Jiménez, A., Turner, L., Valmaseda, A., Gupta, H., De Las Salas, B., Mandomando, I., Wang, C. W., Petersen, J. E. V., Muñoz, J., Gascón, J., Macete, E., Alonso, P. L., Chitnis, C. E., Bassat, Q. & Mayor, A. Cytoadhesion to gC1qR through Plasmodium Falciparum Erythrocyte Membrane Protein 1 in Severe Malaria. *PLOS Pathogens* **12** (ed Blackman, M. J.) e1006011. ISSN: 1553-7374. doi:10.1371/journal.ppat.1006011 (Nov. 11, 2016).

151. Claessens, A., Adams, Y., Ghumra, A., Lindergard, G., Buchan, C. C., Andisi, C., Bull, P. C., Mok, S., Gupta, A. P., Wang, C. W., Turner, L., Arman, M., Raza, A., Bozdech, Z. & Rowe, J. A. A Subset of Group A-like *Var* Genes Encodes the Malaria Parasite Ligands for Binding to Human Brain Endothelial Cells. *Proceedings of the National Academy of Sciences* **109.** ISSN: 0027-8424, 1091-6490. doi:10.1073/pnas.1120461109 (June 26, 2012).

152. Gillrie, M. R., Avril, M., Brazier, A. J., Davis, S. P., Stins, M. F., Smith, J. D. & Ho, M. Diverse Functional Outcomes of *P Lasmodium Falciparum* Ligation of EPCR: Potential Implications for Malarial Pathogenesis: Divergent Activities of *P. Falciparum* EPCR-binding Domains. *Cellular Microbiology* **17,** 1883–1899. ISSN: 14625814. doi:10.1111/cmi.12479 (Dec. 2015).

153. Bernabeu, M., Gunnarsson, C., Vishnyakova, M., Howard, C. C., Nagao, R. J., Avril, M., Taylor, T. E., Seydel, K. B., Zheng, Y. & Smith, J. D. Binding Heterogeneity of Plasmodium Falciparum to Engineered 3D Brain Microvessels Is Mediated by EPCR and ICAM-1. *mBio* **10** (ed Sibley, L. D.) e00420–19. ISSN: 2161-2129, 2150-7511. doi:10.1128/mBio.00420-19 (June 25, 2019).

154. Li, A., Lim, T. S., Shi, H., Yin, J., Tan, S. J., Li, Z., Low, B. C., Tan, K. S. W. & Lim, C. T. Molecular Mechanistic Insights into the Endothelial Receptor Mediated Cytoadherence of Plasmodium Falciparum-Infected Erythrocytes. *PLoS ONE* **6** (ed Snounou, G.) e16929. ISSN: 1932-6203. doi:10.1371/journal.pone.0016929 (Mar. 17, 2011).

155. Kustatscher, G., Grabowski, P. & Rappsilber, J. Pervasive Coexpression of Spatially Proximal Genes Is Buffered at the Protein Level. *Molecular Systems Biology* **13,** 937. ISSN: 1744-4292, 1744-4292. doi:10.15252/msb.20177548 (Aug. 2017).

156. Chappell, L., Ross, P., Orchard, L., Russell, T. J., Otto, T. D., Berriman, M., Rayner, J. C. & Llinás, M. Refining the Transcriptome of the Human Malaria Parasite Plasmodium Falciparum Using Amplification-Free RNA-seq. *BMC Genomics* **21,** 395. ISSN: 1471-2164. doi:10.1186/s12864-020-06787-5 (Dec. 2020).

157. Wang, C. W., Magistrado, P. A., Nielsen, M. A., Theander, T. G. & Lavstsen, T. Preferential Transcription of Conserved Rif Genes in Two Phenotypically Distinct Plasmodium Falciparum Parasite Lines. *International Journal for Parasitology* **39,** 655–664. ISSN: 00207519. doi:10.1016/j.ijpara.2008.11.014 (May 2009).

158. Tonkin, C. J., Carret, C. K., Duraisingh, M. T., Voss, T. S., Ralph, S. A., Hommel, M., Duffy, M. F., Silva, L. M. D., Scherf, A., Ivens, A., Speed, T. P., Beeson, J. G. & Cowman, A. F. Sir2 Paralogues Cooperate to Regulate Virulence Genes and Antigenic

Variation in Plasmodium Falciparum. *PLoS Biology* **7** (ed Templeton, T. J.) e1000084. ISSN: 1545-7885. doi:10.1371/journal.pbio.1000084 (Apr. 14, 2009).

159. Joergensen, L., Bengtsson, D. C., Bengtsson, A., Ronander, E., Berger, S. S., Turner, L., Dalgaard, M. B., Cham, G. K. K., Victor, M. E., Lavstsen, T., Theander, T. G., Arnot, D. E. & Jensen, A. T. R. Surface Co-Expression of Two Different PfEMP1 Antigens on Single Plasmodium Falciparum-Infected Erythrocytes Facilitates Binding to ICAM1 and PECAM1. *PLoS Pathogens* **6** (ed Kazura, J. W.) e1001083. ISSN: 1553-7374. doi:10.1371/journal.ppat.1001083 (Sept. 2, 2010).

160. Flueck, C., Bartfai, R., Niederwieser, I., Witmer, K., Alako, B. T. F., Moes, S., Bozdech, Z., Jenoe, P., Stunnenberg, H. G. & Voss, T. S. A Major Role for the Plasmodium Falciparum ApiAP2 Protein PfSIP2 in Chromosome End Biology. *PLoS Pathogens* **6** (ed Kim, K.) e1000784. ISSN: 1553-7374. doi:10.1371/journal.ppat.1000784 (Feb. 26, 2010).

161. Guizetti, J., Barcons-Simon, A. & Scherf, A. Trans-Acting GC-rich Non-Coding RNA at *Var* Expression Site Modulates Gene Counting in Malaria Parasite. *Nucleic Acids Research,* gkw664. ISSN: 0305-1048, 1362-4962. doi:10.1093/nar/gkw664 (July 27, 2016).

162. Diffendall, G. & Scherf, A. Deciphering the Plasmodium Falciparum Perinuclear Var Gene Expression Site. *Trends in Parasitology* **40,** 707–716. ISSN: 14714922. doi:10.1016/j.pt.2024.06.002 (Aug. 2024).

163. Chan, J.-A., Fowkes, F. J. I. & Beeson, J. G. Surface Antigens of Plasmodium Falciparum-Infected Erythrocytes as Immune Targets and Malaria Vaccine Candidates. *Cellular and molecular life sciences: CMLS* **71,** 3633–3657. ISSN: 1420-9071. doi:10.1007/s00018-014-1614-3 (Oct. 2014).

164. Duraisingh, M. T., Voss, T. S., Marty, A. J., Duffy, M. F., Good, R. T., Thompson, J. K., Freitas-Junior, L. H., Scherf, A., Crabb, B. S. & Cowman, A. F. Heterochromatin Silencing and Locus Repositioning Linked to Regulation of Virulence Genes in Plasmodium Falciparum. *Cell* **121,** 13–24. ISSN: 00928674. doi:10.1016/j.cell.2005.01.036 (Apr. 2005).

165. Voss, T. S., Kaestli, M., Vogel, D., Bopp, S. & Beck, H.-P. Identification of Nuclear Proteins That Interact Differentially with *Plasmodium Falciparum Var* Gene Promoters. *Molecular Microbiology* **48,** 1593–1607. ISSN: 0950-382X, 1365-2958. doi:10.1046/j.1365-2958.2003.03528.x (June 2003).

166. Maier, A. G., Rug, M., O'Neill, M. T., Brown, M., Chakravorty, S., Szestak, T., Chesson, J., Wu, Y., Hughes, K., Coppel, R. L., Newbold, C., Beeson, J. G., Craig, A., Crabb, B. S. & Cowman, A. F. Exported Proteins Required for Virulence and Rigidity of Plasmodium Falciparum-Infected Human Erythrocytes. *Cell* **134,** 48–61. ISSN: 00928674. doi:10.1016/j.cell.2008.04.051 (July 2008).

167. Oberli, A., Slater, L. M., Cutts, E., Brand, F., Mundwiler-Pachlatko, E., Rusch, S., Masik, M. F. G., Erat, M. C., Beck, H.-P. & Vakonakis, I. A Plasmodium Falciparum PHIST Protein Binds the Virulence Factor PfEMP1 and Comigrates to Knobs on the Host Cell Surface. *FASEB journal: official publication of the Federation of American Societies for Experimental Biology* **28,** 4420–4433. ISSN: 1530-6860. doi:10.1096/fj.14-256057 (Oct. 2014).

168. Sargeant, T. J., Marti, M., Caler, E., Carlton, J. M., Simpson, K., Speed, T. P. & Cowman, A. F. Lineage-Specific Expansion of Proteins Exported to Erythrocytes in Malaria Parasites. *Genome Biology* **7,** R12. ISSN: 1474-760X. doi:10.1186/gb-2006-7-2-r12 (Feb. 20, 2006).

169. Otto, T. D., Gilabert, A., Crellen, T., Böhme, U., Arnathau, C., Sanders, M., Oyola, S. O., Okouga, A. P., Boundenga, L., Willaume, E., Ngoubangoye, B., Moukodoum, N. D., Paupy, C., Durand, P., Rougeron, V., Ollomo, B., Renaud, F., Newbold, C., Berriman, M. & Prugnolle, F. Genomes of All Known Members of a Plasmodium Subgenus Reveal Paths to Virulent Human Malaria. *Nature Microbiology* **3,** 687–697. ISSN: 2058-5276. doi:10.1038/s41564-018-0162-2 (May 21, 2018).

170. Wootton, J. C., Feng, X., Ferdig, M. T., Cooper, R. A., Mu, J., Baruch, D. I., Magill, A. J. & Su, X.-z. Genetic Diversity and Chloroquine Selective Sweeps In (2002).

171. Sander, A. F., Lavstsen, T., Rask, T. S., Lisby, M., Salanti, A., Fordyce, S. L., Jespersen, J. S., Carter, R., Deitsch, K. W., Theander, T. G., Pedersen, A. G. & Arnot, D. E. DNA Secondary Structures Are Associated with Recombination in Major *Plas-*

modium Falciparum Variable Surface Antigen Gene Families. *Nucleic Acids Research* **42,** 2270–2281. ISSN: 1362-4962, 0305-1048. doi:10.1093/nar/gkt1174 (Feb. 1, 2014).

172. Simmons, D. Anti-Adhesion Therapies. *Current Opinion in Pharmacology* **5,** 398–404. ISSN: 14714892. doi:10.1016/j.coph.2005.02.009 (Aug. 2005).

173. Marsh, K., Forster, D., Waruiru, C., Mwangi, I., Winstanley, M., Marsh, V., Newton, C., Winstanley, P., Warn, P., Peshu, N., Pasvol, G. & Snow, R. Indicators of Life-Threatening Malaria in African Children. *New England Journal of Medicine* **332,** 1399–1404. ISSN: 0028-4793, 1533-4406. doi:10.1056/NEJM199505253322102 (May 25, 1995).

174. Wahab, A., Shehzad, A., Ayesha, B. & Rahman, H. U. New Inhibitors Predicted for Plasmodium Falciparum Erythrocyte Membrane Protein1 (PfEMP1). *TSF Journal of Biology* **2,** 20–30. ISSN: 3006-0478, 3006-0869. doi:10.69547/TSFJB.020203 (Dec. 15, 2024).

175. Reyes, R. A., Raghavan, S. S. R., Hurlburt, N. K., Introini, V., Bol, S., Kana, I. H., Jensen, R. W., Martinez-Scholze, E., Gestal-Mato, M., López-Gutiérrez, B., Sanz, S., Bancells, C., Fernández-Quintero, M. L., Loeffler, J. R., Ferguson, J. A., Lee, W.-H., Martin, G. M., Theander, T. G., Lusingu, J. P. A., Minja, D. T. R., Ssewanyana, I., Feeney, M. E., Greenhouse, B., Ward, A. B., Bernabeu, M., Pancera, M., Turner, L., Bunnik, E. M. & Lavstsen, T. Broadly Inhibitory Antibodies to Severe Malaria Virulence Proteins. *Nature* **636,** 182–189. ISSN: 0028-0836, 1476-4687. doi:10.1038/s41586-024-08220-3 (Dec. 5, 2024).

176. Röckendorf, N., Nehls, C. & Gutsmann, T. Design of Membrane Active Peptides Considering Multi-Objective Optimization for Biomedical Application. *Membranes* **12,** 180. ISSN: 2077-0375. doi:10.3390/membranes12020180 (Feb. 2, 2022).

177. Röckendorf, N., Borschbach, M. & Frey, A. Molecular Evolution of Peptide Ligands with Custom-Tailored Characteristics for Targeting of Glycostructures. *PLoS Computational Biology* **8** (ed Ofran, Y.) e1002800. ISSN: 1553-7358. doi:10.1371/journal.pcbi.1002800 (Dec. 13, 2012).

178. Lou, J., Zhang, D., Wu, J., Zhu, G., Zhang, M., Tang, J., Fang, Y., He, X. & Cao, J. Antimalarial Activity of Cecropin Antimicrobial Peptides Derived from *Anopheles*

Mosquitoes. *Antimicrobial Agents and Chemotherapy* **68** (ed Odom John, A.) e00311–24. ISSN: 0066-4804, 1098-6596. doi:10.1128/aac.00311-24 (July 9, 2024).

179. Gelhaus, C., Jacobs, T., Andrä, J. & Leippe, M. The Antimicrobial Peptide NK-2, the Core Region of Mammalian NK-Lysin, Kills Intraerythrocytic *Plasmodium Falciparum*. *Antimicrobial Agents and Chemotherapy* **52,** 1713–1720. ISSN: 0066-4804, 1098-6596. doi:10.1128/AAC.01342-07 (May 2008).

180. Föller, M., Huber, S. M. & Lang, F. Erythrocyte Programmed Cell Death. *IUBMB Life* **60,** 661–668. ISSN: 1521-6543, 1521-6551. doi:10.1002/iub.106 (Oct. 2008).

181. Hernández-Castañeda, M. A., Lavergne, M., Casanova, P., Nydegger, B., Merten, C., Subramanian, B. Y., Matthey, P., Lannes, N., Mantel, P.-Y. & Walch, M. A Profound Membrane Reorganization Defines Susceptibility of Plasmodium Falciparum Infected Red Blood Cells to Lysis by Granulysin and Perforin. *Frontiers in Immunology* **12,** 643746. ISSN: 1664-3224. doi:10.3389/fimmu.2021.643746 (May 19, 2021).

182. Sherman, I. W., Prudhomme, J. & Tait, J. F. Altered Membrane Phospholipid Asymmetry in Plasmodium Falciparum-Infected Erythrocytes. *Parasitology Today* **13,** 242–243. ISSN: 01694758. doi:10.1016/S0169-4758(97)85284-2 (June 1997).

183. Vale, N., Aguiar, L. & Gomes, P. Antimicrobial Peptides: A New Class of Antimalarial Drugs? *Frontiers in Pharmacology* **5.** ISSN: 1663-9812. doi:10.3389/fphar.2014.00275 (Dec. 19, 2014).

184. Ghosh, J. K., Shaool, D., Guillaud, P., Cicéron, L., Mazier, D., Kustanovich, I., Shai, Y. & Mor, A. Selective Cytotoxicity of Dermaseptin S3 toward Intraerythrocytic-Plasmodium Falciparum and the Underlying Molecular Basis. *Journal of Biological Chemistry* **272,** 31609–31616. ISSN: 00219258. doi:10.1074/jbc.272.50.31609 (Dec. 1997).

185. Belda, I., Llorà, X. & Giralt, E. Evolutionary Algorithms and de Novo Peptide Design. *Soft Computing* **10,** 295–304. ISSN: 1432-7643, 1433-7479. doi:10.1007/s00500-005-0487-7 (Feb. 2006).

186. Schneider, G. & Schüller, A. in *Ligand-Macromolecular Interactions in Drug Discovery* (ed Roque, A. C. A.) 135–147 (Humana Press, Totowa, NJ, 2010). ISBN: 978-1-60761-243-8 978-1-60761-244-5. doi:10.1007/978-1-60761-244-5_8.

187. Sandberg, M., Eriksson, L., Jonsson, J., Sjöström, M. & Wold, S. New Chemical Descriptors Relevant for the Design of Biologically Active Peptides. A Multivariate Characterization of 87 Amino Acids. *Journal of Medicinal Chemistry* **41,** 2481–2491. ISSN: 0022-2623, 1520-4804. doi:10.1021/jm9700575 (July 1, 1998).

188. Savinov, A., Swanson, S., Keating, A. E. & Li, G.-W. High-Throughput Discovery of Inhibitory Protein Fragments with AlphaFold. *Proceedings of the National Academy of Sciences* **122,** e2322412122. ISSN: 0027-8424, 1091-6490. doi:10.1073/pnas.2322412122 (Feb. 11, 2025).

189. Rask, T. S., Hansen, D. A., Theander, T. G., Gorm Pedersen, A. & Lavstsen, T. Plasmodium Falciparum Erythrocyte Membrane Protein 1 Diversity in Seven Genomes – Divide and Conquer. *PLoS Computational Biology* **6** (ed Eisen, J. A.) e1000933. ISSN: 1553-7358. doi:10.1371/journal.pcbi.1000933 (Sept. 16, 2010).

190. Metwally, N. G., Tauler, M. D. P. M., Torabi, H., Allweier, J., Mohamed, S., Bessemoulin, M., Bouws, P., Alshikh, F., Wu, Y., Temori, M., Schell, T., Rakotonirinalalao, M., Honecker, B., Höhn, K., Jacobs, T., Heine, H. & Bruchhaus, I. Distinct Brain and Lung Endothelial miRNAmRNA Profiles after Exposure to Plasmodium Falciparum-Infected Red Blood Cells. *iScience* **27,** 111265. doi:10.1016/j.isci.2024.111265 (Nov. 15, 2024).

B Acknowledgments

First and foremost, I would like to express my sincere gratitude to my supervisors, **Prof. Dr. Iris Bruchhaus and Prof. Dr. Thomas Gutsmann**. Thank you both for making this doctorate possible and for standing by me with advice and practical support. I truly appreciate your warm encouragement and your valuable input throughout this journey. I would also like to thank **Prof. Dr. Tim Gilberger** for taking the time to examine my thesis.

I also want to thank the whole **team in Borstel**, especially **Dr. Christian Nehls** for his expertise and help with biophysical methods, as well as to **Dr. Niels Röckendorf** for the peptide synthesis and the extensive technical support regarding their application.

I am also deeply grateful to **Dr. Anna Bachmann and Dr. Tobias Spielmann**, who supported me as co-supervisors with their insightful feedback and suggestions.

A special thank you goes to my students: **Florian, David, and Jiwanen**. Your support and motivation were vital to the success of this work, and I truly enjoyed working with you.

To my lab mates, **Susann Ofori and Dr. Pilar**: thank you so much for your help and for being people I could always count on whenever things got tough. You were truly the Yin and Yang of Lab 4, making shure, that it was rarely a boring place to be. I not only enjoyed our time in the lab but also the many relaxed evenings we spent sharing a glass of wine after work.

My deepest thanks go to **my family**. You have always supported me in everything I do and made this path possible for me. Your constant encouragement means the world to me.

Finally, I want to thank my girlfriend, **Agnes**. You were always there for me through all the ups and downs, providing emotional support, critical perspectives, and endless patience. Thank you for everything.